ISSN 1343-2230

CNS-REP-76
December, 2007

Annual Report 2006

Center for Nuclear Study,
Graduate School of Science, the University of Tokyo

Editors
Taku Gunji

Center for Nuclear Study

CNS Reports are available from:
Wako-Branch at RIKEN
Center for Nuclear Study,
Graduate School of Science, the University of Tokyo
2-1 Hirosawa, Wako
351-0198, Japan
Tel: +81-48-464-4191
Fax: +81-48-464-4554

Annual Report 2006

Center for Nuclear Study,
Graduate School of Science, the Univ ersity of Tokyo

Preface

This is the annual report of the Center for Nuclear Study (CNS), Graduate School of Science, the University of Tokyo, for the fiscal year 2006 (April 2006 through March 2007). During this period, a lot of research activities in various fields of nuclear physics have been carried out and a wide variety of fruitful results have been obtained at CNS. This report summarizes research such activities. I hereby mention some highlights of the report.

Deformed structures in neutron-rich Be and B isotopes were studied via in-beam spectroscopy experiments using the position-sensitive γ-ray detector array, CNS GRAPE. High-spin states in ^{48}Ca region populated by fusion reactions of an RI beam and A$\sim$110 region by a ^{20}Ne + ^{96}Zr reaction were investigated by γ-ray measurements using the CNS GRAPE and Clover detectors. Digital pulse shape analysis of the signals from the CNS GRAPE was performed providing a typical 3 dimensional position sensitivity of 2 mm. The CNS GRAPE having such a good position sensitivity will be a powerful tool for new experiments at RIBF.

The research activities with the CNS low-energy RI beam separator CRIB have expanded not only for nuclear physics and nuclear astrophysics, but also to an application science. These activities are also based strongly on the international collaborations. There are some technical developments achieved during the past year. One remarkable achievement is a successful operation of a cryogenic production target, which utilizes liquid Nitrogen for cooling the circulating Hydrogen gas as well as the target cell. This target produces in total roughly ten times more secondary beam intensity than before by increasing the beam durability as well as the target density increase. Actually, low energy ^{7}Be were obtained steadily with an intensity of 2×10^{8} pps with nearly 100 % purity. This will expand our research activities to a new phase in various fields. The research activities include resonant elastic scattering of protons on ^{25}Al and ^{8}B. The direct measurements of astrophysical reactions were also successfully made for the ^{14}O(α,p) reaction and the ^{18}F(p,α)^{15}O reaction. A significant spin-polarized beam of ^{17}N was successfully obtained from the ^{9}Be(^{18}O,^{17}N) reaction for studying material science.

Development of the polarized proton solid target has continued for use in the $p-{}^{8}$He elastic scattering measurement and future experiments at RIBF. The R&D of new light sources of the polarized target has been started.

The SHARAQ project is going as scheduled collaborating with Sakai group in Department of Physics and RIKEN Nishina center. The magnets of the SHARAQ spectrometer have been constructed and will be installed by the summer of 2007. The design of the high resolution beam line has been finished. RIKEN Nishina center will construct the beam line based on the MOU between University of Tokyo and RIKEN engaged in December 2006. An international collaboration with GANIL for the focal plane detectors was initiated in the end of FY2006.

The experimental study in the PHENIX experiment at Relativistic Heavy Ion Collider (RHIC) at Brookhaven National Laboratory have made a steady progress toward the understanding of hot and dense matter created by colliding gold nuclei at relativistic energies. The CNS group has been playing major roles in producing results for various physics subjects which include energy loss mechanism for light and heavy quarks, and J/ψ production in $\mathrm{Cu}+\mathrm{Cu}$, and $\mathrm{Au}+\mathrm{Au}$ collisions. The study of basic performances of gas electron multiplier (GEM), a new type of gaseous detector, has been performed. R & D of a UV-photon detector with GEM have been made, and development of a readout system for 2-D imaging has started.

Contribution of CNS to upgrade the AVF cyclotron is described as follows: (1) HyperECR has been playing roles to deliver the high intense gaseous or meta l ion beams to the AVF cyclotron. Gaseous ion beam such as ^{83}Kr^{23+} 0.033eμA was extracted from AVF h owever 5.45 eμA was injected to the AVF. The continuous extraction of Li^{3+} beam for one week has been established by using large volume crucible with pure Li sample. (2) Development of charge breeding ECR ion source (CBECR) is being proceeded. Si ngly charged ion source was adopted to the 10kV acceleration stage and

extracted beam has been measured by ma gnetic mass analyser. (3) Proof of the glaser lens GLI38 of AVF cyclotron has been done to enlarge a c onvergence power of the vertical beam injection line. (4) Computer model of the present AVF cyclotron was constructed to study the cen ter region for harmonic number of 1, 2 and 3.

Theoretical studies have been carried out by large-scale nuclear structure calculations in collaboration with RIKEN Nishina Center and the Department of Physics, University of Tokyo. Shell-model calculations, in particular, those by the Monte Carlo Shell Model, have produced crucial results to clarify the evolution of nuclear shells in particular in exotic nuclei and the role of the tensor force on it, modifying the picture of the island of inversion, for instance. Other aspects, for instance, the cluster structure of light nuclei, have been studied also. Many of such theoretical studies have been made in collaboration with various groups over the world.

The 5th CNS International Summer School (CISS06) has been organized in August 2006 with many invited lecturers including four foreign distinguished physicists. There were 96 participants from 7 countries mainly from Asia.

Finally, I thank Ms. M. Hirano and other administrative stuff members for their heartful contributions throughout the year.

Takaharu Otsuka
Director of CNS

Table of Contents

1a. Experimental Nuclear Physics: Low and Intermediate Energies

1b. Experimental Nuclear Physics: PHENIX Experiment at BNL-RHIC

2. Accelerator and Instrumentation

3. Theoretical Nuclear Physics

4. Other Activities

Appendices

Experimental Nuclear Physics: Low and Intermediate Energies

On the Waiting Point at A=30 in X-ray Bursts: ^{30}S(α, p)^{33}Cl with CRIB

D. Kahl[a], A. A. Chen[a], J. Chen[a], S. Hayakawa[b], A. Kim[c], S. Kubono[b], S. Michimasa[b], K. Setoodehnia[a], Y. Wakabayashi[b], H. Yamaguchi[b],

[a] *Department of Physics & Astronomy, McMaster University (Canada)*
[b] *Center for Nuclear Study, Graduate School of Science, University of Tokyo (Japan)*
[c] *Department of Physics, Ewha Womans University (Korea)*

1. Introduction

The understanding of energy generation in Type I X-Rays bursts will be enhanced by a direct measurment of the ^{30}S(α,p)^{33}Cl reaction. Very little is known about the compound nucleus ^{34}Ar above the alpha threshold, and the reaction in question has yet to be measured experimentially [1, 2]. The experimenters undertook two days of ^{30}S beam development at the CNS radioactive ion beam separator CRIB facility [3] of the University of Tokyo at RIKEN during December 2006 in preparation for a planned experiment measuring the ^{30}S(α,p)^{33}Cl reaction directly in inverse kinematics at an energy range corresponding to astrophysical burst temperatures of interest.

Models of energy generation in Type I X-Ray burst are constrained by the observations of bursts with multiple peaks in their bolometric luminosity [4, 5, 6, 7]. Recently, Fisker *et al.* [8] argued that previous theories of heat transport impedance and coronal radiation scattering are unsatisfying explanations of the burst light-curves, and instead proposed a nuclear waiting-point impedence at the proton-rich nucleus ^{30}S. Nuclear reaction networks in burst conditions (T = 1 to 1.5 GK) indicate that the burning pathway passes through ^{30}S. However, proton capture on ^{30}S will be in equilibrium with the photodisintegration of ^{31}Cl, and the β^+ decay of ^{30}S has a lifetime on the order of burst luminosity rise-times, making the reaction rate of ^{30}S(α,p) crucial for a proper understanding of how the burning proceeds thereafter [4, 9].

Previous work on α-capture reactions on unstable, T_z = –1 ($T_z \equiv$ (N – Z)/2), even-even nuclei at A $\approx$ 20 revealed they are dominated by a few narrow natural-parity, α-cluster resonances in the reaction channel of the respective compound nuclei [10, 11, 12]. If one assumes that this property of nuclei holds true up to A=30, a strong case is made for directly measuring the cross section of the ^{30}S(α,p)^{33}Cl reaction rather than relying on Hauser-Feshbach statistical modeling. By varying the theoretical rate of ^{30}S(α,p) by a factor of 100, burst models show that if the cross section is sufficiently large enough, the resulting light curve exhibits a notably different shape [8, 13]. As explosive stellar nucleosynthesis models have a large number of parameters, these should be experimentally constrained whenever possible.

2. Setup and Method

At the CRIB there are four focal planes of interest, denoted F0, F1, F2, and F3, respectively. The production target of the secondary beam is located at F0. After the first magnetic dipole is the momentum dispersive focal plane, F1, followed by a double achromatic focal plane, F2 [3]. Finally, a Wien filter is used before the scattering chamber F3.

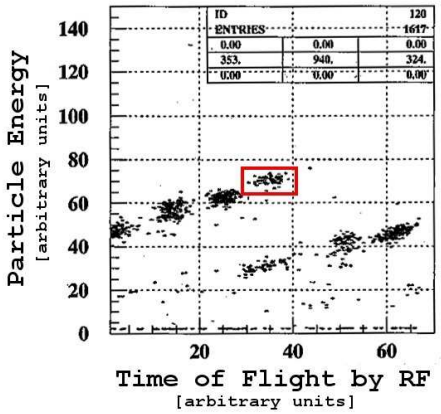

Figure 1. Sample on-line calibration spectrum used for particle identification at F2. $^{30}S^{16+}$ is enclosed in the solid box, with a purity of 7.4%. The abscissa data is obtained by comparing the cyclotron RF signal with the triggering of the PPAC and SSD at F2, and the ordinate data is only from the SSD at F2. Both axes are plotted in channels.

The ^{30}S beam, via ^{3}He(^{28}Si,n)^{30}S, is among the heaviest secondary radioactive beams yet developed for experimental use at the CRIB facility [14]. A $^{28}Si^{9+}$ primary beam, produced by an ECR ion source, accelerated by the RIKEN AVF Cyclotron up to the energy 6.9 MeV/u with an intesity of 100 pnA entered the CRIB and impinged on a 2.5 μm havar windowed gas cell of ^{3}He held at 400 Torr and cooled to 80K with LN_2 located at F0. By inserting one parallel plate avalanche counter (PPAC) at F1 and a second PPAC and a silicon strip detector (SSD) at F2, the magnet rigidity and F1 slit positioning are optimized by considering particle time-of-flight versus energy (see Figure 1) [3]. The PPACs used in this experiment have 4 μm mylar outer windows, and 1.5 μm mylar on the X cathod, anode, and Y cathod [15]. The ion identification spectrum is compared to the LISE simulation [16]. The Wien filter was held at 64 kV.

Event by event trajectory and particle identification is obtained from a second set of PPACs (separation 60 cm) at F3. The future experiment will measure ^{30}S(α,p)^{33}Cl in inverse kinematics by bombarding a havar windowed, He-filled gas cell, kept at laboratory temperature. Reaction particles are then detected at three forward angles (0, 17, 27 degrees) by ΔE-E telescopes. The ΔE telescopes are 16 by 16 channel position-sensative silicon detectors (PSD) with

a thickness of 75 μm, followed by two 1500 μm SSD E telescopes. The reaction protons of interest will be stopped within the first SSD, while the second SSD will be used to veto background events.

Reactions will then be reconstructed from proton detection in coincidence with ^{30}S ions detected in the upstream PPACs at F3. By considering only coincidence data from the F3 PPACs and ΔE-E telescopes, events of interest may be distinguished from background events. The semi-cylindrical target gas cell is designed and tested to hold up to 2 atmosphere over-pressure, is crafted from aluminum, and has dimension 6.7 cm wide (given by the width of the front face) and 3.8 cm long (given by the radius of the semi-cylinder). The entrance window is a 2.5 μm havar foil 1 cm in diameter, while the curved exit window is a 5 μm havar foil (in order to stop the beam) 1 cm tall and wide enough to allow reaction protons to escape at an angle of up to 45 degrees. The curved exit window ensures that the energy loss of protons that emerge from a given interaction point within the gas is independent of the angle [17]. The pressure of the He fill-gas will be set to scan the energy region of interest based on the available secondary beam energy at the target; this pressure is expected to be one atmosphere or less.

3. Results

After the first 36 hours of development, a $^{30}S^{16+}$ beam of 1.8 kpps per 100 pnA arrived at the secondary target at 11.3 ± 1.8 MeV and purity of 13%; a maximum purity for $^{30}S^{16+}$ at F3 of 56% was achieved for lower beam currents. The Gamow window for the ^{30}S(α,p)^{33}Cl reaction at 1 GK is E_{cm} 1.41 to 2.34 MeV, which requires the beam to scan an energy of 12.0 to 19.9 MeV in the laboratory [18]. Calculations using a statistical model reaction cross section indicate that a ^{30}S beam with intensity of the order 10^5 pps is required to observe 200 ^{30}S(α,p)^{33}Cl reaction protons after 250 hours of data collection under our conditions [19]. Although the prospects to increase the purity of the 11.3 MeV $^{30}S^{16+}$ beam above 13% appeared very promising, due to time contraints and the consideration that the beam intensity was two orders of magnitude lower than we desire, we chose to scan other charge states of ^{30}S.

In the remaining 12 hours of the development run, we developed a $^{30}S^{15+}$ beam to get a higher seconary beam intensity at F3. A $^{30}S^{15+}$ beam of 3 kpps per 20 pnA at 9 MeV was delivered to the secondary target. In order to best separate out the $^{28}Si^{14+}$ contamination, the primary beam intensity was reduced to 20 pnA, but an excess of $^{28}Si^{14+}$ contamination still resulted in a purity of only 2.1% on target.

The secondary target gas cell was designed based on the consideration that the beam diameter would not exceed 1 cm; because the resulting ^{30}S beam had a diameter of 1.5 cm, the gas cell was successfully modified in May 2007 to make the entance window 2 cm in diameter, and the rear window 2 cm tall.

Since the beam development run, the Wien filter has attained higher potentials up to 90 kV, increasing the abiliy to purify contaminated beams by a factor of nearly 1.5 [20]. A higher Wien filter potential may allow the future development of ^{30}S beams with lower charge states (i.e. not fully ionizied), as it is seen that lower charge states have higher intensities but also more Si contamination and so require more purification. It is also possible to decrease the PPAC outer foil thickness by a factor of 2 using 2μm mylar, reducing the beam energy loss as it traverses F3 and thus increase the beam energy delivered to the secondary target. Finally, data analysis is currently underway in order to determine how the primary beam, primary target, and secondary beam development may be further optimized based on the results of the development run to increase the secondary beam energy, purity and count rate on target during the next planned ^{30}S beam production run.

4. Acknowledgements

This experiment was made possible through the CNS and RIKEN collaboration. The McMaster University group is appreciative of funding from the National Science and Engineering Research Council of Canada.

References

[1] P. Endt, Nucl. Phys. A **521** (1990) 1.
[2] P. Endt, Nucl. Phys. A **633** (1998) 1.
[3] S. Kubono *et al.*, Eur. Phys. J. A **13** (2002) 217.
[4] M. Sztajno, J. van Paradijs, W. H. C Lewin and J. Trümper, ApJ **299** (1985) 487.
[5] J. van Paradijs, M. Sztajno, W. H. G. Lewin, J. Trümper, W. D. Vacca, and M. van der Klis, MNRAS, **221** (1986) 617.
[6] W. Penninx, E. Damen, J. van Paradijs, and W. H. G. Lewin, A&A, **208** (1989) 146.
[7] E. Kuulkers, J. Homan, M. van der Klis, W.H.G. Lewin, and M. Méndez, A&A 382 (2002) 947.
[8] J. Fisker, F. -K. Thielemann, and M. Wiescher, Ap. J. Lett. **608** (2004) 61.
[9] H. Schatz *et al.*, Phys. Rev. Lett. **79** (1997) 3845.
[10]W. Bradfield-Smith *et al.*, Phys. Rev. C **59** (1999) 3402.
[11]D. Groombridge *et al.*, Phys. Rev. C **66** (2002) 055802.
[12]S. Dababneh *et al.*, Phys. Rev. C **68** (2003) 025801.
[13]S. E. Woosley *et al.*, Ap. J. Supp. **151** (2004) 75.
[14]W. Bohne *et al.*, Nucl. Phys. A **378** (1982) 525.
[15]H. Kumagai *et al.*, Nuc. Inst. and Meth. A **470** (2001) 562.
[16]O. Tarasov, D. Bazin, Nucl. Phys. A **746** (2004) 411.
[17]Proposal for this experiment, accepted by CNS PA Committee.
[18]C. Rolfs, *Cauldrons in the Cosmos*, University of Chicago Press (1988).
[19]T. Rauscer and F. -K. Thielemann, At. Data Nucl. Data Tables **79** (2001) 47.
[20]S. Kubono, private communication (2007).

Astrophysically Important ^{26}Si States studied with the ^{28}Si($^{4}He,^{6}He$)^{26}Si Reaction

Y. K. Kwon, C. S. Lee, J. Y. Moon, J. H. Lee, J. Y. Kim, S. Kubono[a], N. Iwasa[b], K. Inafuku[b], H. Yamaguchi[a], J. J. He[a], A. Saito[a], Y. Wakabayashi[a], H. Fujikawa[a], G. Amadio[a], L. H. Khiem[c], M. Tanaka[d], A. Chen[e], S. Kato[f], Y. Fuchi[d], and N. Fukunishi[g]

Department of Physics, Chung-Ang University, Korea
[a]*Center for Nuclear Study, Graduate School of Science, University of Tokyo*
[b]*Department of Physics, Tohoku University*
[c]*Institute of Physics and Electronics, Vietnam*
[d]*KEK (The High Energy Accelerator Organization)*
[e]*Department of Physics and Astronomy, McMaster University, Canada*
[f]*Department of Physics, Yamagata University*
[g]*RIKEN (The Institute of Physical and Chemical Research)*

1. Introduction

^{26}Al is the first cosmic radioactivity ever detected through its characteristic 1.809-MeV gamma ray line. One possible source for the production of ^{26}Al is a nova explosion. Under the nova environment, ^{25}Al$(p,\gamma)^{26}$Si reaction is the key reaction to produce ^{26}Si. The uncertainty of ^{25}Al$(p,\gamma)^{26}$Si reaction rate is mainly due to the lack of nuclear structure information of ^{26}Si above the proton threshold ($Q_{p\gamma}$ = 5.518 MeV).

Illiadis et al. [1] made a detail survey of the past data on ^{26}Si and derived tentative spin-parity assignments based on conjunction with shell-model calculations and mirror-nucleus considerations. They concluded that the ^{25}Al$(p,\gamma)^{26}$Si reaction rate is dominated by a 3^+ unnatural-parity state (E_x = 5970(100) keV) in ^{26}Si under the typical nova temperature (T_9 = 0.1 - 0.4 K). Motivated by this suggestion, several experiments [2,3,4,5] have been performed to confirm the 3^+ state. However, as summarized in Table 1, there are discrepancies in spin-parity assignment of the 3^+ state. To solve this contradiction, we have decided to study the level structure of ^{26}Si with ^{28}Si($^{4}He,^{6}He$)^{26}Si reaction. Direct transitions to unnatural parity states especially like 3^+ are forbidden to first order in (*p,t*) reaction, but allowed in ($^{4}He,^{6}He$) reaction [6]. There are several experiments reporting enhanced cross sections for the excitation of unnatural-parity 3^+ state via ($^{4}He,^{6}He$) reaction [7, 8].

(p,t) [2]		(p,t) [3]		$(^3He,n\gamma)$ [4]		$(^3He,^6He)$ [5]	
E_x	J^π	E_x	J^π	E_x	J^π	E_x	J^π
–	–	–	–	5670(4)	1^{+a}	5678(8)	1^{+b}
5916(2)	0^{+c}	5914(2)	3^{+d}	5912(4)	3^{+a}	–	–
–	–	–	–	5946(4)	0^{+a}	5945(8)	3^{+b}

[a] From the Hauser-Feshbach calculations [4].
[b] From mirror nuclei considerations [5].
[c] From DWBA analysis [2].
[d] From consideration of multi-step process [3].

Table 1. Previously measured excitation energies (units in keV) and spin-parities in ^{26}Si.

2. Experiment

The ^{28}Si($^{4}He,^{6}He$)^{26}Si reaction was studied using the high resolution quadrupole-dipole-dipole (QDD) magnetic spectrograph (PA) at Center for Nuclear Study (CNS), University of Tokyo. A beam of ^{4}He at 120 MeV was extracted from RIKEN linear accelerator (RILAC) + RIKEN ring cyclotron (RRC). Beam intensity was typically 70 enA at the target position. Beam transportation with dispersion matching mode was adopted for the optimized condition of PA system. A self-supporting natural silicon target (thickness $\sim$ 1 mg/cm^2) was used. ^{6}He particles were measured at four angles, 8^o, 11^o, 15^o and 20^o in the lab system. Because of the low cross section, the PA slit with aperture of 5 msr was used. For the particles identification, utilized are the energy-loss (ΔE), energy (E) and time-of-flight (TOF) information. Also, with the incident angle information and the drift-time distribution, the background was eliminated as much as possible. Internal energy calibration was used to determine the excitation energy in ^{26}Si. The well-known states that were populated with the ^{24}Mg($^{3}He,n\gamma$)^{26}Si reaction [9] were used for the calibration. The overall energy resolution was about 90 keV in FWHM.

3. Result and discussion

Total of 22 excited states in ^{26}Si were observed, including eleven above the proton threshold. The excitation energies below the proton threshold level agreed well with those from previous experimental results.

The 7018 keV level which was only observed by Bardayan et al. [2] was confirmed in our measurement. Among the strong candidates for the unnatural parity states at E_x = 5678 keV, 5916 keV and 5945 keV, the 5918(8) keV state was only observed within the uncertainty of energy. The energy resolution of our system was not sufficient to resolve the observed levels at E_x = 5916 and 5945 keV. As shown in Figure 1, along the measured angles, there was possible systematic trend that would suggest the centroid of 5918(8) keV peak was shifting. Also, in the total summed energy spectrum through the all measured angles, the width of peak at the 5918(8) keV seems to be wider than other peaks. It suggested that the peak of 5918 keV may correspond to the

doublet state.

We observed a new state at E_x = 6101 keV. This new state was examined using the scattering-angle kinematics. If it came from other reactions, the position of peak should shift a little, depending on the measured angles. As shown in Figure 1, the 6101 keV state was observed in two different angles (8^o and 20^o in the lab system). Also we checked all possible contamination peaks thoroughly. As a result, we concluded that the 6101 keV state could be the new state.

Due to the lack of measured angles (only four forward angles) and low statistics, spin-parity assignment cold not be made from the present measurement. To directly assign the spin-parity with the angular distribution data, the more statistics and more number of measured angles are required.

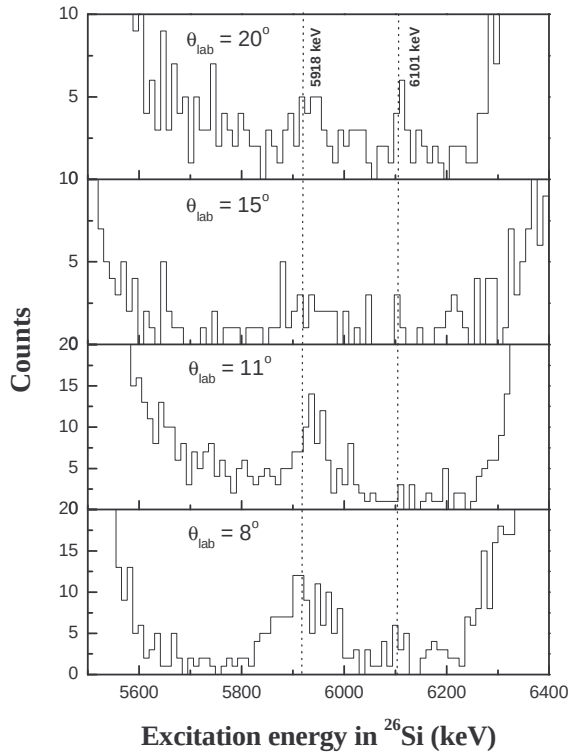

Figure 1. Excitation energy spectra in the region 5.5 MeV $\leq E_x \leq$ 6.4 MeV in ^{26}Si.

References

[1] C. Illiadis et al., Phys. Rev. C **53**, 475 (1996).
[2] D. Bardayan et al., Phys. Rev. C **65**, 032801(R) (2002).
[3] D. Bardayan et al., Phys. Rev. C **74**, 04584 (2007).
[4] Y. Parpottas et al., Phys. Rev. C **70**, 065805 (2004).
[5] J. A. Caggiano et al., Phys. Rev. C **65**, 055801 (2002).
[6] M. H. Tanaka et al., Phy. Lett. B **104**, 265 (1981).
[7] M. E. Rickey, H. E. Wegner, and K. W. Jones, Phys. Rev. Lett. **13**, 444 (1964).
[8] M. H. Tanaka and S. Kubono, Phys. Lett. B **161**, 52 (1985).
[9] R. A. I. Bell et al., Nucl. Phys. **A133**, 337 (1969).

Study of Astrophysically Important States in ^{26}Si through Elastic Scattering with CRIB

J. Chen[a], A. A. Chen[a], G. Amadio[b], S. Cherubini[h], M. La .Cognata[h], H. Fujikawa[b], S. Hayakawa[b], N. Iwasa[j], D. Kahl[a], S. Kubono[b], Y. Kurihawa[b], Y. K. Kwon[c], J Y. Moon[c], M. Niikura[b], S. Nishimura[f], A. Odahara[e], J. Pearson[a], R. Pizzone[h], A. Saito[b], C. Signorini[i], T. Teranishi[d], Y. Togano[g], Y. Wakabayashi[b], H. Yamaguchi[b],

[a] *Department of Physics and Astronomy, McMaster University, Canada*
[b] *Center for Nuclear Study, Graduate School of Science, University of Tokyo, Japan*
[c] *Department of Physics, Chung-Ang University, South Korea*
[d] *Department of Physics, Kyushu University, Japan*
[e] *Department of Physics, Nishinippon Institute of Technology, Japan*
[f] *RIKEN(The Institute of Physical and Chemical Research)*
[g] *Department of Physics, Rikkyo University, Japan*
[h] *Department of Physics, University of Catania and INFN, Italy*
[i] *Department of Physics, University of Padova and INFN, Italy*
[j] *Department of Physics, Tohoku University, Japan*

1. Introduction

The astrophysically important states in ^{26}Si have been studied with different reactions [1,2,3,4] because they contribute dominantly in the ^{25}Al(p,γ)^{26}Si reaction rate at nova temperatures, which consequently determines the 26Al production rate. But the results from these experiments are not consistent in the spin-parity assignments for the 5.912 MeV and 5.946 MeV states. To improve such uncertain situation and confirm the states found in these experiments, an elastic scattering of ^{25}Al+p was performed with CRIB at RIKEN.

The thick target method with inverse kinematics [5, 6] is used. Advantage of this method is that a wide range of energy levels can be scanned simultaneously with only one beam energy and the scattered proton can be detected only at forward angles in the laboratory. The energy of center-of-mass (or resonance energy) can be obtained or calculated from the measured proton energy as follows:

$$E_{cm} = \frac{m_p}{m_p + M} E_{M,lab} = \frac{m_p + M}{4Mcos^2\theta_{lab}} E_{p,lab}$$

where M and m_p are the mass numbers of beam nucleus and proton; $E_{M,lab}$, $E_{p,lab}$ and θ_{lab} are the beam energy, proton energy and scattering angle in the lab frame, respectively. With this method, for example, for 3.4 MeV/A ^{25}Al beam, it is possible to scan E_{cm} from 0 to about 3.3 MeV corresponding to a range of excited states from 5.515 MeV (^{25}Al+p threshold) to about 8.8 MeV.

2. Experimental Details

A test experiment was performed at CRIB [7] using 7.5 MeV/A ^{24}Mg primary beam. The reaction ^{2}H(^{24}Mg,n)^{25}Al was used to produce the secondary ^{25}Al beam with energy of about 3.4 MeV/A. Beams with purity of about 50% and intensity up to 1.2×10^{6} particles per second were obtained with a thick polyethylene (CH_2) target. The secondary beam was identified by two PPACs (parallel plate avalanche counter) which were also used for beam tracking to determine beam position on target and the scattering angle combined with the recoil position measured with PSD (position-sensitive silicon detector). The elastically scattered protons after the target were measured by 3 sets of ΔE-E telescopes at 0^o, 17^o and 27^o, respectively. Each set of telescope consists of one 75μm double-sided 16ch$\times$16ch PSD and two 1500μm single channel SSDs (silicon strip detectors). Right above the target 10 NaI detectors were used to detect γ-rays from the decay of the first excited state of the ^{25}Al produced in the inelastic scattering.

The Si detectors –PSDs and SSDs– were calibrated separately. A further calibration with proton beams of 5 MeV, 9 MeV and 14 MeV was made to correct the different pulse height defect of alpha's in the Si detector [8]. Since the energy range of proton in the PSD used in this experiment is about 2 MeV, the proton beams will punch through the PSDs, enabling the ΔE-E telescope to be calibrated as a whole.

The scattered protons were identified using ΔE versus E spectrum which is only used for separating the protons punching through the PSD, and also the PSD energy versus TOF which can identify both protons punching through the PSD and the ones stopped in the PSD. Figure 1 and 2 show the particle identification of protons.

3. Analysis and Preliminary Results

When using the thick target method, the energy loss of the scattered proton traveling through the remaining part of the target must be taken into account. The following steps were performed to correct such energy loss for proton energies measured with the Si detector event by event. The range of the ^{25}Al beam in the CH_2 is determined and then divided into 5000 equal parts. Then from the front end of the target, the residual energy of the ^{25}Al beam is calculated at each part by Ziegler's routines [9], along with the proton energy at the scattering spot. Knowing the path length which proton travels in the target, its energy after the target

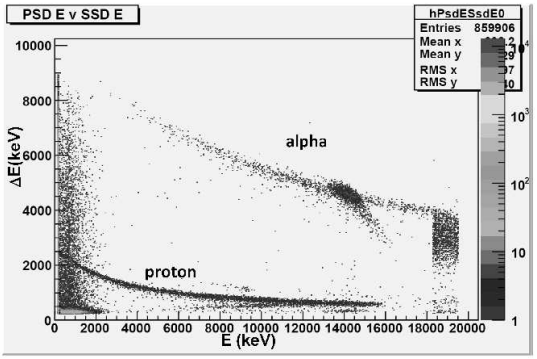

Figure 1. 2-D histogram of E versus ΔE for the silicon telescope at zero degree only for identifying scattered protons penetrating PSD.

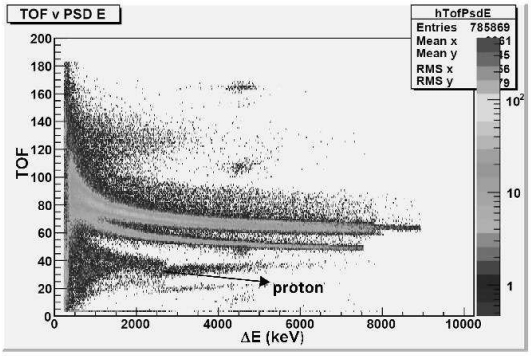

Figure 2. 2-D histogram of ΔE versus time-of-flight for identifying scattered protons both penetrating PSD and stopping in PSD.

is obtained and compared with the measured proton energy in a single event. The on-spot proton energy of this event, that is, the energy of the proton with energy loss corrected, is then directly deduced from the final match of the comparison.

The total yields of background protons of different energies from a carbon target are normalized by the inverse ratio of the energy-dependent stopping power of the proton in the CH_2 and C targets as well as the ratio of the total number of beam events for each target times the number density of carbon in the target:

$$Y = I\sigma n\Delta x = I\sigma n\Delta E/\frac{dE}{dx}(E).$$

where the *I* represents the accumulated number of events,*n* is the number density of the target material and Δx is the target thickness per energy bin ΔE in the spectrum, which is inversely proportional to the stopping power of proton at the corresponding energy. From the above formula,the excitation function can be obtained from the yield spectrum by multiplying *Y* and the energy-dependent stopping power dE/dx since $\sigma \propto Y \times \frac{dE}{dx}$.

Figure 3 shows a proton spectrum after correcting the energy loss in target.

An R-Matrix [10] fit to the excitation function will be used to extract physical parameters such as energy levels and proton widths. Assuming only one open channel(elastic scattering) and only one level per J^π, then the single-channel single-level R-Matrix formula will be used:

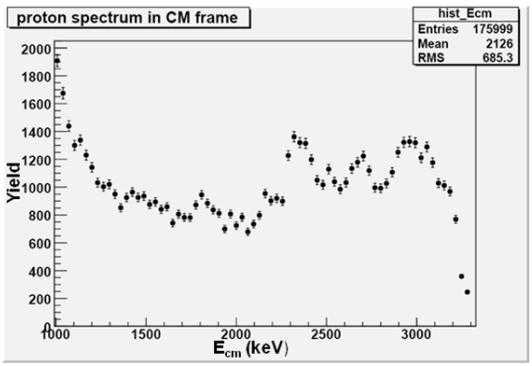

Figure 3. Measured proton spectrum in the center of mass frame with energy loss corrected and background subtracted. There are evident signatures of resonances in the spectrum. We aim to acquire more statistics to identify more states.

$$\frac{d\sigma}{d\Omega} = \frac{\pi}{k^2}[(2I_1+1)(2I_2+1)]\sum_{ss'}(CT+RT+IT).$$

where I_1, I_2 are the spins of the nuclei in the entrance channel; s, s' are the channel spins of the entrance and the exit channels; CT, RT, and IT are the Coulomb term, resonant term and interference term, respectively. All terms depend on the single-channel single-level R function:

$$R = \frac{\gamma^2}{E_\lambda - E}$$

where γ and E_λ are the reduced level width and resonance energy respectively, the two physical parameters to be extracted from the fitting.

For further consideration of the inelastic scattering to the excited state in ^{25}Al, the multi-channel R-Matrix analysis will be applied.

The analysis is in progress.

References

[1] D. W. Bardayan *et al.*, Phys. Rev. C **65** (2002) 032801.
[2] J. A. Caggiano *et al.*, Phys. Rev. C **65** (2002) 055801.
[3] Y. Parpottas *et al.*, Phys. Rev. C **70** (2004) 065805.
[4] D. W. Bardayan *et al.*, Phys. Rev. C **74** (2006) 045804.
[5] S. Kubono, Nucl. Phys. A **693** (2001) 221-248.
[6] A. H. Hernández *et al.*, NIM. B **143** (1998) 569-574
[7] S. Kubono *et al.*, Eur. Physi. J. A **13** (2002) 217-220
[8] N. J. Hansen, NIM **96** (1971) 373
[9] J.F. Ziegler, The Stopping and Ranges of Ions in Matter, vols. 3 and 5, Pergamon Press, Oxford, 1980.
[10]A. M. Lane, and R. G. Thomas, Rev. Mod. Phys. **30** (1958) 257

Development of the Secondary ^{46}Cr Beam produced by Fusion Reactions

Y. Wakabayashi[a] H. Yamaguchi[a] S. Hayakawa[a] G. Amadio[a] S. Nishimura[b], A. Kim[c], D. N. Binh[d], Y. Gono[b], and S. Kubono[a]

[a] *Center for Nuclear Study, Graduate School of Science, University of Tokyo*
[b] *RIKEN (The Institute of Physical and Chemical Research)*
[c] *Department of Physics, Ewha Woman University*
[d] *Institute of Physics and Electronic, Vietnam Academy of Science and Technology*

1. Introduction

For the rapid proton capture process (rp-process) in X-ray burst and the core-collapse stage of supernova, proton-rich pf-shell nuclei far from stability play important roles [1]. Studies of the β and electron capture decays of these proton-rich pf-shell nuclei are of great astrophysical interest. These decays involved in the charged-current processes, e.g. $p \rightarrow n + e^+ + \nu$, are predominated by the Fermi and Gamow-Teller (GT) transitions. Information on the GT transitions can be derived directly from β-decay measurements. Recently, studies were performed for several proton-rich pf-shell nuclei [2, 3, 4, 5]. However, the GT transition strengths (B(GT)'s) of these proton-rich nuclei far from stability were measured for only a few low-lying states with large uncertainties due to the small production cross sections and short half lives. To determine the B(GT) accurately, it is important to know the feeding ratio and the half-life of the β-decay accurately.

In this study, the final purpose of the experiment is to measure the properties of ^{46}Cr, namely, i) the total half-life of the β-decay with an accuracy better than 10 %, ii) the decay branching ratios to the ground state (Fermi transition) and the GT states accurately, iii) higher excited GT states if exist.

Since the cross section of ^{46}Cr production was very low, less than 100 μb, here we report on test experiments carried out using other dominant products, such as ^{46}Ti.

2. Experimental procedure

Test experiments with different primary beam conditions were performed using the CNS low-energy RI beam separator (CRIB) [6, 7]. A self-supporting ^{12}C primary target of 0.4 mg/cm^2 was set as the production target. Primary beams of ^{40}Ar^{11+} of 4.5 MeV/u and ^{40}Ca^{11+} of 5.6 MeV/u were used to bombard the ^{12}C target to produce the secondary beam. A parallel-plate avalanche counter (PPAC) was set at a dispersive focal plane (F1) for beam monitoring. Another PPAC and a Si detector of 1.5 mm thickness were installed for particle identification (PI) at an achromatic focal plane (F2). For PI, a monolithic Si detector [8] was also placed behind the PPAC at F1. This Si detector consists of 1.5-μm-thick and 500-μm-thick layers that are used as ΔE and E counters, respectively. A Ge detector was set at 260 mm from the ^{12}C primary target for measuring γ rays emitted from the fusion reaction products at F0. A 2.2-μm-thick Havar foil was installed at the entrance of the F0 chamber to enclose helium gas. The vacuum chambers of CRIB were filled with helium gas of 20 Torr at maximum.

3. Experimental results

Figure 1 shows a singles spectrum measured by the Ge detector placed at F0. In the measurement of the ^{12}C + ^{40}Ar scattering, the primary beam intensity was limited to 10 enA due to the maximum count rate of the Ge detector. The bombarding energy was 4.1 MeV/u at the target since the havar foil was placed at the entrance of F0 chamber. Gamma rays emitted from $^{45-48}$Ti, $^{47-49}$V and ^{49}Cr were identified as shown in Fig. 1. Sharp peaks, such as 1173 and 1333 keV emitted from the β-decays of ^{60}Co, were the background γ-rays.

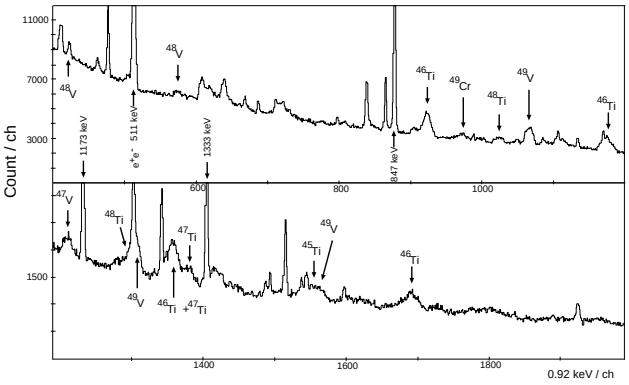

Figure 1. Singles spectrum of Ge detector placed at F0.

The optimum GARIS condition [9] was searched by changing the gas pressure for $Z \approx 20$ region with energies of around 4 MeV using a primary beam. The full width at half maximum (FWHM) of the momentum distribution became narrower from 5.4 to 3.2 % when the helium gas pressure was increased from 6 to 20 Torr. However, PPAC did not work over 20 Torr, and thus the optimum He gas pressure was not determined.

The particle identification using the ΔE-E counter telescope of the monolithic Si detector placed at F1 was performed under a helium gas pressure of 8 Torr. To confirm that the fusion reaction products reached at the ΔE-E counter, the coincidence of the ΔE counter and Ge detector was measured. In this measurement, Bρ value of D1 magnet was set to 0.5864 Tm for ^{46}Ti, which were the most dominant products in the ^{40}Ar+^{12}C scattering. The momentum slits at F1 was set to $\pm$20 mm, corresponding to the FWHM

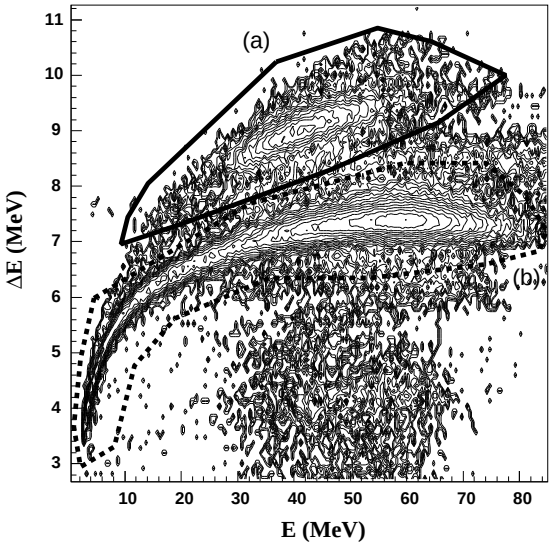

Figure 2. ΔE-E spectrum obtained by the monolithic Si detector placed at F1. The part (a) and (b) surrounded by dash and solid line indicate the components of the primary beam and the fusion reaction products, respectively.

of 2.5%.

Figure 2 shows a spectrum of the monolithic Si detector for PI. The part (a) surrounded by the dashed line indicates the component of the primary beam. The part (b) surrounded by the solid line is considered to be that of the fusion reaction products. The spectrum of the Ge detector gated on the part of the fusion reaction products is shown in Fig. 3. Several peaks emitted from fusion products, such as ^{46}Ti, ^{48}V and ^{49}V, were observed. Therefore, the part (b) in Fig. 2 certainly corresponds to the fusion products.

Further analysis for the ^{40}Ca+^{12}C scattering is now in progress.

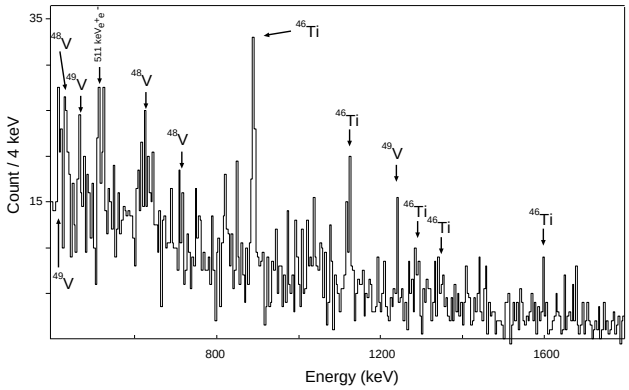

Figure 3. Gamma-ray spectrum of Ge detector obtained by gating on the part of the fusion reaction products.

References

[1] K. Langanke and G. Martinez-Pinedo, Rev. Mod. Phys. **75**, 819 (2003).

[2] T.K. Onishi et al., Phys. Rev. C **72**, 024308 (2005).

[3] V.T. Koslowsky et al., Nucl. Phys. A **624**, 293 (1997).

[4] I. Reusen et al., Phys. Rev. C **59**, 2416 (1999).

[5] A. Jokinen et al., Eur. Phys. J. A **3**, 271 (1998).

[6] S. Kubono et al., Eur. Phys. J. A **13**, 217 (2002).

[7] Y. Yanagisawa et al., Nucl. Instrum. Methods Phys. Res. A **539**, 73 (2005).

[8] A. Musumarra et al., Nucl. Instrum. Methods Phys. Res. B **409**, 414 (1998).

[9] H. Miyatake et al., Nucl. Instrum. Methods Phys. Res. B **26**, 309 (1987).

Feasibility Study of Direct Measurement of (α, p) Reaction with ^{21}Na Radioactive Beam at CRIB

L.H. Khiem[a], D.N. Binh[a], S. Kubono[b], H. Yamaguchi[b], Y. Wakabayashi[b], S. Hayakawa[b] and A. Kim[c]

[a] *Institute of Physics and Electronics, Vietnamese Academy for Science and Technology*
[b] *Center for Nuclear Study, Graduate School of Science, University of Tokyo*
[c] *Department of Physics, Ewha Womans University, seoul, Korea*

1. Introduction

Nucleosynthesis in the NeNa cycle during nova outbursts leads to the synthesis of the astronomically important ^{22}Na nucleus. Its beta decay leads to the emission of a 1.275 MeV gamma-ray, following population of the first excited state of ^{22}Ne. This gamma-ray is an ideal observable for nova events. Thus far, observational searches performed with NASA's COMPTEL on-board CGRO satellite of five ONe novae have not found this gamma-ray signature [1]. Whereas the inferred upper limits are in agreement with recent results from ONe nova models [2], the reduction of the nuclear uncertainties associated with the main reactions involved in the synthesis of ^{22}Na is critically important in order to predict how much ^{22}Na can be produced in a typical nova event, and at what distance a nova explosion is expected to provide a detectable flux of γ-rays.

Synthesis of ^{22}Na in novae takes place following two possible reaction paths : in the first path (called "cold" NeNa cycle), ^{21}Na forms from the seed ^{20}Ne which then leads to ^{21}Na(β^+)^{21}Ne(p,γ)^{22}Na. In the second path, associated with higher temperatures (called "hot" NeNa cycle), proton capture on ^{21}Na dominates over its β-decay, followed by ^{21}Na(p,γ)^{22}Mg(β^+)^{22}Na. There is little net mass flow from ^{22}Mg to ^{23}Al due to the low Q value for photo disintegration of ^{23}Al. However, the observed ^{22}Na abundance was much smaller than the predicted value by current models of ONe novae. People believe that the unknown rate of ^{21}Na(p,γ) is the main source of uncertainty associated with calculating the amount of ^{22}Na in nova outbursts [3] but even when using the more correct value recently obtained by TRIUMF-ISAC groupe [4], the problem still unsolved. There is another possibility, by which the abundance of ^{22}Na will be reduced. The predicted ^{22}Na abundance might be reduced by the ^{21}Na(α,p)^{24}Mg reaction bypassing the production of ^{22}Na. Therefore, the purpose of our study is to perform a direct measurement of the rates of ^{21}Na(α,p)^{24}Mg for the first time.

The other motivation is to significantly advance knowledge of the nuclear level structure of ^{25}Al. Indeed there is limited information concerning even the position of states in the compound system ^{25}Al at and above the α particle threshold energy of 9.1569 MeV. So far, only two levels above this threshold have been reported. They are at 9.275 and 9.415 MeV respectively [5]. Also from strictly nuclear physics view point, the study of the structure of exotic nuclei has gained significant importance since the advent of radioactive beam facilities. These open up an invaluable means to experimentally access nuclei for which very little is known at present.

Recently, we have performed a test experiment for studying the resonance scattering of ^{21}Na beam on ^{4}He gas target. The experiment was performed using the CRIB facility at RIKEN, Japan. The purpose of this test experiment is to study the feasibility of direct measurement of (α,p) reaction with ^{21}Na radioactive beam using CRIB. In this report, the result of the test experiment will be presented.

2. Experimental procedure and results

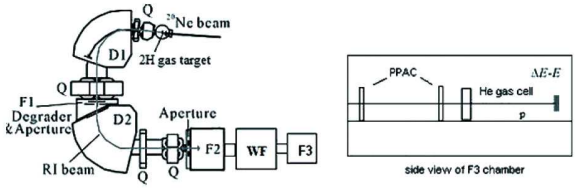

Figure 1. CRIB and experimental setup in F3 chamber.

The experiment was performed using CNS Radioactive Ion Beam Separator (CRIB) facility at RIKEN [6]. The experimental setup is shown schematically in Fig.1. The ^{21}Na secondary beam was produced via ^{2}H(^{20}Ne^{6+},^{21}Na)n reaction. The ^{20}Ne^{6+} primary beam was accelerated by the AVF cyclotron in RIKEN.The ^{2}H gas was contained within the gas-cell at F0. The length of ^{2}H target gas-cell is 80 cm and the pressure of gas was 360 torr. It was cooled down to temperature of 77 K by liquid nitrogen. The energy of the primary beam was checked by measuring its value at F1 without production target. This value was 1.177 Tm, which corresponds to 5.99 MeV/u. The momentum of the ^{21}Na secondary beam was analyzed in the dipole magnet D1 and the beam reaches at the momentum dispersive focal plane F1. At F1, the momentum of the particle was selected by a slit and then the beam was focused achromatically at the second focal plane F2. The particles can be clearly identified at F2 by the ΔE-TOF method, where TOF indicates the time-of-flight between RF signal from cyclotron and a Parallel-Plate Avalanche Counters (PPAC) at F2, and ΔE indicates the energy measured by a Si detector downstream of this PPAC. In fig.2, the particle identification spectrum

was presented. There are some other radioactive isotopes together with our desired ^{21}Na beam.The purity of $^{21}Na^{11+}$ is 8.54%. With a primary beam of 5 enA (5.2 x 10^9 pps) and the width of F1 slit was 10mm centered at -30mm (optimal condition), a $^{21}Na^{11+}$ secondary beam intensity of 1.0x10^4 pps was measured. Therefore, a 1.2 x 10^7 pps $^{21}Na^{11+}$ secondary will be achievable if 1 pμA $^{20}Ne^{6+}$ primary beam was used. In order to further separate the $^{21}Na^{11+}$ particles from other contaminant particles, the Wien Filter was used and its high-voltage of 100 KV was set. The particle identification spectrum after the Wien Filter was shown in Fig.3 and the purity of $^{21}Na^{11+}$ after the filter is about 94 %. We have estimated the transmission between F2 and F3 and its value is about 36 %.

The He gas target and detectors for tracking the ^{21}Na

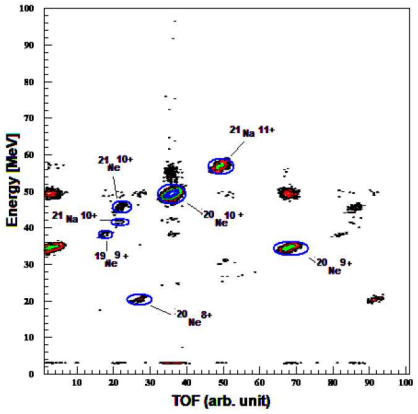

Figure 2. Particle identification at F2

beam and for proton measurement in this experiment were installed in the scattering chamber at the downstream of the Wien filter. Two PPACs measured the timing and position of the incoming ^{21}Na beam. The timing information was used for making event triggers, and also for the particle identification with the time-of-flight (TOF) method. The position of the beam and the incident angle at the target were determined by extrapolating the positions measured by the PPACs. The He target was a new gas cell of a semi-cylindrical design, with a length of about 3 cm (given by the radius of the semi-cylinder). The entrance window was made of a havar foil of 2.5 μm thickness. The exit havar window was 10 μm thick. The cell was filled with 380 torr of He gas. The He gas-cell was thick enough to stop all of the ^{21}Na beam. A multi-layered silicon detector set, referred to as ΔE-E telescope, was used for measuring the energy and angular distribution of the recoil protons. ΔE-E telescope consisted of a ΔE counter of 70 μm thickness following by an E counter of 1.5 mm thickness, all of which had an area of 50 mm x 50 mm. It was placed 23 cm distant from the target at 0^o. The maximum energy of the recoil protons was about 14.6 MeV, and the silicon detectors were sufficiently thick to stop all the recoil protons in them. Using this ΔE-E telescope, we can identify the recoil protons from other particles. The further data analysis is now in progress.

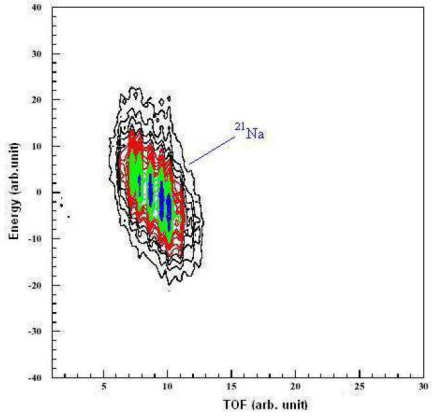

Figure 3. Particle identification after Wien Filter

3. Summary

In the test experiment, we have produced the secondary $^{21}Na^{11+}$ beam using the ^{2}H(^{20}Ne,^{21}Na)n reaction. About 1.2x10^7 pps of $^{21}Na^{11+}$ secondary beam will be achievable if 1 pμA $^{20}Ne^{6+}$ primary beam is used. The purity of $^{21}Na^{11+}$ at F1 is 8.54 %. By using the Wien filter, the purity of $^{21}Na^{11+}$ before the He gas target cell is about 94 %. The transmission between F2 and F3 is about 36 %. The energy spectrum of recoil protons have been observed by the Si ΔE-E telescope. It confirms the feasibility of our proposal for direct measurement of (α,p) reaction with ^{21}Na radioactive beam using CRIB.

References

[1] A.F.Iyudin et al., Astron. Astrophys. **300** (1995) 422.
[2] J.Jose and M. Hernanz, Astrophys.J. **494** (1998) 680.
[3] N.A.Smirnova *et al.*, Phys. Rev. C **62** (2000) 045803.
[4] S.Bishop *et al.*,Phys. Rev. Lett. **90** (2003) 162501-1.
[5] P.M.Endt, Nucl. Phys. A **521** (1990) 153.
[6] S.Kubono *et al.*, Eur. Phys. J, A **13** (2002) 217.

Feasibility Study of the ^{11}C$(\alpha, p)^{14}$N Reaction at CRIB

S. Hayakawa, S. Kubono, H. Yamaguchi, Y. Wakabayashi, S. Michimasa, A. Kim[a], K.I. Hahn[a], T.E. Choi[a] J.L. Kim[a], J.S. Yoo[a], T. Teranishi[e] H.S. Jung[c], Y.K. Kwon[c], K.W. Lee[c] and A. Chen[d]

Center for Nuclear Study, Graduate School of Science, the University of Tokyo
[a]*Department of Physics, Ewha Womans University*
[b]*Department of Physics, Kyushu University*
[c]*Department of Physics, Chung-Ang University*
[d]*Department of Physics, McMaster University*

1. Introduction

The first generation of stars formed after the Big Bang is belived to have included a large number of very massive stars of greater than 100 solar masses [1]. Though long after they died, it is important to understand these initial stars for their effect on the early universe through massive supernovae and nucleosynthesis. An interesting example is the lowest-metallicity stars which still exist and are observable. They are regarded as the second generation of stars formed from the remnants of supernovae of the first generation of stars [2].

A unique feature of the first generation of stars was a complete lack of initial seed nuclei for the CNO cycle, as no elements heavier than boron were produced in the Big Bang. Massive and rapid energy generation is needed to stabilize a very large star against collapse and to trigger an explosion. The CNO cycle can generate energy at much higher rates in massive stars as compared to the p-p chains, which are limited by the slow rate of the weak-force-reaction $p + p \rightarrow d + e^+ + \nu_e$. The CNO cycle is also important as a trigger to induce a supernova explosion at the last stage of a steller evolution. Wischer *et al.* [1] investigated the posibility of the "hot proton-proton chains", which expand up to A=11 mass region close to the proton drip line at higher temperatures and densities, cicumventing the slow triple-α process in producing CNO material by a sequence of proton- and α- capture reactions. Therfore, nuclei near the proton drip line in the hot p-p chains, such as ^{9}C and ^{11}C, can produce CNO isotopes via subsequent reactions, ^{9}C$(\alpha, p)^{14}$N, ^{11}C$(p, \gamma)^{12}$N and ^{11}C$(\alpha, p)^{14}$N.

To investigate above reactions, precise informations of the cross sections over energy ranges relevant to such steller temperatures are desirable. The ^{11}C$(\alpha, p)^{14}$N reaction is interesting beacuse of following reasons.

Alpha capture on ^{11}C populates the compound nucleus ^{15}O at high excitation energies from the alpha threshold of 10.22 MeV up to 13 MeV, corresponding to the steller temperature of 0-3 GK. In this energy range the level structure of ^{15}O as well as of its mirror nucleus ^{15}N is well studied [3]. More than 20 levels, mostly broad, have been observed within 2 MeV above the alpha threshold. The reaction rate can be calculated based on the experimental investigation of the inverse reaction ^{14}N$(p, \alpha)^{11}$C by Ingalls *et al.* [4]. However, possible reaction contributions to the first excited state of ^{14}N, ^{11}C$(\alpha, p_1)^{14}$N*, are not included in the total reaction rate. The first excited state is located at $E_x = 2.313$ MeV with $J^\pi = 0^+$. Wiescher *et al.* [1] investigated the ^{11}C$(\alpha, p)^{14}$N reaction rate by calculating the Hauser-Feshbach cross section with the code SMOKER [5], including contributions of the ^{11}C$(\alpha, p_1)^{14}$N*, but there is no experiment reported. Therefore, we are planning to measure the excitation function of the ^{11}C$(\alpha, p)^{14}$N reaction which have not directly been measured yet.

2. The ^{11}C$(\alpha, p)^{14}$N Reaction

When we produced a low-energy ^{14}O beam using the CNS low-energy radioactive ion beam separator (CRIB) [6] for an experiment, a low-energy ^{11}C beam was also obtained. We had about 7.2% ^{11}C of the secondary beam for some runs in this experiment, and thus we decided to analyze the ^{11}C$(\alpha, p)^{14}$N reaction data to study the experimental feasibility of this reaction.

A primary beam of ^{14}N was accelerated up to an energy of 8.23 MeV/u at the RIKEN AVF cyclotron with $K = 70$. The maximum intensity of the beam was 620 pnA. The primary beam bombarded a H_2 gas target with a thickness of 1.9 mg/cm^2. The target gas was cooled down to 80-90 K using a liquid-nitrogen cooling gas target system which was recently installed for an intense beam production [7], and confined in a cell with entrance and exit window foils. The gas pressure was set to 600 Torr and Havar foils of 2.5-μm thick were used for the windows. A 12.5-μm-thick Havar foil was installed behind the production target cell as an energy degrader. The secondary particles were momentum-analyzed at the momentum dispersive focal plane (F1), subsequently focused achromatically on the second focal plane (F2). After that they passed through a Wien filter to reduce remaining contamination with the high voltages of +50 kV and -53 kV, then focused in the experimental chamber (F3). The purities of ^{14}O and ^{11}C were respectively 8.9% and 1.9% at F2, 89% and 7.2% at F3 after the Wien filter.

Though this setup was optimized for the ^{14}O beam, ^{11}C was also observed in RF-TOF spectrum (Fig.1) at F3. RF here stands for the Time-of-Flight from the production target to the first PPAC at F3, while TOF means the Time-of-Flight between the two PPACs in F3 chamber. The ^{11}C was produced from the ^{14}N$(p, \alpha)^{11}$C reaction, which has the cross section reaching a local maximum of about 200 mb at $E_{^{14}\mathrm{N}} = 7.4$ MeV/u [8]. The observed ^{11}C beam had the count rate of about 5×10^3 pps, the purity of 7.2% on the entrance window of the secondary target and the peak energy of 11.5 MeV.

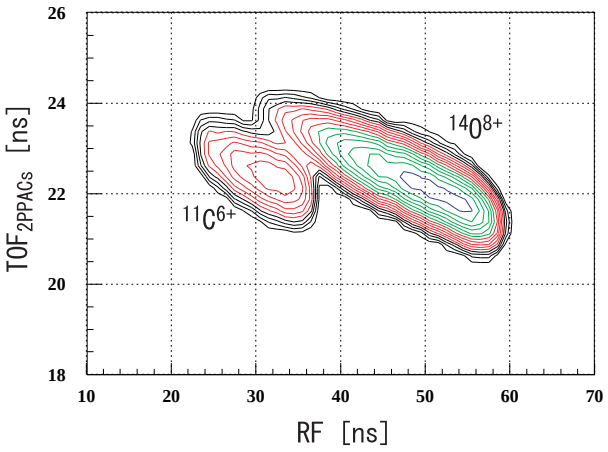

Figure 1. Particle identification in RF vs. TOF spectrum.

We adopted the thick-target method to determine the excitation function. A wide energy range which corresponds to the steller temperature of 0-6 GK could be scanned in the helium gas target. The setup inside the scattering chamber (F3) is described below. The secondary beam was monitored with two parallel-plate avalanche counters (PPACs) [9]. The secondary target is a semi-cylindrical gas cell with a thickness of 36 mm. The entrance window is a 2.5-μm-thick Havar foil and has a diameter of 20 mm. The exit window is a 10-μm-thick Mylar foil covering a wide range of angles. Helium gas was confined in the gas cell with a thickness of 0.5 mg/cm^2. Identification of the protons was performed by 5 sets of ΔE-E telescopes using silicon detectors mostly covering the angular range from -85° to +85°.

In principle, the origins of the protons can be identified in the spectrum of the total energy deposit in the ΔE-E detectors versus the TOF between the PPAC and the E detector. In the 0° telescope, two groups of protons of defferent origins were observed. One of them is considered to be the background protons from either F0 or F1 through an unusual way. The origin of the other one must be either the (α, p) reaction or the elastic scattering in a set of Mylar foil in the PPACs at F3, but further analysis is needed to identify it. A similar assemblage of protons can be seen in the telescope around 45°, except most of the background protons either from PPACs or F0 target beacuse only protons from the secondary target could geometrically reach the telescope at 45°. The two small fractions around 6.5 and 7.6 MeV seem to correspond to the known resonances seen in the ^{14}N$(p, \alpha)^{11}$C reaction [4] with reasonable yields.

3. Summary and Plan of Experiment

A detailed analysis of the present data provids useful information for a further experiment of the ^{11}C$(\alpha, p)^{14}$N reaction. The origins of background protons surely need to be identified to reduce them. The ^{11}B$(p, n)^{11}$C reaction may be easier to produce a ^{11}C beam since the yield is expected as large as that of the ^{14}N$(p, \alpha)^{11}$C reaction and less contamination is expected. In addition, the primary beam has less energy straggling in the production target, i.e., a large acceptance of the beam is available. The secondary beam should be defined more sharply in energy. A scanning region of the excitaion energy in the compound nucleus ^{15}O should be devided into several narrower regions to observe ^{11}C$(\alpha, p_1)^{14}$N* uniquely.

References

[1] M. Wiescher *et al.*, Astrophys. J.**343** (1989) 352. Phys. Rev. Lett. **57** (1986) 1801.
[2] N. Iwamoto *et al.*, Nature **309** (2005) 451.
[3] F. Ajzenberg-Selove, Nucl. Phys. A**523** (1991) 1.
[4] P.D. Ingalls, J.S. Schweitzer and B.D. Anderson Phys. Rev. C **13** (1976) 524.
[5] F.K. Thielemann, M. Arnould, J.W. Truran 1987, in *Advances in Nuclear Astrophysics*, ed. E. Vamgioni-Flam *et al.*, p.525.
[6] S. Kubono *et al.*, Eur. Phys. J. A**13** (2002) 217.
[7] H. Yamaguchi *et al.*, CNS Annual Report 2006 p.?(2007).
[8] S. Takacs *et al.*, Nucl. Instru. Meth. B**211** (2003) 169.
[9] H. Kumagai *et al.*, Nucl. Instru. Meth. A**470** (2001) 562.

In-Beam γ-Ray Measurement in ^{20}Ne + ^{96}Zr Reaction

E. Ideguchi, S. Ota, T. Koike[a], K. Shirotori[a], M. Liu, Y. Zheng

Center for Nuclear Study, Graduate School of Science, University of Tokyo
[a]Department of Physics, Tohoku University

Since the discovery of the superdeformed (SD) rotational band in ^{152}Dy [1], studies of SD states have been extensively performed both experimentally and theoretically. So far SD bands have been observed in A$\sim$40, 60, 80, 130, 150, and 190 regions [2] with an aid of large Ge detector arrays such as Euroball [3] and Gammasphere [4]. Recent calculations using a cranked Strutinsky method and a four-dimensional shape space representing quadrupole, octupole, hexadecapole, and necking degrees of freedom predict that a new region of SD states in A$\sim$100 nuclei with 45<Z<49 and 57<N<65 [5]. Experimentally, a presence of SD band is reported in ^{108}Cd [6] and it is suggested to have the most deformed structure identified in any nucleus. Since the appearance of such extremely deformed nucleus is not fully understood, systematic investigations of SD nuclei in this region both experimentally and theoretically will be helpful to elucidate it.

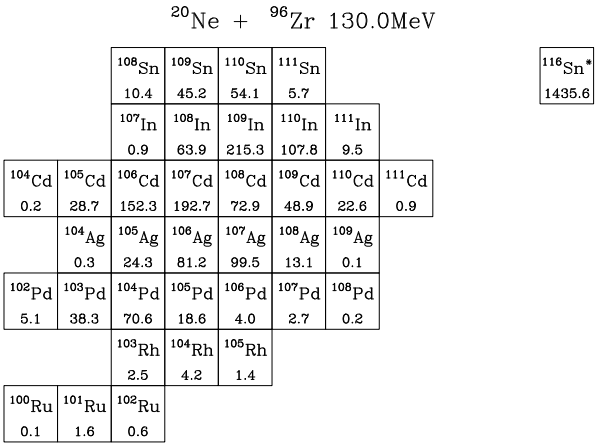

Figure 1. Cross sections for evaporation residues in the ^{20}Ne+^{96}Zr reaction at 130 MeV calculated by CASCADE code [7]. The number in each box is the cross section in milli-barn. In the box of compound nucleus, ^{116}Sn, total fusion cross-section is shown.

In order to find new SD nuclei in A$\sim$100 region with 45<Z<49 and 57<N<65 systematically, we plan to perform in-beam γ-ray measurements using a ^{20}Ne + ^{96}Zr reaction to investigate high-spin states of ^{109}In and ^{107}Cd next to the ^{108}Cd. Figure 1 shows calculated cross-sections of evaporation residues in the ^{20}Ne + ^{96}Zr reaction at a ^{20}Ne beam energy of 130 MeV by using a CASCADE code [7]. As shown in the figure, many evaporation channels will open in this reaction and therefore it is necessary to select the channel using a charged particle filter to identify ^{109}In and ^{107}Cd. To realize such measurement, we plan to use a detector system composed of Hyperball-2 Ge detector array and a Si-Ball charged particle filter [8]. In this report, results of a test experiment to check the performance of the detector system and γ-ray background are presented.

The experiment was performed at the Cyclotron and Radioisotope Center, Tohoku University. The ^{20}Ne ions, accelerated by the 930 cyclotron to an energy of 130 MeV, were used to bombard a target of 1 mg/cm^2 ^{96}Zr self-supporting foil. High-spin states in ^{109}In and ^{107}Cd were populated by ^{96}Zr(^{20}Ne,1p6n)^{109}In and ^{96}Zr(^{20}Ne,1α5n)^{107}Cd reaction, respectively. Prompt γ rays were detected by three Ge detectors mounted on the Hyperball-2 detector array frame. One Ge detector was placed at the angle of 60° and the other two Ge's were at 137° relative to the beam direction. Each Ge detector was shielded with BGO counters for Compton background suppression. Evaporated charged particles in the reaction were detected by the Si-Ball charged particle filter which consists of 20 Si detector elements. In this measurement, five detectors placed at most forwrd angle were removed in order to avoid the beam stopping on the Au absorber foil put in front of Si detector, and accordingly 15 Si detectors were used. Inlet and outlet hole size of the Si-Ball chamber was set to 10 mm diameter so that the beam goes through the target without hitting the beam tube.

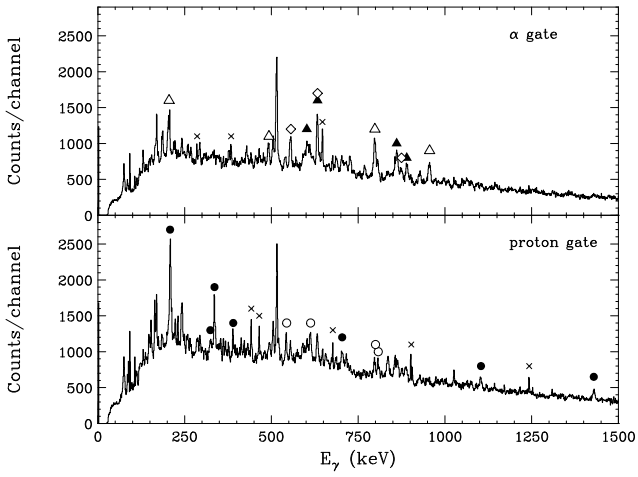

Figure 2. Projection spectra of $\gamma\gamma$ coincidence data gated by 1 α (upper panel) and 1 proton (lower panel), respectively. In the upper panel, γ peaks of ^{106}Cd, ^{107}Cd, and ^{108}Cd are marked by open triangles, filled triangles, and open diamonds, respectively. In the lower panel, γ peaks of ^{109}In and ^{110}In are marked by filled circles and open circles, respectively.

Figure 2 shows γ-ray projection spectra of $\gamma\gamma$ coincidence data after Doppler correction gated by 1 α (upper panel) and 1 proton (lower panel) detection. In the α gated spectrum γ-ray peaks of ^{106}Cd, ^{107}Cd, and ^{108}Cd appeared

clearly as indicated by filled triangles, open triangles, and open diamonds, respectively, in the figure. In the proton gated spectrum γ-ray peaks of ^{109}In and ^{110}In are presented (filled circles and open circles, respectively). Sharp peaks in the figures (shown by cross) are due to stopped γ peaks created by ^{20}Ne beam with Al target frame. Gamma peaks of ^{42}Ca (1α1p channel), ^{39}K (2α channel), and ^{38}Ar (2α1p) were strongly observed in the spectrum before Doppler correction. Main background in the data are these stopped γ peaks and a 511 keV peak by e^+e^- decay after β^+ decay. These stopped peaks will be reduced by careful beam tuning and making smaller beam spot size on target. Other accidental background due to room background will be reduced by taking trigger conditions as triple γ coincidence and placing Pb sheild around the beam dump.

Longer beam time is planned to perform in-beam γ ray spectroscopy to investigate high-spin states in ^{107}Cd and ^{109}In.

References

[1] P.J. Twin *et al.*, Phys. Rev. Lett. **57** (1986) 811.
[2] B. Sing, R. Zysina, R.B. Firestone, Nucl. Data Sheet **97** (2002) 241.
[3] J. Simpson, Z. Phys. A **358** (1997) 139.
[4] I.Y. Lee, Nucl. Phys. **A520** (1990) 641c.
[5] R.R. Chasman, Phys. Rev. C**64** (2001) 024311.
[6] R.M. Clark *et al.*, Phys. Rev. Lett. **87** (2001) 202502.
[7] F. Fühlhofer, Nucl. Phys. A**280** (1977) 267.
[8] T. Kuroyanagi *et al.*, Nucl. Instrum. and Methods, A **316** (1992) 289.

Proton Inelastic Scattering Study on Very Neutron-rich Nuclei with $A/Z = 3$

S. Michimasa, Y. Yanagisawa[a], K. Inafuku,[b], N. Aoi[a], Z. Elekes[c], Zs. Fülöp[c], Y. Ichikawa[d], N. Iwasa[b], K. Kurita[e], M. Kurokawa[a], T. Machida[e], T. Motobayashi[a], T. Nakamura[f], T. Nakabayashi,[f] M. Notani[g], H. J. Ong[a], T. K. Onishi[d], H. Otsu[a], H. Sakurai[a], M. Shinohara[f], T. Sumikama[h], S. Takeuchi[a], K. Tanaka[a], Y. Togano[e], K. Yamada[a], M. Yamaguchi[i], and K. Yoneda[a]

Center for Nuclear Study, Graduate School of Science, University of Tokyo
[a]*RIKEN (The Institute of Physical and Chemical Research)*
[b]*Department of Physics, Tohoku University*
[c]*ATOMKI, Hungary*
[d]*Department of Physics, University of Tokyo*
[e]*Department of Physics, Rikkyo University*
[f]*Department of Physics, Tokyo Institute of Technology*
[g]*Argonne National Laboratory, USA*
[h]*Department of Physics, Faculty of Science and Technology, Tokyo University of Science*
[i]*National Institute of Advanced Industrial Science and Technology*

1. Introduction

We report here on the in-beam γ-ray spectroscopy of the very neutron-rich nucleus locating at around $A/Z = 3$ using proton inelastic scattering. The present experiment has been designed for sd–pf shell nuclei, such as ^{42}Si, ^{36}Mg, ^{30}Ne and ^{27}F. The ^{42}Si nucleus is located at proton subshell closure and neutron shell closure, and hence possibility has been raised of disappearance of the conventional neutron magic number of $N = 28$ [1,2,3]. So far no excitation level in ^{42}Si was reported. The present experiment was aimed at measuring the excitation energy of the first 2^+ state and the deformation length in ^{42}Si. The ^{36}Mg nucleus is located in the middle of the shell closures of $N = 20$ and 28, and is closer to the neutron drip line than nuclei belonging to the so-called 'island of inversion'. In previous experimental studies on neutron-rich magnesium isotopes, ^{32}Mg was reported to be a well-deformed nucleus [4] and the disappearance of the magicity at $N = 20$ was indicated. For ^{34}Mg, the deformation was reported to be larger than that of ^{32}Mg [5]. The present study is the first experiment to investigate the low-lying excited states in ^{36}Mg. The ^{30}Ne and ^{27}F nuclei were investigated by proton inelastic scattering measurements, and de-excitation γ-rays were reported at $791(26)$ keV in ^{30}Ne [6] and at $504(15)$ keV and $777(19)$ keV in ^{27}F [7]. The present experiment will provide identification of γ cascades and discussions on deformation for these nuclei.

2. Experiment

The experiment was performed at the unstable nuclear beam line RIPS at RIKEN. Figure 1 shows a schematic view of the present setup. Ions of ^{48}Ca were accelerated up to 63 MeV/nucleon using the acceleration scheme of RFQ-RILAC-CSM-RRC. The average intensity of the primary beam was $\sim$80 particle nA. The primary target was a ^{181}Ta plate with a thickness of 150 μm or an enriched ^{64}Ni plate with a thickness of 200 μm. The fragmentation reaction of ^{48}Ca with ^{64}Ni has been reported to produce effectively nuclei with $Z > 10$ and $A/Z \sim 3$ [8]. A radioactive beam near $A/Z = 3$ was isotopically separated by RIPS [9]. The momentum acceptance was set to be 6%. For good separation an energy degrader was placed at first momentum-dispersive focal plane (F1). Particle identification of the secondary beam was performed by a standard method based on the energy deposit (ΔE), time of flight (TOF), and magnetic rigidity ($B\rho$). The magnetic rigidity of the fragments was deduced from the position on the F1 measured using a parallel-plate avalanche counter (PPAC). ΔE was obtained from the silicon detector arranged at the first achromatic focus (F2), and the TOF was measured between plastic scintillators placed at F2 and the second achromatic focus (F3). The secondary beam bombarded a liquid hydrogen target [10] of 105 mg/cm^2 with havar foil windows, which was placed at F3. To obtain a sufficient mass resolution for the reaction products, the TOF spectrometer [11] was placed downstream of the secondary target. The scattered particles were detected using a telescope arranged at the end of the beam line, which consisted of a 100-μm silicon detector and two NaI(Tl) scintillators. The identification of the scattered particles was performed by the TOF-ΔE-E method. The scattering angle of the particle was measured using the three PPACs placed before and after the secondary target. De-excitation γ rays from the inelastically scattered particle were detected using 160 NaI(Tl) scintillators (DALI2) [12] surrounding the secondary target.

3. Present Status of Analysis

Figure 2 shows the identification of the particles involved in the secondary beam. The fragments located at $A/Z = 3$ were clearly identified, and their intensities were approximately 0.05–1 counts per second. Further analysis is now in progress for outgoing particles and de-excitation γ rays. The excitation energies of the first 2^+ states and the deformation lengths of $A/Z = 3$ nuclei obtained from the

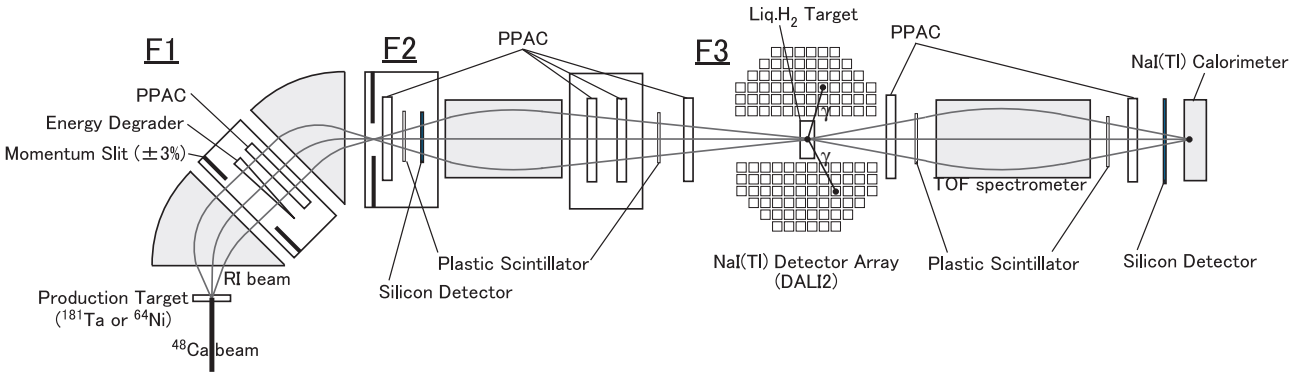

Figure 1. Schematic view of the present experimental setup.

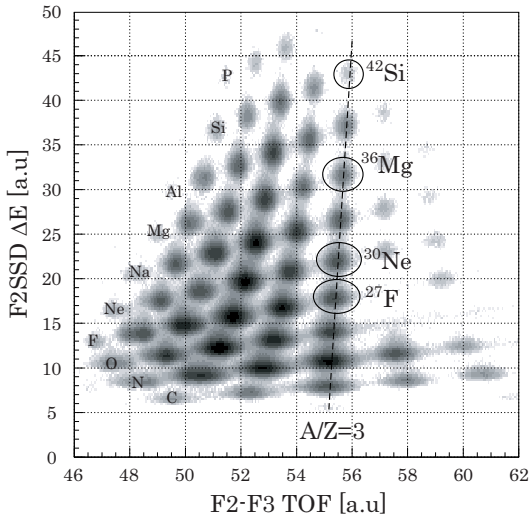

Figure 2. Identification of the particles involved in the secondary beam. The horizontal and vertical axes correspond to the TOF between F2 and F3, and to the energy deposited in the F2 Si detector, respectively.

present experiment will provide basic information on nuclear structure in very neutron-rich sd–pf nuclei.

References

[1] S. Grévy et al., Phys. Lett. B **594**, 252 (2004).
[2] J. Fridmann et al., Nature(London) **435**, 922 (2005).
[3] J. Fridmann et al., Phys. Rev. C **74**, 034313 (2006).
[4] T. Motobayashi et al., Phys. Lett. B **346**, 9 (1995).
[5] H. Iwasaki et al., Phys. Lett. B **522**, 227 (2001).
[6] Y. Yanagisawa et al., Phys. Lett. B **566**, 84 (2003).
[7] Z. Elekes et al., Phys. Lett. B **599**, 17 (2004).
[8] M.Lewitowicz et al., Z. Phys. A **335**, 117 (1990).
[9] T. Kubo et al., Nucl. Instrum. Methods Phys. Res. B **70**, 309 (1992).
[10] H. Ryuto et al., Nucl. Instrum. Methods Phys. Res. A **555**, 1 (2005).
[11] N. Aoi et al., RIKEN Accel. Prog. Rep. **38**, 176 (2005).
[12] S. Takeuchi et al., RIKEN Accel. Prog. Rep. **36**, 148 (2003).

Proton Intruder State in ^{13}B

S. Ota, S. Shimoura, H. Iwasaki[a], M. Kurokawa[b], S. Michimasa, N. Aoi[b], H. Baba[b], K. Demichi[c], Z. Elekes[d], T. Fukuchi[e], T. Gomi[b], S. Kanno[b], S. Kubono, K. Kurita[c], K. Hasegawa[c], E. Ideguchi, N. Iwasa[f], Y.U. Matsuyama[c], K. Miller[g], T. Minemura[b], T. Motobayashi[b], T. Murakami[h], M. Notani[i], A. Odahara[c], A. Saito[a], H. Sakurai[b], E. Takeshita[b], S. Takeuchi[b], M. Tamaki, T. Teranishi[j], Y. Yanagisawa[b], K. Yamada[b], M. Ishihara[b],

Center for Nuclear Study, University of Tokyo
[a]*Department of Physics, University of Tokyo*
[b]*RIKEN Nishina Center for Accelerator-based Science*
[c]*Department of Physics, Rikkyo University*
[d]*Hungarian Acad Sci, Inst. Nucl. Res.*
[e]*Department of Physics, Osaka University*
[f]*Department of Physics, Tohoku University*
[g]*NSCL, Michigan State University*
[h]*Department of Physics, Kyoto University*
[i]*Argonne National Laboratory, Argonne*
[j]*Department of Physics, Kyushu University*

1. Introduction

The existence of intruder states in the light neutron-rich unstable nuclei is one of the evidences for the melting of shell closure and for the change of the shell structure. In ^{11}Be nuclei, the parity of the ground state is positive originated from $\nu(s1/2)$ orbit lowering below $p1/2$-orbit by 0.3 MeV [1]. In ^{12}Be, there is 1^- state at 2.7 MeV excitation energy [2]. These small excitation energies indicate the narrow gap between p- and sd-orbit of the neutron shell in ^{11,12}Be. These intruder states in the ^{11,12}Be are well reproduced by a shell model calculation with the effective interaction involving the monopole effect [3] of the tensor force. The small gap between p- and sd-shell can be found also in the deformed mean field formed in the deformed nuclei like Nilsson diagram where the gap between p- and sd-shell seems to become smaller with large deformation parameter, like $\beta_2 \sim 0.6 - 0.7$ in ^{12}Be [4]. The change of the shell structure may happen not only in the neutron shell but also in the proton shell, since the tensor force between the proton and the neutron is expected to change both the neutron orbit and proton orbit [5]. In the present study, we focus on the proton shell structure in ^{13}B by investigating the proton single particle state.

The ^{13}B nucleus has one more proton than the ^{12}Be and also $N = 8$ neutron-rich unstable nuclei. Its ground state is believed to be spherical based on the measured nuclear moments [6, 7], which is represented by an $sd-$shell model calculation [8]. However, the properties of the excited states are not clear yet since their spins and parities are not assigned yet. One can expect excited states with proton single particle nature affected by the monopole effect of the tensor force or affected by the deformed mean field originated by the deformed ^{12}Be core. In this paper, we report the change of the proton shell structure studied via the measurement of ^{4}He(^{12}Be,^{13}Bγ)X reaction.

2. Experiment

The experiment was performed at RIPS course in RIBF, RIKEN. A beam of ^{12}Be of 50 *A*MeV, as a fragment of ^{18}O, was separated by RIPS and bombarded a liquid helium target of 143 ± 5mg/cm^2 thickness. The incident particle and the outgoing particle were identified on an event-by-event basis by means of TOF-ΔE and TOF-ΔE-E method, respectively. The momentum vector of the incident particle is monitored by two plastic scintillators and PPACs. That of outgoing particle are monitored by plastic scintillator hodoscope at the end of beam line. De-excitation gamma rays are detected by an array of 6 germanium detectors: Gamma-Ray detector Array with Position and Energy sensitivities (GRAPE) [9]. The typical efficiency and intrinsic resolution are 2.7 keV (σ) and 0.6%, respectively, for 661 keV gamma rays. The energy resolution of 1.3 % (FWHM) is achieved for the Doppler-corrected gamma ray of 2.1 MeV ($\beta \sim 0.3$) by adopting the method of the pulse shape analysis [9, 10]. The detail of the experimental setup can be seen in Ref. [11]

3. Result and Discussion

Figure 1 shows the energy spectrum of the de-excitation γ rays measured in coincidence with ^{13}B after correcting the Doppler shift. The intensities of the transition gamma rays was extracted by the decomposition of the energy spectrum by fitting the experimental spectrum with the response functions simulated by GEANT4 and the accidentally coincident background obtained from experimental data. In the fitting, no cascade decay is assumed. In order to deduce the angular distribution of the differential cross section, the energy spectra in coincidence with ^{13}B scattering to every 0.5-degree angular region up to 6 deg in the laboratory frame are fitted in the same way described above. The resultant angular distribution corresponding to 4.83-MeV excitation is shown in Fig. 2. The transferred angular

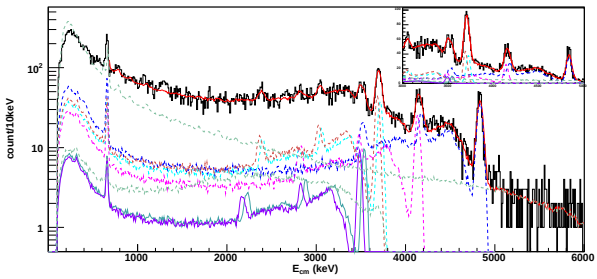

Figure 1. Doppler-corrected γ-ray spectrum in coincidence with ^{13}B.

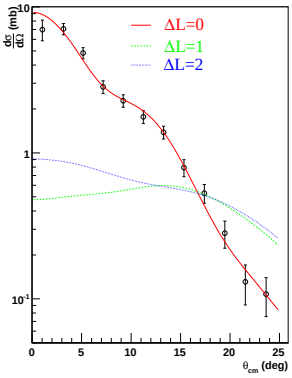

Figure 2. Angular distribution of 4.83-MeV excited ^{13}B. Experimental datum are indicated by closed circle with statistical errors. Solid, dotted and dashed curves indicate the DWBA prediction with assumptions of ΔL = 0, 1, and 2, respectively. About optical potentials, see context.

momentum was deduced to be ΔL = 0 by distorted-wave Born approximation (DWBA) analysis. Hence, we assigned the spin and parity 1/2$^+$ to 4.83 MeV excited state, for the first time. The spectroscopic strength C^2S, where S is a spectroscopic factor and C^2 is an isospin Clebsch-Gordan coefficient, was deduced to be 0.20 ± 0.02 for the excited state. For the DWBA calculation, optical potentials for entrance and exit channel were obtained by adopting single folding model used in Ref. [12]. The obtained optical potentials were approximated to be Woods-Saxon form. In the optical potential parameters, the same value were taken for $r_0(= 1.1fm)$ and $a(= 0.94fm)$, for real part and imaginary part, and for entrance and exit channel. The depth of the potentials, $V_i = -72.6$, $W_i = -42.7$, $V_f = -113.6$, and $W_f = -32.6$ in MeV are used for entrance channel (i) and exit channel (f), respectively. A shell model calculation for ^{13}B(^{12}Be) with a new Hamiltonian [3], which represents the melting of shell closure of $N = 8$, was performed with a shell model calculation code, OXBASH [13]. The calculations were done with maximum 2 and 3 $\hbar\omega$ excitation for ^{12}Be and ^{13}B, respectively. However, the shell model calculation cannot predict the excited state of 1/2$^+$ corresponding to the experimental one. For this discrepancy, we introduce a simple model of the deformed mean field, i.e. Nilsson model. The deformed mean field is provided by the large deformed ^{12}Be core. The $1/2^+$ state arises with the configuration of $(\pi[220\frac{1}{2}])^1$ to the ^{12}Be(g.s.) core. The $\pi[220\frac{1}{2}]$ orbit gains energy and comes down at the large deformation. The probability of spherical $2s_{1/2}$ in $[220\frac{1}{2}]$ is $S = 0.273$ with deformation $\delta = 0.4$ [14]. The fact the $1/2^+$ state locates at low-lying region of 4.83 MeV excitation energy can be explained by the Nilsson model. The spherical ground state in ^{13}B can be also predicted by Nilsson model. In the ground state of ^{13}B, the last proton sits in $[101\frac{1}{2}]$ orbit. The $[101\frac{1}{2}]$ orbit will lose energy at the large deformation so that the spherical configuration will be favored in the ground state while the deformed configuration will be favored in the one proton excitation to sd-shell. Based on this discussion, the $1/2^+$ state at 4.83 MeV in ^{13}B is an intruder state from sd-shell due to the deformation of core nucleus. Recent AMD calculation [15] indicates the first $1/2^+$ state is deformed rather than spherical and has proton excited configuration. This result also supports the deformation of $1/2^+$ state at 4.83 MeV.

4. Summary

We have studied proton transfer reaction on ^{12}Be in inverse kinematics. The spin and pritiy of the 4.83-MeV excited state was assigned to be 1/2$^+$ for the first time. The spectroscopic strength was also obtained to be 0.20 ± 0.02. This state is a proton intruder state from $sd-$shell and its configuration may be represented by the Nilsson model. The shell model calculation may need an effect of deformation. The present study indicates a dynamical change of the shell structure in proton shell with the excitation of the proton.

References

[1] D. Wilkinson, et al., Phys. Rev. 113 (1959) 563.
[2] H. Iwasaki, et al., Phys. Lett. B 491 (2000) 8.
[3] T. Suzuki, et al., Phys. Rev. C 67 (2003) 044302.
[4] H. Iwasaki, et al., Phys. Lett. B 481 (2000) 7.
[5] T. Otsuka, et al., Phys. Rev. Let. 95 (2005) 232502.
[6] T. Nagatomo, et al., Nucl. Phys. A 746 (2004) 505c.
[7] T. Nagatomo, et al., Nucl. Phys. A 746 (2004) 509c.
[8] H. Sagawa, K. Asahi, Phys. Rev. C 63 (2001) 064310.
[9] S. Shimoura, Nucl. Instr. and Meth. A 525 (2004) 188.
[10] M. Kurokawa, et al., IEEE TRANSACTIONS ON NUCLEAR SCIENCE 50 (2003) 1309.
[11] S. Ota, et al., CNS Annual Report 2002 (2003) 14.
[12] G. R. Satchler, Phys. Rev. C 55 (1997) 285.
[13] B. A. Brown, et al., The computer code OXBASH, MSU-NSLC report 524 (1988).
[14] A. Bohr, B. R. Mottelson, Nuclear Structure, Vol II, World Scientific.
[15] Y. Kanada-En'yo, et al., *submitted to* Phys. Rev C (arXiv:0706.3503v1).

Study of High-spin States in ^{109}In

Y. Zheng, E. Ideguchi, S. Ota, A. Yoshida[a], T. Morikawa[b], M. Liu, T. Murakami[a], S. Shimoura, M. Niikura, S. Michimasa, D. Suzuki[c], T. Nakao[c], M. Kurokawa[d], H. Baba[d], T. Koike[e], T. Fukuchi[f], and T .Suzuki[f]

Center for Nuclear Study, Graduate School of Science, University of Tokyo
[a]*Department of Physics, Kyoto University*
[b]*Department of Physics, Kyushu University*
[c]*Department of Physics, University of Tokyo*
[d]*RIKEN(The Institute of Physical and Chemical Research)*
[e]*Department of Physics, Tohoku University*
[f]*Department of Physics, Osaka University*

1. Introduction

Nuclei in the $Z \sim 50$, $A \sim 110$ mass region are of great interest for providing a rich picture in nuclear structure. Due to the $Z = 50$ shell closure, single-particle motions will dominate the excitation schemes of these nuclei. However, other excitation mechanisms also play a role in generating angular momentum such as collective rotations exhibiting smooth band terminations [1] and magnetic rotations (M1 bands) [2]. Recent theoretical calculations predict that a region of shape minima at deformations with $2:1$ axis ratios (or larger) exists at high angular momentum in A ~ 110 nuclei. A superdeformed (SD) band was observed experimentally in ^{108}Cd and it was suggested to be among the most deformed structures ever observed [3]. In this region, ^{109}In is also expected to have smooth band termination, M1 band, and SD band at high-spin states. It would be of interest to find these excitation modes in ^{109}In and to understand the mechanism of the occurrence of SD band. So far, the yrast states of ^{109}In have previously been studied only upto a spin of $31/2\,\hbar$ [4]. The object of the present work was to extend the level scheme of ^{109}In to higher spin and search for these interesting nuclear structures. In this report, preliminary result of the research is presented.

2. Measurement

The experiment was performed at RIKEN accelerator research facility. High-spin states in ^{109}In were populated by using the ^{96}Zr(^{20}Ne, 1p6n)^{109}In reaction. The ^{20}Ne beam was provided by the AVF cyclotron. The ^{96}Zr target had a thickness of 1 mg/cm^2. To determine the optimum beam energy to produce ^{109}In, excitation functions of the evaporation residues were calculated by using the statistical model code, CASCADE [5]. In the energy region around 6.5 MeV/A, nuclei in the evaporation channels of 1p5n-1p7n ($^{108-110}$In), and 1α4n-1α6n ($^{106-108}$Cd) will be mainly produced. Gamma-ray yields of these nuclei were measured at the 6.5 MeV/A beam energy by using a coaxial Ge detector placed at 90°. Production cross-sections have been extracted from the experimental data. The results are shown in table 1 compared with CASCADE calculation. Although there is a discrepancy in production cross-sections between the experimental result and the calculation, the relative yields of the nuclei are consistent with the calculation (see table 1) and ^{109}In has a largest production cross-section ($\sim$ 129mb) among the residual nuclei at the 6.5 MeV/A energy, this energy was used in the remainder of the experiment to populate high-spin states in ^{109}In.

Nuclide (exit channel)	production cross-section (mb) CASCADE calculation	experiment
^{109}In (1p6n)	215.3	129 ± 3
^{107}Cd (2p7n)	192.7	111 ± 3
^{106}Cd (2p8n)	152.3	90 ± 8
^{110}In (1p5n)	107.8	73 ± 3
^{108}Cd (2p6n)	72.9	69 ± 3
^{108}In (1p7n)	63.9	37 ± 2

Table 1. The production cross-sections.

Gamma rays from the high-spin states in the residual nuclei were measured by GRAPE and two clover Ge detectors at forward angle. In this experiment the GRAPE was composed of 17 detectors. These detectors were placed around the target to cover the angle range between 60° and 120° and had an efficiency of $\sim 4\%$. Evaporated charged particles were simultaneously measured by using a Si Ball, a 4π array of 11 Si detectors which has been developed for the in-beam study of nuclei requiring a high degree of channel selectivity. Protons and α particles can be identified by gating different energy region in the energy spectrum of Si detector. High selectivity will therefore be obtained by combining the Ge detector array with the Si Ball which allows the selection on the particle emission of interest. With a trigger condition of seven or more Ge detectors firing in coincidence, a total of 160×10^6 events was collected. The gamma-ray detectors were calibrated with ^{133}Ba, ^{152}Eu and ^{56,60}Co standard sources; typical energy resolution of the two clover and the GRAPE (in add-back mode) detectors was about 2.5-3 keV at full width at half maximum (FWHM) for the 1332.5 keV line. The energy of Doppler-shifted gamma rays emitting from moving nuclei was also corrected by using an average value of β (2%) and taking the center of each segment for the position information on the interaction points of the incident gamma rays. After accurate gain matching, the coincidence events were sorted into total matrix and charged-particle emission

selected matrices for off-line analysis.

3. Analysis and Result

The energy spectra of gamma rays from this work are shown in Figure 1. The top panel shows the total spectrum and the bottom is the charged-particle gated spectrum ($1\mathrm{p}0\alpha$) which corresponds to the $1\mathrm{p}x\mathrm{n}$ channels. Compared to the total spectrum, We can see that the background is significantly reduced and the gamma lines from ^{109}In and ^{110}In appear clearly in the particle-gated spectrum. This shows that the particle emission selection by using the Si Ball discriminates against other reaction channels effectively. Low-lying states of nuclei ^{109}In and ^{110}In were previously studied. Gamma-ray assignments were performed by using previously reported peak energies. In figure 1(bottom), gamma peaks at 245, 336, 1028, 1104 and 1429 keV appeared strongly which are yrast cascade transitions of ^{109}In. The 241, 544, 613 and 808 keV peaks of ^{110}In also appeared clearly. The strong peak at 209 keV is a doublet of transitions in ^{109}In and ^{110}In.

In order to assign new gamma rays to ^{109}In and extend the level scheme of ^{109}In to higher spin region, an analysis of the gamma-gamma coincidence has been performed. Gated spectra were produced for each of the gamma rays assigned to ^{109}In previously. Based on the coincidences with the known gamma rays, a new observed transition with the energy of 633 keV was assigned to ^{109}In. The coincidence spectrum gated by the 1104, 208, 336 and 390 keV known gamma-lines in ^{109}In is shown in figure 2(a) for energy range from 180 to 700 keV and (b) from 700 to 1450 keV. Although the new 633 keV transition is quite weak, it can be seen clearly in figure 2(a) and is in coincidence with all the gamma lines marked in the gated spectrum. Among these, the peaks at 208, 390, 708, 324 and 409 keV are dipole cascade transitions from the M1 band in ^{109}In as shown in figure 2(c). Based on the coincidence relations with the transitions of the M1 band and intensity balance (the intensity of the 633 keV transition is weaker than other transitions in the M1 band), the 633 keV transition was temporarily placed on the top of the M1 band. An interesting feature of this sequence of cascade transitions was that the energies of the transitions exhibit a steady increase from the $21/2^-$ to the $27/2^-$states, while the subsequent $29/2^- \rightarrow 27/2^-$transition is lower in energy, beyond which the transition energies become regular again. Similar structure has also been reported in the neighboring odd-A In isotopes [6]. This behavior of M1 band indicates that the fully aligned $\pi(g_{9/2})^{-1} \otimes \nu(h_{11/2}, g_{7/2})$ configuration with the other neutrons in the $\mathrm{d}_{5/2}$ and $\mathrm{g}_{7/2}$ orbitals coupled to a spin zero, is probably the dominant component of the configuration for the $27/2^-$ state in ^{109}In. The subsequent spin is generated by the gradual alignment of the neutrons in the $\mathrm{d}_{5/2}$ and $\mathrm{g}_{7/2}$ orbitals.

In summary, the yrast cascade transitions of ^{109}In appeared clearly in the gamma-ray spectra gated by the Si Ball and the 633 keV new transition was found and placed on the top of the M1 band in ^{109}In. Further analysis of cross-talk events in adjacent detectors is needed to reduce the Compton background.

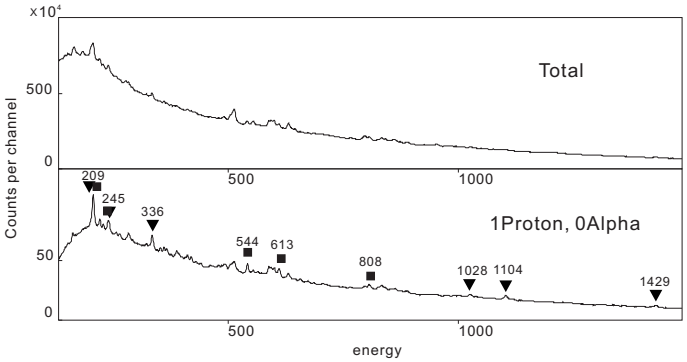

Figure 1. Comparison between the total gamma-ray spectrum (top) and particle-gated gamma-ray spectrum (bottom). Gamma-lines of selected nuclei are labeled by their energies.

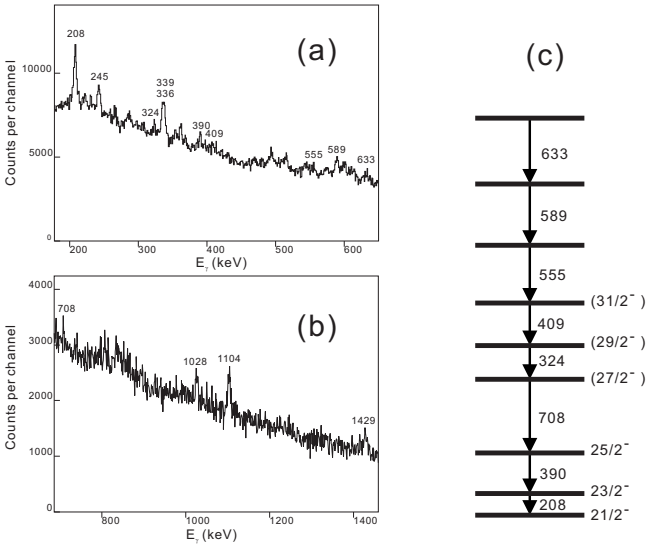

Figure 2. The coincidence spectrum of ^{109}In gated by the 1104, 208, 336 and 390 keV known gamma-lines. The M1 band of ^{109}In (c), in which a new transition of 633 keV has been added to the top.

References

[1] I. Ragnarsson *et al.*, Phys. Rev. Lett. **74**, (1995) 3935.
[2] A. Gadea *et al.*, Phys. Rev. C **55**, (1997) R1.
[3] R.M. Clark *et al.*, Phys. Rev. Lett. **87** (2001) 202502.
[4] J. Kownacki *et al.*, Nucl. Phys. A **627** (1997) 239.
[5] F. Fühlhofer, Nucl. Phys. A **280** (1977) 267.
[6] S.K. Tandel *et al.*, Phys. Rev. C **58**, (1998) 3738.

Study of High-spin States in A∼30 Nuclei

M. L. Liu, E. Ideguchi, T. Morikawa[a], Y. Toh[b], M. Koizumi[b], M. Oshima[b], B. Cederwall[c], K. Furutaka[b], Y. Hatsukawa[b], M. Sugawara[d], Y. Zheng *Center for Nuclear Study, Graduate School of Science, University of Tokyo*
[a] *Department of Physics, Kyushu University*
[b] *Japan Atomic Energy Agency*
[c] *Department of Physics, Royal Institute of Technology*
[d] *Chiba Institute of Technology*

1. Introduction

Study of high-spin states in A $\sim$ 30 nuclei has been extensively made in the past few years. Several interesting phenomena were investigated in this mass region such as level structures of mirror nuclei, shape coexistence, and the interplay between single-particle and collective motion; even largely deformed states were observed in this mass region [1, 2]. Because of the presence of largely deformed shell gap in N=20, it will be interesting to search for largely deformed structure at high-spin states in ^{36}S and its neighbouring nuclei.

2. Experiment

In-beam γ-ray spectroscopic experiment was performed to study high-spin states of ^{36}S with neutron number N=20 and its neighbouring nuclei through the reaction ^{24}Mg(^{18}O, α2p)^{36}S reaction at a beam energy of 70 MeV, at which energy the yields of ^{36}S were large. The $^{18}O^{6+}$ beam was provided by the tandem accelerator of Japan Atomic Energy Agency (JAEA). The target was an isotopically enriched ^{24}Mg metallic foil of 1 mg/cm^2 thickness with an 8 mg/cm^2 ^{nat}Pb backing. The GEMINI [3] γ-ray detector array was used. The array consisting of 14 hyperpure germanium detectors with bismuth germanate anti-Compton (AC) shields was used to detect γ rays. The HPGe detectors were placed at 47°(4 Ge's), 72°(2 Ge's), 90°(2 Ge's), 105°(4 Ge's), 144°(1 Ge) and 147°(1 Ge) with respect to the beam direction. The HPGe detectors were calibrated by using standard γ-rays sources of ^{133}Ba, ^{152}Eu and ^{56}Co. Due to the low Coulomb barrier of light mass A $\sim$ 30 nuclei, the cross sections of reaction channels with evaporation of charge particles in the final state become very large. Many competing channels are therefore open and dominant for the present projectile and target combination. To select the reaction channels, a charge particle ball consisting of 20 ΔE Si detectors surrounding the target was employed. Events were collected when at least two HPGe detectors and one Si detector were fired in coincidence. To observe the fast transitions de-exciting the short-lived levels (higher-lying and large-deformed states), a 490 μg/cm^2 thick target without backing was also used in the experiment.

3. Analysis and Results

Based on the γ-γ coincidence relationship and γ-ray energy sum, a level scheme for ^{36}S was constructed. The γ-γ coincidence relationship and the level scheme can be seen in Fig. 1. The ordering of transitions in the level scheme was determined according to the γ-ray relative intensities. The present level scheme is the same as the published one in Ref. [4]. We didn't observe γ rays de-exciting the high-lying states in ^{36}S. It is mainly because many open exit channels and smaller reaction cross section $\sim$ 10 mb for ^{36}S compared with the $\sim$ 600-mb total cross section lead to low statistics. Figure 2 indicates the typical γ-ray and charge particle gated spectra obtained from current analysis. γ rays emitted from ^{33}P, ^{34}S, ^{35}Cl, ^{38}Ar and ^{39}K nuclei can be seen in the spectra. Three new 1026-, 1297- and 1431-keV γ rays were observed in ^{33}P [5], which de-excite high-lying states with spin $\sim$ 15/2 $\hbar$(see Figure 2 A). The 1001-keV gate in Figure 2 B comes from the the ^{34}S $5^- \rightarrow 4^+$ decay [6]. The ^{35}Cl nucleus was populated most strongly in the experiment and we observed most of the known non-yrast transitions [7] (see Figure 2 C). The topmost level observed in this experiment is the 11.617-MeV state of ^{38}Ar with spin and parity 11^- and the corresponding decay is the1441-keV gate in Figure 2 D [8]. We also observed the yrast transitions of ^{39}K, shown in Figure 2 E [9].

References

[1] E. Ideguchi et al., Phys. Rev. Lett. **87** (2001) 222501.
[2] C. E. Svensson et al., Phys. Rev. Lett. **85** (2000) 2693.
[3] K. Furuno et al., Nucl. Instrum. Methods A **421** (1999) 211.
[4] X. Liang et al., Phys. Rev. C. **66** (2002) 014302.
[5] E. H. Berkowitz et al., Nucl. Phys. A **140** (1970) 173.
[6] P. Mason et al., Phys. Rev. C. **71** (2005) 014316.
[7] R. kshetri et al., Nucl. Phys. A **781** (2007) 277.
[8] D. Rudolph et al., Phys. Rev. C. **65** (2002) 034305.
[9] Th. Andersson et al., Eur. Phys. J. A **6** (1999) 5.

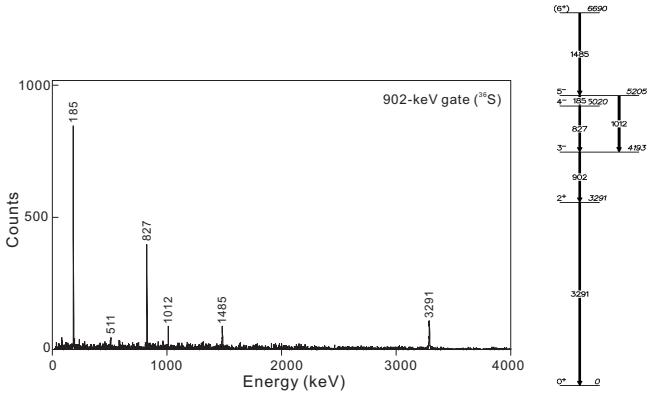

Figure 1. The Gamma-ray spectrum gated on the 902-keV transition and level scheme of ^{36}S deduced from present work.

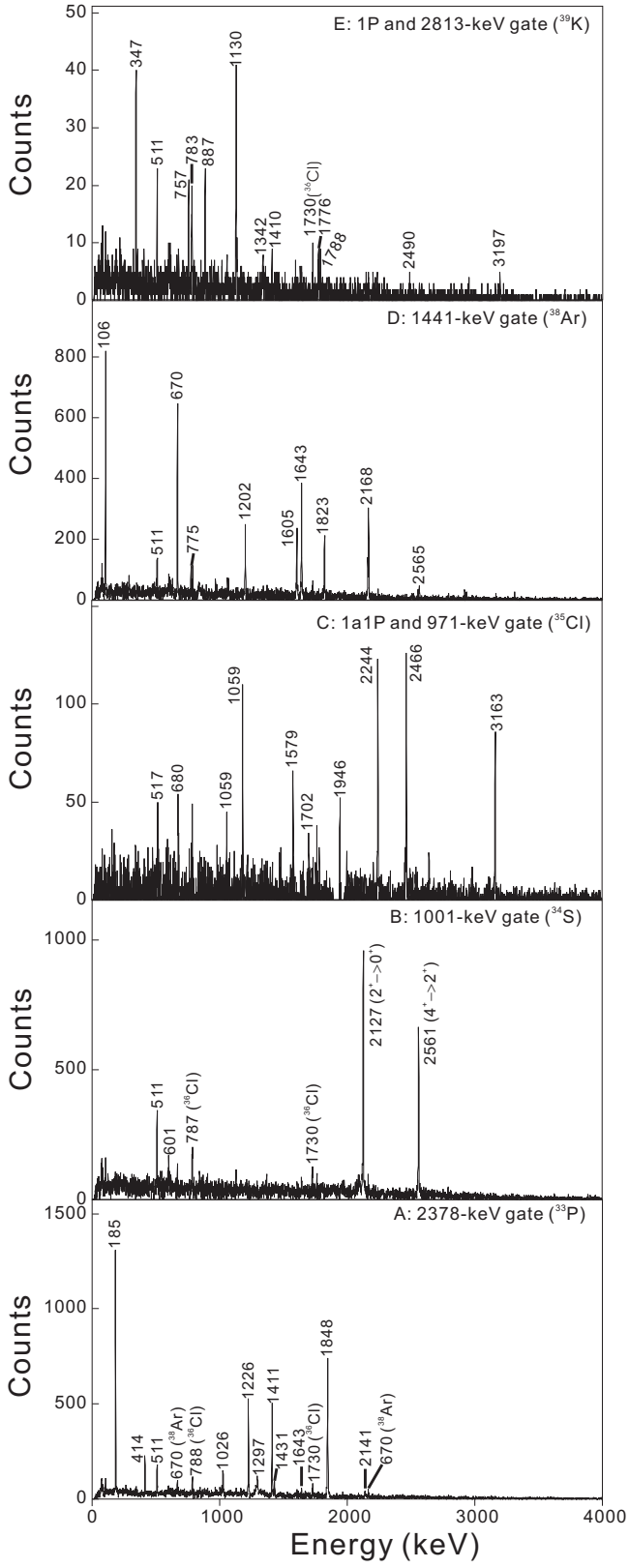

Figure 2. Gamma-ray Spectra produced in the reaction ^{18}O+^{24}Mg.

Study of High-spin States in $^{49-51}$Ti

M. Niikura, E. Ideguchi, N. Aoi[a], H. Baba[a], T. Fukuchi[b], Y. Ichikawa[c], H. Iwasaki[c], T. Kubo[a], M. Kurokawa[a], M. Liu, S. Michimasa[a], T. Ohnishi[a], T. K. Onishi[c], S. Ota, S. Shimoura, H. Suzuki[c], D. Suzuki[c], Y. Wakabayashi, K. Yoshida[a] and Y. Zheng

Center for Nuclear Study, Graduate School of Science, University of Tokyo
[a]RIKEN (The Institute of Physical and Chemical Research)
[b]Department of Physics, Graduate School of Science, Osaka University
[c]Department of Physics, Graduate School of Science, University of Tokyo

1. Introduction

In-beam γ-ray spectroscopy by fusion-evaporation reaction is one of the most efficient methods of studying nuclear structure at high-spin, since a large amount of angular momentum can be brought into the system. However, nuclei produced via fusion-evaporation reactions using stable isotope beams are limited, in many cases, to the proton-rich side relative to the β-stability line. In order to investigate the high-spin states of neutron-rich nuclei by the fusion-evaporation reaction, it is necessary to use neutron-rich secondary beams. In ^{50}Ti and its neighbors, the onset of deformed collective states due to the presence of deformed shell gaps in $Z = 22$ and $N = 28$ is expected at high spin. In this report, the in-beam γ-ray spectroscopy in $^{49-51}$Ti by secondary fusion reaction, $^{46}\mathrm{Ar} + ^{9}\mathrm{Be}$, are described.

2. Experiment

The experiment was performed at the RIKEN Projectile-fragment Separator (RIPS) facility in RIKEN [1]. A secondary ^{46}Ar beam was produced by projectile fragmentation of 64-A-MeV ^{48}Ca beam and its energy was lowered using aluminum degraders placed at the first and second focal planes of RIPS. The secondary beam bombarded a 10-μm-thick ^{9}Be target placed at the third focal plane to induce secondary fusion reactions, $^{9}\mathrm{Be}\left(^{46}\mathrm{Ar}, xn\right)^{55-x}\mathrm{Ti}$.

Gamma rays emitted from the high-spin states of evaporation residues were detected by the CNS Gamma-Ray detector Array with Position and Energy sensitivity (GRAPE) [4] together with two clover and one coaxial germanium detectors. These γ-ray detectors were placed around the secondary target to cover the angular range between 30° and 120° relative to the beam direction. In order to correct the Doppler-shift effect of γ rays emitted from fast moving particle ($\beta \sim 0.08$), pulse-shape analysis was performed for CNS-GRAPE [5] to determine the interaction points of the detected γ rays.

Details on the production of a secondary beam and experimental setup are reported in ref. [2, 3].

3. Analysis and results

A Doppler correction was carried out based on the beam position at the target, velocity of the outgoing particles and interaction points of the γ rays in the germanium detectors. Figure 1 shows a Doppler-corrected γ-ray spectrum, wherein we confirmed known cascade γ transitions from the spin $(19/2)^-$, (11^+) and (13/2,17/2) states in ^{49}Ti, ^{50}Ti and ^{51}Ti [6, 7, 8], respectively.

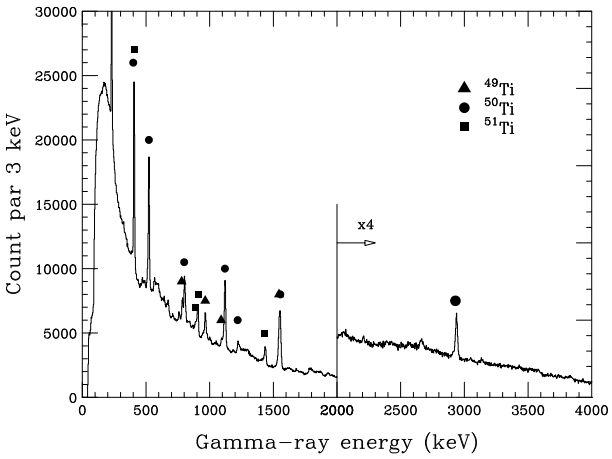

Figure 1. Doppler-corrected γ-ray spectrum. Gamma rays from ^{49}Ti,^{50}Ti and ^{51}Ti are marked by closed triangle, closed circle and closed square, respectively.

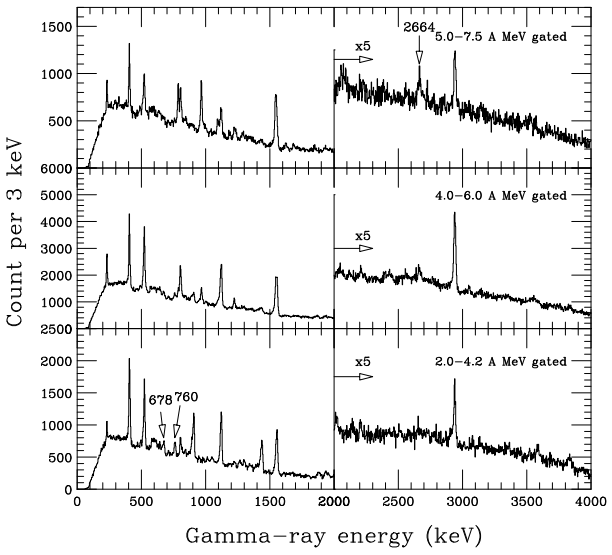

Figure 2. Relative γ-ray yields of ^{51}Ti as a function of the incident beam energy.

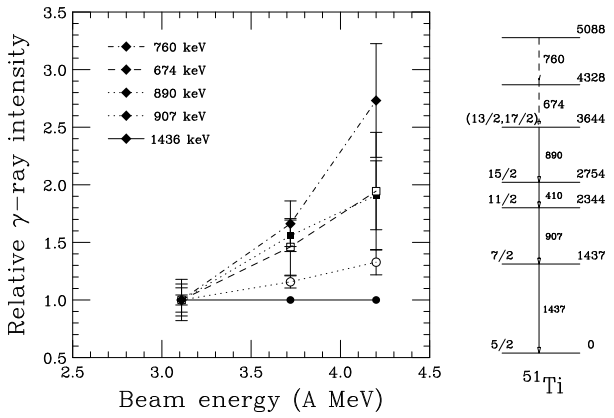

Figure 3. Excitation function of the γ rays in ^{51}Ti (left) and proposed level scheme of ^{51}Ti (right).

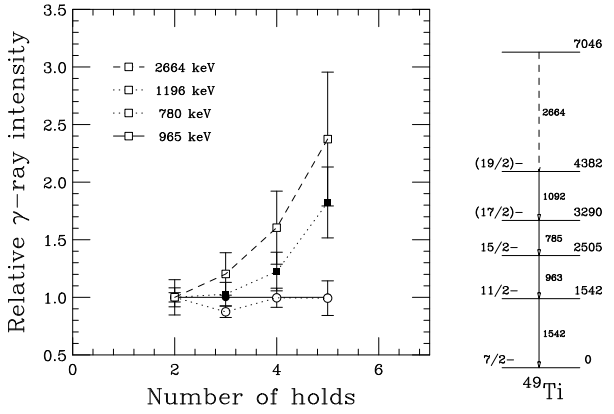

Figure 4. Relative γ-ray yields as a function of detected γ-ray multiplicities (left) and proposed level scheme of ^{49}Ti (right).

The energy of ^{46}Ar beam was broadened between 2 and 8 A MeV at the center of the target due to the energy straggling after passing through the degraders and the beamline detectors. Since cross sections of fusion reactions depend strongly on the incident beam energy, excitation function can help identifying the evaporation channel. Figure 2 shows γ-ray spectra by gating different regions of the beam energy. In the spectra, we observe new γ-transition at 674 and 760 keV in ^{51}Ti and at 2664 keV in ^{49}Ti, respectively.

In the left panel of fig. 3, normalized γ-ray yields of ^{51}Ti relative to that of the lowest γ transition at 1437 keV were plotted as a function of the incident beam energy. As a beam energy increases, larger angular momentum can be brought to the system and consequently a relative population of higher spin states will increases. The behavior of relative γ-ray yields of the known transitions support the previously reported order of the cascade decay. Since the newly observed 684 and 760 keV transitions are largely populated in higher incident beam-energy region than the other transitions, they are assigned as the transitions above the known (13/2,17/2) state at 3644 keV (right panel of fig. 3).

The left panel of Fig. 4 shows the relative yield of the observed γ-rays of ^{49}Ti as a function of detected γ-ray multiplicities. The γ-ray yields are normalized to the intensity of the known 963 keV transition. Because the newly observed γ rays at 2664 keV is enhanced in the high-multiplicity spectrum, this γ-ray is placed above the known 4382 keV state (see the right panel of Fig. 4).

4. Summary

We have performed in-beam γ-ray spectroscopy by the fusion-evaporation reaction using secondary beam. The new γ transition from high-spin states in ^{51}Ti and ^{49}Ti were identified and level scheme were constructed. Further analysis to assign spins for the newly observed states using angular distribution is now in progress.

References

[1] T. Kubo *et al.*, Nucl. Instrum. Methods **B70** (1992) 309.
[2] E. Ideugchi *et al.*, Eur. Phys. J. **A25** (2005) 429.
[3] M. Niikura *et al.*, CNS Ann. Rep. **2005** (2006) 29.
[4] S. Shimoura, Nucl. Instrum. Methods **A525** (2004) 188.
[5] M. Kurokawa *et al.*, IEEE Trans. Nucl. Sci. **50** (2003) 1309.
[6] M. Behar *et al.*, Nucl. Phys. **A366** (1981) 61.
[7] B. Gass *et al.*, Phys. Rev. Lett. **40** (1978) 1313.
[8] S. E. Arnell *et al.*, Phys. Scr. **6** (1972) 222.

Measurement of pd Breakup Reaction at 250 MeV for the Study of 3NF Effects

Y. Maeda[a], M. Dozono[a], K. Hatanaka[c], E. Ihara[a], T. Kawabata, T. Matsubara[c], S. Noji[b], T. Sagara[a], S. Sakaguchi, H. Sakai[b], Y. Sasamoto, M. Sasano[b], K. Sekiguchi[d], Y. Shimizu, K. Suda[c], M. Takechi[d], Y. Tameshige[c], A. Tamii[c], T. Uesaka, T. Wakasa[a] and K. Yako[b]

Center for Nuclear Study, Graduate School of Science, University of Tokyo
[a]Department of Physics, Kyushu University
[b]Department of Physics, University of Tokyo
[c]Research Center for Nuclear Physics, Osaka University
[d]RIKEN (The Institute of Physical and Chemical Research)

To describe the properties of nuclear system as a consequence of the nuclear force between nucleons is one of the most important objective. The modern NN potentials reproduce the experimental NN data up to a laboratory energy of 350 MeV very accurately. When applied to many body ($>$ 2N) systems, however, the NN potentials alone fail to predict the experimental data. This discrepancy between the data and the theoretical predictions based on the NN force can be considered as the effects of the three-nucleon force (3NF). Recently, from the experimental side, the 3NF effects have been actively studied by the measurements of nucleon-deuteron elastic scattering at intermediate energy region. At 135MeV/A, the calculations with NN forces only fail to reproduce the highly precise data of the cross sections and the vector analyzing powers for the dp elastic scattering [1]. But these discrepancies are filled by adding the 2π exchange 3NFs. It supports the theoretical prediction that the Nd elastic scattering at intermediate energy is a good probe to study the 3NF effects. When we go to 250MeV, however, the large discrepancy between Nd cross sections and NN force predictions can be partially removed by including the 3NF [2, 3] into the calculations. This result is very different from the case at 135MeV/A. Addition to that, recent calculations including the relativistic corrections [4] or the Coulomb interaction [5] show that these effects are too small to explain the discrepancy between the data and the theory [3]. This discrepancy might be explained by the inclusion of $\pi-\rho$ or $\rho-\rho$ exchange type 3NFs or relativistic 3NFs. More studies from both experimental and theoretical sides are expected to solve it.

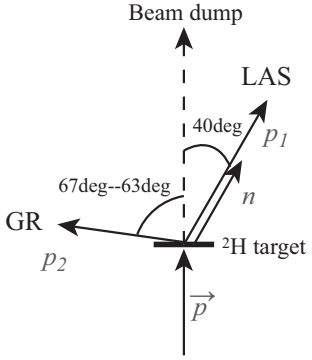

Figure 1. The schematic view of the experimental setup.

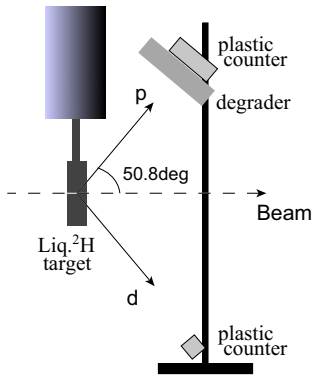

Figure 2. The schematic view of the luminosity monitor installed in the scattering chamber.

For the next step of the 3NF study at higher energy region, the breakup reactions are expected to reveal more significant 3NF effects because the total cross sections of the breakup reactions are predicted to become larger than that of the elastic reactions [6]. However the three-nucleon final state of the breakup reaction is kinematically much more complicated than that of the elastic reaction. In this work, we selected the kinematical condition which include the final state interaction (FSI) region and avoid the Coulomb force effects between the particles under the FSI,

$$\vec{p} + d \rightarrow (p_1 n)_{FSI} + p_2.$$

The measurement was performed at the West experimental hall in the Research Center for Nuclear Physics (RCNP) of Osaka University. Figure1 shows the schematic view of the experimental setup. The polarized proton beam was accelerated to 250 MeV and bombarded a deuteron target in the scattering chamber. The typical beam polarization was 0.7.

We used the liquid deuteron target (LDT) [7] as the deuteron target. This LDT has windows of aramid foil with thickness of 12 μm. We installed the luminosity monitor in the scattering chamber to monitor the thickness of the LDT throughout the measurements. Figure2 shows the schematic view of the luminosity monitor which was designed to measure the pd elastic scattering. The scattered protons and recoiled deuterons were detected in kinematical coincidence by the plastic scintillation counters set at $\theta_p = \theta_d = 50.8°$. For the normalization purpose, the deuterated polyethylene (CD_2) foil [8] was used as the deuteron target. The thick-

ness of the LDT was about 30mg/cm^2 during the measurement.

Two protons in the final state were momentum analyzed by the Large Acceptance Spectrometer (LAS) and the Grand Raiden Spectrometer (GR), respectively. The proton in the FSI (p_1) was analyzed by LAS fixed at $\theta_{lab} = 40°$. The LAS covered the energy range of 50 - 115 MeV of p_1 by changing its magnetic field. The other proton (p_2) was analyzed by GR at $\theta_{lab} = 63° - 67°$. The setting angle and the magnetic field of GR were changed to cover the kinematical condition that the neutron which was not detected in this work scattered to $\theta_{lab} = \theta_{LAS} = 40°$. The energy range of the detected p_2 was 115 - 120 MeV. From the measurement of p_1 and p_2 as described above, the momentum of the neutron was derived and the energy correlation between p_1 and n (S-curve) was obtained.

Figure3 shows the missing mass spectrum of (p, pp) reaction with the LDT target. The peak around 940 MeV represents the neutrons from pd breakup reactions. To subtract the contribution from the window foils of the LDT, we also carried out the measurement with the gas deuteron target using the LDT system. Addition to that, we also subtracted the contribution from the accidental coincidence events of GR and LAS (Fig.3). After the subtraction of these background contributions, we obtained a neutron mass resolution of 1.15MeV FWHM.

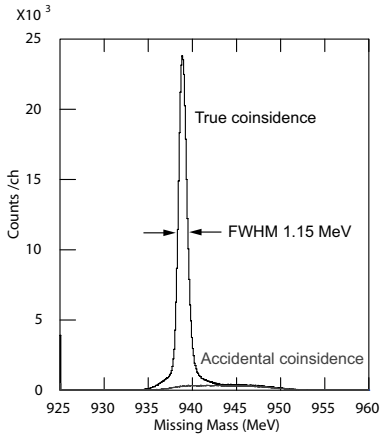

Figure 3. The missing mass spectra obtained by Liq.^{2}H(p,pp) measurements was shown by the black line, which include both the true coincidence and the accidental coincidence events. The contribution of the accidental coincidence events only was represented by the gray line.

The preliminary results of the vector analyzing power were shown by solid circles in Fig.4. The results of the theoretical calculations [10] with CD-Bonn only (dashed line) and that with CD-Bonn and Tucson-Melbourne (TM) 3NF [9] were also represented in the figure. These predictions include the correction according to the experimental acceptances of the solid angle. We can see that the data was well reproduced by the prediction without 3NF around the FSI but the the data seems to prefer the prediction with 3NF in the region far from the FSI. The results of the differential cross section were under analysis now.

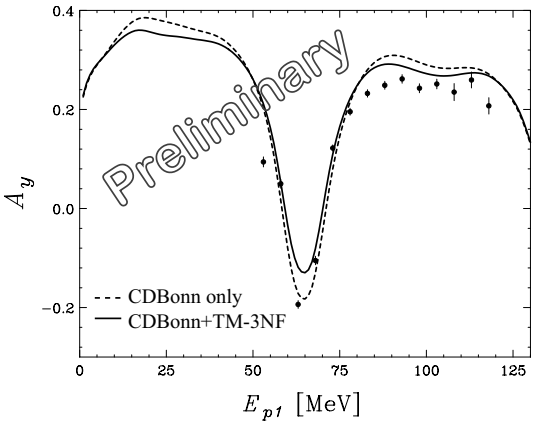

Figure 4. The results of the vector analyzing power are shown by the solid circles with the statistical errors. The horizontal axis is the energy of p_1 which was detected by using LAS. The theoretical predictions based on the CD-Bonn potential with (solid line) or without (dashed line) TM-3NF.

References

[1] K. Sekiguchi *et al.*, Phys. Rev. C **65** (2002) 034003.
[2] K. Hatanaka *et al.*, Phys. Rev. C **66** (2002) 044002.
[3] Y. Maeda *et al.*, Phys. Rev. C, in print.
[4] H. Witała, *et al.*, Phys. Rev. C **71** (2002) 054001.
[5] A. Deltuva *et al.*, Phys. Rev. C **67** (2003) 034001.
[6] J. Kuroś-Żołnierczuk *et al.*, Phys. Rev. C **66**, 024003 (2002).
[7] K. Sagara *et al.*, RCNP Annual Report, 1995, p.158.
[8] Y. Maeda *et al.*, Nucl. Instrum. Meth. A **490** (2002) 518.
[9] S.A. Coon *et al.*, Nucl. Phys. A **317** (1979) 242.
[10]H. Kamada, private communication.

Cluster States in ^{13}C

Y. Sasamoto, T. Kawabata , T. Uesaka , K. Suda , Y. Maeda , S. Sakaguchi , K. Itoh[a], K. Hatanaka[b], M. Fujiwara[b], A. Tamii[b], Y. Shimizu[b], K. Nakanishi[b], K. Kawase[b], H. Hashimoto[b], Y. Tameshige[b], H. Matsubara[b], M. Itoh[c], H. P. Yoshida[d] and M. Uchida[e]

Center for Nuclear Study, Graduate School of Science, University of Tokyo
[a]*Department of Physics, Saitama University*
[b]*Research Center for Nuclear Physics (RCNP), Osaka University*
[c]*Cyclotron and Radioisotope Center (CYRIC), Tohoku University*
[d]*Department of Physics, Kyusyu University*
[e]*Department of Physics, Tokyo Institute of Technology*

Alpha clustering is one of the important concepts in the nuclear structure. Alpha cluster states in self-conjugate $4N$ nuclei are expected to appear near α-decay thresholds as shown in the Ikeda diagram [1]. For example, it has been suggested that the 7.65-MeV 0_2^+ state in ^{12}C, which is strongly excited by the monopole transition, has a 3α configuration [2]. This state locates at 0.39 MeV above the 3α-decay threshold energy, and is not described by shell-model (SM) calculations. Recently, this state is theoretically considered to have the dilute-gas-like structure [3].

The next natural question is whether such a dilute state of clusters exists in the $A \neq 4N$ nuclei. Recently, it is proposed that the $3/2_3^-$ state in ^{11}B is a candidate for the dilute cluster state where a proton hole in the $p_{3/2}$ orbit couples to the 0_2^+ state in ^{12}C [4, 5]. The $3/2_3^-$ state in ^{11}B at $E_x =$ 8.56 MeV, which is located just 100-keV below the α-decay threshold, is strongly excited by the monopole transition.

The large monopole strength for the $3/2_3^-$ state in ^{11}B, which is not explained by the SM calculations, is reasonably well described by the antisymmetrized molecular dynamics (AMD) calculation. According to the AMD calculation, the $3/2_3^-$ state has a loosely bound $2\alpha + t$ cluster structure with a dilute density. It is pointed out that the large monopole transition strength is one of the possible evidences for dilute cluster states.

Similar cluster states where a proton in the $p_{1/2}$ orbit instead of a proton hole in the $p_{3/2}$ orbit couples to the 0_2^+ state in ^{12}C are expected in ^{13}C. Such cluster states are considered to be excited by the monopole transitions similar to the $3/2_3^-$ state in ^{11}B. Therefore, it is important to measure the monopole transition strengths in ^{13}C for the clarification of the cluster structure. Since the spin-parity of the ground state in ^{13}C is $1/2^-$, the $1/2_2^-$ at $E_x = 8.86$ MeV and $1/2_3^-$ at $E_x = 11.08$ MeV states, which are allowed to be excited by the monopole transition, are candidates for such cluster states.

For the measurement of the monopole strengths, the inelastic alpha scattering is a good probe. Since only the isoscalar natural parity transitions are allowed in the (α, α') reaction, the reaction mechanism is expected to be simple. In the present work, we measured the inelastic alpha scattering at forward angles where the monopole transition is enhanced and searched for the cluster states in ^{13}C.

The experiment was performed by using a 400-MeV alpha beam at the Research Center for Nuclear Physics, Osaka University. The self-supporting ^{13}C and ^{nat}C targets with the thickness of 1.5 and 0.5 mg/cm^2 prepared by a thermal cracking method [6] were used. The alpha particles scattered from the target were momentum analyzed by the magnetic spectrometer Grand Raiden (GR). In order to obtain the isoscalar transition strengths, the cross sections for the ^{13}C(α,α') and ^{nat}C(α,α') reactions were measured at forward angles of θ = 0°–19.4°.

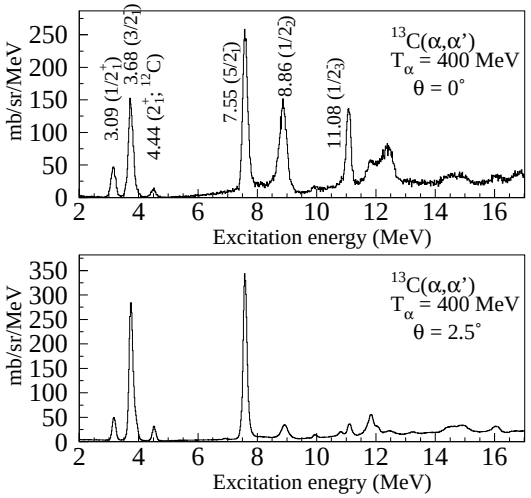

Figure 1. Energy spectra for the ^{13}C(α,α') reaction at 0° and 2.5°.

Figure 1 shows the energy spectra for the ^{13}C(α,α') reaction at 0° and 2.5°. The $5/2_1^-$ state at $E_x = 7.55$ MeV is strongly excited both at 0° and 2.5°. The angular distribution of the cross sections for this state is expected to be almost flat at forward angles. The angular distributions have the characteristic shape corresponding to the transferred angular momentum. The distribution of monopole transition has a forward peak, and that of quadrupole transition is almost flat at forward angles. Therefore, this state is suggested to be dominantly excited by the quadrupole transition. On the other hand, the $1/2_2^-$ and the $1/2_3^-$ states are strongly observed only at 0°. The cross sections for these states rapidly decrease as increasing the scattering angle. Therefore it is concluded that these two states are excited by the monopole transitions. Since the bump around

$E_x = 12.5$ MeV is also strongly observed only at 0°, the 12.5-MeV state is considered to be excited by the monopole transition in similar to the $1/2^-_2$ and $1/2^-_3$ states. Thus, the spin-parity of this state is assigned to be $1/2^-$, although the $1/2^-$ state around $E_x = 12.5$ MeV have not been reported in ref. [7].

The measured cross sections for the $5/2^-_1$, $1/2^-_2$, and $1/2^-_3$ states are compared with the distorted-wave Born approximation (DWBA) calculation in Fig. 2. Since only the natural-parity transitions are allowed in the inelastic alpha scattering, the allowed transfered spin-parity ΔJ^π exciting the $5/2^-$ and $1/2^-$ states are 2^+ and 0^+, respectively. Thus, the cross sections for the $\Delta J^\pi = 0^+$ and 2^+ transitions are calculated using the DWBA calculation. The transition potentials used in the DWBA calculation were obtained from the deformed potential model [8]. It is found that the measured cross sections in Fig. 2 have the characteristic shape depending on the transferred angular momentum.

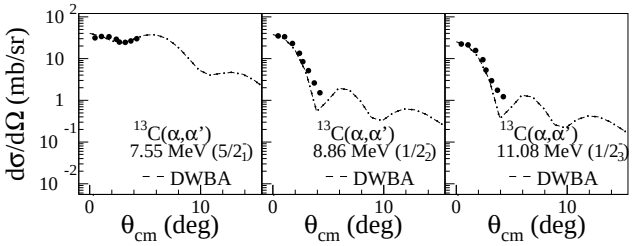

Figure 2. Cross sections for the ^{13}C(α, α') reaction at E_α = 400 MeV. Dashed-lines show the DWBA calculation.

The hadron scattering at forward angles and at intermediate energies have a good proportionality between the cross sections and the relevant excitation strengths. Assuming that the transition potential for the ^{13}C(α, α') reaction is similar to that for the ^{12}C(α, α') reaction, the following relation can be approximately used,

$$B(\mathrm{E}\lambda; \mathrm{IS} :^{13}\mathrm{C}) = \frac{\text{cross section } (^{13}\mathrm{C})}{\text{cross section } (^{12}\mathrm{C})} \times B(\mathrm{E}\lambda; \mathrm{IS} :^{12}\mathrm{C}), \quad (1)$$

where $B(\mathrm{E}\lambda; \mathrm{IS} : \mathrm{A})$ is the isoscalar transition strength with a multipolarity of λ for a nucleus A.

The isoscalar strengths in ^{13}C were deduced from Eq. (1) by using the isoscalar monopole strengths $B(\mathrm{E0}; \mathrm{IS} :^{12}\mathrm{C}) = 120$ fm^4 for the 0^+_2 state and the quadrupole strengths $B(\mathrm{E2}; \mathrm{IS} :^{12}\mathrm{C}) = 94$ fm^4 for the 2^+_1 state in ^{12}C taken from ref. [7] and [9]. The obtained isoscalar transition strengths in ^{13}C are tabulated in Table 1. Theoretical predictions by the SM calculation are also listed for comparison. The SM calculation was performed by using the SFO (Suzuki-Fujimoto-Otsuka) interactions within the 0–2$\hbar\omega$ configuration space [10]. The theoretical level scheme for the negative-parity states are compared with the experiment in Fig. 3. The SM calculation reasonably explains the experimental level scheme below $E_x = 10$ MeV.

For the $5/2^-_1$ state, the predicted quadrupole strength is relatively smaller than the experimental value. The large monopole strengths were observed for the $1/2^-_2$ and $1/2^-_3$ states although the SM calculation gives the extremely small monopole strengths. The large monopole strengths for the $1/2^-_2$ and $1/2^-_3$ states are reflection of the exotic structure of these states which are not described by the SM calculation. Therefore, the $1/2^-_2$ and $1/2^-_3$ states are inferred to be cluster states. For further clarification, the present results should be compared with the cluster model calculations.

Table 1. Measured transition strengths compared with the SM predictions.

		Experiment	Shell-model
J^π	E_x (MeV)	$B(\mathrm{E2}; \mathrm{IS})$ (fm^4)	$B(\mathrm{E2}; \mathrm{IS})$ (fm^4)
$5/2^-_1$	7.55	77 ± 8	44
J^π	E_x (MeV)	$B(\mathrm{E0}; \mathrm{IS})$ (fm^4)	$B(\mathrm{E0}; \mathrm{IS})$ (fm^4)
$1/2^-_2$	8.86	55 ± 6	$\sim$0
$1/2^-_3$	11.08	35 ± 4	$\sim$0

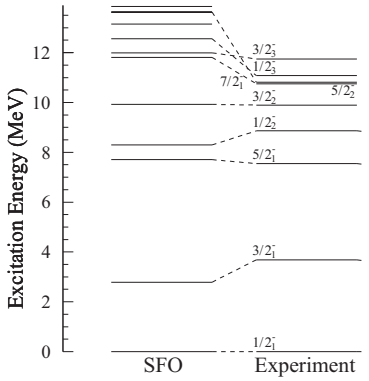

Figure 3. Experimental and theoretical energy level schemes for negative parity states in ^{13}C.

References

[1] K. Ikeda *et al. Prog. Theor. Phys. Suppl. Extra Number* (1968) 464.
[2] H. Morinaga, *Phys. Rev.* **101** (1956) 254.
[3] A. Tohsaki *et al. , Phys. Rev. Lett.* **87** (2001) 192501.
[4] T. Kawabata *et al. , Phys. Rev. C* **70** (2004) 034318.
[5] T. Kawabata *et al. , Phys. Lett. B* **646** (2007) 6.
[6] I. Sugai *et al. , Nucl. Instrum. Methods* **A521** (2004) 227.
[7] F. Ajzenberg-Selove , *Nucl. Phys.* **A506** (1990) 1.
[8] M. N. Harakeh *et al. , Giant Resonance* Clarendon Press, Oxford, (2001).
[9] S. Raman, , *At. Data Nucl. Data Tables* **78** 1 (2001) 1.
[10]T. Suzuki, *et al. ,Phys. Rev. C* **67** (2003) 044302.

Spin-orbit Potential of p+^{6}He Studied with Polarized Proton

S. Sakaguchi, T. Uesaka, T. Wakui[a], T. Kawabata, N. Aoi[b], Y. Hashimoto[c], M. Ichikawa[d], Y. Ichikawa[e], K. Itoh[f], M. Itoh[a], H. Iwasaki[e], T. Kawahara[g], H. Kuboki[e], Y. Maeda,[h], R. Matsuo[d], T. Nakao[e], H. Okamura[i], H. Sakai[e], N. Sakamoto[b], Y. Sasamoto, M. Sasano[e], Y. Satou[c], K. Sekiguchi[b], M. Shinohara[c], K. Suda,[i], D. Suzuki[e], Y. Takahashi[e], A. Tamii[i], K. Yako[e], and M. Yamaguchi[b]

Center for Nuclear Study, Graduate School of Science, University of Tokyo
[a]*Cyclotron and Radioisotope Center, Tohoku University*
[b]*RIKEN (The Institute of Physical and Chemical Research)*
[c]*Department of Physics, Tokyo Institute of Technology*
[d]*Department of Physics, Tohoku University*
[e]*Department of Physics, University of Tokyo*
[f]*Department of Physics, Saitama University*
[g]*Department of Physics, Toho University*
[h]*Kyushu University*
[i]*Research Center for Nuclear Physics, Osaka University*

1. Introduction

Direct reactions induced by polarized protons have revealed various aspects of nuclear structure and reaction mechanisms in the study of stable nuclei. However, there has been no scattering experiment of unstable nuclei and polarized protons until 2003 [1] due to the lack of polarized proton target that can be used in RI beam experiments. In this situation, a solid polarized proton target has been constructed at CNS [2,3]. Applicability of the target in RI beam experiments was realized, for the first time, by its modest operating condition of $B = 0.1$ T and $T = 100$ K.

Making use of the polarized solid proton target, vector analyzing power was measured for the $\vec{p}$+^{6}He elastic scattering at 71 MeV/u. The aim of the measurement is to determine the spin-orbit term in the optical potential of p+^{6}He elastic scattering. Since the spin-orbit interaction is a nuclear surface effect, the shape of spin-orbit potential should be closely related to the surface structure of ^{6}He.

2. Experiment

The experiment was carried out at RIKEN Accelerator Research Facility (RARF) using RIKEN Projectile-fragment Separator (RIPS). A ^{6}He beam was produced through the projectile fragmentation of a ^{12}C beam with an energy of 92 MeV/u bombarded on to a ^{9}Be target. The energy and the typical intensity of the ^{6}He beam were 71 MeV/u and 2.5×10^5 pps, respectively. The purity of the beam was 95%. The spot size on the secondary target was 10 mm FWHM in diameter. The material of the solid polarized proton target was a single naphthalene crystal doped with 0.005 mol% of pentacene. The diameter and the thickness of the crystal were 14 mm and 1 mm, respectively. The number of protons in the target was $4.29 \pm 0.17 \times 10^{21}$ cm^{-2}. The average and the maximum polarization were 13.8% and 20.4%, respectively.

3. Results and Microscopic Calculation

Identification of ^{6}He particles was carried out by the $\Delta E - E$ method. Protons were identified using the correlation between the scattering angle and the total energy. The $\vec{p}$+^{6}He elastic scattering events were selected by requiring kinematical consistency to identified particles. Analyzing power was deduced, canceling spurious asymmetry, by

$$A_y = \frac{1}{\overline{P_y}} \frac{\sqrt{N_L^{\uparrow} N_R^{\downarrow}} - \sqrt{N_R^{\uparrow} N_L^{\downarrow}}}{\sqrt{N_L^{\uparrow} N_R^{\downarrow}} + \sqrt{N_R^{\uparrow} N_L^{\downarrow}}}. \quad (1)$$

Here, $\overline{P_y}$ is the average polarization of the target. N_i^j is the yield where the subscript and the superscript denote a scattering direction and a polarizing direction, respectively. Preliminary results of the differential cross sections and the analyzing powers are shown in Fig. 1 by closed circles. Previously obtained differential cross section data are also plotted by open circles [1] and open squares [4].

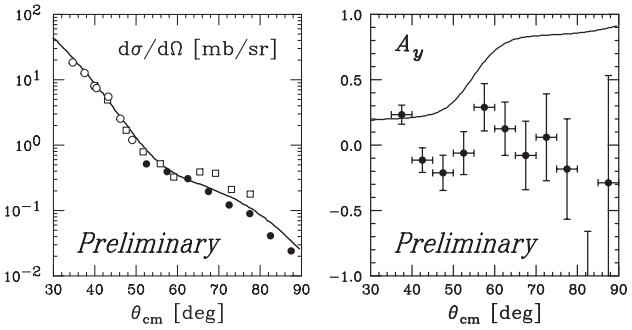

Figure 1. Differential cross sections and analyzing powers for the proton elastic scattering from ^{6}He at 71 MeV/u. See text for details.

Measured differential cross sections and analyzing powers are compared with predictions by microscopic models

based on a g-matrix theory. The analyzing power data exhibit a significant discrepancy with the calculation [5] shown by a solid line in Fig. 1. Calculations based on standard folding model predict positive values in the angular region of $\theta_{CM} < 90^\circ$, while the data take negative values at $\theta_{CM} \approx 50^\circ$ and small absolute values where $\theta_{CM} > 60^\circ$.

4. Phenomenological Optical Model Analysis

For quantitative discussions, we carried out an optical model analysis using phenomenological optical potentials. For the spin-orbit term, we used a Watson-type function:

$$V_{ls}(r) = V_{ls}\left(\frac{\hbar}{m_\pi c}\right)^2 \frac{1}{r_{ls}}\frac{d}{dr} f(r; r_{ls}, a_{ls})(\overrightarrow{\sigma}\cdot\overrightarrow{L}), \quad (2)$$

and also a Thomas-type function:

$$V_{ls}(r) = V_{ls}\left(\frac{\hbar}{m_\pi c}\right)^2 \frac{1}{r}\frac{d}{dr} f(r; r_{ls}, a_{ls})(\overrightarrow{\sigma}\cdot\overrightarrow{L}). \quad (3)$$

Here, $f(r; r_{ls}, a_{ls})$ is a Woods-Saxon type function:

$$f(r; r_{ls}, a_{ls}) = \left[1 + \exp\left(\frac{r - r_{ls}A^{1/3}}{a_{ls}}\right)\right]^{-1}. \quad (4)$$

Figure 2 shows the analyzing power data and fitting results giving the best agreement with the data. Solid and dashsed lines represent the calculations where Watson-type and Thomas-type functions are used, respectively. Preliminarily obtained parameters of the spin-orbit potential are summarized in Table 1.

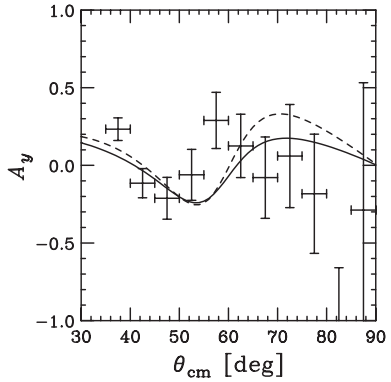

Figure 2. Analyzing power data and fitting results. Solid and dashed lines represent the calculations with Watson-type and Thomas-type functions, respectively.

Parameter	Watson-type	Thomas-type
V_{ls} (MeV)	-1.38	-1.63
r_{ls} (fm)	0.82	0.97
a_{ls} (fm)	1.37	0.96

Table 1. Optical potential parameters giving the best reproduction of the analyzing power data.

Radial shapes of the phenomenological optical potentials are shown in Fig. 3. Real and imaginary parts of central term are shown in the upper panel by solid and dashed lines, respectively. The lower panel shows spin-orbit potentials (solid: Watson-type, dotted: Thomas-type). Watson-type and Thomas-type potentials are consistent in the region of r >1 fm. Microscopically composed spin-orbit potential [6] is also shown by a dashed line in the lower panel of Fig. 3, while this potential does not reproduce the data. Comparison between the phenomenological and microscopic potentials indicates that the spin-orbit potential in ^{6}He should have a long-tail in the region of $r > 2$ or 3 fm for the reproduction of the analyzing power data.

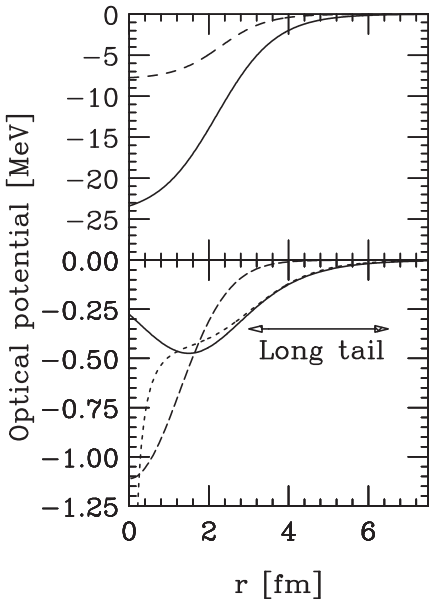

Figure 3. Radial shapes of the phenomenological optical potentials in ^{6}He are shown. Upper and lower panels show a central term and a spin-orbit term, respectively. See text for details.

The unexpected long-tail shape of the spin-orbit potential in ^{6}He may contain important information on the surface structure of the ^{6}He particle, since the spin-orbit interaction is a surface effect. To extract more detailed information, further investigations such as the evaluation of channel coupling effects will be required. Data analysis and theoretical calculations are now in progress.

References

[1] M. Hatano *et al.*, Eur. Phys. J. A **25** (2005) 255.
[2] T. Wakui *et al.*, Nucl. Instrum. and Methods. A **550** (2005) 521.
[3] T. Uesaka *et al.*, Nucl. Instrum. and Methods. A **526** (2004) 186.
[4] A. Korsheninnikov *et al.*, Nucl. Phys. A **617** (1997) 45.
[5] K. Amos, private communication.
[6] Y. Iseri, private communication.

First Production of Spin-polarized ^{17}N Beam using CRIB

K. Shimada[a], D. Nagae[a], K. Asahi[a], T. Arai[a], M. Takemura[a], T. Inoue[a], K. Takase[a], S. Kagami[a], N. Hatakeyama[a], Y. Kobayashi[b], H. Ueno[b], A. Yoshimi[b], D. Kameda[b], T. Nagatomo[b], T. Sugimoto[b], S. Kubono, H. Yamaguchi, Y. Wakabayashi, G. Amadio, S. Hayakawa, J. Murata[c], and H. Kawamura[c]

[a]*Department of Physics, Tokyo Institute of Technology*
[b]*RIKEN Nishina Center*
Center for Nuclear Study, University of Tokyo
[c]*Department of Physics, Rikkyo University*

A beam of radioactive nuclei (RNB) with their spins polarized has been applied to not only studies in nuclear physics but also studies in condensed matter physics. RNBs may even be an exclusive tool for investigating surfaces, layers and nanosized structures, if the energy and spatial distribution of spin-polarized RNBs are controlled with sufficient precision.

One of the most appropriate methods of obtaining such RNBs may be RNB production via inverse-kinematics nucleon-transfer reactions. Spin polarization of a recoil product in a low-energy nucleon-transfer reaction depends on both the recoil angle and the kinetic energy [1]. In the inverse kinematics, by selecting certain regions of the emission angle and the energy, the RNB may be spin-polarized as well as the case of the recoil product.

The angular distribution of the product in the inverse-kinematics reaction is substantially compressed into forward angles, thus facilitating an efficient collection of RNB particles. In addition, the RNB particles can be separated from other species using an in-flight separator. Furthermore, because an experimental site is located far from the production target in our measurements a background radiations originating from the target are reduced.

We are developing a method of producing a spin-polarized ^{17}N ($I^\pi = 1/2^-$, $\mu = 0.352(2)\ \mu_{\rm N}$, $A_\beta = +0.57$, $T_{1/2} = 4.173$ s) beam via the inverse-kinematics reaction using the low-energy in-flight separator CRIB. CRIB consists of a double achromatic system and the Wien filter, and its configuration is shown in Fig. 1. In this experiment the Wien filter was not used. A primary beam of $^{18}O^{7+}$ at 7.0 MeV/u and with an intensity of 240 pnA bombarded a thin Be target of 2.8 mg/cm^2 , which was installed in a target chamber at F0. The ^{17}N beam was produced by nucleon transfer. By limiting the emission angle to $-(0.6°$–$2.8°)$ and the momentum p to 1.84 GeV/c –1.88 GeV/c, the yield of the ^{17}N beam was typically 10^5 cps. Figure 2 (lower part) gives the production yield of ^{17}N beam plotted as a function of the momentum. The β-NMR technique was used to measure the spin polarization P of ^{17}N. The beam was implanted into a single-crystal MgO stopper mounted at the center of the β-NMR system (Fig. 1). A beam-on production time was 6.0 s, which was followed by a beam-off radio-frequency (rf) time of 15 ms for spin manipulation. After the rf time was applied, a β-ray counting time with the beam off was 6.0 s or 10.0 s. A rf oscillating field

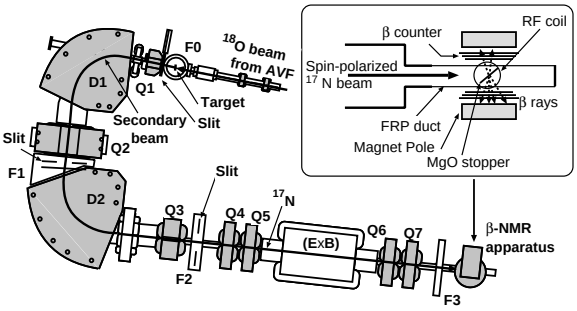

Figure 1. Schematic view of CRIB and β-NMR apparatus.

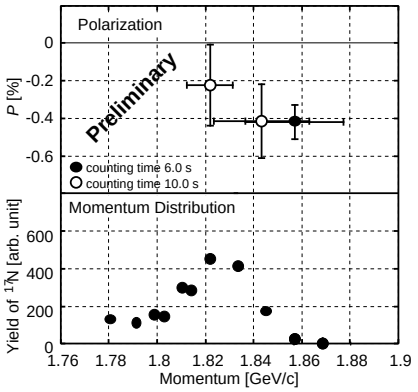

Figure 2. Observed polarization P of ^{17}N. The vertical and horizontal extensions of the data points of P correspond to the uncertainly in P (one standard deviation) and the momentum window, respectively. The observed momentum distribution is also shown.

B_1 was applied perpendicular to an external static magnetic field B_0 which was 707.7 mT . Its frequency and amplitude were 3.798 MHz $\pm$ 1% and 0.2 mT respectively. In the result, the obtained P is shown as a function of momentum of the ^{17}N beam in the upper part of Fig. 2. Maximum $|P|$ obtained in this experiment was 0.42(10)%.

In summary, we succeeded in producing the spin-polarized ^{17}N beam via inverse-kinematics nucleon-transfer reaction.

References

[1] M. Tanaka *et al.*, *Nucl. Phys. A* **263**, 1 (1976).

Experimental Nuclear Physics: PHENIX Experiment at BNL-RHIC

Progress of the PHENIX Experiment and Related Activities in the Year 2006

H. Hamagaki, K. Ozawa, T. Horaguchi, F. Kajihara, T. Gunji, T. Isobe, S.X. Oda, Y. Morino, S. Saito, Y. Aramaki, Y.L. Yamaguchi, S. Sano, J. Kikuchi[a], S. Sugawara[a], Y. Tanaka[b], and T. Fusayasu[b]

Center for Nuclear Study, Graduate School of Science, University of Tokyo
[a] *Advanced Research Institute for Science and Engineering, Waseda University*
[b] *Nagasaki Institute of Advanced Science*

1. Introduction

It is intended in this article to make an overview of the activities of the group whose primary interest is in the study of basic properties of strongly interacting QCD matter.

Current major activity of the group is the international collaborative study at the PHENIX experiment in the Relativistic Heavy Ion Collider (RHIC) of Brookhaven National Laboratory, USA. RHIC is the first collider ever built to find evidence of the phase transition from normal hadronic matter to deconfined quark matter, called quark-gluon plasma (QGP), and to study the properties of the hot QCD matter.

In addition, development of a gaseous detector, named as GEM (Gas Electron Multiplier) has been performed.

2. PHENIX Experiment and RHIC Runs

The CNS group has been participating in the PHENIX experiment as a project supported by the Japan-US cooperation in the field of high energy physics sponsored by MEXT. The PHENIX experiment is one of the major experiments at RHIC, which consists of two central arms (East and West), two muon arms (North and South) and inner detectors for event trigger and event characterization. The PHENIX experiment was designed so as to address as many signatures as possible for QGP formation, by having a very unique capability to measure photons, electrons and muons as well as hadrons.

In the JFY 2006, we have successfully completed the latter half of Run 6, which started in February 2005 and lasted until the end of June 2006, and the first part of Run 7, whose starting date of March 2007 was significantly later than planned because of US-DOE budget problem and will continue until the end of June 2007. Run 6 was totally devoted to polarized p-p collisions. PHENIX accumulated $10.7pb^{-1}$ of p-p collisions at $\sqrt{s}$ = 200 GeV, and run with a lower energy was executed. Only Au+Au collisions is planned for Run 7, and more than four times higher statistics compared to Run 4 will be accumulated.

For this run, two new detectors, HBD and RxNP, were added to the PHENIX experiment. HBD (Hadron Blind Detector) will add high rejection power for Dalitz decay and γ external conversions, which is crucial to access low mass region in the lepton-pairs. A new detector for reaction-plane determination, named as RxNP, will provide higher accuracy for reaction plane determination.

The CNS group has been responsible for operation and calibration of the RICH (Ring Imaging Cherenkov) subsystem, which is a gaseous Cherenkov counter using CO_2 gas as a Cherenkov radiator, and is a primary device for electron identification. It worked without serious problems throughout Run 6, and has been working fine during Run 7.

3. Analysis of the PHENIX Experiment

Major efforts of the CNS group has been on the physics with photons and leptons. Brief introduction is intended in this article as an overview, and details will be described in the following separate articles.

Hard photon production is described well with pQCD calculation, and the high-$p_{\rm T}$ photon yield is expected to be proportional to the number of nucleon-nucleon collisions in the initial stage, which is called $N_{\rm coll}$ scaling. Nuclear effects such as nuclear shadowing and Cronin effect make modifications to this scaling behavior. A PHENIX result on photon yield is consistent with the $N_{\rm coll}$ scaling, which indicates that initial state effects are minor [1]. This result provides strong support to the claim that yield suppression of high-$p_{\rm T}$ hadrons are mainly due to jet quenching effect, that is, energy loss of jet partons in dense medium. Recently, the $p_{\rm T}$ range was successfully extended up to 18 GeV/c. It is surprising that the single-photon yield seems to get suppressed at the highest $p_{\rm T}$ points, deviating from the $N_{\rm coll}$ scaling. The result is described in [2].

Single photon yield in p+p collisions need to be measured with good precision, since it is used as a reference for A-A collisions. In p+p collisions, isolated cut can be used, and the results may provide insight of the production mechanism of single photons. According to a pQCD calculation, a sizeable fraction of photons come from jet-fragmentation process. Status of the analysis is reported in [3].

Sizable yield suppression was found recently for single electrons comparable to the case for light quarks [4]. Single electrons are categorized into two sources; 'photonic' and 'non-photonic'. Main 'non-photonic' sources at the RHIC energies are leptonic decay of charm and bottom mesons. 'Photonic' electrons, majority of which come from Dalitz decay of neutral mesons and external conversion of photons, are severe background sources for measuring 'non-photonic' electrons. The observed large yield suppression of single electron yield is demanding an additional mechanism of energy loss other than gluon bremsstrahlung, which is considered to be a main cause of energy loss for light quarks and gluons. Final results are described in [5].

In order to understand better the energy loss mechanism, it is favorable to determine experimentally the fraction of contributions from charm and bottom quarks. It is shown

through careful simulation studies of electron-hadron correlation in p+p collisions using PYTHIA event generator [6] that the difference of the semi-leptonic decay pattern can be used to to determine the yield ratio between D (charm) and B (bottom) mesons. Current status of the study is described in [7].

The J/ψ yield suppression has been considered to be a key signature of deconfinement of hadronic matter. The CNS group has been taking a leading role in the analysis of J/ψ productions. Final results from the RUN-4 of the J/ψ yield and p_T distribution as a function of centrality in Au-Au have been obtained [8]. Near-final results for Cu + Cu collisions from the Run 5 are also presented [9]. Yield suppression larger than expected from the cold nuclear matter effect obtained from the measurement in d + Au collisions at RHIC [10] is clearly seen in the both cases.

In order to account for centrality dependence of the J/ψ yield in Au + Au collisions, a model is made which is based on the hydro-dynamical model for space-time evolution of the colliding system and sequential melting scheme of J/ψ and excited states of quarkonium [11].

One of the research subjects at RHIC with critical importance is low-mass vector mesons and low-mass lepton-pair continuum. Low-mass vector mesons should provide information relevant to chiral symmetry restoration. Importance of thermal-radiation measurement cannot be over-emphasized. In order to cope with the huge combinatorial background from Dalitz decay and external γ conversion, the HBD detector was installed for RUN-7. Current status of low-mass electron-pairs in Au-Au and Cu-Cu collisions is presented in [12].

In the heavy-ion collisions at RHIC, probability may be sizable of producing exotic nuclear or partonic entities through coalescence of particles both in the partonic and hadronic stages, simply because of large particle density. Abundant strangeness could help producing multi-strangeness hadrons. A search was made for deeply-bound K- nuclei, which was predicted to exist by Yamazaki and Akaishi [13] and is a hot topic in the field of hadron physics. Current status of the search is described in [14].

4. R & D efforts

Development and application of GEM (gas electron multiplier) has been a central R & D subjects of our group in the last few years. GEM, originally developed at CERN [15], has very simple structure having regularly arrayed holes pierced through a polyimide sheet with typical thickness of 50μm with both sides coated by copper foils with thickness of $\sim 5\mu$m which serve as electrodes.

A new GEM was developed which uses a different method for making holes [16], and extensive study of basic performance has been performed.

Recently, a GEM with thickness two to three times thicker than the standard GEM has been developed. Advantage of thicker GEM could be more stable operation with lower operation voltage, since higher gain per unit length is expected. Current status is described in [17].

As an application, development of Cherenkov counter with CsI photo-cathode has been made. A special GEM with additional Ni and Au layers coated on the Cu electrode was needed to prevent Chemical reaction between CsI and Cu. Achievement is described in [18]

GEM is very suited for two-dimensional imaging with X-rays or neutrons. Development of readout circuit with custom ASIC for charge integration has started. Current status is described in [19].

5. Summary and Outlook

In the year 2006, the PHENIX experiment completed Run 6 with p + p collisions at $\sqrt{s_{NN}} = 200$ GeV and $\sqrt{s_{NN}} = 63$ GeV, and have been executing the first half of Run 7 which is dedicated to Au + Au collisions.

The major activities of the CNS groups are presented, which includes data analysis efforts, R & D efforts related to GEM.

In the coming year, efforts are continued on to the PHENIX RUN execution and data analysis. R & D efforts for GEM will also be continued. In addition, active involvement to the ALICE experiment at LHC will be initiated.

References

[1] S.S. Adler, H. Hamagaki, S. Kametani, T. Matsumoto, K. Oyama, K. Ozawa, T. Sakaguchi et al. (PHENIX Collaboration): Phys. Rev. Lett. **94** (2005) 232301.
[2] T. Isobe *et al.*, CNS Annual Report 2006 (2007) 37
[3] T. Horaguchi *et al.*, CNS Annual Report 2006 (2007) 47
[4] S. S. Adler, H. Hamagaki, S. Kametani, T. Matsumoto, K. Oyama, K. Ozawa, T. Sakaguchi et al. (PHENIX Collaboration): Phys.Rev.Lett.96 (2006) 032301.
[5] F. Kajihara *et al.*, CNS Annual Report 2006 (2007) 39
[6] T. Sjostrand, S. Mrenna, and P. Skands: JHEP 05 (2006) 026.
[7] Y. Morino *et al.*, CNS Annual Report 2006 (2007) 49
[8] T. Gunji *et al.*, CNS Annual Report 2006 (2007) 41
[9] S.X. Oda *et al.*, CNS Annual Report 2006 (2007) 43
[10] S.S. Adler, H. Hamagaki, M. Inuzuka, F. Kajihara, S. Kametanai, T. Kawabata, T. Matsumoto, K. Oyama, K. Ozawa, T. Sakaguchi et al. (PHENIX Collaboration): Phys.Rev.Lett.96 (2006) 012304.
[11] T. Gunji *et al.*, CNS Annual Report 2006 (2007) 51
[12] K. Ozawa *et al.*, in this report.
[13] T. Yamazaki and Y. Akaishi: Phys. Rev. C **65** (2002) 044005.
[14] Y. Morino *et al.*, CNS Annual Report 2006 (2007) 45
[15] F. Sauli: Nucl. Instr. and Meth. A 386 (1997) 531.
[16] M. Inuzuka et al.: Nucl. Instr. and Meth. A 525 (2004) 529 – 534.
[17] Y.L. Yamaguchi *et al.*, CNS Annual Report 2006 (2007) 79
[18] Y. Aramaki *et al.*, in this report.
[19] S. Sano *et al.*, CNS Annual Report 2006 (2007) 83

Measurements of Low-Mass Vector Mesons at RHIC

K. Ozawa[a], H. Hamagaki[b], F. Kajihara[b], T. Gunji[b], T. Isobe[b], S.X. Oda[b], Y. Morino[b], Y. Aramaki[b], Y.L. Yamaguchi[b] for the PHENIX collaboration

[a]*Department of Physics, Graduate School of Science, University*
[b]*Center for Nuclear Study, Graduate School of Science, University of Tokyo*

1. Introduction

In 7 years study of hot and dense nuclear matter with Relativistic Heavy Ion Collider (RHIC) at Brookhaven National Laboratory (BNL), many new phenomena have been discovered. The PHENIX experiment produced many new results on a wide range of physics subjects, including charged and neutral hadron production, single electron production, and event isotropy [1].

In spite of these fruitful results, there are still remaining questions to be answered to further characterize the state of matter formed at RHIC. In particular, chiral properties of the dense matter produced has not been obtained. For the study of the chiral properties, $\phi(1020)$ is an interesting meson because the restoration of approximate chiral symmetry at high temperature may modify its mass and width [2]. These modifications can be shown directly in the line shape of the $\phi \longrightarrow e^+e^-$ peak. Here, the measurements with lepton decays are essential, since leptons are not interact with the medium and carry direct information about conditions and properties of the medium. In addition to line shape measurements, the branching fraction of $\phi \longrightarrow K^+K^-$ and $\phi \longrightarrow e^+e^-$ could changed when the ϕ decays in medium [3]. Results on $\phi \longrightarrow K^+K^-$ in Au+Au collisions are already published in Ref. [4] and results on lepton decay channels are waited for a long time.

In this paper, the current results on $\phi \longrightarrow e^+e^-$ in p+p collisions are reported, since measurements in p+p collisions are important as a baseline. The analysis shows t he capability of the PHENIX detector and the baseline of this measurement. Also, an upgrade plan for the PHENIX detector to improve measurements in Au+Au collisions is briefly discussed. Statistics of measurements in Au+Au collisions is currently very poor as shown in Ref. [5] and will be improved using the data in 2007.

2. ϕ meson measurements at PHENIX

The PHENIX experiment is specifically designed to measure low-mass lepton pairs. The current PHENIX detector consists of two central spectrometer arms for detecting electrons. Each central arm covers pseudo-rapidity of $|\eta| < 0.35$, transverse momentum of $p_T > 0.2$ GeV/c, and azimuthal angle of $\delta\phi$=$\pi/2$. Further details of the detector design and performance are given in Ref. [6].

During the fifth running period (Run5), RHIC delivered a luminosity of approximately 3.8 $p\mathrm{b}^{-1}$ to the PHENIX intersection region within a vertex z range ($|z| < 30$ cm). PHENIX successfully accumulated p+p events of 85 $\times 10^{12}$ equivalent at $\sqrt{s} = 200$ GeV.

PHENIX has an excellent electron identification capability that is necessary to separate electrons from the much more abundant charged pions. The RICH provides a threshold selection for electrons and the Electromagnetic Calorimeter (EMC) confirms the matching of the tracked momentum and electromagnetic energy (E/p). Since electrons deposit all of their energy in the EMC, E/p for electrons should be approximately unity. Fig. 1 shows $(E-p)/p/\sigma$ distribution. Here the σ stands for the standard deviation of $(E-p)/p$.

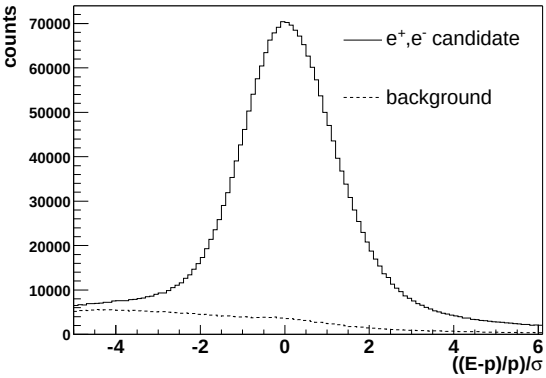

Figure 1. $(E-p)/p/\sigma$ distribution.

Analysis of Run5 data is underway and the first results is appeared using a part of data. Figure 2 shows the e^+e^- invariant mass distribution. The spectrum is fitted by exponential background and Gaussian convoluted Relativistic Breit-Wigner distribution. There is a clear peak around the ϕ mass with a signal strength of $894 \pm 46(\mathrm{stat})$. The mass peak and width values agree with the values from the Particle Data Group and experimental mass resolution. Results shows that PHENIX has enough resolution for the measurement.

In addition to mass shape measurements of ϕ meson, yield measurements are also important. Several efficiencies need to be evaluated to obtain the production cross section of ϕ meson in p+p collisions at $\sqrt{s_{NN}} = 200$ GeV. Especially, PHENIX has a single electron trigger in p+p collisions and the trigger efficiency for ϕ should be evaluated. The trigger required corresponding hits both in RICH and EMC. When one electron or positron from ϕ decay satisfies trigger condition, ϕ meson is triggered. the total trigger efficiency has strong $\mathrm{p_T}$ dependence due to an energy threshold of EMC. Results of yield measurements in p+p collisions will appear soon. Figure 3 shows trigger efficiency for ϕ meson as a function of $\mathrm{p_T}$. Results show that 50% of trigger efficiency is kept even at low $\mathrm{p_T}$ region.

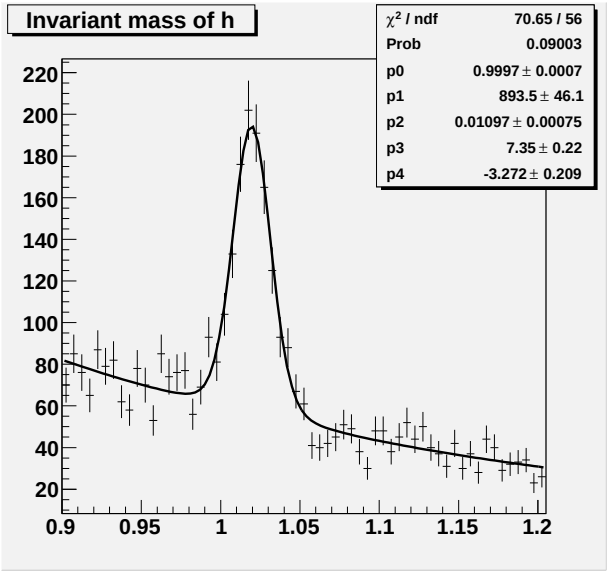

Figure 2. e^+e^- invariant mass distribution in p+p collisions at $\sqrt{s_{NN}} = 200$ GeV in Run5.

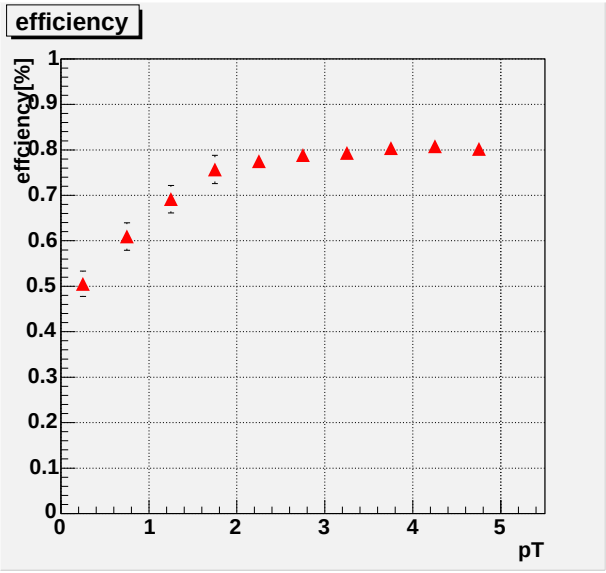

Figure 3. Trigger efficiency for ϕ meson as a function of p_T

3. Hadron Blind Detector

To figure out hot nuclear matter effects on ϕ meson production, the significant improvement of the statistics and the suppression of the combinatorial background are needed in Au+Au data. For the statistics, we are performing a long Au+Au data acquisition period in 2007. In this run, we will have four times more statistics. The suppression of the combinatorial background will be achieved with a newly installed detector, as described below.

To extend the capability of the measurement of lepton pairs, several upgrade projects of the detector are currently underway. The difficulty of the measurement of low mass dileptons comes from the large combinatorial background, which is mainly coming from π^0 Dalitz decays and external conversion of photons. Thus, for this measurement, a Dalitz rejecter with a large rejection power covering a large solid angle is needed.

The proposed Dalitz rejecter is composed of two essential elements; zero magnetic field, and improved electron identification detector. The electron identification detector under zero field conditions eliminates electron-positron pairs from Dalitz decays and gamma conversions, since such pairs have a very small angle and the detector can identify very close two hits.

The zero magnetic field is realized by canceling the magnetic field produced by the outer coils of the PHENIX central magnet with the reverse magnetic field produced by a set of inner coils.

To realize electron identification near the vertex region, a hadron blind detector (HBD), which is a threshold-type Čerenkov counter using CF_4 as a radiator gas [7], is proposed. The detector consists of a 50 cm long radiator, directly coupled in a windowless configuration to a triple GEM detector which has CsI photocathode evaporated on the top face of the first GEM foil, and pad readout at the bottom of the GEM stack [8].

The R&D phase to demonstrate the validity of the HBD concept is complete. A test of a prototype detector was performed at PHENIX using electrons from p-p collisions. The preliminary result of the test showed that electrons produce enough number of photoelectrons. The final detector is installed in PHENIX and operated in 2007. New results with new detector will come soon.

4. Summary

The yield of ϕ mesons are measured for the first time using e^+e^- decay mode in p+p collisions at $\sqrt{s_{NN}} = 200$ GeV. The mass peak and width values agree with the values from the Particle Data Group and experimental resolution.

In the future, a Hadron Blind Detector will be installed in PHENIX that will enhance our capabilities of rejecting external photon conversion and Dalitz pairs, and will result in a significant reduction of the large combinatorial background. This will open up the possibility of studying chiral symmetry restoration as well as thermal di-electrons.

References

[1] K. Adcox *et al.*, nucl-ex/0410003, PHENIX whitepaper
[2] V. Koch, Int. J. Mod. Phys. **E6**, (1997) 203. R. Rapp, Nucl. Phys. **A661**, (1999) 238c
[3] D. Lissauer *et al.*, Phys. Lett. B253, 15 (1991).
[4] S.S. Adler *et al.*, Phys. Rev. C72, (2005) 014903.
[5] K. Ozawa *et al.*, CNS Annual Report 2005 43 (2006).
[6] K. Adcox *et al.*, Nucl. Inst. Meth. **A499**, (2003) 469.
[7] Z. Fraenkel *et al.*, Proposal for a Hadron Blind detector for PHENIX, PHENIX Technical Note **391** (2001).
[8] A. Kozlov *et al.*, Nucl. Inst. Meth.**A523** (2004) 345.

Direct Photon Production in $\sqrt{s_{\rm NN}} = 200$ GeV Au+Au Collisions studied with RHIC-PHENIX

T. Isobe, H. Hamagaki, T. Sakaguchi[a], G. David[a], and B. Sahlmueller[b] for the PHENIX Collaboration

Center for Nuclear Study, Graduate School of Science, University of Tokyo
[a]Brookhaven National Laboratory, USA
[b]University of Muenster, Germany

1. Introduction

Direct photon is a powerful probe to study the initial state of matter created in relativistic heavy ion collisions since photons do not interact strongly once produced. They are emitted in all stages of the collision: in the initial state where photon production can be described by pQCD, in the Quark-Gluon Plasma (QGP), dominated by thermal emission, and in the final hadron-gas phase [1]. In addition, high transverse momentum ($p_{\rm T}$) photons are expected to be produced by the interaction of jet partons with dense matter.

The direct photon yields measured by the PHENIX experiment in the heavy ion collisions during the RHIC-Year2 are in good agreement with a NLO pQCD calculation scaled by the number of binary nucleon-nucleon collisions within experimental errors and theoretical uncertainties [2]. While this suggests that the initial hard scattering probability is not reduced, the result is in contradict to a naive expectation of yield suppression in Au+Au collisions compared to the binary scaled NLO pQCD calculation, since direct photons in the calculation consist of prompt photons produced directly in hard scattering and jet fragmentation photons from hard scattered partons which in turn would be suppressed due to the jet-quenching effect. In order to study this nuclear effect more precisely, direct photon data in p+p collisions with good quality has been desired as a reference.

The PHENIX experiment [3] is capable of measuring photons with two types of highly segmented electromagnetic calorimeters (EMCal) [4]. One is a lead scintillator sampling calorimeter (PbSc), and the other is a lead glass Cherenkov calorimeter (PbGl).

For the measurement of direct photons presented here, the conventional subtraction method has been used. π^0 and η mesons are reconstructed via their two-photon decay mode. The decay background photons were estimated based on the measured π^0 and η spectra. The $p_{\rm T}$ spectra of direct photons are obtained by subtracting the spectra of decay photons from the $p_{\rm T}$ spectra of inclusive photons. The details of the direct photon measurement is found in [5].

The direct photon spectra in $\sqrt{s} = 200$ GeV p+p collisions based upon RHIC-Year3 data have been published in [6]. The data are consistent with the NLO pQCD calculation within the uncertainties. The new large amount of data in RHIC-Year5 ($\int Ldt$ = 3.8 pb^{-1}) makes it possible to extend the $p_{\rm T}$ range of the direct photon cross-section, and provides a good reference to evaluate the nuclear modification on direct photon production in Au+Au collisions.

2. Direct Photon Spectra

PHENIX recorded high-statistics Au+Au data in RHIC-Year4 ($\int Ldt$ = 241 μb^{-1}). The new data allow us to measure direct photons and to evaluate their nuclear modification up to very high-$p_{\rm T}$. Owing to the strong suppression of neutral hadrons in heavy ion collisions [7], the signal-to-noise ratio of direct photons improves significantly at high-$p_{\rm T}$ ($p_{\rm T} > 5$ GeV/c). The direct photon excess ratio ($R = \gamma_{\rm all}/\gamma_{\rm bg}$) is about 3 at $p_{\rm T} = 10$ GeV/c in the most central (0-10 %) Au+Au collisions. Figure 1 shows direct photon spectra as a function of $p_{\rm T}$ for nine centralities and minimum-bias of Au+Au collisions at $\sqrt{s_{\rm NN}} = 200$ GeV. The spectra shown here are obtained using only the PbSc calorimeter. The solid curves show the binary scaled fit to the RHIC-Year5 p+p direct photon preliminary data.

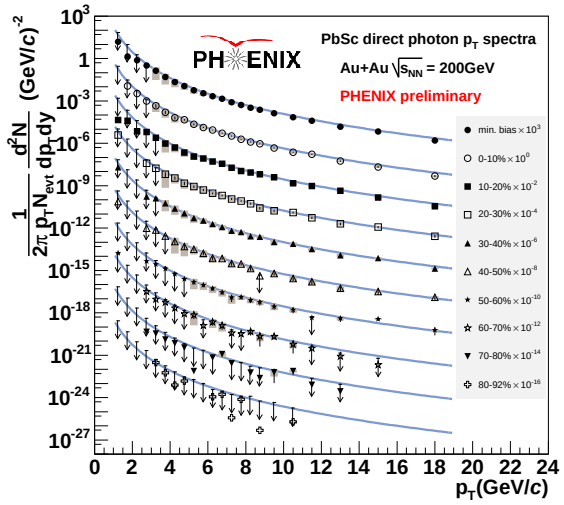

Figure 1. Direct photon invariant yields as a function of $p_{\rm T}$ for nine centrality selections and minimum bias Au+Au collisions at $\sqrt{s_{\rm NN}} = 200$ GeV. In addition to the statistical and $p_{\rm T}$-uncorrelated errors, $p_{\rm T}$-correlated errors are shown on the data points as boxes. Arrows indicate measurements consistent with zero yield with the tail of the arrow indicating the 90 % confidence level upper limit. The solid curves are binary scaled p+p direct photon parameterizations.

3. Nuclear Modification Factor for Direct Photon

The amount of nuclear modification can be quantified using a nuclear modification factor ($R_{\rm AA}$). $R_{\rm AA}$ is the ratio between the measured yield and the expected yield from

the p+p result, and is defined as

$$R_{\rm AA}({\rm p_T}) = \frac{d^2N^{\rm AA}/d{\rm p_T}dy}{\langle T_{\rm AA}(b)\rangle\, d^2\sigma^{\rm pp}/d{\rm p_T}dy}, \qquad (1)$$

where the numerator is the invariant direct photon yield per unit rapidity in Au+Au collisions and the denominator is the expected yield from p+p collisions scaled by the nuclear overlapping function ($\langle T_{\rm AA}(b)\rangle = \langle N_{\rm coll}(b)\rangle / \sigma_{\rm pp}$) in Au+Au. If the reaction is just the superposition of hard scatterings, unmodified by nuclear effects, the factor $\rm R_{AA}$ is unity.

Figure 2 shows $\rm R_{AA}$ of direct photons as a function of $p_{\rm T}$ in the most central (0-10 %) Au+Au collisions at $\sqrt{s_{\rm NN}} =$ 200 GeV. While $\rm R_{AA}$ of direct photons is consistent with unity at $p_{\rm T} < 14$ GeV/c, it seems to be below unity at very high-$p_{\rm T}$ ($p_{\rm T} > 14$ GeV/c).

A few possible factors would contribute to this yield suppression at high-$p_{\rm T}$. An initial state effect which is expected to contribute to the suppression at high-$p_{\rm T}$ is the so-called isospin effect. The parton distribution function (PDF) of constituent quarks of a proton (*uud*) is different from these of neutrons (*udd*), then the direct photon production in Au+Au collisions can not be represented completely only with the binary scaled p+p collisions. According to the NLO pQCD calculation, the magnitude due to this effect is obtained from the superposition of cross-section in p+p, p+n and n+n collisions, and estimated to be ~ 0.8 at $p_{\rm T}$ = 20 GeV/c,

In addition to the isospin effect, the violation of binary scaling due to jet quenching of partons prior to its fragmentation is also possible. As described before, direct photons in NLO pQCD are composed of "prompt" photons produced directly in hard scattering and jet "fragmentation" photons from hard scattered partons, which would be suppressed due to the jet-quenching effect. On the assumption of similar suppression of fragmentation photon yield with hadron yield, the $\rm R_{AA}$ of direct photon in the most central Au+Au collisions is estimated to be ~ 0.75, which would be more suppressed if the isospin effect is also taken into account.

However, the relative yield of fragmentation photons with respect to prompt photons are expected to be larger at medium-$p_{\rm T}$ region according to the NLO pQCD calculation. Thus, the suppression of direct photon yield is expected to be larger at medium-$p_{\rm T}$ region, and an explanation why $\rm R_{AA}$ is not suppressed at the medium-$p_{\rm T}$ region is needed. One possible effect is conversion, often referred as jet-photon conversion, which produces photons via Compton-like scattering of the jet partons with slow partons in the hot medium [8]. The agreement with NLO pQCD calculations can just be an accidental coincidence caused by mutually counterbalancing effects of jet-photon conversion and energy loss of jet partons themselves. While theorists try to reproduce the direct photon $\rm R_{AA}$ [10, 9], none of them have been successful in reproducing completely the data.

In order to measure $\rm R_{AA}$ of direct photons more precisely at very high-$p_{\rm T}$, it is necessary to measure high-$p_{\rm T}$ direct photon with the PbGl calorimeter. The main source of the systematic error on the high-$p_{\rm T}$ direct photon measurement is the correction for shower merging effect, where two photons from same π^0 would merge due to the finite EMCal tower size. Thus, the PbGl calorimeter has better granularity than PbSc, and the error due to this effect would be improved .

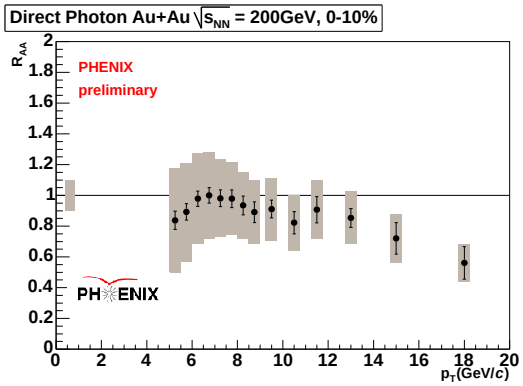

Figure 2. Direct photon $\rm R_{AA}$ measured with PbSc as a function of $p_{\rm T}$ in the most central (0-10 %) collisions compared with theoretical calculations [9, 10]. For comparison, $\rm R_{AA}$ using NLO pQCD calculation is shown as dotted line. In addition to the statistical and $p_{\rm T}$-uncorrelated errors, $p_{\rm T}$-correlated errors are shown on the data points as boxes, and an overall systematic error of $\rm T_{AA}$ normalization is shown at 1.

4. Summary

The measurements of high-$p_{\rm T}$ direct photons in Au+Au collisions at $\sqrt{s_{\rm NN}} = 200$ GeV are presented. The direct photon signal is extracted as a function of the Au+Au collision centrality and $\rm R_{AA}$ is calculated using the p+p direct photon data. The $\rm R_{AA}$ of very high-$p_{\rm T}$ direct photon seems to be below unity in the most central collisions.

References

[1] S. Turbide, R. Rapp and C. Gale *Phys. Rev.* C **69** (2004) 014903.
[2] S.S. Adler *et al. Phys. Rev. Lett.* **94** (2005) 232301.
[3] K. Adcox *et al. Nucl. Instr. and Meth.* A **499** (2003) 469.
[4] L. Aphecetche *et al. Nucl. Instr. and Meth.* A **499** (2003) 521.
[5] T. Isobe *et al.* CNS Annual Report **05** (2006) 51.
[6] S.S. Adler *et al. Phys. Rev. Lett.* **98** (2007) 012002.
[7] S.S. Adler *et al. Phys. Rev. Lett.* **91** (2003) 072301.
[8] R.J. Fries, B. Müller and D.K. Srivastava *Phys. Rev.* C **72** (2005) 041902.
[9] S. Turbide, C. Gale, S. Jeon and G.D. Moore *Phys. Rev.* C **72** (2005) 014906.
[10] F. Arleo *JHEP* **0609** (2006) 015.

Heavy Quark Measurement by Single Electrons in $\sqrt{s_{NN}}$ = 200 GeV Au+Au Collisions[†]

F. Kajihara, Y. Akiba[a], R. Averbeck[b], A. Dion[b], T. Gunji, H. Hamagaki, and K. Ozawa, for the *PHENIX* Collaboration

Center for Nuclear Study, Graduate School of Science, the University of Tokyo
[a]*RIKEN (The Institute of Physical and Chemical Research), Wako, Saitama*
[b]*Department of Physics and Astronomy, Stony Brook University, SUNY, Stony Brook, NY, USA*

1. Introduction

Strong suppressions of π^0 and the other light hadrons at high transverse momentum ($p_{\rm T}$) have been observed in high-energy heavy-ion collisions at the Relativistic Heavy Ion Collider (RHIC) [1,2,3]. The suppression is due to significant energy loss of partons through an extremely dense matter created in the collisions. Further insight into properties of the produced medium can be gained from the production and propagation of heavy quarks (charm or bottom). In heavy ion collisions, the total yield of heavy-flavor decay electrons has been found to scale with the number of nucleon-nucleon collisions [4]. Energy loss via gluon radiation is expected to be reduced for quarks with larger mass due to suppression of the forward radiation [5]. Consequently, smaller high-$p_{\rm T}$ suppression is expected for charm and bottom quarks compared to light quarks, with the absolute values and their $p_{\rm T}$ dependences being sensitive to the properties of the medium.

2. Experiment and Analysis

The PHENIX experiment took high statistic data at $\sqrt{s_{\rm NN}} = 200$ GeV in Run-4 Au + Au collisions (2004). Electrons ($e^{\pm}$) in $0.3 < p_{\rm T}^e < 9.0$ GeV/c were measured by central arm detectors, each covering azimuthal angle $\Delta\phi = \pi/2$ and pseudo-rapidity $|\Delta\eta| < 0.35$ [6]. Reconstruction of charged tracks required the hit information of Drift Chambers and Pad Chambers. Electrons were identified with Ring-Imaging Čerenkov Counters and ElectroMagnetic Calorimeters. All measured electrons can be categorized into two groups: *photonic* and *nonphotonic*. Photonic electrons are mainly generated from photon-conversions and Dalitz decays of mesons such as π^0 and η, while signal electrons from open charm/bottom decays are dominant sources of nonphotonic electrons. Two methods were applied to extract nonphotonic electrons [4, 7]. The first one is called "*cocktail subtraction*" method. In this method, all possible photonic electron components are reconstructed using a hadron-decay simulator on the basis of measured π^0 spectra [1,3], and are subtract them from the inclusive electron spectrum. Cocktail method is effective to count signal electrons at high-$p_{\rm T}^e$, where the signal to background ratio is large. The second one is "*converter subtraction*" method. In the experiment, special runs were performed with a photon converter, a brass sheet (1.68 % radiation length) around the beam pipe. The photon converter enhances the only electron yield produced by external photon conversion ($P(p_{\rm T}^e)$) by a certain amount. The ratio of photonic electron yield with/without the converter is defined as R_γ, which can be evaluated within 3% systematic error by a GEANT-based Monte-Carlo simulation. The measured inclusive electron yield $I(p_{\rm T}^e)$ is given as $I(p_{\rm T}^e) = P(p_{\rm T}^e) + N(p_{\rm T}^e)$ without the converter and $I'(p_{\rm T}^e) = R_\gamma \cdot P(p_{\rm T}^e) + N(p_{\rm T}^e)$ with the converter. Nonphotonic electron yield ($N(p_{\rm T}^e)$) is obtained by solving these relations. Backgrounds in the nonphotonic electrons are mainly produced from weak decays of Kaon (K_{e3}), vector meson decays and Drell-Yan processes. Kaon contributes less than 10 % at $p_{\rm T}^e = 0.5$ GeV/c compared to photonic electron yields, while vector mesons are very small, and Drell-Yan process is negligible in the $p_{\rm T}^e$ range of our measurement. Backgrounds from Kaon and vector mesons are evaluated utilizing the data measured by the PHENIX.

3. Results

The resulting invariant differential yields of heavy-flavor decay electrons in Au + Au collisions are shown in Fig. 1. To quantify the suppression, the nuclear modification factor, $R_{\rm AuAu}(p_{\rm T}^e)$ is shown in Fig. 2.

$$R_{\rm AuAu}(p_{\rm T}^e) = \frac{dN^e_{\rm AuAu}/dp_{\rm T}^e}{\langle N_{\rm coll}\rangle \times dN^e_{pp}/dp_{\rm T}^e} \quad (1)$$

$$= \frac{dN^e_{\rm AuAu}/dp_{\rm T}^e}{\langle T_{\rm AuAu}\rangle \times d\sigma^e_{pp}/dp_{\rm T}^e}. \quad (2)$$

Here, σ^e_{pp} is the cross section of heavy-flavor decay electrons in p + p collisions [7], $\langle N_{\rm coll}\rangle$ is the number of binary collisions of partons, and $\langle T_{\rm AuAu}\rangle$ is the nuclear thickness function for Au + Au and $\langle N_{\rm coll}\rangle = \langle T_{\rm AuAu}\rangle \times \sigma^e_{pp}$. Very strong suppression is clearly seen at high-$p_{\rm T}^e$ in central collisions (centrality class: 0-10 %), comparable to the suppression observed for π^0 [1,3]. A perturbative QCD calculation with radiative energy loss is shown (curve I) [8], but it is known that this model overestimates the observed elliptic flow (v_2) of heavy-flavor electrons. A calculation including elastic scattering mediated by resonance excitation is also shown (curve II) [9]. This result is achieved with short thermalization time (τ) of heavy quarks, which is translated into a diffusion coefficient $D_{\rm HQ} \times (2\pi T) = 4-6$ in this model. Energy loss is calculated in terms of $D_{\rm HQ}$ as well (curve III) in [10]. These calculations suggest that small τ is required to reproduce the data. Figure 3 shows $R_{\rm AuAu}$ as a function of the number of participant ($N_{\rm part}$). For $p_{\rm T}^e > 0, 3$

[†]Published as A. Adare *et al.*, Phys. Rev. Lett. 98, 172301 (2007).

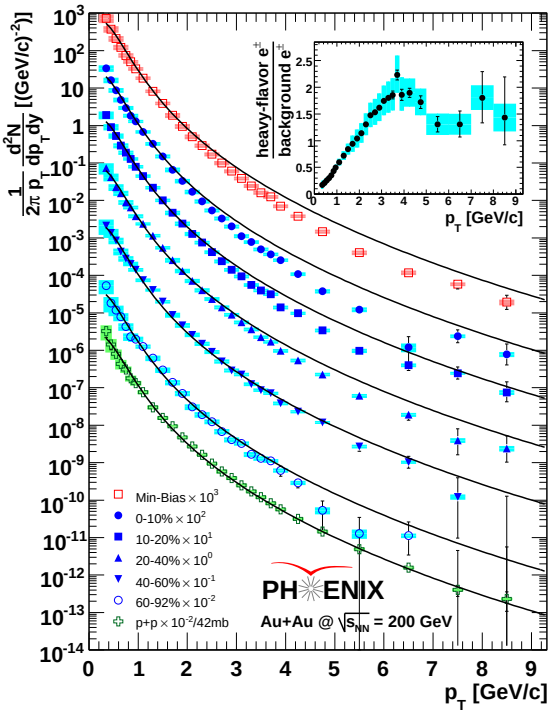

Figure 1. Invariant yields of electrons from heavy-flavor decays for different Au + Au centrality classes and for $p + p$ collisions, scaled by powers of ten for clarity. The solid lines are the result of a fixed-order-plus-next-to-leading-log (FONLL) pQCD calculation [11] normalized to the $p + p$ data and scaled with $\langle T_{\rm AuAu} \rangle$ for each Au + Au centrality class. The insert shows the ratio of heavy-flavor to background electrons for minimum bias Au + Au collisions. Error bars (boxes) depict statistical (systematic) uncertainties.

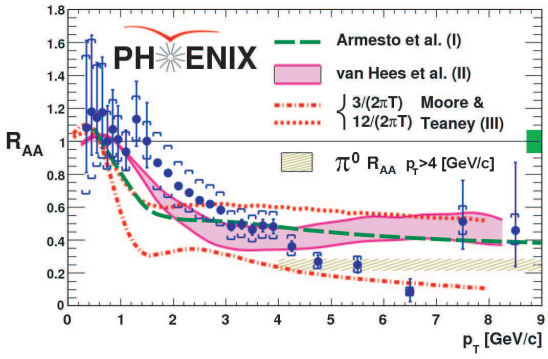

Figure 2. $R_{\rm AuAu}$ of heavy-flavor decay electrons in Au + Au collisions for 0–10% centrality class, compared with π^0 data and model calculations. The box at $R_{\rm AuAu} = 1$ shows the uncertainty in $\langle T_{\rm AuAu} \rangle$.

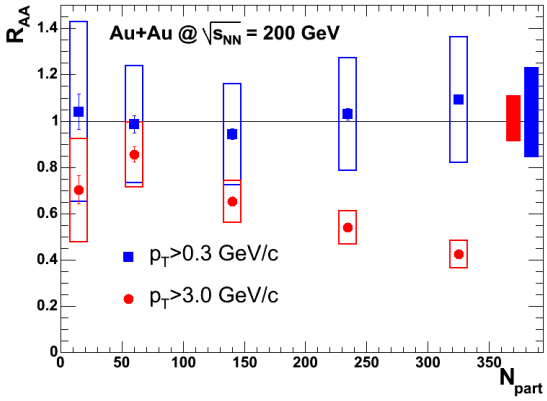

Figure 3. $R_{\rm AuAu}$ of heavy-flavor decay electrons with $p_{\rm T}^e$ above 0.3 and 3 GeV/c as a function of centrality given by $N_{\rm part}$. Error bars (brackets) depict statistical (point-by-point systematic) uncertainties. The right (left) box at $R_{\rm AuAu} = 1$ shows the relative uncertainty from the $p + p$ reference common to all points for $p_{\rm T}^e > 0.3$ (3) GeV/c.

GeV/c, $R_{\rm AuAu}$ is close to unity for all $N_{\rm part}$, which indicates binary scaling of the total heavy-flavor yield works. For $p_{\rm T}^e > 3$ GeV/c, the $R_{\rm AuAu}$ decreases systematically with $N_{\rm part}$. These behaviors reflect the observed strong suppression at high-$p_{\rm T}^e$ in central collisions.

4. Summary and Outlook

In conclusion, electrons from semileptonic decays of heavy quarks have been measured for $0.3 < p_{\rm T}^e < 9.0$ GeV/c in Au + Au collisions at $\sqrt{s_{NN}} = 200$ GeV. $R_{\rm AuAu}$ shows a very strong suppressive effect. The result suggests very high dense medium is created so that even heavy quarks lose their energy. To understand it more clearly, we need to separate the contributions from charm or bottom in the future experiment. The mass difference will provide more information on the energy-loss mechanism in the high dense matter.

References

[1] S. S. Adler *et al.*, Phys. Rev. Lett. **91**, 072301, (2003).
[2] J. Adams *et al.*, Phys. Rev. Lett. **91**, 172302, (2003).
[3] S. S. Adler *et al.*, Phys. Rev. Lett. **96**, 202301, (2006).
[4] S. S. Adler *et al.*, Phys. Rev. Lett. **95**, 082301, (2005).
[5] Y. L. Dokshitzer *et al.*, Phys. Lett. **B519**, 199, (2001).
[6] K. Adcox *et al.*, Nucl. Instrum. Meth. A**499**, 469, (2003).
[7] A. Adare *et al.*, Phys. Rev. Lett. **97**, 252002, (2006).
[8] N. Armesto *et al.*, Phys. Lett. **B637**, 362 (2006)
[9] H. van Hees *et al.*, Phys. Rev. **C73**, 034913 (2006)
[10] G. D. Moore *et al.*, Phys. Rev. **C71**, 064904 (2005).
[11] M. Cacciari *et al.*, Phys. Rev. Lett. **95**, 122001, (2005).

Measurement of $J/\psi \to e^+e^-$ in Au+Au Collisions at $\sqrt{s_{NN}}$ = 200 GeV at RHIC-PHENIX

T. Gunji, H. Hamagaki, K. Ozawa, Y. Akiba[a], C.L. Silva[b], X. Wei[c], for the PHENIX collaboration

Center for Nuclear Study, Graduate School of Science, University of Tokyo, Japan
[a] *RIKEN (The institute of Physics and Chemical Research), Japan*
[b] *Universidade de São Paulo, Instituto de Física, Brazil*
[c] *RIKEN BNL Research Center, Brookhaven National Laboratory, USA*

1. Introduction

It is predicted by the lattice Quantum ChromDynamics (QCD) calculations that there is a phase transition from ordinary nuclear matter to the deconfined state composed of quarks and gluons, called Quark-Gluon-Plasma (QGP), at high temperature ($T_c \sim 170$ MeV) [1]. Relativistic heavy ion collisions provide the unique opportunity to realize such a phase transition in the laboratory and to study the detail properties of QGP.

Suppression of the J/ψ yield in heavy ion collisions has been considered as one of the unambiguous signatures of the formation of QGP, since J/ψ is expected to melt in QGP due to the color Debye screening effect [2].

There have been two scenarios proposed for the J/ψ production in heavy ion collisions. The first scenario is based on the substantial charmonium dissociation due to gluons and comoving particles supplemented with the regeneration of J/ψ due to $c\bar{c}$ recombination. The second scenario is based on the sequential melting of the charmonia [7]. Recent quenched lattice QCD calculations show that the melting temperature of J/ψ would be $\sim 2T_c$ while χ_c and ψ' would melt just above T_c [8, 9]. This leads to the J/ψ suppression first from the absence of the feed down to J/ψ from χ_c and ψ' due to their melting at lower temperature, and second from the directly produced J/ψ [10].

Besides these effects, cold nuclear matter effects (CNM) such as nuclear absorption and gluon shadowing are expected to modify the J/ψ production in heavy ion collisions. Therefore it is very important to study J/ψ production as functions of collision systems, collision energies, collision species, rapidity, and transverse momentum p_T.

2. Data analysis

The PHENIX experiment recorded the integrated luminosity of $\sim$ 240 μb^{-1} in Au+Au collisions at the center of mass energy per nucleon pairs ($\sqrt{s_{NN}}$) of 200 GeV in 2004.

The PHENIX experiment consists of two central arm spectrometers, each of which covers the pseudo-rapidity range $|\eta| < 0.35$ and 90 degrees in azimuthal angle, and two forward spectrometers covering $1.2 < |\eta| < 2.4$ with full azimuthal acceptance [11]. The central arm spectrometers are composed of Drift Chambers (DC), Pad Chambers (PC), Ring Imaging Cerenkov Counters (RICH) and two types of Electromagnetic Calorimeters (EMCal). Electrons are identified by matching the charged tracks to the clusters in EMCal and to the rings in RICH.

J/ψ yield is obtained from the e^+e^- invariant mass spectrum after subtracting combinatorial background using an event mixing method. The numbers of reconstructed J/ψ's are $\sim$1000 in Au+Au collisions. The invariant J/ψ yield is extracted by correcting the number of recorded events, the acceptance of e^+e^- pairs from J/ψ and efficiency of the spectrometers for the electron identification [12].

3. Results

Nuclear modification factor, R_{AA}, is a useful variable to quantify the nuclear effects in A+A collisions compared to that in $p+p$ collisions, which is defined as follows:

$$R_{AA}(b) = \frac{dN/dy_{AA}(b)}{dN/dy_{pp}\langle N_{col}(b)\rangle}, \qquad (1)$$

where $dN/dy_{AA}(b)$ and dN/dy_{pp} correspond to the yield in A+A and $p+p$ collisions, respectively, and $\langle N_{col}(b)\rangle$ is the average number of nucleon-nucleon collisions for a given impact parameter of b. Figure 1 shows R_{AA} in Au+Au collisions at mid-rapidity as a function of the number of participant nucleons N_{part}, where the expected R_{AA} due to the CNM effects are shown for the case of the nuclear absorption cross section (σ_{abs}) of 0, 1, and 2 mb as solid, dashed and dotted lines, respectively [13]. R_{AA} due to the CNM effects is estimated from the measured J/ψ suppression in d+Au collisions at RHIC energy,

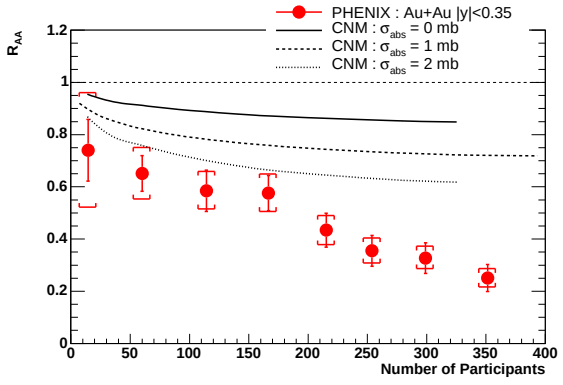

Figure 1. R_{AA} as a function of the number of participants. Solid, dashed and dotted lines are the expected R_{AA} due to the CNM effects with the nuclear absorption cross section (σ_{abs}) of 0, 1, and 2 mb, respectively. Bars and brackets are correlated and non-correlated errors with respect to the N_{part}, respectively.

where σ_{abs} is constrained to be less than 2 mb from experimental data [14]. Errors shown in Fig. 1 are grouped into two categories. Bars are the point-to-point non-correlated errors for which the points can move independently one from the other. Brackets are the point-to-point correlated errors for which the points can move coherently. It is clearly shown that the J/ψ suppression in Au+Au collisions is stronger than the expectations from CNM effects.

Figure 2 shows the comparison of R_{AA} in Au+Au collisions to the models involving dissociation of J/ψ by thermal gluons and recombination of J/ψ from $c\bar{c}$ pairs [3, 4], where dashed, dotted and solid lines correspond to the contribution of dissociation, recombination and sum of these two processes, respectively. The magnitude is reproduced better when the recombination is included, but the trend of R_{AA} can not be reproduced well.

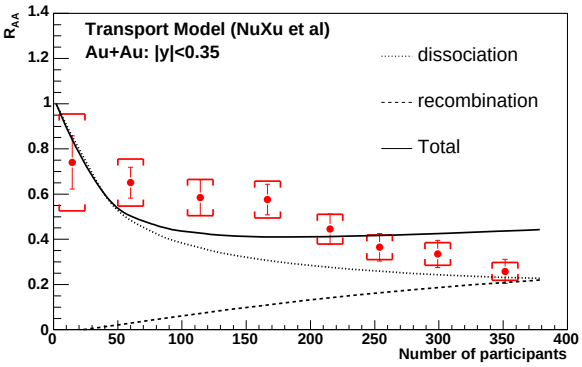

Figure 2. Comparison of J/ψ R_{AA} to that expected from the dissociation by the thermal gluons and the recombination of J/ψ from initially produced $c\bar{c}$ pairs [3].

To define the experimental survival probability in hot and dense medium, R_{AA} was divided by that expected from CNM effects (R_{AA}/CNM), where R_{AA} with σ_{abs} of 1 mb was used as CNM effects. Figure 3 shows R_{AA}/CNM as a function of the Bjorken energy density in Pb+Pb and In+In collisions at SPS energy ($\sqrt{s_{NN}} = 17.3$ GeV) and Au+Au collisions at RHIC [15]. J/ψ suppression at SPS can be interpreted as the melting of only χ_c and ψ' and associated feed down to J/ψ. It is seen that J/ψ suppression at RHIC is comparable below the Bjorken energy density of 4 GeV/fm^3 and and stronger for more than the Bjorken energy density of 4 GeV/fm^3, which suggests the melting of directly produced J/ψ in central Au+Au collisions. Quantitative study of the sequential melting of J/ψ in evolving quark-gluon-fluid has been developed by the authors and is reported in Ref. [16].

4. Summary

J/ψ production at mid-rapidity in Au+Au collisions has been measured using e^+e^- decay channel at RHIC-PHENIX. It is shown that J/ψ production is suppressed by a factor of 4 in central Au+Au collisions and the suppression is beyond the cold nuclear matter effects. The destruction of J/ψ by thermal gluon predicts stronger suppression, and a magnitude of the suppression is compatible with the

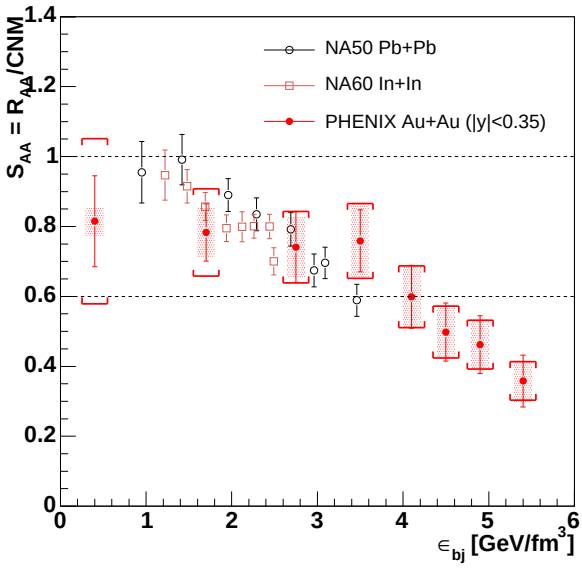

Figure 3. Experimental survival probability of J/ψ in the medium as a function of the Bjorken energy density at RHIC energy and at SPS energy [15].

inclusion of recombination. However, the trend is still not well reproduced and further investigation of the charm production and transport in QGP will be necessary. R_{AA}/CNM at RHIC energy shows the J/ψ suppression around mid-central Au+Au collisions is comparable with that at SPS energy and is stronger in central Au+Au collisions, which may suggest the melting of directly produced J/ψ.

References

[1] T. Hatsuda, hep-ph/0702293.
[2] T. Matsui and H. Satz, Phys. Lett. **B 178**, (1986) 416.
[3] L. Yan, P. Zhuang, and N. Xu, Phys. Rev. Lett. **97**, 232301 (2006).
[4] R. Rapp, Eur. Phys. J. **C43**, 91 (2005).
[5] R. Thews, Nucl.Phys. **A783**, 301 (2007).
[6] A. Andronic *et al.*, nucl-th/0701079.
[7] F. Karsch, D. Kharzeev, and H. Satz, Phys. Lett. **B637**, 75 (2006).
[8] M. Asakawa and T. Hatsuda, Phys. Rev. Lett. **92**, 012001 (2004).
[9] S. Datta *et al.*, Phys. Rev. **D69**, 094507 (2004);
[10] H. Satz, Nucl. Phys. **A783**, 249 (2007).
[11] K. Adcox, *et al.*, (PHENIX Collaboration), Nucl. Instr. and Meth. **A 499** (2003) 469.
[12] A. Adare *et al.* (PHENIX Collaboration), nucl-ex/0611020.
[13] R. Vogt, Acta Phys. Hung. **A25**, 97 (2006).
[14] S. S. Adler *et al.*, Phys. Rev. Lett **96**, 012304 (2006).
[15] T. Gunji (PHENIX Collaboration), nucl-ex/0703004.
[16] T. Gunji, *et al.*, CNS Annual Report 2006 (2007) 51

Measurement of J/ψ via Di-electron Decay in Cu+Cu Collisions at RHIC-PHENIX

S.X. Oda, H. Hamagaki, K. Ozawa, Y. Akiba[a], K. Das[b], A.D. Frawley[b], and W. Xie[c], for the PHENIX collaboration

Center for Nuclear Study, Graduate School of Science, University of Tokyo
[a]RIKEN(The Institute of Physics and Chemical Research)
[b]Florida State University
[c]RIKEN BNL Research Center, Brookhaven National Laboratory

1. Introduction

High-energy heavy ion collision experiments are performed to create and study the quark gluon plasma (QGP). $J/\psi(3097)$ meson will dissociate in the hot QGP by the color Debye screening and its yield will be suppressed [1]. Therefore, J/ψ has been considered as one of the most promising probes of the QGP for twenty years. However, the yield will be modified by other processes such as cold nuclear matter effects [2, 3], feed down from the excited charmonium states (ψ' and χ_c) and bottom quarks [4], and recombination of initially uncorrelated charm quarks [5, 6]. To disentangle these effects, one needs to study the J/ψ production with several system sizes and energy densities. J/ψ has di-lepton (e^+e^-, $\mu^+\mu^-$) decay channels and the leptons have the advantage that they are experimentally easily identified.

2. Experiment and analysis

The PHENIX experiment at RHIC collected ^{63}Cu+^{63}Cu collision data in 2005 to study the dependence on the collision species and energies. The center of mass energies per nucleon pair were $\sqrt{s_{NN}}$=200 and 62.4 GeV, and those integrated luminosities were 3.06 nb^{-1} and 0.19 nb^{-1}, respectively. The advantage of light Cu ions is that one can obtain precise data at the small number of participants, $N_{part} < 100$, with high luminosity.

The analysis of 200-GeV Cu+Cu data is ongoing and the current results are presented in this report.

J/ψ is measured at mid rapidity ($|y| < 0.35, \Delta\phi = 90^\circ \times 2$) by the di-electron decay channel ($BR = 5.94\%$) and at forward rapidity by di-muon (5.93%).

The collision vertex and centrality, which corresponds to the impact parameter, of an event are determined by beam-beam counters (BBC) in the Cu+Cu collisions. The z-coordinate (beam direction) of collision vertex is required to be located at the detector center within $\pm$30 cm. The BBC trigger efficiency of an inelastic Cu+Cu collision is estimated to be $94 \pm 2\%$. The number of nucleon-nucleon collisions, N_{coll}, and N_{part} are estimated by Monte Carlo Glauber calculation. In a peripheral collision, the number of charged particles is small and there is a large ambiguity in centrality determination. Therefore, the maximum number of centrality bins would be seven (0–10, 10–20, $\cdots$, 50–60 and 60–94%) for 200-GeV Cu+Cu collisions.

Charged particle tracks at mid rapidity are measured by drift chambers (DC) and pad chambers (PC). The tracking codes were carefully checked to improve reliability.

Ring imaging Cherenkov counters (RICH) detect Cherenkov photons emitted from electrons. The number of hit photo tubes in the ring region of an electron candidate is required to be greater than one.

Information of electromagnetic calorimeters (EMC) is used for track (in two directions, z and ϕ) and energy matching for electron identification. Since the effect of the stray magnetic field is not well taken into account in the PHENIX tracking, track matching parameter calibration was needed. The ratio of the EMC energy to the track momentum, $E/p \sim 1$, is used for electron identification. Since the E/p value has the momentum dependence, calibration for the energy matching parameter was also needed. The recalibration was performed so that the three matching parameters have standard normal distributions. $\pm 4\sigma$ cuts for z and ϕ directions and a $> -2\sigma$ cut for energy are used in the analysis.

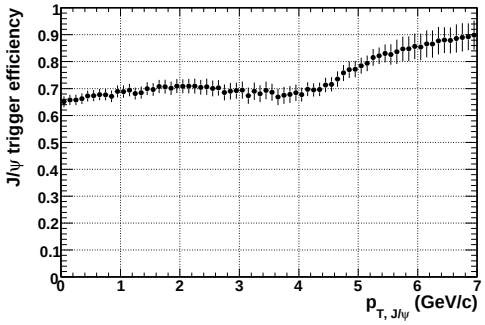

Figure 1. The J/ψ trigger efficiency as a function of J/ψ transverse momentum for the 1.2-GeV energy threshold and the centrality bin 0-10%.

Data was recorded with a hardware single electron trigger (ERT) requiring a signal above an energy threshold of 1.2 or 0.8 GeV in the EMC and a corresponding RICH hit. The single electron trigger efficiency including random benefit is defined by the ratio of the number of electrons in triggered events and the one of minimum bias (MB) events. The single electron trigger efficiency was determined as a function of momentum for eight EMC sectors and seven centrality bins. J/ψ trigger efficiency was calculated for each centrality bin as a function of transverse momentum, $p_{T,J/\psi}$, from the single electron trigger efficiency with single J/ψ simulation samples. Figure 1 shows the J/ψ trigger efficiency as a function of $p_{T,J/\psi}$ for the

1.2-GeV threshold and the centrality bin 0-10%.

During the data taking, a software di-electron filter was additionally used to reduce the data size for a quick analysis. However, the whole data was reconstructed without the software di-electron filter by the end of 2006 and the final results will be obtained with the whole data.

Quality assurance (QA) of collected data was performed based on the mean numbers of electrons and positrons per event. The QA with MB and ERT events assure detector performance and trigger performance, respectively. The analyzed number of ERT events is 286 million and corresponds to 6.39 billion MB events.

Detector acceptance and electron identification efficiency were evaluated with GEANT3 simulation. In the simulation, detector dead maps of DC, PC, EMC and RICH, made from real data, were used to taken into account detector inefficiency. The acceptance of J/ψ including efficiency is 1.8% and 0.6% at $p_{T,J/\psi} = 0$ and 5 GeV/c, respectively. Inefficiency due to high multiplicity was also estimated and it is 4% for the most central collisions.

Figure 2 shows the invariant mass spectrum of di-electrons. The mass window of 2.9–3.3 GeV/c^2 is used to count the number of J/ψ and the like-sign method is used to estimate combinatorial background, $N_{J/\psi} = N_{e^+e^-} - (N_{e^+e^+} + N_{e^-e^-})$. The observed number of J/ψ is 1685 ± 57.

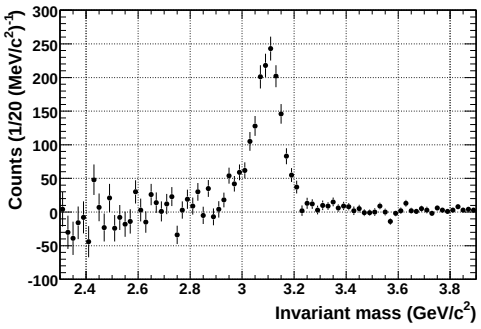

Figure 2. The subtracted invariant mass spectrum of di-electrons.

3. Results

To quantify the difference between the superposition of nucleon-nucleon collisions and a nucleus-nucleus collision, the nuclear modification factor is defined as follows, $R_{AA} = (Y_{AA}/N_{coll})\,/Y_{pp}$, where Y_{AA} is the J/ψ yield in a nucleus-nucleus collision and Y_{pp} is the J/ψ yield in a $p+p$ collision. The $\sqrt{s} = 200$ GeV $p+p$ collision data taken in 2003 [7] is used as a reference.

Figure 3 shows the nuclear modification factor as a function of N_{part}. The solid lines, brackets and boxes are the statistical, point systematic and overall systematic errors, respectively. Strong suppression is observed in the most central collisions. Lines from model calculations are also shown in Fig. 3. The cold nuclear matter model (dashed line) [2] underpredicts the data. The comover model (dot-dashed line) [3], which was successful in describing the SPS data, overpredicts the suppression at RHIC. The recombination model (solid line) [5] also underpredicts the suppression.

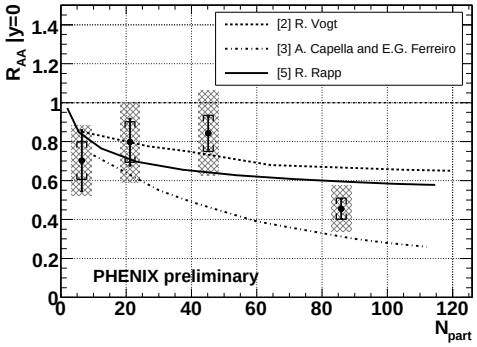

Figure 3. The nuclear modification factor of J/ψ as a function of the number of participants.

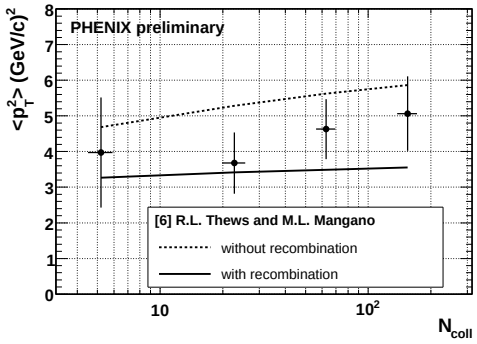

Figure 4. The mean square of the transverse momentum of J/ψ as a function of the number of collisions.

Figure 4 shows the mean square of the transverse momentum, $\langle p_T^2 \rangle$, as a function of N_{coll}. There is no significant centrality dependence of $\langle p_T^2 \rangle$. Theoretical predictions with recombination (solid line) and without recombination (dashed line) [6] are also shown in Fig. 4.

4. Summary

J/ψ is a good probe for the deconfined QGP. J/ψ created in Cu+Cu collisions was measured via di-electron decay at RHIC-PHENIX and the analysis is ongoing. Strong suppression beyond cold nuclear matter effect is observed.

References

[1] T. Matsui and H. Satz, Nucl. Phys. **A757** (1986) 184.
[2] R. Vogt, Acta Phys. Hung. **A25** (2006) 97.
[3] A. Capella and E.G. Ferreiro, Eur. Phys. J. **C42** (2005) 419.
[4] H. Satz, J.Phys. **G32** (2006) R25.
[5] R. Rapp, Eur. Phys. J. **C43** (2005) 91.
[6] R.L. Thews and M.L. Mangano, Phys. Rev. **C73** (2006) 014904.
[7] S.S Adler, et al., Phys. Rev. Lett. **96** (2006) 012304.

A Search for Deeply Bound K^- State at RHIC-PHENIX

Y. Morino, H. Hamagaki, and K. Ozawa,
for the PHENIX Collaboration

Center for Nuclear Study, Graduate School of Science, University of Tokyo

1. Introduction

Existence of bound anti-K states with a large binding energy was predicted by Akaishi and Yamazaki as an answer for kaonic hydrogen puzzle [1]. They predicted a bunch of bound K^- states based on effective K^-N and NN interactions, as summarized at Table 1. The characteristic features of bound K^- states are a large biding energy and a high nuclear density. It is important to find evidence of bound K^- states and to study the properties for understanding K^-N interaction.
The first experimental sign of bound K^- states has been reported by KEK E471 experiment, measuring single K^- clusters , $ppnK^-$ and $pnnK^-$ [2]. FINUDA experiment reported that they observed ppK^- cluster [5]. These experiments were performed at stopped K^- reactions.

On the other hand, at Relativistic Heavy Ion Collisions (RHIC), similar single K^- clusters and also double K^- clusters with a larger binding energy (∼200MeV) might be produced. There are two possible formation processes at RHIC, cascade evolution of K^- clusters and direct formation from Quark Gluon Plasma, since an abundant number of strange quarks which will become seeds for K^- clusters exist in very high density medium [4] and biding energies of K^- clusters are large. For a search for deeply bound K states at RHIC, invariant mass spectroscopy can be used.

Table 1. Summay of predictedK^- clusters. M: total mass[MeV]. E_K:total binding energy[MeV]. Γ_K decay width[MeV].$\rho(0)$: nucleaon density [fm^{-3}] [1].

K^- cluster	Mc^2 [MeV]	E_k [MeV]	Γ_K [MeV]	$\rho(0)$ [fm^{-3}]
pK^-	1407	27	40	0.59
ppK^-	2322	48	61	0.52
$pppK^-$	3211	97	13	1.56
$ppnK^-$	3192	118	21	1.50
ppK^-K^-	2747	117	35	
$ppnK^-K^-$	3582	221	37	2.97
$pppK^-K^-$	3580	220		

2. PHENIX experiment

The PHENIX experiment is the one of largest experiments at RHIC. Beam Beam Counter (BBC) and Zero Degree Calorimeter (ZDC) are used for event characterization and event trigger. Charged particle tracking is performed at Drift Chamber (DC) and charged particle identification is performed with using timing information at Time Of Flight counter (TOF) and Electromagnetic Calorimeter (EMCal). PHENIX provides excellent tracking and particle identification capabilities to search the bound K^- states.

3. Analysis

At PHENIX, the following K- clusters can be reconstructed, because PHENIX provides excellent tracking and particle identification capabilities for charged tracks.

$$ppK^- \rightarrow X(2.32GeV) \rightarrow \Lambda + p$$
$$pppK^- \rightarrow X(3.21GeV) \rightarrow \Lambda + p + p$$
$$ppK^-K^- \rightarrow X(2.75GeV) \rightarrow \Lambda + \Lambda,$$
$$pppK^-K^- \rightarrow X(3.58GeV) \rightarrow \Lambda + \Lambda + p.$$

Here, Λ can be reconstructed via Λ →p+π^- decay. Figure 1 shows invariat mass distribution of p+π^-. Solid line is from Au+Au collisions at $\sqrt{s_{NN}}$=200 GeV and dotted line is background calculated by event mixing. Here, pairs with invariant mass from 1.10 GeV to 1.13 GeV are identified as Λ. Since PHENIX does not have inner

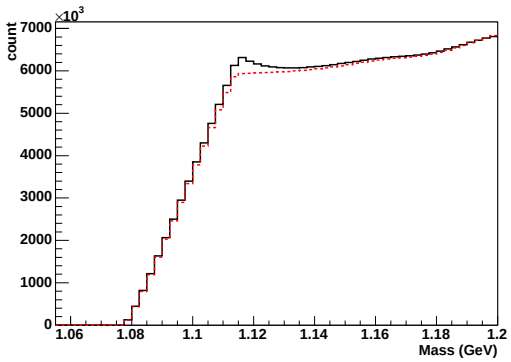

Figure 1. Invariat mass distributions of p+π^-. Solid lines are real data and dotted lines are background by event mixing.

trackers, background of Λ can not be reduced using vertex cut when bound K^- states are reconstructed. Date from Au+Au (2004) collisions at $\sqrt{s_{NN}}$=200 GeV and Cu+Cu (2005) at $\sqrt{s_{NN}}$=62.4 GeV collisions were analized. Number of analyzed events is about 800 M for Au+Au collisions and 250 M for Cu+Cu collisions.

4. Result

Figure 2 shows invariant mass distributions some of the predicted decay products of bound K^- states. Left figures are for real data and background. Solid lines are real data and dotted lines are background. Backgrounds are estimated by event mixing and normalized by the number of entries at unphysical region. Right figures are background subtracted invariant mass distributions. Panels (a) are from Λ and p

for ppK^- cluster, whose predicted mass is 2.32 GeV, in Au+Au $\sqrt{s_{NN}}$=200 GeV collisions. Panels (b) are also from Λ and p for ppK^- cluster in Cu+Cu $\sqrt{s_{NN}}$=62.4 GeV collisions. FINUDA reported mass of ppK^- cluster (panel (a) and (b)) was 2.26GeV and the width was 67MeV [4].
Panels (c) are from Λ, p and p for $pppK^-$ cluster, whose predicted mass is 3.21 GeV, in Au+Au $\sqrt{s_{NN}}$=200 GeV collisions. Panels (d) are from Λ and Λ for ppK^-K^- cluster, whose predicted mass is 2.75 GeV, in Au+Au $\sqrt{s_{NN}}$=200 GeV collisions. Panels (e) are from Λ, Λ and p for $pppK^-K^-$ cluster, whose predicted mass is 3.58 GeV, in Au+Au $\sqrt{s_{NN}}$=200 GeV collisions. In right figures, vertical dotted line indicates the sum of mass of decay products. Resonance should be searched below this sum. In these figures, significant peaks are not observed in any of the channels.

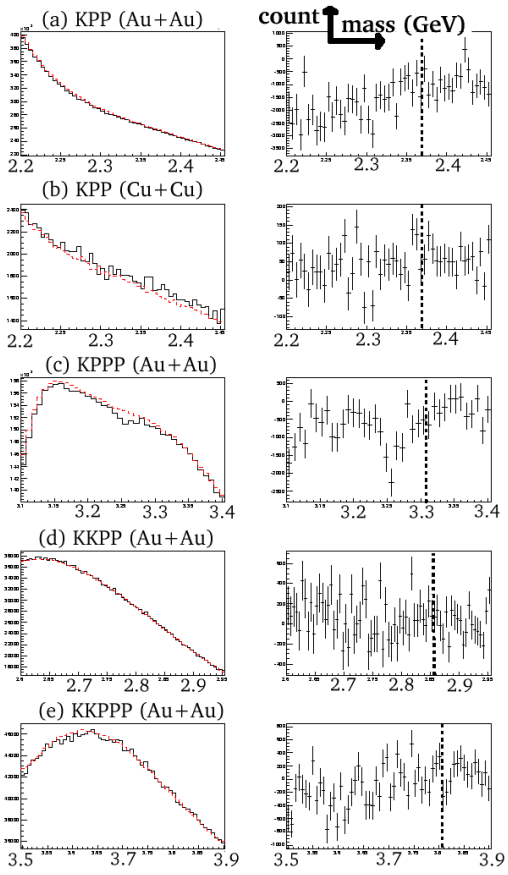

Figure 2. Left figures are for real data and background invariant mass distributions. Solid lines are real data and dotted lines are background. Right figures are background subtracted invariant mass distributions. Panels (a) are from Λ and p at Au+Au $\sqrt{s_{NN}}$=200 GeV collisions. Panels (b) are from Λ and p at Cu+Cu $\sqrt{s_{NN}}$=200 GeV collisions. Panels (c) are from Λ, p and p at Au+Au $\sqrt{s_{NN}}$=200 GeV collisions. Panels (d) are from Λ and Λ at Au+Au $\sqrt{s_{NN}}$=200 GeV collisions. Panels (e) are from Λ, Λ and p at Au+Au $\sqrt{s_{NN}}$=200 GeV collisions. In right figures, dotted line indicates the sum of mass of decay products.

5. Discussion

Figure 3 shows excitation function of the yields of K^- bound states relative to Λ yields at Au+Au collisions, based on a statistical model calculation [3]. Using this function and Λ yield at Au+Au $\sqrt{s_{NN}}$=200 GeV collisions, number of K^- clusters whose decay products will enter in PHENIX detector can be estimated. The results of the estimation at Au+Au $\sqrt{s_{NN}}$=200 GeV collisions are summarized in Table 2. Quick Monte-Carlo simulation was used and m_t scaling for K^- clusters was assumed for this estimation. ppK^- cluster could not be seen due large background and statistics is not enough for other K^- clusters according to this estimation .

Table 2. Summary of K^- clusters which will enter in PHENIX detector at Au+Au $\sqrt{s_{NN}}$=200 GeV collisions

K^- cluster	number/1event
ppK^-	3.4×10^{-6}
$pppK^-$	4.3×10^{-8}
ppK^-K^-	1.1×10^{-8}
$pppK^-K^-$	1.3×10^{-12}

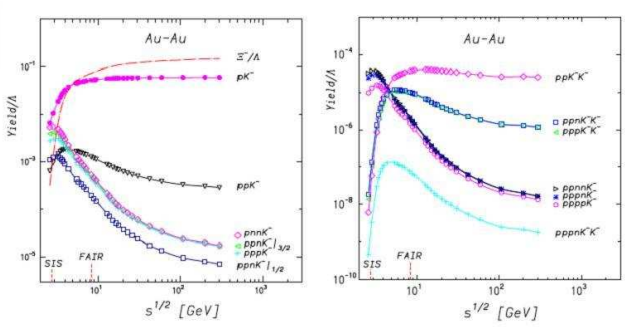

Figure 3. Excitation function of the yields of K^- bound states relative to Λ yields at Au+Au collisions [3].

6. Conclusion

Deeply bound K states are not observed at RHIC-PHENIX. Background rejection with vertex detection and higher statistics will be needed.

References

[1] Yamazaki and Akaishi Phys.Rev.**C65**(2002) 044005.
[2] T. Suzuki *et al.*,Nucl. Phys.**A 754** (2005) 375.
[3] A. Andronic *et al*, Nucl.Phys.**A765** (2006)
[4] T. Yamazaki *et al*, Phys.Let **B587**, 167 (2004)
[5] FINUDA collaboration, Phys.Rev.Let **94**, 212303 (2005).

Measurement of the Direct Photon Production in Polarized Proton-Proton Collisions at $\sqrt{s} = 200$GeV with PHENIX

T. Horaguchi[a] for the PHENIX Collaboration

[a]*Department of Physical Science, Graduate School of Science, Hiroshima University*

It had been believed that the proton spin is carried by the quark spin. The spin dependent structure function measurements started at SLAC. In 1988, the European Muon Collaboration (EMC) measured spin dependent structure function with higher statistics and in a wider kinematic range, and reported that the contribution of quark spin to proton spin is only $12 \pm 9 \pm 14\%$ [2, 3]. This result is called "Spin Puzzle". Later, other experiments measured the contribution of quark spin for proton and neutron spin and reported consistent results with EMC. The proton spin consists of the spin of the quarks, the gluons, and their angular momentum. The proton spin can be written as follows;

$$\frac{1}{2} = \frac{1}{2}\Delta\Sigma + \Delta G + L_q + L_g, \quad (1)$$

where $\Delta\Sigma$ and ΔG are the contribution of quark and gluon spin to the proton spin and L_q and L_g are those of the orbital angular momentum of quarks and gluons, respectively. The measurement of the polarized gluon distribution function (Δg) is important for understanding the origin of the proton spin. HERMES [4], SMC [5], and COMPASS [6] have reported measurements sensitive to the Δg using a deep inelastic scattering. Another approach to the Δg is a measurement of the particles which are produced by quark-gluon or gluon-gluon interaction in polarized proton-proton collisions. At RHIC, the Δg can be measured directly, precisely, and over a large range of gluon momentum fraction with several independent processes. The Δg can be evaluated from double spin asymmetry (A_{LL}) which can be written to Leading-Order (LO) as follows [7];

$$A_{LL} = \frac{1}{P_1 P_2}\frac{N_{++} - N_{+-}}{N_{++} + N_{+-}} \quad (2)$$

$$\approx \frac{\sum_{f_1,f_2,f} \Delta f_1 \times \Delta f_2}{\sum_{f_1,f_2,f} f_1 \times f_2 \times [d\hat{\sigma}^{f_1 f_2 \to f X'}] \times D_f} \quad (3)$$

$$\times \left[d\hat{\sigma}^{f_1 f_2 \to f X'} \hat{a}_{LL}^{f_1 f_2 \to f X'}\right] \times D_f \quad (4)$$

where P_1 and P_2 are the beam polarizations, N_{++} represents the number of observed particles when helicity of beam1 is + and helicity of beam2 is +. N_{+-} represents the number of particles when helicity of beam1 is $+$ and helicity of beam2 is $-$.

Direct photon production is a very useful tool of measurement of the Δg. The measurement of the direct photon cross section is a test of perturbative Quantum ChromoDynamics (pQCD), and it gives us the polarized and unpolarized gluon distribution in the nucleon [1]. Because the direct photon is produced directly by parton scattering, there is no ambiguity of the fragmentation function. Additionally, a direct photon is detected more easier than jet because it does not spread like a jet. A_{LL} in direct photon production can disentangle the sign of Δg due to absence of the gluon-gluon scattering process. On the other hand, the difficulty is in its poor statistics compared with other channels.

The Relativistic Heavy Ion Collider (RHIC) at BNL is operated as the first polarized proton-proton collider in the world with beam energy range from 50 GeV to 250 GeV. In PHENIX, data with an integrated luminosity of $3.8\mathrm{pb}^{-1}$ for longitudinally polarized collisions with 47% average polarization have been collected in the run of year 2005 at $\sqrt{s} =$ 200 GeV. It is 40 times larger in figure of merit for A_{LL} than the past year.

The PHENIX detector consists of four instrumented spectrometers and beam detectors. One of the instrumented spectrometers is called Central Arm. The 'Central Arm' consists of tracking chambers [Drift Chamber (DC), Pad Chamber (PC)], particle identification detectors [Ring Imaiging Cherenkov Detector (RICH), Time Expansion Chamber (TEC), Time Of Flight Counter (TOF)] and ElectroMagnetic Calorimeter (EMCal). The Central Arm covers the azimuthal angle of 180° and the pseudo rapidity range from -0.35 to 0.35. Photons with high transverse momentum (p_T) are detected by the EMCal with high p_T trigger. Another one is called the 'Muon Arm'. The Muon Arm consists of Muon Tracker (MuTr) and Muon Identifier (MuID). These arms cover the azimuth angle of 360° and the pseudo rapidity range of $1.2 < |\eta| < 2.4$. The beam detectors are Zero Degree Calorimeter (ZDC), Beam Beam Counters (BBC). The PHENIX Beam Detectors are used to measure the z-vertex to produce the trigger timing and to measure the luminosity in heavy ion and proton-proton collisions. The ZDC is also used as a local polarimeter to monitor the direction of the proton beam polarization.

Figure 1 (left) shows the final plot of the cross section for direct photon using 2003 data with pQCD calculation with CTEQ6M PDF with different scale factor [8]. The cross section was measured over 4 orders of magnitude. The measured p_T range is from 3.25 GeV/c to 16 GeV/c. Figure 1 (right) shows the fraction of the direct photon with BFG2 fragmentation functions with three different scale factors and GRV fragmentation function [8]. The result shows many of direct photons are isolated and theory predictions agree well with the result at high p_T region. The theoretical curves show larger values than the data points at low p_T region, which is due to the effect of underlying event in the data. π^0 photons from jets are suppressed as we expected qualitatively. Figure 2 (left) shows the preliminary plot of the cross section for direct photon using 2005 data with pQCD calculation with CTEQ6M PDF with different scale factor. The wide p_T renge from 5 GeV/c to 24 GeV/c is covered. The cross section was measured over 4 orders of magnitude. The pQCD caculation describes the data well over all measured p_T region. The result is consistent with

2003 data. Figure 2 (right) shows the preliminary plot of the cross seciton for direct photon with isolation cut method. The isolation cut method is to require that the direct photon candidate is not accompanied by any other particle inside a cone of a certain radius

$$R = \sqrt{\Delta\phi^2 + \Delta\eta^2} \tag{5}$$

in the η-ϕ space. The wide p_T range from 5 GeV/c to 24 GeV/c is covered. The 4 orders of magnitude on the cross section is obtained. The result is consistent with 2005 data.

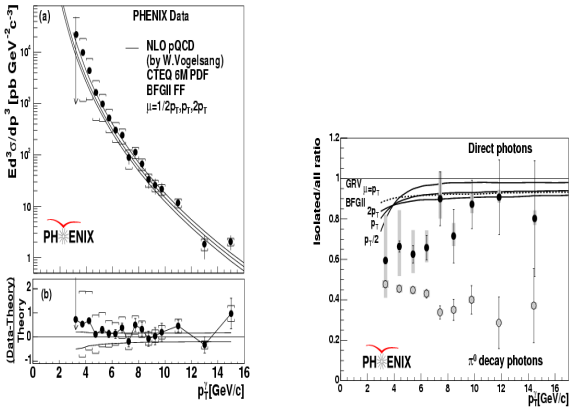

Figure 1. Left figure shows the final plot of the cross section for direct photon using 2003 data with pQCD calculation with CTEQ6M PDF with different scale factor. Right figure shows the fraction of the direct photon with BFG2 fragmentation functions with three different scale factors and GRV fragmentation function [8].

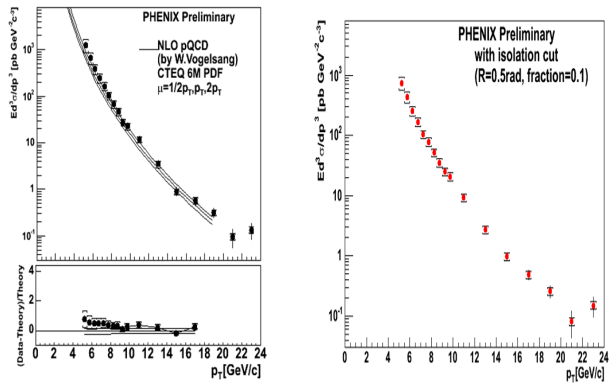

Figure 2. Left figure shows the preliminary plot of the cross section for direct photon using 2005 data with pQCD calculation with CTEQ6m PDF with different scale factor. Right figure shows the preliminary plot of the cross seciton for direct photon with isolation cut method.

At this moment, only the cross section is presented and more statistics is needed to measure the A_{LL} with sufficient accuracy. The expected A_{LL} with luminosity of $65\mathrm{pb}^{-1}$ and beam polarization of 70% is shown in Figure 3.

The study of Δg is on going at the RHIC-PHENIX experiment at BNL. RHIC was operated the long spin run in 2005 and 2006 successfully. The latest results of the measurement of the direct photon are presented here. More precise measurement will be obtained in the near future and determined the sign of Δg by direct photon measurement. Moreover, it is needed to cover wide range of Bjorken x to determine the integral of Δg. Run at $\sqrt{s} = 500$ GeV will be able to reach smaller x region.

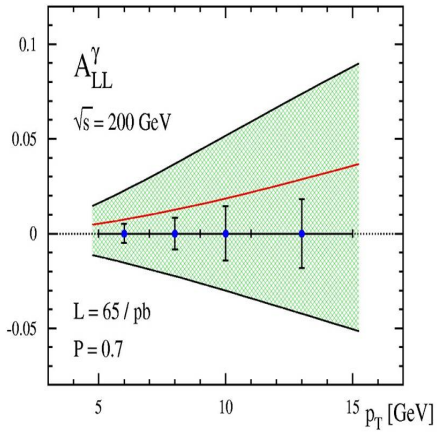

Figure 3. Figure shows the expected A_{LL}^{γ} as a function of p_T with luminosity of $65\mathrm{pb}^{-1}$ and beam polarization of 70% with theoritical curves.

References

[1] W. Vogelsang and M. R. Whalley, J. Phys. G **23**, A1 (1997).

[2] J. Ashman *et al.* [European Muon Collaboration], Phys. Lett. B **206**, 364 (1988).

[3] J. Ashman *et al.* [European Muon Collaboration], Nucl. Phys. B **328**, 1 (1989).

[4] A. Airapetian *et al.* [HERMES Collaboration], Phys. Rev. Lett. **84**, 2584 (2000) [arXiv:hep-ex/9907020].

[5] B. Adeva *et al.* [Spin Muon Collaboration (SMC)], "Spin asymmetries for events with high p(T) hadrons in DIS and an Phys. Rev. D **70**, 012002 (2004) [arXiv:hep-ex/0402010].

[6] E. S. Ageev *et al.* [COMPASS Collaboration], "Gluon polarization in the nucleon from quasi-real photoproduction of Phys. Lett. B **633**, 25 (2006) [arXiv:hep-ex/0511028].

[7] G. Bunce, N. Saito, J. Soffer and W. Vogelsang, Ann. Rev. Nucl. Part. Sci. **50**, 525 (2000) [arXiv:hep-ph/0007218].

[8] S. S. Adler *et al.* [PHENIX Collaboration], Phys. Rev. Lett. **98**, 012002 (2007) [arXiv:hep-ex/0609031].

Measurement of Single Electrons from Charm and Bottom via Electron-hadron Correlation in $\sqrt{s} = 200$ GeV $p + p$ Collisions at RHIC-PHENIX

Y. Morino, H. Hamagaki, K. Ozawa, T. Gunji and Y. Akiba [a],
for the PHENIX Collaboration

Center for Nuclear Study, Graduate School of Science, University of Tokyo
[a] RIKEN (The institute of Physics and Chemical Research)

1. Introduction

It is predicted from lattice Quantum Chromo Dynamics (QCD) calculations that a phase transition from hadronic matter to a plasma of deconfined quarks and gluons, called quark-gluon plasma (QGP) occurs at high energy density. The physics goal of Relativistic Heavy Ion Collider (RHIC) is to realize such a phase transition and study the properties of QGP, which is important to understand QCD under extreme hot and dense condition.

Heavy quark (charm and bottom) measurement is a good probe to study the effect of final state interactions in the extreme hot and dense medium such as parton energy loss, since heavy quarks is created only at the initial stage of the collisions due to their large mass. Heavy quarks are predicted to lose less energy in the hot and dense medium than light quarks because of their large masses, and to have much longer thermal equilibration time constants [1].

The PHENIX experiment is one of largest experiments at RHIC. Since PHENIX provides excellent electron identification capability, heavy quarks are measured via electrons which are produced from semi-leptonic decays of heavy flavor mesons. Inclusive electrons include photonic electrons and non-photonic electrons. Photonic electrons are mainly from γ conversion and π^0 daliz decay. The dominant source of non-photonic electrons is semi-leptonic decay of heavy quarks. Measurement of heavy quarks is performed with non-photonic electrons, that is, by subtraction photonic electrons from inclusive electrons, at PHENIX. PHENIX has measured non-photonic electrons in $0.3 < p_{\rm T} < 9.0$ GeV/c in Au+Au collisions at $\sqrt{s_{NN}} = 200$ GeV and reported a very large suppression for heavy quarks similar to light mesons [2]. The energy loss mechanism of heavy quarks in the medium is still an open question. For understanding energy loss mechanism of heavy quarks, a ratio of single electron from charm over bottom is one of the most critical parameter. The ratio of single electron from charm over bottom has not be determined experimentally and theoretical calculations have still a large uncertainty at $\sqrt{s_{NN}} = 200$ GeV collisions. It can be said that determination of this ratio is one of the most important measurements at RHIC.

2. Analysis

The ratio of single electron from charm over bottom could be studied by utilizing the difference of semi-leptonic decay pattern between D and B meson at PHENIX. Electron-hadron correlation provides information of semi-leptonic decay. It is a good way to compare unlike charge sign electron-hadron pairs with like charge sign electron-hadron pairs for the study of semi-leptonic decay, since only weak decay make unlike sign electron-hadron pairs different from between like sign pairs.

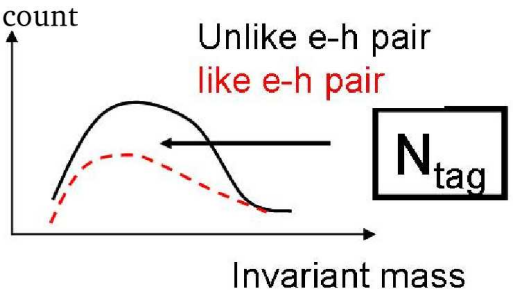

Figure 1. A conceptual view of invariant mass distributions of unlike sign pairs and like sign pairs.

Figure 1 shows a conceptual view of invariant mass distributions of unlike sign pairs and like sign pairs. Here, N_{tag} is defined as number of unlike sign pair entries N_{unlike} minus number of like sign pair entries N_{like}. Tagging efficiency ϵ_{data} is defined as follows using number of non-photonic electrons N_e.

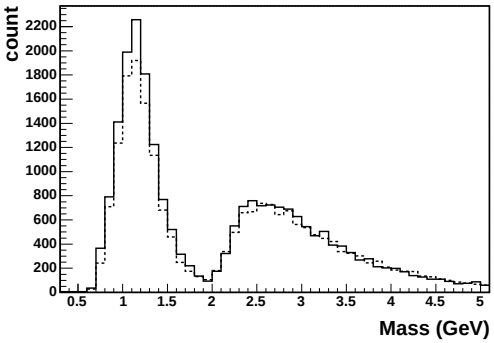

Figure 2. Invariant mass distributions of unlike sign pairs and like sign pairs at p+p collisions at $\sqrt{s_{NN}} = 200$ GeV. Solid line is the distribution of unlike sign pairs and dotted line is the one of like sign pairs.

$$\epsilon_{data} \equiv \frac{N_{tag}}{N_e} = \frac{N_{c\to tag} + N_{b\to tag}}{N_{c\to e} + N_{b\to e}}$$

Here, c (b) means charm (bottom). ϵ_{data} will be calculated from data analysis. The ratio of the number of single elec-

trons from charm over bottom can be calculated as follows.

$$\frac{b \to e}{c \to e + b \to e} = \frac{\epsilon_c - \epsilon_{data}}{\epsilon_c - \epsilon_b},$$

$$\epsilon_c \equiv \frac{N_{c \to tag}}{N_{c \to e}},\ \epsilon_b \equiv \frac{N_{b \to tag}}{N_{b \to e}},$$

where $\epsilon_{c\ (b)}$ is a tagging efficiency in the case of charm (bottom) production and will be calculated from a simulation.

The merit of this method is that cross sections of charm and bottom in PYTHIA simulation have no effect for calculation of tagging efficiency. Since the tagging efficiency is determined only by decay kinematics and the production ratio of D or B meson to the first order, we do not need to care about the large uncertainty of PYTHIA simulation in heavy quark production cross sections.

3. Result

Figure 2 shows invariant mass distributions of unlike sign pairs and like sign pairs at p+p collisions at $\sqrt{s_{NN}} = 200$ GeV . The solid line is the distribution of unlike sign pairs and the dotted line is the one of like sign pairs. The transverse momentum of electrons were selected with $2.0 < p_{\rm T} < 4.0$ GeV/c and The transverse momentum of hadrons was selected with $0.4 < p_{\rm T} < 4.0$ GeV/c. Mass of hadron was assigned kaon when invariant mass was calculated, since main component of the difference between unlike pairs and like pairs will be D$\to$ e + K +ν decay. The difference between unlike sign electron-hadron pairs and like sign pairs can be seen clearly in 0.5<invariant mass<2.0 GeV, which means semi-leptonic decay of D meson is the main component of the difference.
For calculation of $\epsilon_{c\ (b)}$, PYTHIA simulation, which is event generator based on Leading Order Calculation, was used [3]. Generated events were simulated by PISA, which is a Monte Carlo simulation based on GEANT 3.21, for PHENIX detector configuration, and was processed as the same way for the real data.

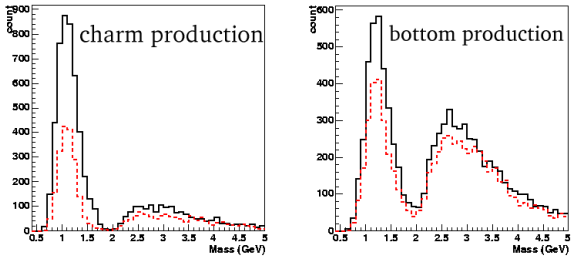

Figure 3. Calculated invarinant mass distributions of unlike sign pairs and like sign pairs from PYTHIA simulation. Solid line is the distribution of unlike sign pairs and dotted line is the one of like sign pairs. Left panel is in the case of charm production and right panel is in the case of bottom production.

Figure 3 shows invarinant mass distributions of unlike sign pairs and like sign pairs from PYTHIA simulation. Solid line is the distribution of unlike sign pairs and dotted line is the one of like sign pairs. Left panel is in the case of charm production and right panel is in the case of bottom production.
Figure 4 shows subtracted and normalized invarinat mass distributions of real data and PYTHIA simulation. The distributions of like sign pairs are subtracted from the distributions of unlike sign pairs. In the case of real data, the distribution is normalized by the number of non-photinic electrons. The number of non-photonic electrons was calculated by cocktail method [4]. In the case of simulation, the distributions is normalized by the number of electrons, since all of created electrons are from semi-leptonic decay. Open triangles are for real data. Closed circles are PYTHIA simulation in the case of charm production and open circles are in the case of bottom production. Closed triangles are PYTHIA simulation result, when we assume $b \to e/(c \to e + b \to e)$ is 0.3. Real data agrees well with PYTHIA result when cham and bottom results are mixed up. This provides additional confidence for mesurements of heavy quarks at PHENIX.

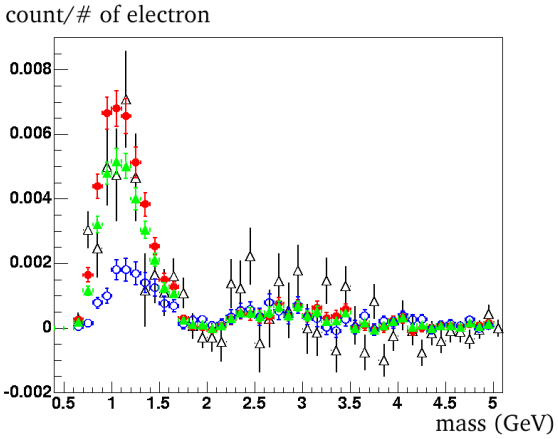

Figure 4. Subtracted and normalized invariant mass distribution of real data and PYTHIA simulation. Open triangles are for the data. Closed circles are PYTHIA simulation in the case of charm production and open circles are in the case of bottom production. Closed triangles are PYTHIA simulation result, when we assume $b \to e/(c \to e + b \to e)$ is 0.3.

4. Summary and Outlook

The difference of invariant mass distribution between unlike sign electron-hadron pairs and like sign pairs are clearly seen. This difference is accounted by the D and B meson semi-leptonic decays. This adds a confidence for measurements of heavy quarks at PHENIX. $b \to e/(c \to e+b \to e)$ will be determined by calculation of tagging efficiency.

References

[1] Y.L. Dokshizer*et al.*, Phys. Lett,**B519**, 199,(2001).
[2] A. Adare *et al.*, Phys. Rev. Lett. **98**, 172301 (2007)
[3] Pythia6 http://projects.hepforge.org/pythia6 .
[4] A. Adare *et al.*, Phys. Rev. Lett. **97**, 252002 (2006).

J/ψ Suppression in Quark-Gluon-Fluid at RHIC

T. Gunji, H. Hamagaki, T. Hatsuda[a], T. Hirano[a]

Center for Nuclear Study, Graduate School of Science, University of Tokyo, Japan
[a]Department of Physics, Graduate School of Science, University of Tokyo, Japan

1. Introduction

A new state of matter composed of deconfined quarks and gluons, the Quark-Gluon Plasma (QGP), is expected to be formed in relativistic heavy-ion collisions if the system reaches a temperature larger than the critical value $T_{\rm c} \sim 170$ MeV [1]. To find an evidence of QGP, the heavy quarkonia (J/ψ, ψ', $\chi_{\rm c}$, and Υ) have long been considered as the most promising probe, since they are supposed to melt away due to the color Debye screening at sufficiently high temperature [2]. Recent lattice QCD studies show that J/ψ would survive up to about $2T_{\rm c}$ while χ_c and ψ' would melt just above $T_{\rm c}$ [3, 4]. Because of such differences, the heavy quarkonia may be used as a thermometer of QGP.

J/ψ production in Au+Au collisions at the center of mass energy per nucleon pair of 200 GeV has been measured by PHENIX at the Relativistic Heavy Ion Collier (RHIC) [5]. It is observed that J/ψ yield in central Au+Au collisions is suppressed by a factor of 4 at mid-rapidity relative to that in $p+p$ collisions scaled by the average number of binary collisions. The suppression is stronger than that expected from cold nuclear matter (CNM) effects extrapolated from the J/ψ production in d+Au collisions at RHIC [6, 7, 8].

It has been proposed that J/ψ suppression at RHIC can be understood as the sequential melting of the charmonia [9], where the melting of χ_c and ψ' and associated absence of the feed down to J/ψ would occur at lower temperature and the melting of directly produced J/ψ at higher temperature. We have developed a hydro+J/ψ model to investigate the sequential charmonia suppression in a dynamically evolving matter produced in Au+Au collisions at RHIC energy, where hot quark-gluon matter is described by the relativistic hydrodynamics [11] and J/ψ, $\chi_{\rm c}$, and ψ' are treated as an impurity traversing through the matter.

2. Hydro+J/ψ Model

The relativistic hydrodynamical calculation describing the space-time evolution of the QGP fluid [10] has been exploited to study the pseudo-rapidity dependence of charged particle multiplicity, azimuthal anisotropy, and disappearance of back-to-back jet correlation [11, 12].

Figure 1 shows the local calculated temperature as functions of x (upper) and y (lower) for various proper time ($\tau = \sqrt{t^2 - z^2}$) at mid-rapidity ($z = 0$) in Au+Au collisions at $\sqrt{s_{\rm NN}}$ = 200 GeV. The left and right panels are for the case at $b = 2.1$ fm and $b = 8.5$ fm, which correspond to the number of participant nucleons ($N_{\rm part}$) of 351 and 114, respectively. Here x and y are transverse coordinates and the centers of two colliding nuclei are located at $(x, y) = (b/2, 0)$ and $(-b/2, 0)$ with an impact parameter b. The initial J/ψ, χ_c, and ψ's in the transverse plane at

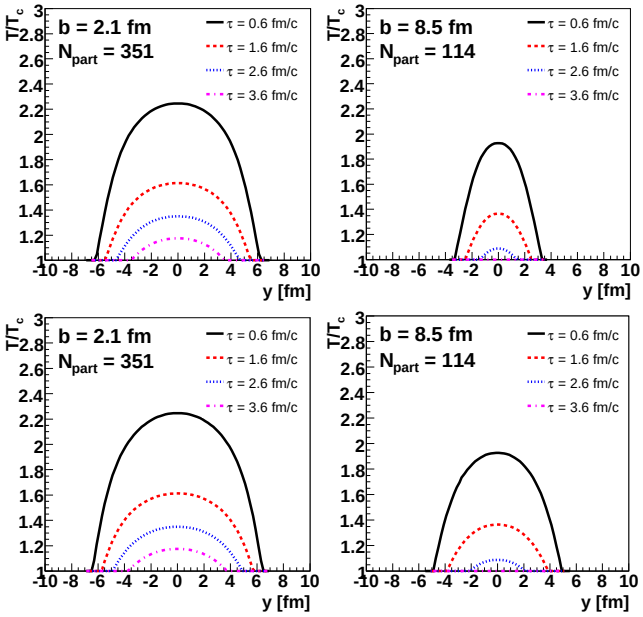

Figure 1. Local temperature in the unit of $T_{\rm c}$ as functions of the transverse coordinates, x (upper) and y (lower), for various proper time (τ) at mid-rapidity. The impact parameters are $b = 2.1$ fm (left) and $b = 8.5$ fm (right).

mid-rapidity are distributed according to the spatial distribution of the number of nucleon-nucleon collisions calculated from the Glauber model for a given impact parameter. Transverse momentum ($p_{\rm T}$) is distributed according to the measured p_T spectrum of J/ψ at RHIC [5].

The survival probability of J/ψ suffering from dissociation along its path inside the expanding fluid may be expressed as

$$S_{J/\psi}(\boldsymbol{x}_{J/\psi}(\tau)) = \exp\left[-\int_{\tau_0}^{\tau} \Gamma_{\rm dis}(T(\boldsymbol{x}_{J/\psi}(\tau')))d\tau'\right], \quad (1)$$

where $\Gamma_{\rm dis}(T(\boldsymbol{x}_{J/\psi}(\tau)))$ is the decay width at temperature T and $\boldsymbol{x}_{J/\psi}(\tau)$ is the transverse position of J/ψ at proper time τ. Information on $\Gamma_{\rm dis}(T)$ is rather scarce at present because the matter is still in non-perturbative region $T \sim (1-2)T_{\rm c}$. We make a simplest threshold ansatz: $\Gamma_{\rm dis}(T) = \infty$ (0) for T larger (smaller) than the melting temperature of J/ψ, $T_{J/\psi}$.

We assume a common melting temperature $T_{\psi'} = T_{\chi_{\rm c}} \equiv T_\chi$ for $\chi_{\rm c}$ and ψ' and then the total survival probability of J/ψ is obtained by taking into account the total feed down fraction $f_{\rm FD}$ from $\chi_c + \psi'$ to J/ψ as

$$S^{\rm tot}_{J/\psi} = (1 - f_{\rm FD})S_{J/\psi} + f_{\rm FD}S_\chi, \quad (2)$$

where S_χ denotes the survival probability of χ_c or ψ' .

In this calculation, $T_{J/\psi,\chi_c,\psi'}$ and $f_{\rm FD}$ are free parameters since $T_{J/\psi,\chi_c,\psi'}$ has not been determined theoretically well and $f_{\rm FD}$ has not been measured at RHIC energy and $f_{\rm FD}$ in other energies has still a large uncertainty [13].

3. Results

Experimental survival probability in the mid-rapidity of J/ψ in Au+Au collisions at RHIC is shown as filled circles in Fig. 2, where gluon shadowing and nuclear absorption with $\sigma_{\rm abs} = 1$ mb are taken into account as CNM effects [8]. Bars and brackets correspond to the uncorrelated and correlated errors with respect to $N_{\rm part}$, respectively [5]. Boxes correspond to the uncertainties associated with the nuclear absorption cross section of 0 mb $-$ 2 mb [8]. The solid line corresponds to the net survival probability $S^{\rm tot}_{J/\psi}$ obtained from our hydro+J/ψ model with the best fit parameters ($\chi^2 = 0.86$ for $N_{\rm part} \geq 50$) as follows:

$$(T_{J/\psi}, T_\chi, f_{\rm FD}) = (2.02T_{\rm c}, 1.22T_{\rm c}, 0.30), \qquad (3)$$

while $S_{J/\psi}$ and S_χ are shown by dashed and dotted lines, respectively.

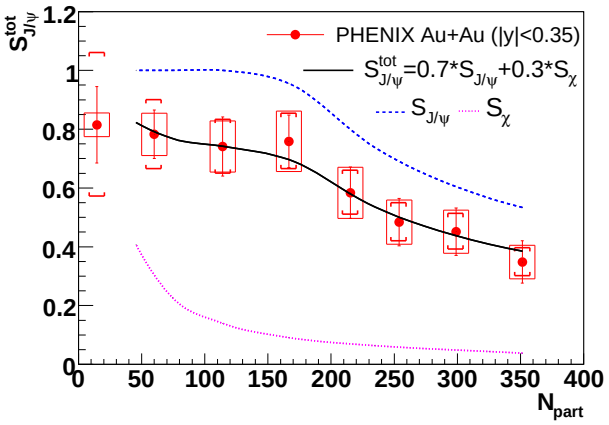

Figure 2. Survival probabilities $S^{\rm tot}_{J/\psi}$ (solid line), $S_{J/\psi}$ (dashed line), and S_χ (dotted line) in the hydro+J/ψ model as a function of the number of participants $N_{\rm part}$ with $(T_{J/\psi}, T_\chi, f_{\rm FD}) = (2.02T_{\rm c}, 1.22T_{\rm c}, 0.30)$. Filled symbols are the experimental survival probability in the mid-rapidity of J/ψ in Au+Au collisions at RHIC [5, 8].

Decreasing of $S^{\rm tot}_{J/\psi}$ with increasing $N_{\rm part}$ is reproduced quite well with the scenario of sequential melting in expanding fluid: Onset of genuine J/ψ suppression around $N_{\rm part} \sim 160$ can be clearly seen by the dashed line in Fig. 2, which results from the fact that the highest temperature of the matter reaches to $T_{J/\psi}$ at this centrality. Gradual decrease of $S^{\rm tot}_{J/\psi}$ above $N_{\rm part} \sim 160$ reflects the fact that the transverse area with $T > T_{J/\psi}$ increases.

We show, in Fig. 3, the χ^2 contour plot in the plane of $T_{J/\psi}/T_{\rm c}$ and $T_\chi/T_{\rm c}$ with $f_{\rm FD}$ being fixed to 0.30. The cross symbol corresponds to Eq.(3) which gives minimum χ^2. Solid and dashed lines correspond to the 1σ and 2σ contours, respectively. It is seen that $T_{J/\psi}$ can be determined in a narrow region around $2.02T_{\rm c}$, while T_χ is not well determined because the feed-down effect is not a dominant contribution to $S^{\rm tot}_{J/\psi}$.

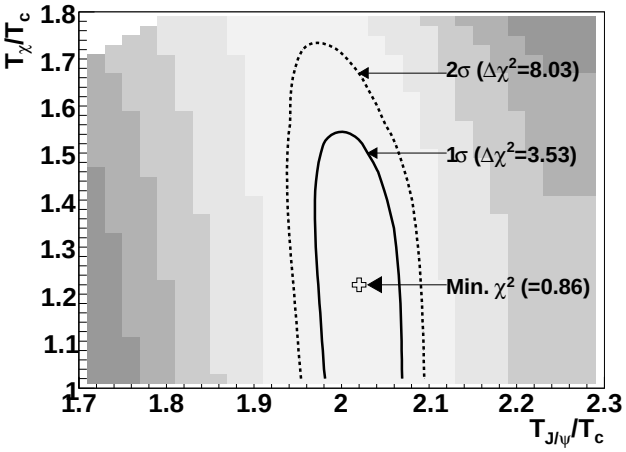

Figure 3. χ^2 contour in $T_{J/\psi}/T_{\rm c} - T_\chi/T_{\rm c}$ plane with $f_{\rm FD}$ being fixed to 0.30. Cross symbol corresponds to $(T_{J/\psi}, T_\chi) = (2.02T_{\rm c}, 1.22T_{\rm c})$. Solid and dashed lines correspond to the 1σ and 2σ contours, respectively.

4. Summary

We have investigated J/ψ suppression at mid-rapidity in Au+Au collisions at RHIC by using a hydro+J/ψ model which serves as a dynamical approach to the sequential charmonia suppression. Comparing the model and the survival probability $S^{\rm tot}_{J/\psi}$ in Au+Au collisions at RHIC, observed J/ψ suppression pattern is described quite well with $T_{J/\psi} \simeq 2.0T_{\rm c}$. It is noticeable that the RHIC data analyzed with the state-of-the-art hydrodynamics leads to a rather solid value for the melting temperature of J/ψ to be around $2T_{\rm c}$. Application of this model to J/ψ suppression at forward rapidity in Au+Au and at both rapidities in Cu+Cu collisions is underway.

References

[1] Reviewed in T. Hatsuda, hep-ph/0702293.
[2] T. Matsui and H. Satz, Phys. Lett. **B 178**, 416 (1986).
[3] M. Asakawa and T. Hatsuda, Phys. Rev. Lett. **92**, 012001 (2004).
[4] S. Datta *et al.*, Phys. Rev. **D69**, 094507 (2004);
[5] A. Adare *et al.* (PHENIX Collaboration), nucl-ex/0611020.
[6] S. S. Adler *et al.*, Phys. Rev. Lett **96**, 012304 (2006).
[7] R. Vogt, Acta Phys. Hung. **A25**, 97 (2006).
[8] T. Gunji (PHENIX Collaboration), nucl-ex/0703004.
[9] F. Karsch, D. Kharzeev, and H. Satz, Phys. Lett. **B637**, 75 (2006).
[10] http://tkynt2.phys.s.u-tokyo.ac.jp/~hirano/parevo/parevo.html
[11] T. Hirano, Phys. Rev. **C65**, 011901 (2002); T. Hirano and K. Tsuda, *ibid.* **C66**, 054905 (2002).
[12] T. Hirano and Y. Nara, Phys. Rev. **C68**, 064902 (2003); **C69**, 034908 (2004); Phys. Rev. Lett. **91**, 082301 (2003); M. Isse *et al.*, nucl-th/0702068.
[13] I. Abt *et al.*, Phys. Lett. **B561**, 61 (2003).

Accelerator and Instrumentation

Development of High Current Single Charge Ion Sources for CNS-CBECR

S. Watanabe, Y. Ohshiro, S. Yamaka, S. Kubono, H. Nakagawa[a], T. Hattori[b]

Center for Nuclear Study, Graduate School of Science, University of Tokyo
[a]RIKEN (The Institute of Physical and Chemical Research)
[b]Tokyo Institute of Technology

1. Introduction

In order to develop the high current, highly charge state metallic ion source [1], an additional charge stripping of incoming singly charged ions has been studied by using Charge Breeder Electron Cyclotron Resonance (CBECR) ion source. [2] A CNS-CBECR ion source comprises a single charge ion source ($\sim 10keV$), electrostatic ion guide, beam decelerator ($\sim 5eV$), ECR plasma chamber, mirror coils and beam extraction system. A differential pumping system is equipped between the primary ion source and the ECR plasma chamber. Detail of the CNS-CBECR ion source is described in the elsewhere. This report describes the development of the high current single charge ion sources. A volume type ion source and a magnetron sputtering type metal ion source are described, respectively.

2. Volume type ion source

The volume type ion source Model-1, called VIS-1, is shown in Fig. 1. [3] Inner diameters of an anode and an extraction holes are both 4 mm. Distance between the anode and extraction electrodes is designed at 8 mm. In order to adopt the VIS-1 to the CNS-CBECR, structure of beam extraction part was modified (VIS-2). A beam extraction voltage of VIS-2 is enlarged up to 15 kV because maximum extraction voltage of CNS-CBECR is designed at 15 kV. An insulator of the VIS-1 is made of Teflon for working voltage at 6 kV. The insulator of VIS-2 is changed from Teflon to MC-Nylon. The diameter of extraction hole of VIS-2 is changed from 4 mm to 8 mm, however anode hole is 4 mm. A distance between the anode hole and the extraction hole of VIS-2 is increased from 8 mm to 17 mm. A design study of vacuum pressures of the primary ion source, ion guide and decelerator has been carried out. For example, the VIS-2 should keep the Argon gas pressure at 3 mTorr in the plasma chamber. This gas pressure is higher than the plasma chamber of ECR ion source. This pressure difference will be kept/isolated by using a differential pumping system located at the ion guide system, which is composed of both the 500 L/s TMP. The Ar beam current density is proportional to a hot cathode arc power in the VIS-2. Cooling capability was strengthened in order to increase a hot cathode arc power, keeping plasma chamber temperature constant. A Cu pipe with 2 mm diameter is welded around the outer wall of the plasma chamber. The anode electrode is also cooled by circulating water going through in the 8 mm Cu pipe welded around the anode electrode.

The performance of VIS-2 has been tested. The schematic drawing of the test stand is shown in Fig. 2. The ion beam containing various charge states of all ion extracted is transported along the beam line. Magnetic sector

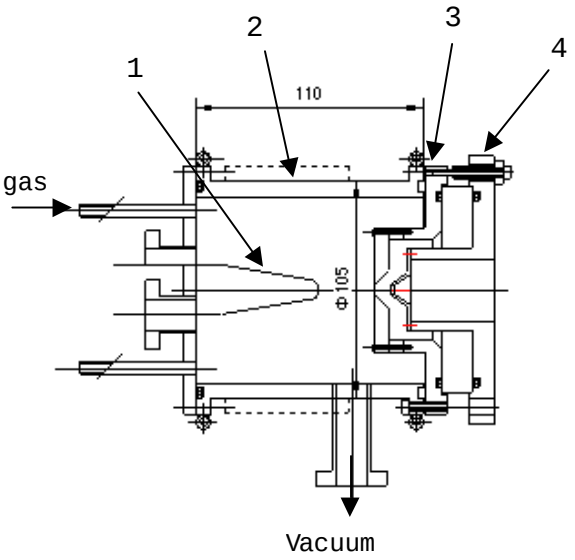

Figure 1. Volume type ion source (VIS-1). Components in the figure, 1=Filament, 2=plasma chamber wall, 3=anode electrode, 4=Extraction electrode.

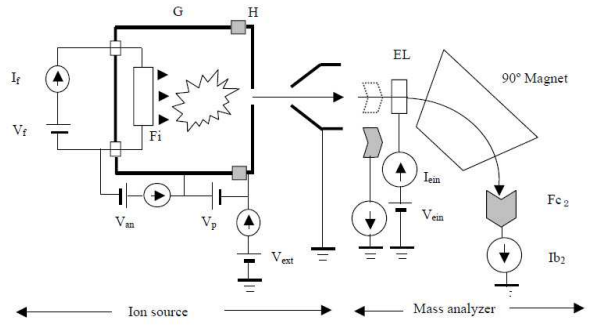

Figure 2. Schematic of mass analysis of VIS-2

mass analyzer is used to separate ions with desired charge to mass ratio and to transport them to the other vacuum chamber for the ion beam experiment. To obtain the sufficient resolution in the charge state analysis, the mean radius of the trajectory in the sector magnet is chosen to be 350 mm. In addition, ions are focused before the magnet by the Einzel lens. The distance between the entrance slit and the edge of the magnet is fixed at 687 mm. The angle of the beam axis to the edge plane of the magnet is chosen to be $123.0\,\mathrm{deg}$ so that the ion beam is double focused at the exit slit on the focal plane. The mass-resolution $M/\Delta M$ was estimated to be 370 when it was supposed that the width of the each slit was 1 mm and that the extraction voltage and the variation were 10 kV and 100 V, respectively.

Extracted ion current Ib1 from the VIS-2 is 0.94 mA when

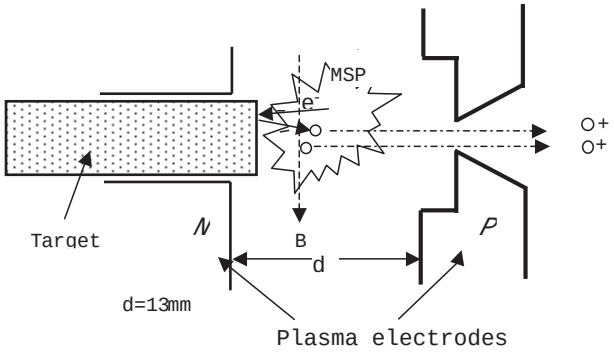

Figure 3. Cross-sectional view of the plasma chamber of metal ion source Magnetic field B is applied in parallel to the surface of target sample.

Vext = 10 kV, Vp = 0 V, Van = 82.6 V, Ian = 5.10 A and If = 40.5 A, respectively. Typical mass spectrum after sweeping by $90\,\mathrm{deg}$ magnet is tabulated in table 1.

In table 1, peak position (P.P) is a distance from a starting point of a X axis (mm) on a pen recorder, which is corresponding to the excitation curent of $90\,\mathrm{deg}$ magnet. $B\rho$ of each spectrum is normalized by a peak position of Ar^+ by using the equation, $(B\rho)^2 = 2Vm_pA/qe$. A/q is introduced from relations of $A/q = (B\rho)^2e/Vm_p$ where the V is extraction voltage of Vext10 kV. Vein is +4.5 kV. The HCl^+ is expected from surface of the O-ring because it is excited by plasma discharge.

Table 1. Mass spectrum obtained from the $90\,\mathrm{deg}$ magnet sweeping

No	p.p [mm]	Ib_2 [eμA]	$B\rho$ [Tm]	A/q	Ion
1	202	33	0.09138	40	Ar^+
2	169	0.33	0.07645	28	N_2^+
3	143	2.35	0.06469	20	Ar^{2+}
4	47	0.54	0.02126	2	H_2^+
5	193	0.036	0.08731	36.5	HCl^+

3. Magnetron sputtering type ion source

Schematic drawing of the metal ion source is shown in Fig. 3. Magnetron sputtering plasma (MSP) is a key technology of the metal ion source (MIS). Generated electrons in the MSP collide with the target sample and sputter the atoms. It is seemed that MSP is good solution to extract the metal-ions from the target sample if the sputtered atoms are ionized by ionization collision. Ionized atom is exhausted by electric potential around the anode hole (1 mm diameter shown in Fig. 3). The ionized atom is accelerated by electric potential between the anode and a grand electrode called extraction electrode.

Plasma excitation is carried out continuously by high-frequency electric field between plasma electrodes (P-N in Fig. 3) generated by capacitive coupled rf power source. When Argon gas pressure was 3 mTorr, it checked carrying out plasma ignition, where high frequency electric powers of 20 W, which are 13.56 MHz, are supplied. Plasma ignition was performed by pulsed 10 kV. The rf power feeding was performed to 300 W. Mass analysis of the extracted metal ions has been carried out by using the magnetic sector mass analyzer. Extracted beam current is tabulated in table 2, where extraction voltage is 10 kV and anode hole has a diameter of 1 mm.

The ion current tabulated in table 2 is a result of zero bias voltage at the target sample. If the target sample is biased to negative electric potential compared with plasma chamber, the sputtering rate of target sample will be increased. An effect of negative bias to increase the ion current has been measured. Preliminary test shows that Al^+ ion current is increased 3 times when the target sample is biased at DC -600 V. RF power dependence of the beam current was measured when the rf power is increased from 50 W to 500 W. The resulting Al^+ ion current is increased up to 13.6 times. If we enlarged the extraction hole of 4 times the present diameter, extraction current will be increased up to 16 times. Totally, estimated ion current will be increased up to 652.8 times. If we chosed more powerful negative bias voltage power supply, for example DC-1500 V, we can extract Al^+ beam of 43.7 eμA which is estimated from extrapolation of present ion current of 27 enA.

Table 2. Ion current measured by the magnetic analyzer

Target sample	RF power [W]	Ion current [eμA]
Ar	50	Ar^+ = 4
Ar	50	Ar^{2+} = 0.06
Al	50	Al^+ = 0.027
Cu	50	Cu^+ = 0.002
LiF	50	Li^+ = 0.00085

4. Summary

Development of high current single charge ion sources for CNS-CBECR ion source has been introduced. The extracted total ion current from VIS-2 is 1 mA at extraction voltage of 10 kV. This beam is mainly Ar^+ sufficient to test the performance of CNS-CBECR. Varieties of the ion species, Cu^+, Al^+ and Li^+, have been extracted from the metal ion source. The increase of beam current extracted from the metal ion source is being developed. The negative DC bias to the target material is more effective to increase the beam intensities. This approach is being studied in detail.

References

[1] Y.Ohshiro et al. CNS-REP-69 Nov. 2006, pp57-58.
[2] ECR Charge Breeding Workshop and open collaboration meeting at CERN on the 8-9th of November 2004.
[3] S.Watanabe et al. CNS-REP-66 Aug. 2005, pp61-62.

Improvement of RIKEN K78 AVF Cyclotron

S. Watanabe, S. Kubono, Y. Ohshiro, S. Yamaka, A. Goto[a], M. Kase[a]

Center for Nuclear Study, Graduate School of Science, University of Tokyo
[a]RIKEN (The Institute of Physical and Chemical Research)

1. Introduction

A RIKEN AVF cyclotron is being operated to deliver the beam to the Ring Cyclotron, a CRIB course and beam bombardment course. Contribution of CNS to improve the AVF cyclotron in this physical year is briefly described.

2. HyperECR

Table 1 shows beam species extracted from AVF cyclotron in 2006. Extracted beam energy, beam intensity (C10) and beam transmission efficiency between the ECR and AVF cyclotron (C01/I36) is also listed in Table 1. Development of metal ions is advanced. Since the hot liner is attached to the plasma chamber, Li ion generation associated with new crucible is stable and extraction of large intensity of the Li ions has been attained. By having doubled the capacity of crucible, contiguous operation without changing the sample for one week or more was realized.

In order to increase the metal ion current, optimum setting position of the target sample has been searched. When the crucible or a rod is placed near 1st ECR zone with efficient consumption rate, the metal ions of large intensity is obtained. The metal ions, $^{28}Si^{9+}$, $^{40}Ca^{11+}$, $^{31}P^{9+}$, which can be used for CRIB have been developed.

Table 1. Extracted beam from HyperECR

Ion	Energy (MeV/u)	C10 (eμA)	C01/I36 (%)
H^{+}	14	9.1	11
H^{2+}	3.97	2.8	8.23
$^{6}Li^{3+}$	9.5	1.55	2.6
$^{7}Li^{2+}$	3.4	3.7	3.7
$^{12}C^{4+}$	7	1.3	3.3
$^{13}C^{4+}$	5.54	6.2	18.2
$^{14}N^{6+}$	8.2	5.2	34.7
$^{15}N^{4+}$	5	3.8	4.8
$^{18}O^{5+}$	3.89	2.5	9.6
$^{18}O^{6+}$	6.27	5.2	14.4
$^{20}Ne^{7+}$	7	0.77	10.7
$^{22}Ne^{7+}$	6.25	4.6	35.4
$^{83}Kr^{23+}$	5.45	0.033	4.5

3. Glaser lens

A solenoid coil comprising a Glaser lens GLI38 has been repaired to recover convergence power for a beam injection into the AVF cyclotron. The old one has caused the electrical leak, and convergence power ($F = B^2L$) has become half of specification at the commissioning. In September '06, the GLI38 was extracted from AVF axial injection hole

Figure 1. Overview of the extracted Glaser lens before exchange. Under part is to be exchanged solenoid coil.

(see Fig. 1) and a leak part was replaced with a new one as shown in Fig. 2. We have been measured magnetic field and compared with old one to confirm convergence power. Table 2 shows the convergence power of GLI38 together with GLI37 as part of injection line. By this improvement, limit of beam focusing power is shift to the higher energy side.

Table 2. Convergence power of glaser lens

Name	B^2L (T^2cm)	Icoil max. (A)
GLI38	63	202.6
GLI37	19	334

4. Beam extraction efficiency

A set of trim coils and harmonic coils have been used to attain the appropriate isochronous field. Magnetic field setting is carried out according to the calculation. Actually, a trim coil 1 and 2 are tuned to give a precise turn separation at the deflector entrance. The harmonic coils are available to adjust the injection angle and position of the beam at deflector entrance. These adjustments have been done with the aid of beam diagnostic instruments. The deflector probe as shown in Fig. 2 has a roll to diagnosis the turn separation at deflector entrance. Further more, position and angle of the deflector electrode is tuned to extraction orbit.

In December '06, extraction efficiency η has been confirmed by using $^{14}N^{6+}$ 8.2 MeV/u. Beam currents at ECR ion source was Iecr = 17 eμA. [1] A main probe has been

Figure 2. New glaser lens before installation

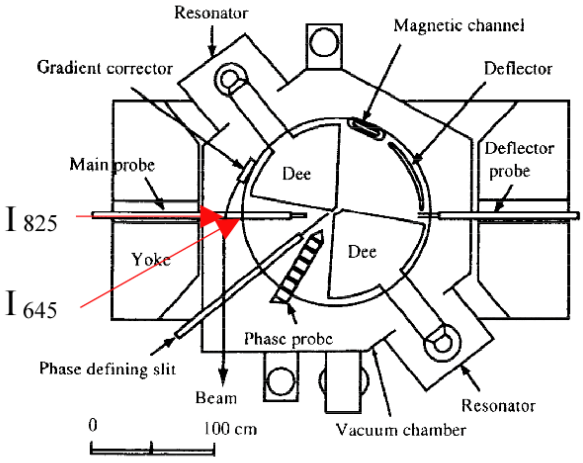

Figure 3. Measurement of extraction efficiency

used to measure the circulating beam at azimuthal angle of 180 deg as shown in Fig. 2. The main probe covers the radial direction between a radius of 78 mm near center region and 963 mm near the beam extraction region. The main probe had measured I645=4.1 eμA where the radius of 645 mm and I825 = 4.0 eμA obtained at radius of 825 mm just before the exit window of the AVF cyclotron. [2] The extraction efficiency defined by η =I825/I645 gives 97%, however extraction efficiency in the traditional operation was 10% or less.

The large efficiency, such as 97%, is the result of adjusting the operation parameter of the AVF cyclotron with sufficient perseverance. We are investigating whether beam monitoring system need to be strengthened in order to trace beam trajectory more reliably and to attain higher beam efficiency. For further precise beam diagnostic, an available space for the installation of beam monitoring devices should be considered.

References

[1] Y. Ohshiro et al. RIKEN Accel. Prog. Rep. 35(2002).
[2] T. Kageyama et al. RIKEN Accel. Prog. Rep. 22 (1988).

Beam Simulation of RIKEN K78 AVF Cyclotron

S. B. Vorozhtsov[b], A. S. Vorozhtsov[b], E. E. Perepelkin[b], S. Watanabe[a], Y. Ohshiro[a], S. Kubono[a], T. Mitsumoto[ad], and A. Goto[c]

[a] *Center for Nuclear Study, Graduate School of Science, University of Tokyo*
[b] *Joint Institute for Nuclear Research, Dubna, Russia*
[c] *RIKEN (The Institute of Physical and Chemical Research)*
[d] *Sumitomo Heavy Industries, Ltd. (SHI)*

1. Introduction

A center region of RIKEN AVF cyclotron was designed to accelerate a beam with harmonic number of 2. In order to expand the utilization of the present cyclotron, design study of the center region for harmonic number of 1, 2 and 3 is being proceeded. A construction of computer model is described in this article.

2. Configuration of electric and magnetic field distributions

An acceleration system model was constructed and its field was estimated with the aid of computer code ASIS. Since the central electrode structure, such as inflector and puller, is an object for possible modifications/optimizations, central electrode has been studied in great details together with acceleration region models (Dee electrodes). Output of computer code together with beam trajectory is shown in Fig. 1.

The 3D E-field map for the whole acceleration region was passed to the beam dynamics program. The 3D E-field map in case of combined structure - Dees, RF-shield, and inflector - was simulated to see the effect of the electrical fringe field in the overlapping field region of all these structures. E-field of the electrostatic deflector (ESD) was estimated. The E-map was passed to the beam dynamics program for extraction process modeling. A model for the magnetic extraction channel is under construction. The magnetic field distributions were also calculated with the aide of computer code TOSCA. [1]

3. Beam simulation

Beam simulations were performed using the above electric and magnetic field distributions. The results are: (1) Substantial increase of the longitudinal beam emittance takes place after passage of the inflector. (2) Comparison of the simulated reference trajectory in the central region and at extraction gives a good agreement with the previous calculations that were performed in the design stage. [2] (3) Calculated beam transmission is close to the experimental one. (4) According to the simulations the major particle losses in the cyclotron are in the central region from the inflector exit to the main probe (initial 2 turns); at the initial $\sim$5 turns due to particles axially hitting the RF system surfaces; Low order harmonics of the magnetic field substantially worsen the radial quality of the beam before extraction. An example of the results of beam simulation is

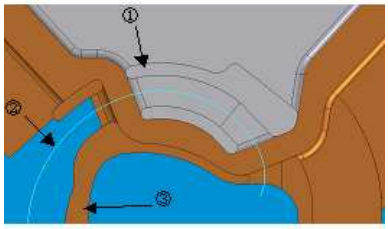

Figure 1. The puller channel and a beam trajectory, where 1=puller channel, 2=beam trajectory, 3= RF shield.

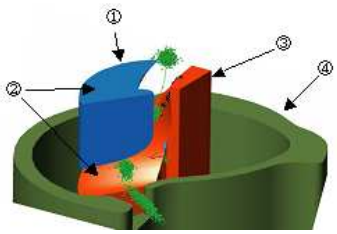

Figure 2. Bunched beam passage through the inflector: 1=bunched beam, 2=inflector, 3=inflector (support), 4=RF shield.

shown in Fig. 2:bunched beam passage through the inflector. In the figure, the bunched beams come from upper side associate with an axial injection line and an ion source.

4. Optimization

Optimization for the existing structure has been studied in order to get higher beam transmission. The major goal is to obtain sufficiently small axial losses during the initial turns. The result could be somewhat improved by some small modification of the electrode dimension at the 2nd turn as well as the inflector parameter, the magnetic field distribution in the center region, and the acceleration voltage. After the modification, loss from the inflector ground to the ESD entrance is 35% instead of 60%.

5. Conclusion

Computer model of the AVF cyclotron in the 1st approximation has been constructed. Some possible effects, having an impact on the transmission and the beam quality have been spotted. Initial optimization study has been conducted.

References

[1] A. S. Vorozhtsov et al, 'Magnetic field of the VINCY Cyclotron', XXXV European Cyclotron Progress Meeting (ECPM 2006), Nice, November 2-4, 2006.

[2] Previous work made by RIKEN AVF cyclotron construction group.

Intense RI Beam Production using a Cryogenic Gas Target at CRIB

H. Yamaguchi, Y. Wakabayashi, S. Hayakawa, G. Amadio, H. Fujikawa, S. Kubono, and D.N. Binh[a]

Center for Nuclear Study, Graduate School of Science, University of Tokyo
[a]Institute of Physics and Electronics, Vietnam Academy of Science and Technology

1. Introduction

A thick and thermostable gas target is relevant for the production of intense RI beams at CRIB (CNS Radio Isotope Beam separator) [1, 2, 3]. In 2006, a cryogenic gas target system was newly developed for CRIB [4]. In that system, the target gas is cooled down to near the liquid nitrogen temperature, to have a thicker target and the stability against the heat. Forced circulation of the target gas can be made in the system, which helps us to avoid the reduction of the effective target thickness [5].

2. Test for the basic features of the target system using heavy-ion beams

We have performed a test experiment of the new cryogenic target system using an RI beam produced at CRIB. In this measurement, hydrogen gas of 760 Torr (at maximum) in a 80 mm-long cell was used as the RI-beam production target. The primary beam used for the production was $^{7}Li^{2+}$ at 5.6 MeV/u, of which the maximum current was 2.8 eμA. The results of the test experiment are described in the following.

2.1. Liquid nitrogen consumption

The measured consumption rate of the liquid nitrogen at the top dewar (see [4]) was 50 ml/min, when there was no gas circulation nor irradiation of the heavy-ion beam. This intrinsic consumption rate is mainly due to the small amount of evaporation of the liquid nitrogen at the top dewar, although the dewar is well covered by thermal-insulating materials. The liquid nitrogen is lost also during the transfer from the storage bottle to the top dewar (transfer efficiency is 70–80%). Considering this efficiency, the total consumption rate amounts to 60 ml/min (about 100 l/day).

The consumption by the heat of the heavy-ion beam is typically much smaller than the intrinsic consumption. The theoretical consumption rate for the heat deposit in this measurement (7.4 W) is 1.3 ml/min.

However, the consumption rate increased when the gas circulation is turned on, as the gas was cooled and warmed repeatedly in its cycle. The measured consumption rate by the circulation was almost linear to the circulation rate, being 13 ml/min per circulation rate of 10 slm (standard liters per minute). .

2.2. Target thickness

The energy of the heavy-ion beam at CRIB can be measured precisely by an analyzing magnet, of which magnetic field strength is monitored with an NMR (Nuclear Magnetic Resonance) probe. Target thickness was determined for various target pressures (200–760 Torr) and circulation rates (0–55 slm), by measuring the energy loss of the beam in the target. The measured thickness was almost proportional to the pressure, indicating the target temperature is constant, independent of the circulation rate. The corresponding temperature, calculated from the measured thickness and pressure, was 85–90 K. This temperature agrees with the measurement by a thermocouple located close to the gas cell, which showed around 88–90 K. The maximum target thickness in this measurement was 2.3 mg/cm^2.

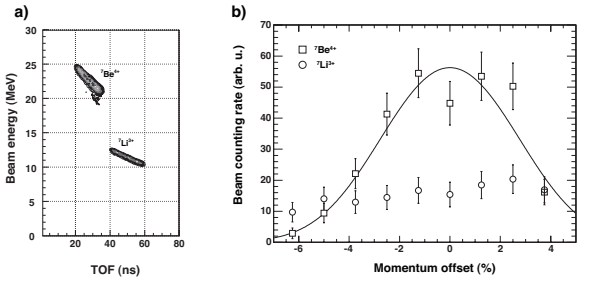

Figure 1. a) Particle identification diagram by the energy and time of flight, b) Momentum distribution of the $^{7}Be^{4+}$beam, together with the contaminant, $^{7}Li^{3+}$. Note that the TOF shown here is from the radio-frequency signal of the cyclotron, and it has an arbitrary time offset for each particle.

2.3. Momentum distribution of the secondary beam

We produced ^{7}Be as the secondary beam from ^{7}Li via (p,n) reaction in inverse kinematics, and its momentum distribution was measured using the analysing magnet of CRIB.

Figure 1a shows the energy and time of flight (TOF) of the detected particles. Two kinds of particles were detected and identified as $^{7}Be^{4+}$ and $^{7}Li^{3+}$, the latter of which came from the primary beam. Other particles were not detected in this measurement. Figure 1b shows the counting rates of $^{7}Be^{4+}$ against the relative momentum offset $\Delta p/p$ (in %) from the center of the distribution, which corresponds to 608 MeV/c (4.0 MeV/u in energy) for the ^{7}Be beam. The counting rates of $^{7}Li^{3+}$ detected in the same measurement are also plotted.

The beam purity of $^{7}Be^{4+}$ is defined as the ratio of the number of $^{7}Be^{4+}$ to the total. The maximum beam purity was determined as 75 % in this measurement. The beam purity is an important index when we evaluate the target thickness reduction by high-current primary beams.

2.4. Intense secondary beam production and circulation rate

Figure 2 shows the production rates of the $^{7}Be^{4+}$ beam, measured for various primary-beam currents and gas circulation rates in the target. The rates are normalized for the momentum acceptance of ± 3 %, and we obtained an intense ^{7}Be beam of 2×10^{8} per second in the best cases. The beam current was measured by a Faraday cup installed

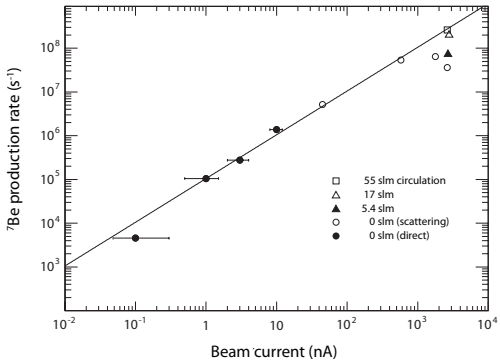

Figure 2. The production rates of the $^7Be^{4+}$ beam. For beam with currents less than 10 nA, the rate was measured with the PPAC (indicated as "direct"). For higher current beams, the rate was determined by counting elastic scattered particles with a gold foil.

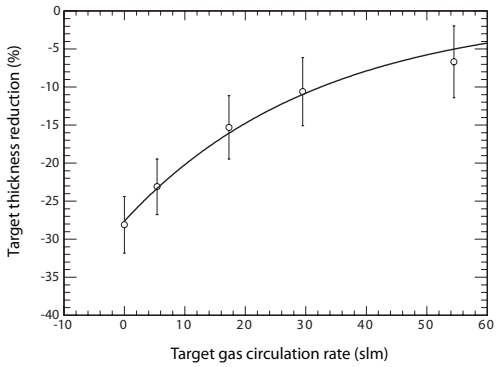

Figure 3. Thickness reduction for the hydrogen gas target of 2.2–2.3 mg/cm^2, irradiated by the $^7Li^{2+}$ beam of 2.7 eμA. The reduction is denoted as the deviation from the standard thickness, measured with a low-current beam. The error is mostly systematic. The data were fitted by an exponential function.

on the beam line.

The production rates were measured by the following two different methods. The first method is a direct measurement using a parallel-plate avalanche counter (PPAC) [6]. The PPAC has an ability to count the beam with the rate up to around 10^6 particles per second. The beam purity was known from the measured TOF. For the case of the beam coming with a much higher rate, we placed a thin (1 μm) gold foil in the beam line, and detected elastically scattered beams by a silicon detector. As the scattered $^7Be^{4+}$ and $^7Li^{3+}$ have different energies which could be clearly identified by the silicon detector, we determined the beam purity with this method as well.

The result shows a good linearity between the production rate and the primary beam current less than 1 eμA. The beam purity remained the same for this current region. However, when the beam current went over 1 eμA, the production rate deviated from the proportional line, and the beam purity started to decrease. This is considered as the thickness-reduction effect caused by the heat [5].

Since we observed the beams with a fixed central momentum, the count rate of $^7Be^{4+}$ decreases by the following two reasons, both arising when the target thickness is reduced. The first reason is simply the reduction of the number of the beam-production reactions, as it is almost proportional to the target thickness. The second reason is the momentum shift of the beam after the target. The central momentum of the beam becomes higher than the normal thickness case, and significant amounts of the beam will go out of the acceptance, which was optimized for the low-current beam conditions.

We evaluated the second effect (momentum shift) using the results shown in Figure 1, and extracted the information on the reduction of the effective target thickness itself.

Figure 3 shows the effective target thicknesses for several circulation rates, when the original target thickness was 2.2–2.3 mg/cm^2, and the $^7Li^{2+}$ beam current was around 2.7 eμA. This result indicates that there was a thermal thickness-reduction effect, which could be minimized by making the circulation of the target gas. The heat deposit by the beam was 5.2 W (corresponding to 65 mW/mm) at the gas, and 2.2 W at the window foils. As shown in the figure, target thickness decreased by about 30 %, when there was no gas circulation. This amount of reduction agrees with the measurement reported in [5], which resulted in a reduction by 30% for the beam of 60 mW/mm.

3. Summary

We obtained an intense (2×10^8 per second) ^{7}Be beam, having the energy of (4.0 ± 0.24) MeV/u. The cryogenic hydrogen gas target was used for the RI-beam production, with the maximum thickness of 2.3 mg/cm^2. We have observed a reduction of the target thickness, possibly due to the high heat deposit of the beam. The reduction was about 30 % at maximum, when the beam deposits heat of 65 mW/mm in the gas. We succeeded in minimizing the reduction effect to around 5 %, by making the gas circulation of 55 slm.

References

[1] S. Kubono *et al.*, Eur. Phys. J. A **13** (2002) 217.
[2] Y. Yanagisawa *et al.*, Nucl. Instrum. Methods Phys. Res., Sect. A **539** (2005) 74.
[3] T. Teranishi *et al.*, Phys. Lett. B **556** (2003) 27.
[4] H. Yamaguchi *et al.*, CNS Annual Report 2005 (2006) 71.
[5] J. Goerres *et al.*, Nucl. Instrum. Methods, 177 (1980) 295.
[6] H. Kumagai, *et al.*, Nucl. Instrum. and Methods **A470** (2001) 562.

Beam Production Test for the Measurement of the ^{18}F + p $\rightarrow \alpha$ + ^{15}O Reaction in Novae

S. Cherubini[a], C. Spitaleri[a], V. Crucillà[a], M. Gulino[a], M. La Cognata[a], L. Lamia[a], R.G. Pizzone[a], S. M. R. Puglia[a], G. Rapisarda[a], S. Romano[a], L. M.L. Sergi[a], S. Tudisco[a], A. Tumino[a], S. Kubono, H. Yamaguchi, Y. Wakabayashi, G. Amadio, S. Hayakawa N. Iwasa[b], S. Kato[c], S. Nishimura[d], T. Teranishi[e]

[a] *D.M.F.C.I.,University of Catania and INFN-LNS, Catania, Italy*
Center for Nuclear Study, Graduate School of Science, University of Tokyo
[b] *Department of Physics, Tohoku University, Sendai, Japan*
[c] *Department of Physics, Yamagata University,Yamagata, Japan*
[d] *RIKEN (The Institute of Physical and Chemical Research), Wako, Japan*
[e] *Kyushu University, Kyushu, Japan*

We plan to measure the cross section of the ^{18}F(p,α)^{15}O reaction in the energy range of interest for the study of the Nova phenomena. We report here on the second ^{18}F beam production test that was performed using the CRIB set-up of the Center for Nuclear Study (CNS) of the University of Tokyo, based at the RIKEN campus in Wako.

Astronomical observations suggest that nova explosions and x-ray bursts occur in close binaries in which the hydrogen-rich material from the outer layers of an extended star is filling its Roche lobe and accreting onto the surface of its companion, a white dwarf or a neutron star, respectively. In such explosive events, the temperatures and densities involved are sufficiently high so that proton and alpha-particle induced nuclear reactions can be fast enough to bypass beta-decay processes. These nuclear reactions involving radioactive nuclei can greatly increase both the rate of energy generation and the total amount of energy produced and can have a dramatic impact on both the isotopic and elemental abundances produced. It has been shown in [1] that classical novae emit γ-ray at and below 511 keV soon after the explosion. The positrons which give rise to the γ emission due to electron-positron annihilation process in the expanding envelope mainly come from ^{18}F β-decay, because its life-time (τ=158 min) is comparable to the time scale when the nova-envelope begins to be transparent to gamma radiation. Thus, the radiation intensity strongly depends on the ^{18}F abundance; for this reason it is necessary to study processes that produce and destroy this isotope in novae. Among these, the ^{18}F(p,α)^{15}O reaction stands as one of the main ^{18}F destruction channels. Consequently, its study in the relevant energy regions is strongly required. ¿From these observations it follows that the reaction ^{18}F(p,α)^{15}O has to be studied in the energy range 100-500 keV (center of mass) roughly. In particular, the contribution to the cross section of the resonance at 330 keV has to be investigated together with the interferences between several other levels occurring in the region of interest. In spite of several attempts to measure this cross section (see e.g. [2]- [15]) the situation is still not satisfactory. For this reason we proposed a new measurement of the ^{18}F(p,α)^{15}O.

We intend to study the excitation function of the ^{18}F(p,α)^{15}O over the full range of astrophysical interest. To this end, we will implement two different experimental approaches. We will make a direct measurement for the higher (i.e. $>$ roughly 400 keV) energy region. Owing to the expected extremely small cross sections of the reaction in the low energy region (200 keV - 400 keV roughly), we will use the Trojan Horse (TH) method [16], [17], [18] in order to explore this part of the excitation function. This will be the first application of the TH method in a reaction where a radioactive ion beam is used.

In 2006 we performed preliminary test of the ^{18}F beam production. The CRIB set-up is shown in figure 1 and described in ref. [19].

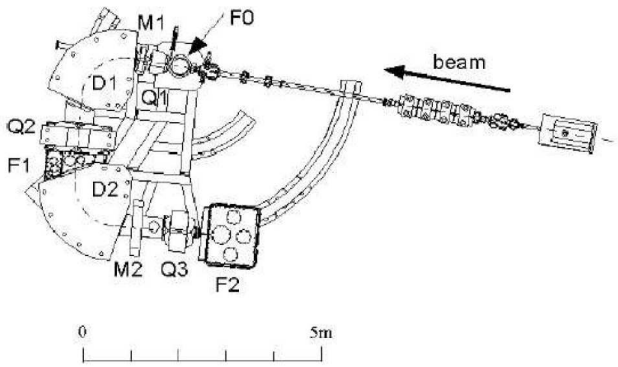

Figure 1. Top view of the CRIB setup

The beam is produced in-flight using the ^{18}O(p,n)^{18}F reaction. A 72 MeV ^{18}O beam of intensity as high as 1 eμA was used to bombard a primary target consisting of a 8 cm long gas cell containing H_2 at a pressure of roughly 600 torr. The products coming from the cell were separated from the primary beam by the CRIB set-up. After the doubly acromatic separator a Wien filter was also used to further purify the the ^{18}F beam. As a result, the beam test showed that it is possible to obtain a practically pure beam of ^{18}F (purity $> 99\%$) and with a good intensity (order of 10^6).

References

[1] A. Coc et al., A.&A., **357** (2000) 561 and references therein.

[2] M. Wiescher and K.U. Kettner, Astrophys. J. **263** (1982) 891.

[3] K.E. Rehm, M. Paul, A.D. Roberts, et al., Phys. Rev. C **52** (1995) R460.

[4] R. Coszach, M. Cogneau, C.R. Bain, et al., 1995, Phys. Lett. B **353** (1998) 184.

[5] K.E. Rehm, M. Paul, A.D. Roberts, et al., Phys. Rev. C **53** (1996) 1950.

[6] K.E. Rehm, C.L. Jiang, M. Paul, et al., Phys. Rev. C **55** (1997) R566.

[7] J.S. Graulich, F. Binon, W. Bradfield-Smith, et al., Nucl. Phys. A **626** (1997) 751.

[8] S. Utku, J.G. Ross, N.P.T. Bateman, et al., Phys. Rev. C **57** (1998) 2731 and C58 (1998) 1354.

[9] Y.M. Butt, J.W. Hammer, M. Jaeger, et al., Phys. Rev. C **58** (1998) R10.

[10] J.-S. Graulich, S. Cherubini, R. Coszach, et al.,Phys. Rev. C **63** (2001) 011302 and references therein.

[11] D.W. Bardayan, J.C. Blackmon, W. Bradfield-Smith, et al., Phys. Rev. C **63** (2001) 065802.

[12] D.W. Bardayan, J.C. Batchelder, J.C. Blackmon, et al., Phys. Rev. Lett. **89** (2002) 262501.

[13] R.L. Kozub, D.W. Bardayan, J.C. Batchelder, et al., Phys. Rev. C **71** (2005) 032801 (R).

[14] R.L. Kozub, D.W. Bardayan, J.C. Batchelder, et al., Nucl. Phys. A **758** (2005) 753c-756c.

[15] N. De Sereville, A. Coc, C. Angulo, et al., Phys. Rev. C **67** (2003) 052801 (R) and references therein.

[16] S. Cherubini, V.N. Kondratyev, M. Lattuada , et al., ApJ **457** (1996) 855

[17] C. Spitaleri, M. Aliotta , S. Cherubini, et al., Phys. Rev. C **60** (1999) 055802

[18] C. Spitaleri, S. Typel, R.G. Pizzone, et al. Phys. Rev. C **63** (2001) 055801

[19] Y. Yanagisawa, S. Kubono, T. Teranishi, et al., Nucl. Instr. Meth. A **539** (2005) 74

SHARAQ Project – Progress in FY2006 –

T. Uesaka , S. Shimoura, H. Sakai[a], K. Nakanishi, A. Saito[a], Y. Sasamoto, S. Michimasa, T. Kawabata, S. Kubono, E. Ideguchi, H. Yamaguchi, T. Kubo[b], and G. P. Berg[c]

Center for Nuclear Study, Graduate School of Science, University of Tokyo
[a] *Department of Physics, Graduate School of Science, University of Tokyo*
[b] *RIKEN (the Institute for Physical and Chemical Research)*
[c] *Department of Physics, Notre Dame University*

SHARAQ project aims to initiate new research activities of nuclear physics by use of a high resolution magnetic spectrometer in radioactive isotope beam experiments. The project has been carried out in collaboration with Sakai group of the Department of Physics and RIKEN Nishina Center. In this report, progress in FY2006 is summarized.

1. Spectrometer

The high-resolution SHARAQ spectrometer is designed to analyze charged particles with a magnetic rigidity of 1.8–6.8 Tm, which provides momentum and angular resolutions of $\delta p/p$ ∼1/15000 and ∼ 1 mrad, respectively. Three of the five magnets making up the spectrometer were newly manufactured in FY2006.

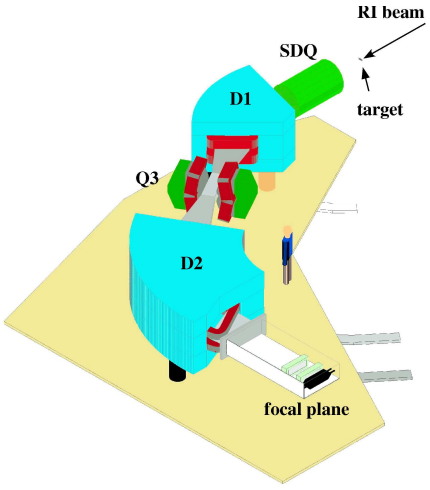

Figure 1. SHARAQ spectrometer

Superconducting doublet quadrupoles (SDQ) are the first part of the spectrometer and used to optimize a beam envelope for achieving required momentum resolution and a required detection solid angle. Its design work started in FY2004, on the basis of the design of superconducting triplet quadrupoles of BigRIPS [1]. Superconducting coils manufactured in FY2005 were mounted on to iron yokes and packed in a cryostat equipped with stand-alone refrigerators. In the cryostat filled with liquid helium, the superconducting coils were successfully cooled down to 4.5 K and a field gradient of 14.1 T/m was produced as designed by applying a DC current of 142 A. They have been already installed in the RIBF building and the field mapping is planned in the beginning of FY2007. Details of the SDQ are described in Ref. [2].

A D2 magnet is the largest magnet in the spectrometer and plays a central role in a momentum analysis. Based on previous studies [3, 4], detailed designs of pole-pieces, yokes, field clamps, and a vacuum chamber have been completed in FY2006 [5]. The magnet was already assembled in the manufacturer factory and is scheduled to be transported to the RIBF building in July of 2007.

The first dipole magnet D1, which has been used in the decommissioned spectrograph SMART, was renovated for the use in SHARAQ. D1 is used to bend a beam by 32.7° with ρ =4.4 m in SHARAQ, while it was originally used as a 60°-bending magnet with ρ =2.4 m in SMART. In addition, the maximum magnetic field increases to 1.55 T from the original value of 1.42 T. To achieve a required field homogeneity of $\Delta B/B \sim 4 \times 10^{-4}$, a modification of pole-pieces shown in Fig. 2 was proposed [6]. The hatched area at corners of the pole-piece in Fig. 2 are taken off with radii of 160 mm and 170 mm at the low- and high-momentum sides, respectively. Additional renovation of side yokes is planned in FY2007.

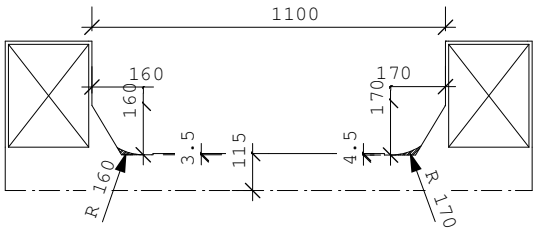

Figure 2. Cross section of the D1 pole piece. The hatched area are taken off.

2. High-resolution Beamline

Detailed design of a high-resolution beamline for SHARAQ has been finalized in FY2006 [7]. Secondary RI beams inevitably have large momentum spreads on the order of 10^{-2}. High momentum and angular resolution measurements with such beams require cancellation of effects due to the spread. Two different methods, a dispersion matching method and an event-by-event tagging method, will be applied in the measurement with SHARAQ. Ion-optical studies have been made to equip the beamline with the both capabilities. A beamline arrangement which achieves required specifications could be found with exist-

ing beam transport elements. Corrections of higher order aberrations by octupole magnets are also studied.

Construction of the beamline will be completed in the beginning of FY2008.

3. Detector R&D

Thin tracking detectors are necessary both in beamline tuning, especially in dispersion matching operation, and in tagging of beam particles during measurements. Development of low-pressure multiwire drift chambers are under way for use as the beamline detectors [8]. Prototypes are manufactured and are being tested with radioactive sources and cosmic rays.

Focal plane tracking detectors should have a position resolution of ~ 0.3 mm in FWHM to achieve the required momentum resolution of $1/15000$. In addition, they should operate at low-pressure of $\sim 10^4$ Pa to minimize multiple scattering which may spoil the angular resolution. Cathode read-out drift chambers (CRDC) are being considered as the detectors capable of covering the focal plane of $\sim 500 \times 300$ mm. Discussion with a GANIL group has been started to fix specifications of CRDCs.

tal area) of the RIBF building. Electricity and cooling water for magnets will be arranged in FY2007.

References

[1] K. Kusaka et al., IEEE Transactions on Applied Superconductivity, **14** (2004) 310.
[2] K. Nakanishi et al., CNS Annual Report 2006 (2007).
[3] G.P.A. Berg, Design Study of a New Dipole Magnet D2 for the SHARAQ Spectrometer, *unpublished*, 2005.
[4] T. Uesaka et al., CNS Annual Report 2005 (2006) 61.
[5] T. Uesaka et al., CNS Annual Report 2006 (2007).
[6] G.P.A. Berg, Evaluation of SMART Dipole for SHARAQ D1, *unpublished*, 2006.
[7] T. Kawabata et al., CNS Annual Report 2006 (2007).
[8] A. Saito et al., CNS Annual Report 2006 (2007).

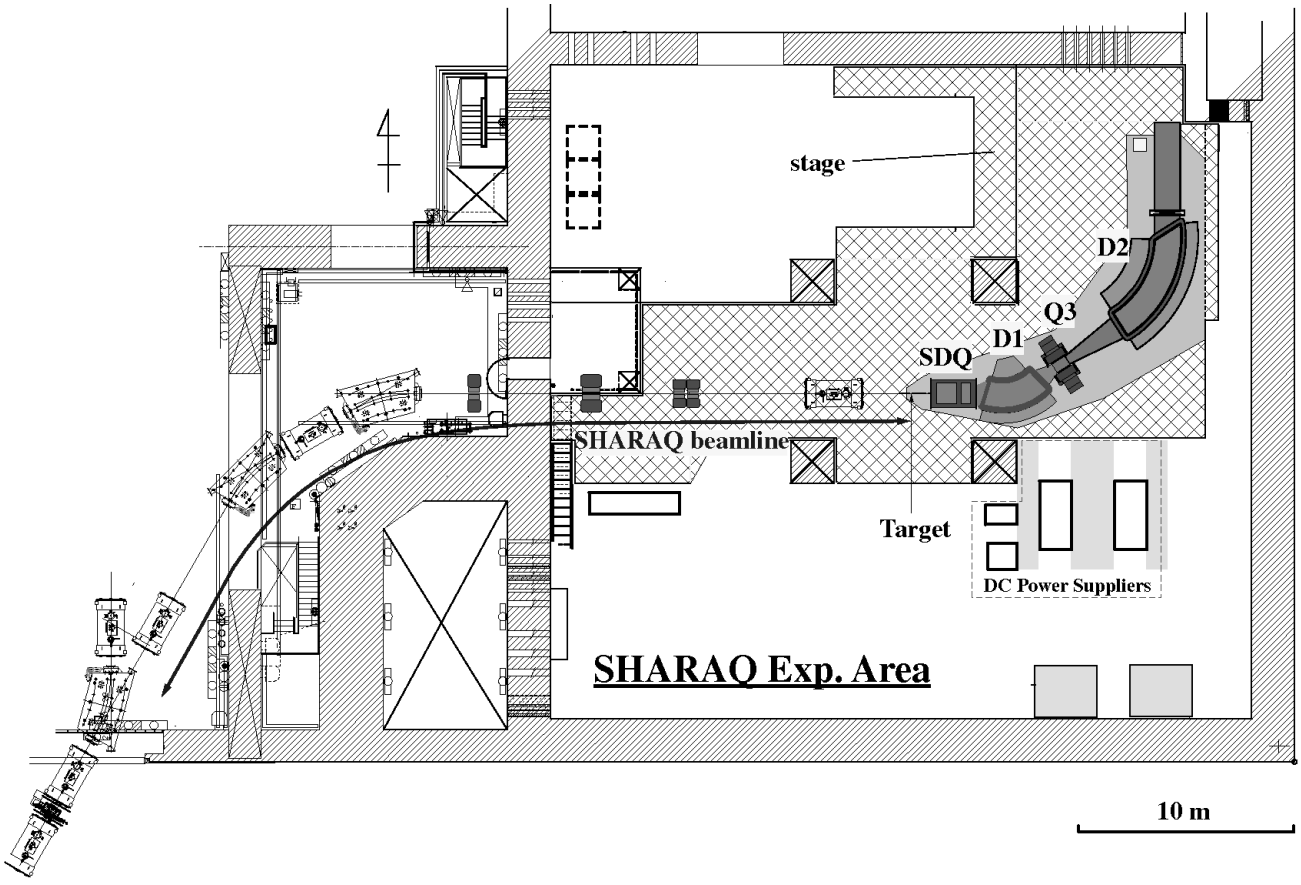

Figure 3. Overview of the SHARAQ experimental area.

4. Experimental Area

The experimental area is being prepared for installation of the SHARAQ spectrometer and the beamline. A stage made of concrete shown by a hatched region in Fig. 3 was placed in the SHARAQ experimental area (E20 experimen-

High Resolution Beam Line for the SHARAQ Spectrometer

T. Kawabata[a], G. P. A. Berg[b], T. Kubo[c], H. Sakai[d], S. Shimoura[a], and T. Uesaka[a]

[a] *Center for Nuclear Study, Graduate School of Science, University of Tokyo*
[b] *Department of Physics, University of Notre Dame*
[c] *RIKEN (The Institute of Physical and Chemical Research)*
[d] *Department of Physics, Graduate School of Science, University of Tokyo*

The construction of the SHARAQ spectrometer started in 2005 at the Center for Nuclear Study [1]. The SHARAQ spectrometer is designed to achieve a high momentum resolution of $\delta p/p \sim 1/15000$ for charged particles with a magnetic rigidity of $B\rho = 6.8$ Tm. The SHARAQ spectrometer will be devoted to the nuclear spectroscopic study using RI beams produced by the RI beam factory (RIBF) at RIKEN. Since the RI beams have a variety of isospin, spin, and internal energy, the RI-beam induced reactions are expected to be useful tools for probing nuclear many body systems.

Since the RI beams generally have a large emittance, the dispersion matching technique [2, 3] must be introduced to perform high resolution measurements. If the dispersions of the SHARAQ spectrometer and its beam line are properly "matched", the missing-mass resolution can be significantly improved better than the momentum spread of the RI beam.

Following the notation of the computer code TRANSPORT [4], the horizontal position x and angle θ at the focal plane of the spectrometer are related to those at the starting point of the beam line by using the transfer matrix elements of the spectrometer (s_{ij}) and beam line (b_{ij}).

$$\begin{aligned} x =&(s_{11}b_{11} + s_{12}b_{21})x_0 \\ &+ (s_{11}b_{12} + s_{12}b_{22})\theta_0 \\ &+ (s_{11}b_{16} + s_{12}b_{26} + s_{16})\delta_0, \qquad (1) \\ \theta =&(s_{21}b_{11} + s_{22}b_{21})x_0 \\ &+ (s_{21}b_{12} + s_{22}b_{22})\theta_0 \\ &+ (s_{21}b_{16} + s_{22}b_{26} + s_{26})\delta_0. \qquad (2) \end{aligned}$$

The x_0, θ_0, and δ_0 are the horizontal position, angle, and fractional momentum deviation from the central trajectory ($\delta \equiv \Delta p/p$) at the starting point of the beam line. When the coefficients of the momentum dependent terms in Eqs. (1) and (2) are zero as

$$s_{11}b_{16} + s_{12}b_{26} + s_{16} = 0, \qquad (3)$$
$$s_{21}b_{16} + s_{22}b_{26} + s_{26} = 0, \qquad (4)$$

the horizontal position and angle at the focal plane are independent of the momentum spread of the beam. Equations (3) and (4) are commonly called as the momenutm- and angular-dispersion matching conditions, respectively. It is necessary for the high-resolution spectroscopy with the secondary RI beam to construct the beam line satisfying these matching conditions. From Eqs. (3), (4), and the SHARAQ design values of s_{ij}, the dispersion matching conditions for the beam-line transfer matrix elements are determined to be $b_{16} = -13.66$ m and $b_{26} = 4.53$ rad.

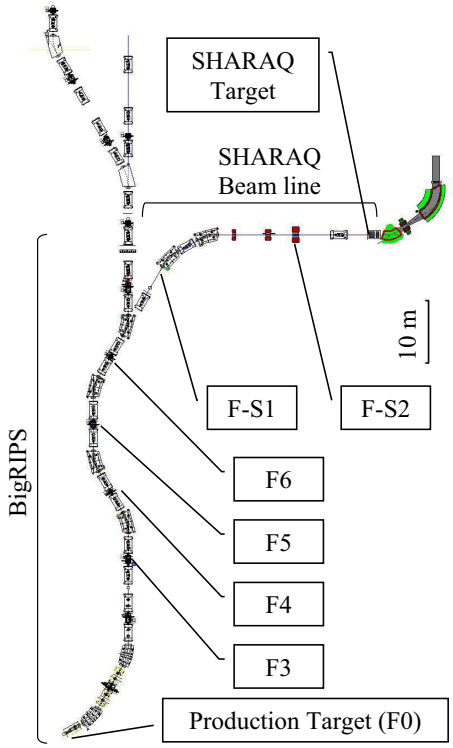

Figure 1. Layout of the SHARAQ spectrometer and the high-resolution beam line at RIBF.

The SHARAQ spectrometer will be installed in the E20 experimental room at RIBF as seen in Fig. 1. Since the RI beam emitted from the production target at F0 is achromatically focused at F3 in the normal beam transport procedure for the BigRIPS fragment separator [5], we determined F3 to be the starting point of the SHARAQ beam line. The SHARAQ beam line shares the magnetic elements with the BigRIPS fragment separator up to F6. After F6, the SHARAQ beam line branches from BigRIPS and bends 60° toward the target. The beam-line layout between the branching point and the SHARAQ target are optimized to satisfy the dispersion matching conditions in the first-order ion optical calculation [6].

The two 30° bending magnets (BM) are used together with the several quadrupole magnets for the beam transport from F6 to the SHARAQ target. Although most of the quadrupole magnets are the super conducting triplet quadrupole magnets (STQ) with the warm bore radius of 12 cm [7], only the doublet (DQ) and singlet (SQ) quadrupole magnets are the normal conducting magnets. DQ and SQ are located between BM-S2 and STQ-S3. The

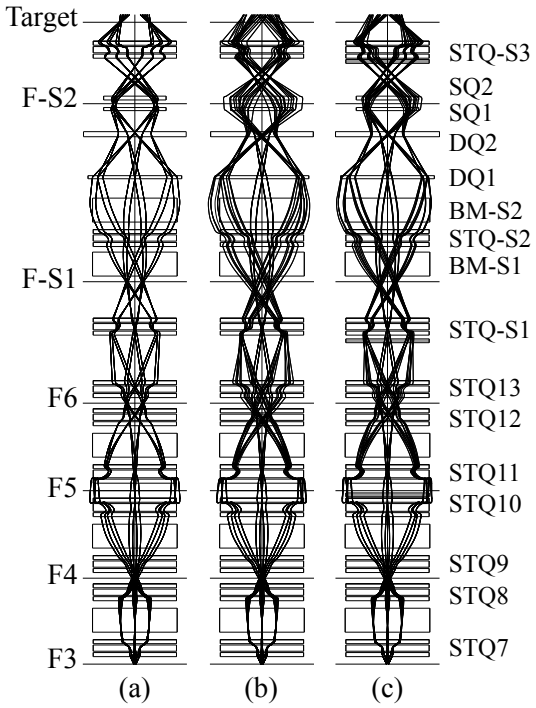

Figure 2. Envelopes of the dispersive beam transport from F3 to the SHARAQ target in the horizontal plane. Trajectories for particles with $x_0 = \pm 3$ mm, $y_0 = \pm 3$ mm, $\theta_0 = \pm 10$ and 0 mr, $\phi_0 = \pm 30$ and 0 mr, and $\delta_0 = \pm 0.3\%$ in the first order calculation are shown in (a), whereas those in the third order calculation without and with octupole magnets are in (b) and (c), respectively. The octupole magnets are show by the gray rectangles in (c).

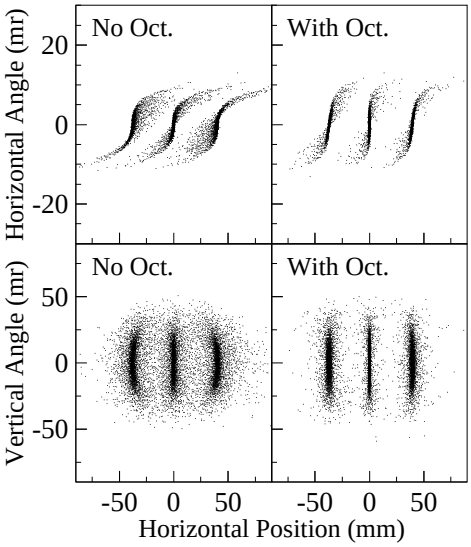

Figure 3. Correlation between the horizontal position on the SHARAQ target and the horizontal and vertical angles at F3. The left and right panels show the correlation patterns before and after octupole magnets are installed.

maximum magnetic rigidity of the beam line is 8.5 Tm, which is limited by the maximum field gradient of 15 T/m of STQ.

The precise ion optical calculation was performed using the computer code COSY INFINITY [8] with measured magnetic field maps of BM and STQ. Envelopes of the beam trajectories in the horizontal plane are shown in Fig. 2. Trajectories are drawn for particles with $x_0 = \pm 3$ mm, $y_0 = \pm 3$ mm, $\theta_0 = \pm 10$ and 0 mr, $\phi_0 = \pm 30$ and 0 mr, and $\delta_0 = \pm 0.3\%$, respectively. Figure 2(a) shows trajectories in the first-order calculation whereas Fig. 2(b) shows those in the 3rd-order calculation. Since the secondary RI beams have a large emittance, the higher order aberration deteriorates the missing-mass resolution. To correct such higher order effects, the multipole magnets should be installed. The best layout of the multipole magnets are searched, and it is found that the higher order aberration is effectively suppressed when three ocutupole magnets are installed at F5 and at the upper streams of STQ-S1 and STQ-S3 as seen in Fig. 2(c).

To examine the beam profile on the SHARAQ target, Monte Carlo calculation was carried out. A monochromatic beam with the momentum of $\delta_0 = 0$ or $\pm 0.3\%$ was transported from F3 to the SHARAQ target using the calculated beam transfer matrix. The beam spot size and the angular spreads at F3 were assumed to be $\Delta x_0 = \Delta y_0 = \pm 0.5$ mm, $\Delta\theta_0 = \pm 10$ mr, and $\Delta\phi_0 = \pm 30$ mr. The expected correlation between the horizontal position on the SHARAQ target and the horizontal and vertical angles at F3 is shown in Fig. 3. The left panels show the correlation when the three octupole magnets are not installed, whereas the right panels show the correlation when the octupole magnets are installed. Three loci seen in each panel correspond to the three assumed beam momenta of $\delta = 0$ and $\pm 0.3\%$. It is clearly seen that the octupole magnets actually suppress the higher order aberration.

The construction of the SHARAQ beam line will be started soon, and the first beam will be delivered to the SHARAQ spectrometer in 2008.

References

[1] T. Uesaka *et al.*, CNS Annual Report 2005 (2006) 61.
[2] B. L. Cohen, Rev. Sci. Instr. **30** (1959) 415.
[3] T. Wakasa *et al.*, Nucl. Instrum. Methods. A **482** (2002) 79, and references therein.
[4] K. L. Brown *et al.*, SLAC Report No. 91 Rev. 1, 1974 (unpublished).
[5] T. Kubo, Nucl. Instrum. Methods. B **204** (2003) 97.
[6] T. Kawabata *et al.*, CNS Annual Report 2005 (2006) 63.
[7] K. Kusaka *et al.*, IEEE Trans. Appl. Supercond. **14** (2004) 310.
[8] M. Berz *et al.*, Computer code COSY INFINITY, http://bt.pa.msu.edu/index_files/cosy.htm.

Developments of Multiwire Drift Chambers for SHARAQ Beamline

A. Saito, S. Shimoura[a], T. Kawabata[a], Y. Sasamoto[a], T. Uesaka[a] and H. Sakai

Department of Physics, University of Tokyo
[a]*Center for Nuclear Study, Graduate School of Science, University of Tokyo*

We are developing beamline detectors that will be used at the high-resolution beamline for the SHARAQ spectrometer, which are now under construction at RI Beam Factory (RIBF) [1, 2]. The spectrometer is designed to achieve a resolving power of $p/\delta p \sim 1.5 \times 10^4$ and an angular resolution better than 1 mrad for charged particles with magnetic rigidity of 6.8 Tm at the maximum. The beamline for the SHARAQ spectrometer is designed to fulfill dispersion-matching conditions when combined with the SHARAQ spectrometer [3]. The simultaneous achievement of lateral dispersion matching and angular dispersion matching conditions are crucially important in the use of the SHARAQ spectrometer for RI beams, which necessarily accompany a large momentum spread. Details of the dispersion-matched beamline is described in other reports [3]. A dispersion matching technique and/or the event-by-event tagging of the beam momentum will be introduced to compensate for the energy spread of the RI beam. Figure 1 shows the calculated optics of dispersive beam transport. The event-by-event tagging and tracking are needed at F3 for monitoring image size and at the target position to measure the momentum vector of the RI beam. There are several requirements for the tracking detectors. The thickness of the detectors should be as small as $\sim 10^{-4}$ of radiation length to reduce the effects of multiple scattering in the detectors to $\sim$0.1 mrad. Detection efficiency should be high even for light RI beams such as ^{8}He at 300 A MeV. The position resolution is required to be less than 300 μm at FWHM. The maximum counting rate should be 1 MHz for the dispersive beam transport.

In order to realize the performance described above, low-pressure multiwire drift chambers (LP-MWDC's) are being developed. A low-pressure operation at around 10–20 kPa is needed to reduce multiple scattering in the detector to 0.1 mrad. The anode and potential wires are 12.5-μmϕ Au-W and 75-μmϕ Au-Cu, respectively. The size of one cell is 5×5 mm^2. The maximum counting rate of each cell is 10^4–10^5 Hz for dispersive beam transport. The specifications are summarized in Table 1. The signals from the anode wires are amplified and discriminated by the REPIC RPA-130 64-ch. preamplifier and discriminator card. The timing signals from RPA-130 are digitized by CAEN V1190A/B multi-hit TDC.

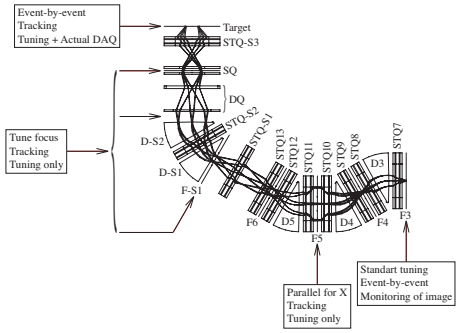

Figure 1. Calculated optics of the dispersive beam transport.

Table 1. Specifications of the beamline detectors.

	LP-MWDC	LP-MWDC with stripped cathodes
position resolution	$<$300 μm†	
efficiency	$>$95%†	
multiple scattering	$\sim$0.1 mrad†	$\sim$0.1 mrad†
counting rate	$\sim$1 MHz†	
anode wire	12.5 μmϕ	20 μmϕ
potential wire	75 μmϕ	75 μmϕ
cell size	5×5 mm^2	6×6 mm^2
anode-cathode pitch	2.4 mm	2.5 mm
cathode	2 μm^t	1.5 μm^t
gas	i-C_4H_{10}	i-C_4H_{10}
gas pressure	10–20 kPa†	10–20 kPa†

† designed value.

In addition, we are developing LP-MWDC with stripped cathodes. The structure of the detector is shown in Fig. 2. The anode and potential wires and the electronics are the same as those for LP-MWDC described above. The cathodes are stripped with 2.5 mm pitch and the signals are read out using the delay lines that were developed for the PPAC [4]. Since the latter readout system has only four channels, the number of channels can be reduced. Their prototypes are now being tested.

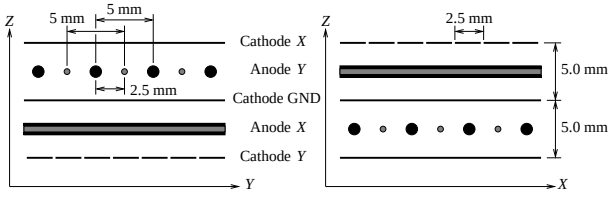

Figure 2. Schematic view of the LP-MWDC with stripped cathodes.

References

[1] T. Uesaka et al.: Eur. Phys. J. **A** (RNB7 conf. proc.) in press.
[2] T. Uesaka et al.: CNS Ann. Rep. 2005 (2006) 61.
[3] T. Kawabata et al.: CNS Ann. Rep. 2005 (2006) 63.
[4] H. Kumagai et al.: Nucl. Instrum. Meth. in Phys. Res. **A470** (2004) 562.

Figure 3. The Low-pressure multi-wire drift chamber.

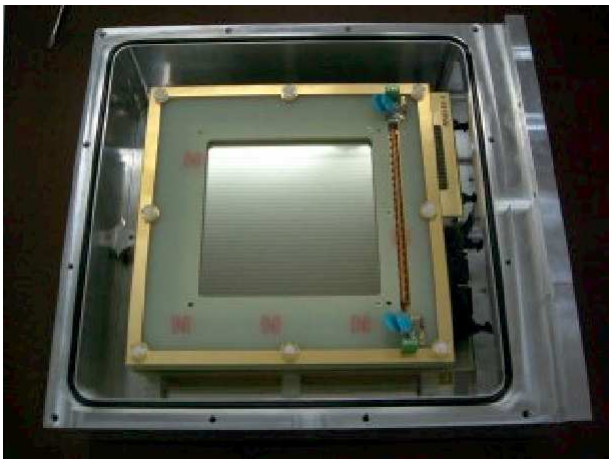

Figure 4. The Low-pressure multi-wire drift chamber with stripped cathodes.

New Dipole Magnet for the SHARAQ Spectrometer

T. Uesaka , K. Nakanishi, Y. Sasamoto, S. Shimoura, H. Sakai[a], A. Saito[a], S. Michimasa, T. Kawabata, and G. P. Berg[b]

Center for Nuclear Study, Graduate School of Science, University of Tokyo
[a] *Department of Physics, Graduate School of Science, University of Tokyo*
[b] *Department of Physics, Notre Dame University*

A second dipole magnet, D2, of the SHARAQ spectrometer [1] has been manufactured in FY2006. The D2 magnet is a 60° bending magnet with a pole gap of 200 mm. It is designed to achieve a magnetic homogeneity of the order of $\sim 10^{-4}$ for a magnetic field range of 0.4–1.55 T. The final design of the D2 magnet was completed by introducing several modifications to that described in Refs. [2, 3].

The pole pieces have a 1400 mm width with fillets on both sides, in the original design [2, 3], to produce a homogeneous magnetic field in the region ±400 mm around the central orbit. The fillets of 200 mm and 180 mm radii at the high- and low momentum sides, respectively, are approximated by 10-step functions as shown in Fig. 1. Rose shims with a thickness of 1 mm are placed on both sides.

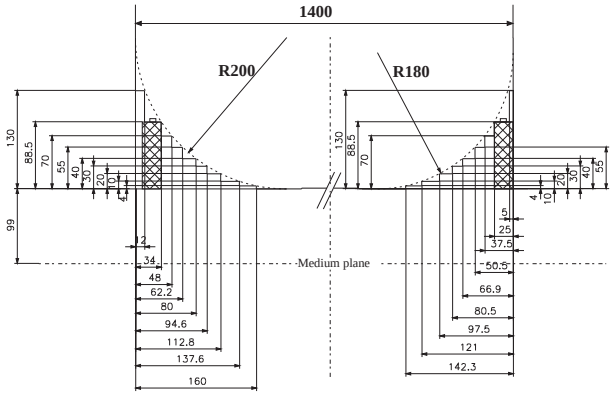

Figure 1. Cross section of the D2 pole piece.

Two-dimensional magnetic field calculations were made to evaluate resulting field homogeneities. Lengths of Rose shims were optimized to balance field homogeneities at high and low field strengths. A magnetization property of the actual pole pieces material was used in the calculation. Figure 2 shows the magnetic field distributions obtained for Rose shim length of 44 mm and 49 mm at the high- and low- momentum sides, respectively. Radial dependences of magnetic field strength in the medium plane are shown for $B = 1.57$ T and 0.40 T in upper and lower panels. A region used in the spectrometer, $R = 4400 \pm 400$ mm is indicated with shades. At the high field strength of $B \sim 1.55$ T, the field at $\Delta R = 400$ mm decreases by 4×10^{-4} due to iron saturation, while noses of $\Delta B/B = 4 \times 10^{-4}$ appears at the low field of $B \sim 0.4$ T. Thus it is found that the required field homogeneity can be achieved by the considered magnetic pole geometry.

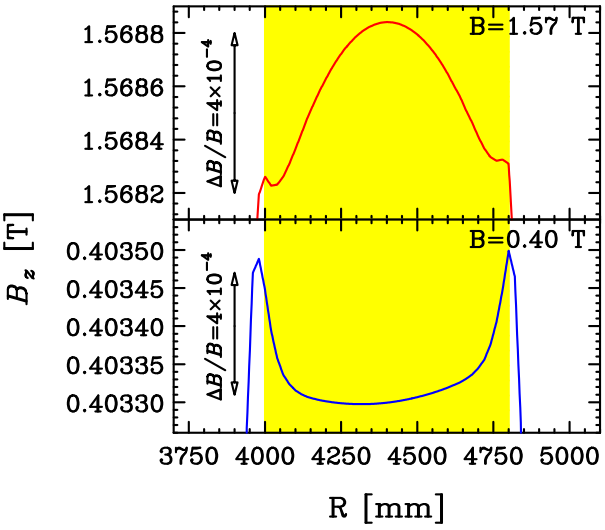

Figure 2. Calculated field distributions at B=1.57 T and 0.40 T.

The end profile of the magnet is shown in Fig. 3. Rogowski profile [5] is introduced to entrance and exit edges of the D2 magnet. The Rogowski curve shown by dashed line in the figure is approximated by a 11-step function in the actual design.

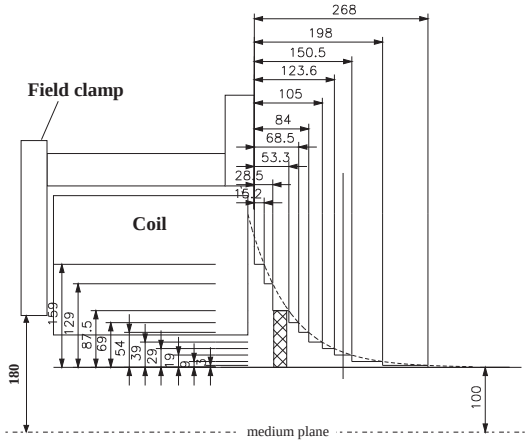

Figure 3. End profile of the D2 magnet.

A field clamp is placed to limit extending fringing field. The height of the field clamp was determined to be 180 mm from the medium plane. Magnetic field calculations show that change of the effective field boundary depending on the field strength is as small as 5 mm in the range of $B = 0.4$–1.55 T.

The entrance pole of D2 has a 3rd-order polynomial shape to minimize higher-order aberrations. The polynomial coefficients of the physical pole edge shaping were determined to give the effective field boundary required from the ion-optical calculations [4]. Figure 4 shows a photo of the D2 entrance edge.

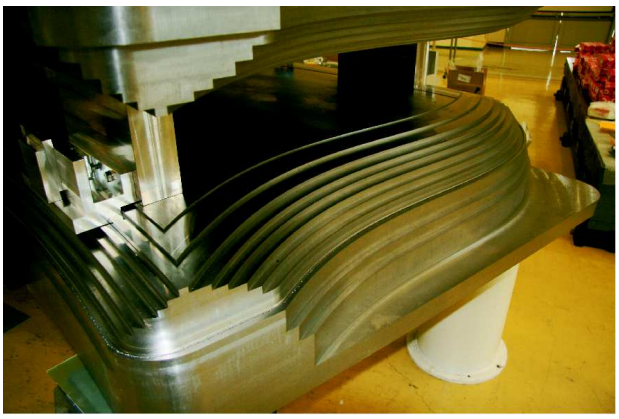

Figure 4. 3rd-order polynomial shaping of the D2 entrance.

A vacuum chamber is inserted between the pole pieces. The vacuum chamber (shown by a hatched squares in Fig. 1 and 3) is sealed by O-rings seating in groovse on the pole surfaces. Pole spacers are also placed between the pole pieces to fix the gap spacing to be 200 mm with a precision of 0.05 mm.

Figure 5 shows the assembled D2 magnet at the manufacturer factory.

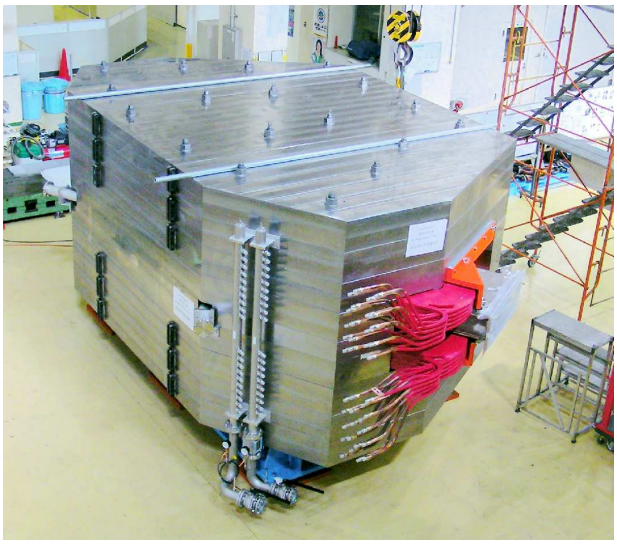

Figure 5. Photo of the D2 magnet.

The magnet will be installed at the SHARAQ experimental area of RI Beam Factory in August 2007. After the installation, field mapping measurements will be carried out.

References

[1] T. Uesaka et al., CNS Annual Report 2006.
[2] T. Uesaka et al., CNS Annual Report 2005
[3] G.P.A. Berg, Design Study of a New Dipole Magnet D2 for the SHARAQ Spectrometer, *unpublished*, 2005.
[4] T. Uesaka et al., CNS Annual Report 2005
[5] W. Rogowski, Archive fur Elektrotechnik **12** (1923) 1.

Superconducting Doublet Quadrupole Magnet for the SHARAQ Spectrometer

K. Nakanishi, T. Kubo[a], S. Michimasa, A. Saito[b], H. Sakai[b], Y. Sasamoto, S. Shimoura and T. Uesaka

Center for Nuclear Study, Graduate School of Science, University of Tokyo
[a]*RIKEN (The Institute of Physical and Chemical Research)*
[b]*Department of Physics, University of Tokyo*

The SHARAQ (Spectroscopy with High-resoluation Analyzer and RadioActive Quantum beams) spectrometer is the high-resolution *QQDQD*-type magnetic spectrometer constructed at the RI Beam Factory (RIBF) at RIKEN [1]. The designed magnetic rigidities are 1.8 - 6.8 Tm, which correspond to an energy range of 40 - 440 MeV/A for $A/Z = 2$ main particles. The characteristic of the spectrometer is the high momentum resolution of $p/\Delta p \sim 15,000$ and a high angular resolution $\delta\theta \sim 1$ mrad.

RI beams are produced at the production target in the BigRIPS and transported to the SHARAQ target position through the BigRIPS [2] and a SHARAQ beam lines [3]. The beam lines and the spectrometer are fully dispersion matched. Simultaneous lateral and angular dispersion matching are essential for the high spacial and angular resolution in measurements.

The SHARAQ spectrometer consists of three quadrupole and two dipole magnets. The first doublet quadrupole (SDQ : Superconducting Doublet Quadrupole) consists of two superconducting quadrupoles, Q1000 and Q500. The basic design followed the superconducting triplet quadrupoles of BigRIPS [4]. Q1000 and Q500 coils have effective lengths of 500 mm and 1000 mm, respectively. The former is a vertical forcusing magnet and the latter vice verse. The specification of the SDQ magnet are summarized in Table. 1. The whole appearance of the magnet is shown in Fig. 1. The others are normal conducting type. D1 and Q3 magnets are inherited from the SMART spectrometer. SDQ and D2 are newly designed for the SHARAQ spectrometer.

Scattered particle at the target of the SHARAQ are firstly dispersed horizontally and focused vertically. Because the RI beams are secondary beam and have large dispersions, the scattered particles are widely spread in space. Flat magnetic fields in large space are needed so that the SDQ magnets are constructed in superconducting type. Additionally, the warm bore radius of the SDQ magnet are required to be large in order not to lose the acceptance of the spectrometer. On the other hand, the vertical dispersion is much small in the dispersion matching transportation. The vertical length of the duct can be kept small. The SDQ vacuum chamber design has been changed to be a wide horizontal aperture in lozenge-shape of 170 mm in height and 230 mm in width, while the original BigRIPS STQ has a circular aperture with 240 mm in diameter.

The SDQ had been manufactured in the TOSHIBA cooperation and transported to the RIBF facility in May 2007. A series of the performance examination has been performed successfully. The remaining magnets will be moved to the E20 experimental room in the RIBF building and the SHARAQ spectrometer will be assembled in Summer in 2007. Before the assembly, the SDQ is independently appraised its performance and the magnetic-field is measured.

To achieve the designed spectroscopy, not only searching an appropriate transportation method but precise magnetic-field mapping are deeply required. We aim to measure the magnetic-field and excitation characteristic of the SDQ magnet. The precise mappings help us to know the matrix elements in the beam transportation in the spectrometer. The designed momentum resolution is $p/\Delta p \sim 15,000$ and the required accuracy of the field mapping is the same order, $\sim 10^{-4}$. To realize such resolution, the important point of the measurement is the accuracy of the magnetic field measurement and position determination and the stabilities of the devices.

The field-mapper supplied for the SDQ is appropriated from the one, which was designed for a BigRIPS STQ magnet with air-core. It has a long cylinder and is inserted to a magnet duct in the direction on the beam axis. The total length of the SDQ is 521 mm smaller than one of the STQ. In order to fit the duct length of the SDQ, two extension supports were prepared in each flange.

The field-mapper has a rotatable arm to support one to four hall probes. Two stepping motors can independently control the probe position at around and along with the beam axis, respectively. The measurable ranges are in 0° - 360° with 0.03° of minimum step and in 2,500 mm on the beam axis with 0.01 mm minimum step, respectively.

The hall probes prepared for the mapping are the 3-axis type, which are designed for the measurement of all three perpendicular components of the magnetic field within a 250 μm $\times$ 250 μm $\times$ 250 μm cube. This type is appropriate for the measurement of fringing fields from magnets, coils and for the other homogeneity characterizations. Active area of each elementary sensor is 50 $\times$ 50 μm. The overall dimensions are ϕ10 $\times$ 20 mm. The mean temperature coefficient of sensitivity at room temperature is enough small (2×10^{-4} K^{-1}).

To satisfy the designed resolution of the spectrometer, the performance of the probe is suitable. On the other hands, the position accuracies of the probes and the field-mapper and measurement intervals are crucial points. The position accuracies are decided on less than 0.1 mm at throughout the measurement region. The reproductivity of the positions for the hall probes and the mapper is guaranteed by using the knock-ping between hall probe holder and mapper. The total position accuracies were confirmed within 0.1 mm.

	Q500	Q1000
Field gradient (T/m)	14.1	14.1
Operating current (A)	142	135
Effective length (mm)	500	1000
Coil length (mm)	440	940
Turn	1403	1403
Inductance (H)	0 - 162	
	18.4 - 8.9	35.0 - 16.7
Stored energy (kJ)	128	275
Warm bore radius (mm)	horizontal direction : 170	
	vertical direction : 115	

Table 1. The specification of the superconducting quadrupole for the SHARAQ spectrometer.

The field mapping has just started spring 2007. The data are still preliminary and needed to be calibrated with the precision analyzed deliberately from now on.

Figure 1. The SHARAQ SDQ magnet.

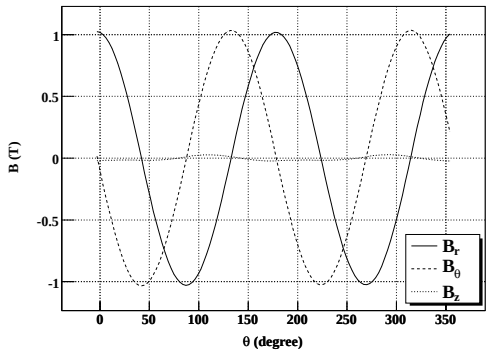

Figure 2. The first magnetic field measurement at the middle point of the beam axis direction in Q1000 coil. The hall probe were placed at the distance of 90 mm from the rotational axis of the field mapper. Measurement step in angular direction was 3°. The solid, dashed and dotted lines are the magnetic field in x-, y- and z-directions, respectively.

References

[1] T. Uesaka *et al.*, CNS Annual Report 2005.

[2] T. Kubo, Nucl. Instrum. Meth. Phys. Res. B **204** (2003) 97.

[3] T. Kawabata *et al.*, RIKEN Accel. Prog. Rep. **39** (2006), CNS Annual Report 2005.

[4] K. Kusaka *et al.*, IEEE Trans. Appl. Supercond. **14** (2004) 310.

Analyzing Power Measurement for the Deuteron-Proton Elastic Scattering at 2.0 GeV

K. Suda,[a,*], T. Uesaka[a], V. P. Ladygin[b], T. Kawabata[a], Y. Maeda[a,†], K. Itoh[c], S. Sakaguchi[a], Y. Sasamoto[a], H. Sakai[a,d], K. Sekiguchi[e], P. K. Kurilkin[b], Yu. V. Gurchin[b], A. Yu. Isupov[b], M. Janek[b,f], J. -T. Karachuk[b,g], A. N. Khrenov[b], A. S. Kiselev[b], V. A. Kizka[b], J. Kliman[b,h], V. A. Krasnov[b], A. N. Livanov[b], A. I. Malakhov[b], V. Matoucek[h], M. Morhac[h], S. M. Piyadin[b], S. G. Reznikov[b], I. Turzo[h], and T. A. Vasiliev[b]

[a] *Center for Nuclear Study, Graduate School of Science, University of Tokyo*
[b] *Joint Institute for Nuclear Research, Russia*
[c] *Department of Physics, Saitama University*
[d] *Department of Physics, University of Tokyo*
[e] *RIKEN (The Institute of Physical and Chemical Research)*
[f] *P. J. Šafárik University, Slovakia*
[g] *Advanced Research Institute for Electrical Engineering, Romania*
[h] *Institute of Physics Slovak Academy of Sciences, Slovakia*

1. Introduction

A high-energy deuteron beam polarimeter based on the d-p elastic scattering was constructed at the internal target station (ITS) of Nuclotron at JINR [1]. The ITS polarimeter will be used for the spin physics programs with polarized deuteron beams at 1.0 – 2.0 GeV. It will also be a unique tool to study the three-nucleon forces with emphasis on the energy dependence of the d-p elastic scattering in the range between 300 and 800 MeV.

As we reported in Ref. [2], the analyzing powers for the d-p elastic scattering at 880 MeV obtained by using this polarimeter are large enough at certain scattering angles, which indicates usefulness of this reaction for the deuteron polarimetry in GeV energy region. The d-p elastic scattering events were easily identified because of a sufficiently large S/N ratio (>10). However, at higher incident energy up to 2 GeV, the S/N ratio becomes worse due to a large contribution from carbon in a polyethylene target. This contribution is considered to be mainly the quasi-free d-p scattering (QFS), and it can have large analyzing powers as free d-p elastic scattering. Therefore, the QFS from carbon will also be a possible candidate for a polarimetry, if analyzing powers for this reaction have large values. In this report, we present the results for the analyzing power measurement at 2 GeV performed at JINR in June, 2005.

2. Experiment

Analyzing power measurement at 2 GeV using the ITS polarimeter was performed following the measurement at 880 MeV at JINR [2]. The experimental conditions were almost the same as that at 880 MeV. The vector and tensor polarized deuteron beams were provided by the cryogenic atomic beam source POLARIS. Two modes of vector and tensor polarizations were used as well as unpolarized mode, $(P_Z, P_{ZZ}) = (+1/3, 1), (+1/3, -1)$, and $(0, 0)$, where the values are theoretical maxima. Typical beam intensity was 3×10^7 particles/spill, and the spill duration was 8 seconds.

The details of the polarimeter was described in Ref. [3,2]. A polyethylene (CH_2) sheet of 10 μm thickness was employed as a target, as well as carbon wires for the background measurement. The polarized beams were used only for the CH_2 target at 2 GeV, while unpolarized beams for the carbon. Analyzing powers for the QFS from carbon can be extracted from the CH_2 data. The detectors covered scattering angles ranging from 60° to 135° in c.m.s. angles. The scattered deuterons and recoiled protons were detected by using plastic scintillation detectors.

3. Analysis

The d-p elastic scattering events were identified in the same manner as that for 880 MeV [2]. Figure 1 shows time difference between deuteron and proton detectors at $\theta_{\rm c.m.} = 60^\circ$ for the polyethylene target. A peak corresponding to the d-p elastic scattering can be observed (shaded area), however, a S/N ratio is poor (~ 0.6) even at this forward angle. At larger angles, events were identified only for the left and right scattering up to $\theta_{\rm c.m.} = 90^\circ$. At $\theta_{\rm c.m.} \geq 100^\circ$, no events for the d-p elastic scattering were identified due to a relatively larger contribution from carbon. Accidental coincidence events were negligible. Figure 2 shows a scatter plot between energy loss of deuteron and that of proton gated by the time difference. A locus corresponding to the d-p elastic scattering was observed, and the region surrounded by dashed lines was selected. Although the carbon contribution is not negligible, no subtraction is performed in this preliminary analysis.

The events for the QFS from carbon were also analyzed. In the time difference, the bump for the QFS was selected as shown in Fig. 1, but the region for the d-p elastic scattering was excluded. The selected region in the energy loss correlation is shown in Fig. 3.

4. Results

The preliminary results of the analyzing powers for the d-p elastic scattering at 2 GeV are shown by closed circles

*Present address: Research Center for Nuclear Physics, Osaka University.
†Present address: Department of Physics, Kyushu University.

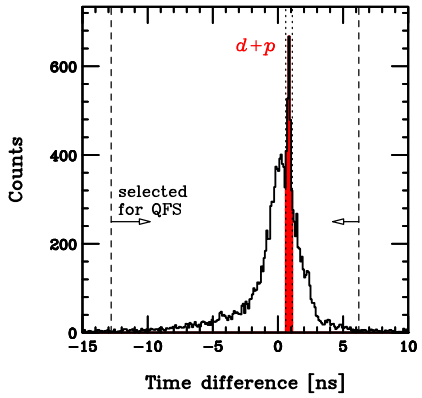

Figure 1. Time difference between deuteron and proton detectors. The solid line shows a spectrum for the polyethylene target. The d-p elastic scattering events were selected by dotted lines. The QFS events were selected by dashed lines, but the d-p elastic scattering events were excluded.

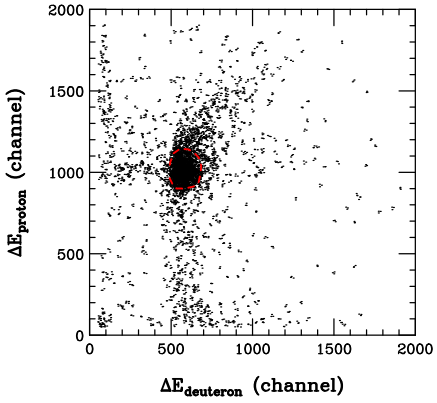

Figure 2. Scatter plot between energy loss of deuteron and that of proton gated by the time difference. A locus corresponding to the d-p elastic scattering can be seen.

in Fig. 4. Only statistical errors are shown. The values are consistent with the data taken from Ref. [4] (open circles).

For the QFS (open squares), a figure of merit can be larger than that for the d-p elastic scattering due to its large cross section. At $\theta_{\rm c.m.} = 60°$, the analyzing powers are about two or three times smaller than that for the d-p elastic scattering, but the cross section is about 10 times larger. Therefore, a figure of merit for the QFS is comparable or larger at this angle. Further analysis is in progress.

References

[1] T. Uesaka *et al.*, CNS Annual Report (2004) 81.
[2] K. Suda *et al.*, CNS Annual Report (2005) 73.
[3] A. I. Malakhov *et al.*, Nucl. Intrum. Methods Phys. Res. **A 440** (2000) 320.
[4] M. Haji-Saied *et al.*, Phys. Rev. C **36** (1987) 2010.

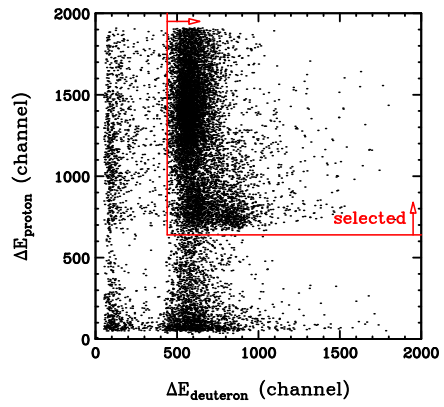

Figure 3. The same plot of Fig. 2, but for the QFS events.

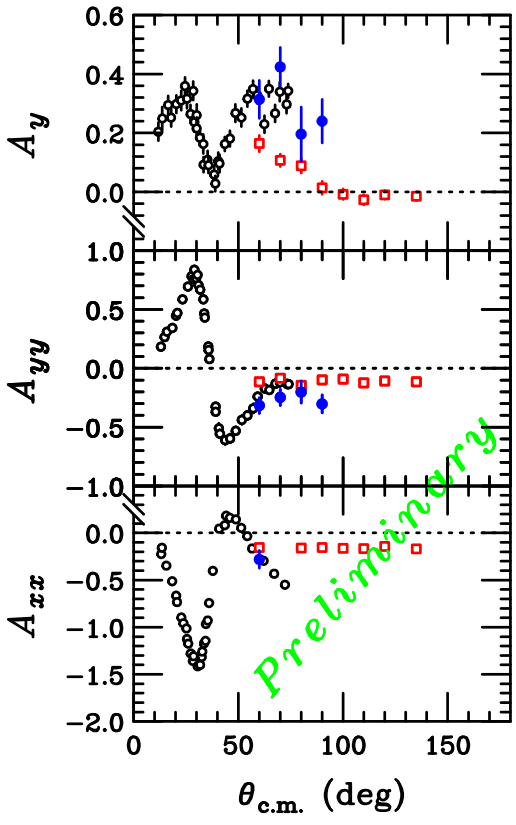

Figure 4. Analyzing powers at $E_d = 2$ GeV. The present data for the d-p elastic scattering are shown by closed circles, and the data taken from Ref. [4] by open circles. The analyzing powers for the QFS are shown by open squares. Only statistical errors are shown for the present data.

Polarized Proton Solid Target by using the High Power LED

T. Kawahara, T. Wakui[a], T. Uesaka[b], S. Sakaguchi[b], and K. Itoh[c]

Department of Physics, Toho University
[a]Cyclotron and Radioisotope Center, Tohoku University
[b]Center for Nuclear Study, Graduate School of Science, University of Tokyo
[c]Gradient School of Science and Engineering, Saitama University

1. Introduction

A polarized proton target for RI-beam experiments should be operated under modest conditions such as a low magnetic field (0.01–0.3T) and a high temperature (77–300K) to detect low-energy recoil protons. One possible method to fulfill the requirements is to make use of a population difference of electrons in Zeeman sublevels in photo excited triplet state of pentacene molecules [1]. Because this population difference is almost independent of temperature and external magnetic-field strength, electrons in the pentacene molecules can be polarized under the modest conditions of B $\sim$ 0.3 T and T $\sim$ 100 K. Thus, a high proton polarization can be achieved by transferring the population difference of electrons to protons. The polarized proton target by this method has been successfully applied to RI-beam experiments [2, 3].

Figure 1 shows a photo-absorption spectrum of pentacene molecules. Currently, an Ar-ion laser with a wavelength of 514 nm is used as the light source to excite the pentacene molecules. Although there is a small absorption peak around this wavelength, the strongest absorption peak is located at 595 nm. This peak is very close to the wavelength of a high power light emission diode (LED), LUXEON III Star. The wavelength of 590 nm is better suited for our use than that of the Ar-ion laser. The high power LED is also advantageous because of its low price and its simple operation in a pulse mode. Recently, we introduced the high power LED as a new light source to excite pentacene molecules.

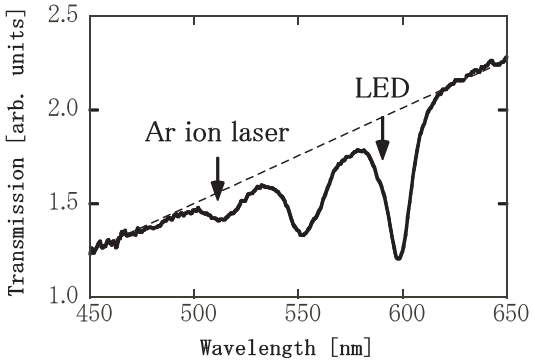

Figure 1. Photo-absorption spectrum of pentacene molecules.

2. The high power LED

The specifications of the high power LED are summarized in Table 1 [4]. A typical optical power of this LED is 0.2 W when it is operated at a current of 1.4 A and a temperature of 25 °C. The diameter of the LED is 20 mm including electrical interconnection pads.

Table 1. LUXEON III Star date-sheet (I=1.4 A,T=25 °C) [4].

Dominant wavelength	min.	584.5 nm
	typ.	590 nm
	max.	597 nm
Optical power	min.	0.135 W
	typ.	0.213 W
Forward voltage	min.	2.31 V
	typ.	2.95 V
	max.	3.51 V
Storage operating temperature	min.	–40 °C
	max.	120 °C

The optical power of the LED depends on its temperature as shown in Fig.2 [4]. Therefore, the LED should be cooled during the operation to obtain a high optical power. A peltier device with a heat sink was used for the cooling. The size of the peltier device was 50 mm$\times$50 mm. We put a high power LED on the peltier device, and attached a platinum thermo resistance to the LED to monitor the temperature.

The LED must be operated in a pulse mode with a frequency of 1 kHz to effectively polarize electrons in the pentacene molecules. For this purpose, we made a circuit to drive the LED in the pulse mode. Since this circuit works as a non-inversion amplifier, a pulse width can be easily changed using an input signal from a function generator. The pulse width was optimized to achieve the highest electron polarization.

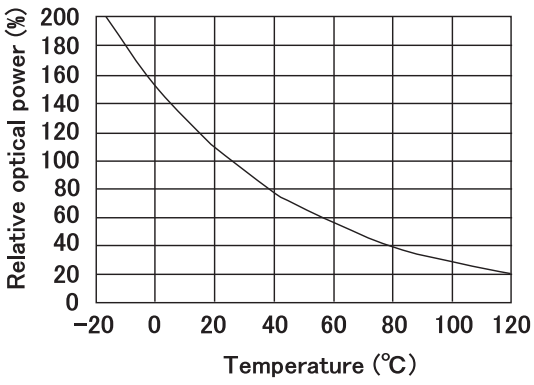

Figure 2. Relative optical power of the high power LED (LUXEON III Star) as a function of temperature.

3. Polarization system

The polarization system consisted of a C–type magnet, an Ar–ion laser for optical excitation, a microwave system for polarization transfer, and an NMR system to measure the proton polarization. The NMR system was also used for a reversal of the polarization axis.

We used a crystal of p-terphenyl doped with pentacene (0.005 mol%) as a target sample. The size of the crystal was 2 mm×3 mm×8 mm. We put the crystal in a sample holder made of thin glass tube. The holder was installed in the microwave cavity which was placed at the center of the C-type magnet, and a static magnetic field of 0.3 T was applied to the sample. The angle between the crystal axis and the magnetic field were carefully adjusted to archive the highest polarization. The resonance frequency of microwave cavity was 9.1 GHz. This cavity had an optical window for the laser irradiation. A 20-mm diameter lens was used as the optical window to focus the laser beam on the target sample. The position of the lens can be adjusted to produce an appropriate spot size of the laser beam on the target sample. When the high power LED was used as a light source, the focus lens had been removed. Instead, the LED and the specially designed lens were directly equipped on the cavity.

4. Result

After parameters of the polarization system were optimized, the target sample was polarized using a high power LED. The LED was operated with a current of 2.2 A, a voltage of 3.5 V, and a pulse width of 2.2 μsec. A build-up curve of the proton polarization with the LED was obtained as shown in Fig.3 (a). For comparison between the LED and the Ar-ion laser, we also measured the proton polarization using the Ar-ion laser after building for 10 minutes as shown by solid circles in Fig.3 (b). The horizontal axis represents the optical power on the target sample. The proton polarization increases with the optical power as shown by solid line in Fig.3 (b). The open circle in Fig.3 (b) denotes the polarization with the LED. It is demonstrated that the LED effectively works as a light source to polarize protons better than the Ar-ion laser. The LED enables 4 times lager polarization than the Ar-ion laser when the same optical power is irradiated on to the target sample. This advantage is exactly what is expected from the larger photon absorption probability at the LED wavelength.

Since the effective optical power obtained from one LED is limited to 20 mW, we need 1000 times as large optical power as the present to achieve practical magnitude of the proton polarization. It is necessary to increase the optical power by introducing large number of LEDs and improving the optical system.

5. Summary

We polarized protons in the target sample by using the high power LED. A p-terphenyl crystal doped with pentacene was used as the target sample. The LED was cooled by the peltier device. The pulse driver was made in order to operate the LED in the pulse mode. We obtained the build-up curve of the proton polarization. We compared the magnitude of polarization by the LED with that by the Ar–ion laser. The polarization with the LED was about 4 times lager than that with the Ar-ion laser, when the same optical power was irradiated to the target sample. However, we still need further development to increase the optical power of the LED for the practical use of the RI-beam experiment.

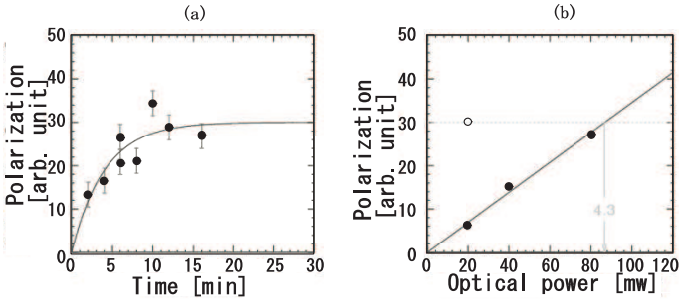

Figure 3. Measured proton polarization. (a) Polarization build–up curve with the high power LED. (b) Comparison of the proton polarization by the LED to that of the an Ar–ion laser.

References

[1] T. Wakui *et al.*, Nucl. Instrum. Methods A **550** (2005) 521.

[2] M. Hatano *et al.*, Eur. Phys. J. A **25** (2005) 255.

[3] S. Sakaguchi *et al.*, CNS Annual Report 2006 (2007).

[4] Power light source LUXEON III Star Technical Data sheet DS46.

Three-Dimensional Position Sensitivity in Segmented Planar HP-Ge Detector Array GRAPE

T. Fukuchi, S. Shimoura[a], E. Ideguchi[a], M. Kurokawa[b], H. Baba[b], S. Ota[a], M. Tamaki[a] and M. Niikura[a]

Department of Physics, Osaka University
[a] *Center for Nuclear Study, Graduate School of Science, University of Tokyo*
[b] *RIKEN (The Institute of Physical and Chemical Research)*

1. Introduction

Recently, new generation of the γ-ray detector using the high-purity germanium (HPGe) semiconductor have been developed by many groups. The feature of the new detector is its position sensitivity with keeping good energy resolution. In most cases, HPGe semiconductor detectors with highly segmented electrodes are used to obtain the position sensitivity. γ-ray interaction point in the detector is determined based on the pulse shape analysis. Particularly, three-dimensional position sensitivity can be achieved by analyzing the pulse shapes of not only the net-charge signals from the charge collecting electrode but also the transient induced signals of neighboring segments. For the pulse shape detection, high-speed waveform digitizer popularizing in recent years is used.

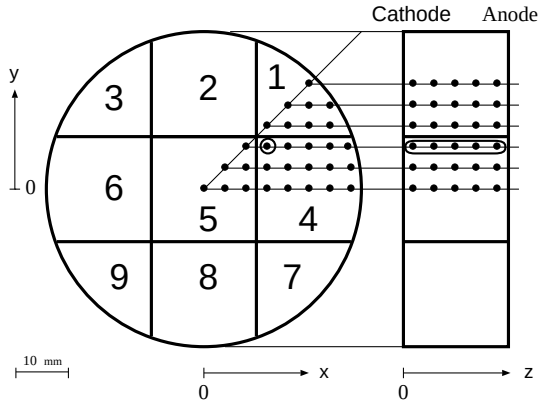

Figure 1. View of a Ge crystal projected in the *xy*-plan (left) and *yz*-plane (right) showing the segmentation boundaries of the outer contacts and the locations of the measured points.

We are using a γ-ray detection system GRAPE (Germanium Array with Position and Energy sensitivity) [1] consisted of 36 planar-type HPGe produced by the company EURISIS. In the GRAPE, the cathode of the crystal is electrically segmented into 9 elements, and γ-ray interaction position of depth direction is extracted by method of pulse shape analysis using an analog technique [2]. In the in-beam γ-ray measurement using high energy accelerator such as RI beam factory at RIKEN, precise Doppler correction is required. In order to achieve it, we have been developing new system which has three-dimensional position sensitivity by pulse shape analysis using sampling ADCs. In this report, expected position sensitivity is described based on these measured pulse shape.

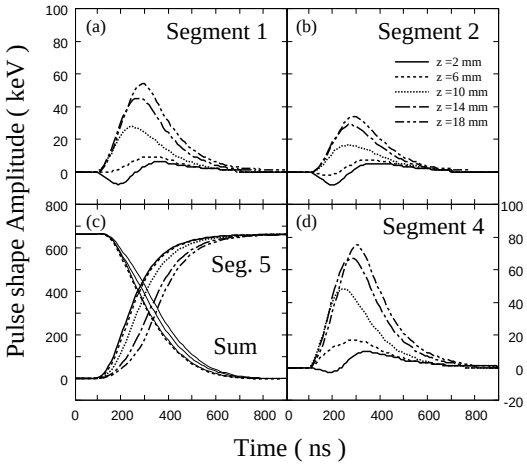

Figure 2. The depth (z-direction) dependence of the average pulse shapes at location x = 8 mm, y = 8 mm, z = 2, 6, 10, 14 and 18 mm.

2. Measured pulse shapes

The pulse shapes in total 145 points covered whole crystal of every 4 mm interval were measured using automatic pulse shape sampling system [3, 4]. These measured positions are shown in Fig. 1. For convenience, we represent the crystal positions by the lateral (x,y) and depth (z) directions. Figure 2 shows examples of depth variation of the pulse shape. These pulses are take in different depth z = (2, 6, 10, 14, 18 mm) at the location (x, y) = (12 mm, 8 mm). The pulse shapes are averaged in each interaction points. The summed signal is shown with segment 5 in reverse polarity. In addition to the variation of signal risetimes of net-charge signals in the segment 5 and summed signals, the amplitudes and polarities of transient signals also change depending on the depth. The position extraction in the lateral direction (x, y) is performed mainly using these transient signals. The positions in the depth direction (z) are mainly determined by the risetime differences of the summed signal and net-charge signal.

The noise level was measured by the sampling ADC data without signal from γ ray. The sampling trigger is generated by clock generator. The measured zero level has r.m.s. of σ = 4.9 keV noise fluctuation. However, because averaging method works a high pass filter, using the 0 level average method, this level can be reduced. The noise level after 1 μsec from the 5 points averaging is σ = 3.0 keV. The 5 points averaging method has been used for the all signal to decide 0 level. Therefore, all signal has σ = 3.0 keV noise

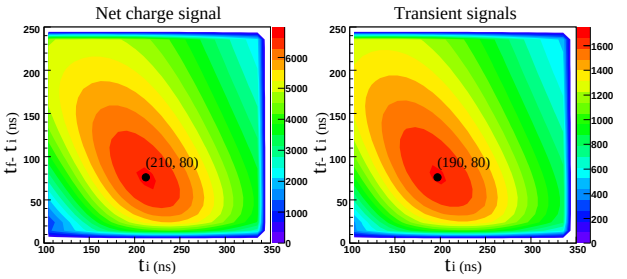

Figure 3. The time range dependence of $(\Delta s_{ij})^2$ value. The net-charge collecting (left) and transient induced signals (right) have different ranges for maximum values. These values are shown in blue.

fluctuations in each sampling time.

3. The expected position sensitivity

In order to estimate expected position sensitivity of γ-ray interacted positions, we follow the procedure of Vetter *et al.* [5], and define a position sensitivity S_{ij} from each pair of points $i = (x_i, y_i, z_i)$ and $j = (x_j, y_j, z_j)$ such that,

$$S_{ij} = r_{ij}/\Delta s_{ij}$$

where r_{ij} is the physical distance between points i and j, and Δs_{ij} quantifies the difference of the signals in terms of the the r.m.s. noise σ = 3.0 keV. Using the difference in the average signal amplitudes $\bar{q}^k(t)$ at the time sample t between the position i and j on contacts k, Δs_{ij} can be given as

$$(\Delta s_{ij})^2 = \sum^{k} \sum_{t=t_i}^{t_f} \frac{[\bar{q}_i^k(t) - \bar{q}_j^k(t)]^2}{2\sigma_k^2}.$$

For the transient induced signals of adjacent segments, these sets of cathode signal k = {2,4,5}, {1,2,5,7,8} and {2,4,6,8} are used for the segment 1,4 and 5, respectively.

Prior to estimate the position sensitivity, to decide the best fitting ranges (t_i, t_f), Δs_{ij} was calculated as a function of t_i and t_f, and best conditions were searched. The example of calculated values are shown in Fig. 3.

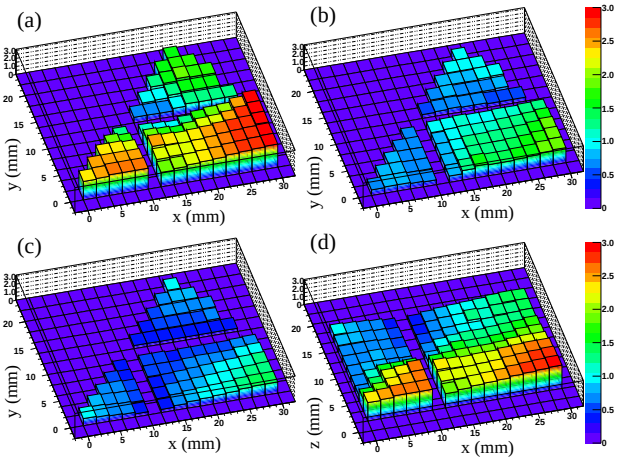

Figure 4. The deduced position sensitivities on the *xy*-plane ((a)(b)(c)) and *xz*-plane (d).

As a result, maximum Δs_{ij} are obtained from the t_{19}-t_{29} and t_{19}-t_{27} for the net-charge collecting and transient induced signals, respectively. These best fitting ranges are narrower than those of typical ranges for the segmented coaxial detectors. The origin of these narrow ranges are its simple variation of the pulse shape. Since these best fitting ranges depend on the γ-ray energies and noise amplitude, it is more effective to vary the fitting ranges as a function of these conditions. However, fixed ranges were used in following calculations.

The examples of obtained position sensitivities are shown in Fig. 4. These figures display sensitivities on *xy*-plane, z = 2 (a), 10 (b), 18 (c) and *xz*-plane, y = 0 (d). In addition to the 3-dimensional position sensitivity, pure depth position sensitivity was calculated based on the pulse shapes of *xy* variations with fixed depth z. Because this pure depth position sensitivity is better than 0.2 mm, the position sensitivity of the lateral (x, y) directions are represented in these figures. Since amplitude of the transient induced signals are smaller in the middle of the segments than those of near boundaries, the position sensitivities of the middle of the segment are worse as compared with those of near boundaries In the *xy*-plane, around z = 2 plane (c) sensitivity is lower, where electrons and holes compensate each other leading to small transient induced signals. Because sensitivity of each segments also depends on the number of adjacent segment, segment 4 and 5 have worse sensitivity as compared with segment 1. The position located at (x, y, z) = (28 mm, 8 mm, 6 mm) in the segment 4 has lowest position sensitivity of 3.13 mm. In the whole volume of the crystal, the mean position resolution for 662-keV γ ray is 1.30 mm. How to transact a large amount of data from the sampling ADCs and multi-hit events in a segment is next subject.

References

[1] T. Shimoura, Nucl. Inst. and Meth. A **525** (2004) 188.
[2] M. Kurokawa *et al.*, IEEE **50** (2003) 1309.
[3] T. Fukuchi *et al.*, CNS Annual Report 2003 (2004) 88.
[4] T. Fukuchi *et al.*, CNS Annual Report 2004 (2005) 73.
[5] K. Vetter *et al.*, Nucl. Inst. and Meth. A **452** (2000) 105.

Development and Performance Evaluation of Thick–GEM at CNS

Y.L. Yamaguchi, H. Hamagaki, K. Ozawa, S.X. Oda, Y. Aramaki, S. Sano and T. Tamagawa[a]

Center for Nuclear Study, Graduate School of Science, University of Tokyo
[a] *RIKEN (The Institute of Physical and Chemical Research)*

1. Introduction

A Gas Electron Multiplier (GEM) [1], which was invented at CERN, is one of Micro Pattern Gas Detectors (MPGDs) having been developed significantly in recent years. A standard GEM consists of a 50 μm thick insulator coated with 5 μm thick metal layers at both sides. It has regularly aligned and densely packed holes. The typical pitch and diameter of the GEM holes are 140 μm and 70 μm, respectively. Hereafter the GEM with a 50 μm thick insulator is referred as 'Standard–GEM'.

In recent years a GEM is fabricated successfully using dry etching in Japan [2, 3]. The GEM fabricated with dry etching has holes with a cylindrical shape while the GEM fabricated with wet etching has holes with a bi-conical shape. It is possible to fabricate GEMs with thicker insulator such as 100 μm and 150 μm using dry etching. They are referred as '100 μm–GEM' and '150 μm–GEM' and collectively called as 'Thick–GEM' in this paper. Since the Thick–GEM is expected to attain higher gain than the Standard–GEM, much safer operation with lower voltage per unit thickness may be possible. In this paper the basic properties of the Thick–GEM are described compared with those of the Standard–GEM.

2. Thick–GEM

It is feasible with the dry etching technique for piercing holes with pitch of 140 μm and diameter of 70 μm in a 100 $\sim$ 150 μm thick metalized polymer sheet. Liquid Crystal Polymer (LCP) is chosen as an insulator of the Thick–GEM because LCP can be pierced easier than other polyimide sheets. The Thick–GEM consists of a 100 μm or 150 μm thick LCP sheet coated with 8 μm thick copper.

	Thickness [μm]	Diameter [μm]	Pitch [μm]
Standard–GEM	50	70	140
100 μm–GEM	100		
150 μm–GEM	150		

Table 1. The geometry of the Thick–GEM and the Standard–GEM such as an insulator thickness, a hole diameter and a hole pitch.

Table 1 shows the geometry of each GEM. The 100 μm–GEM and the 150 μm–GEM are comparable to double and triple layer structure of the Standard–GEM with respect to the total length of the hole for electron multiplication.

The Thick–GEM is expected to attain higher gain than the multi–layer structure of the Standard–GEM. The Thick–GEM has a larger effective path length for multiplication and the effect of electron absorption at the electrodes is smaller than the multi–layer structure of the Standard–GEM since the number of gaps between the GEMs are smaller.

3. Electric Field of Thick–GEM

The electric field in a hole of the Thick–GEM and the Standard–GEM are calculated using Maxwell 3D. The left and right panels in Fig. 1 show the electric field along the hole center and the hole edge, respectively. The z position is defined as the direction perpendicular to the GEM and the top surface of the GEM is located at $z = 0$. The voltage difference per every 50 μm of each GEM, which is denoted by $V_{\rm ref}$, is 250 V. In other words, the voltage applied to each GEM are 250 V, 500 V and 750 V in the case of the Standard–GEM, the 100 μm–GEM and the 150 μm–GEM, respectively. The solid, dash and dot lines represent the results of the 150 μm–GEM, the 100 μm–GEM and the Standard–GEM, respectively.

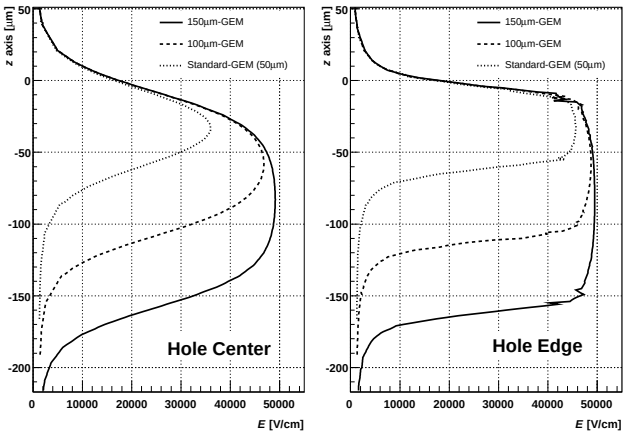

Figure 1. Comparison of the Thick–GEM with the Standard–GEM for the electric field strength along the hole center and the hole edge at $V_{\rm ref} = 250$ V.

It is clearly seen that the electric field of the Thick–GEM is much stronger than the Standard–GEM. The Thick–GEM has larger maximum field and especially the 150 μm–GEM has plateau for $\sim$ 50 μm even at the hole center. On the other hand, the electric field of the Standard–GEM falls down before saturation. Thus it is perfectly expected that the Thick–GEM has larger multiplication than the Standard–GEM.

4. Gain Measurement

4.1. Setup

The measurements were carried out using the single Thick–GEM or the triple Standard–GEM structure. A drift plane, which is made of a metallic mesh, is mounted 3 mm above the upper GEM and readout pads are placed 2 mm below the lower GEM in a chamber. In the case of the triple Standard–GEM structure, the gap between the neighboring GEMs is 2 mm. The high voltage is supplied to each GEM electrode via a chain of 10 MΩ resistors and also to the mesh independently. The chamber is filled with Ar(70%)/CO_2(30%)

or Ar(90%)/CH_4(10%) during the measurements. A thermocouple sensor and a barometer are also placed in the chamber for the purpose of monitoring the temperature and pressure. Their precisions are less than 0.05%.

4.2. $V_{\rm ref}$ Dependence of Gain

Figure 2 shows the gain of the 150 μm–GEM (circle), the 100 μm–GEM (triangle) and the triple Standard–GEM structure (square) as a function of $V_{\rm ref}$ in Ar(70%)/CO_2(30%). The circle, triangle and box symbols represent the results of the 150 μm–GEM, the 100 μm–GEM and the triple Standard–GEM structure, respectively. Each solid line represents a fitted result with an exponential function to each data set. Especially, the result of the 100 μm–GEM is scaled up to the power of 3/2 in order to make comparison with the both results of the 150 μm–GEM and the triple Standard–GEM structure.

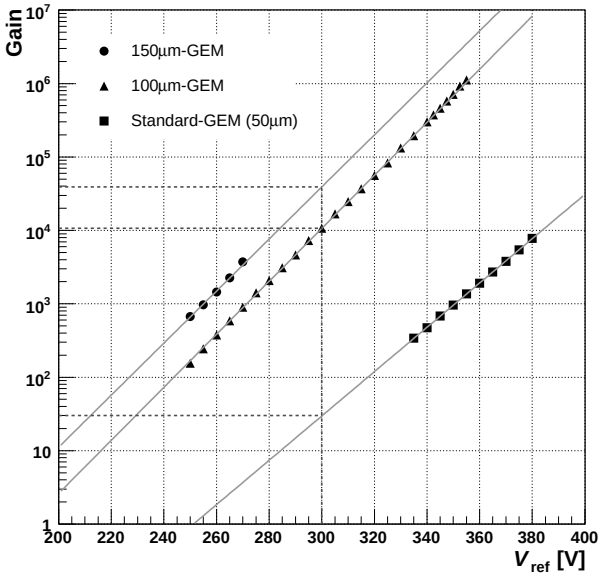

Figure 2. The $V_{\rm ref}$ dependence of the gain for the Thick–GEM compared with the Standard–GEM in Ar(70%)/CO_2(30%).

In the case of the 150 μm–GEM, continuous discharge starts to occur at $V_{\rm ref} = 275$ V and the measurement could not be conducted. Although the current 150 μm–GEM has a problem, it is clearly seen that the Thick–GEM can attain more than 10^3 gain at much lower $V_{\rm ref}$ than the triple Standard–GEM structure as expected. In Table 2 listed

	Gain at $V_{\rm ref}$=300 V	Magnification Ratio
150 μm–GEM	3.9×10^4	1.3×10^3
100 μm–GEM	1.1×10^4	3.6×10^2
Standard–GEM	30	1

Table 2. The comparison of the Thick–GEMs with the Standard–GEM in a value of the gain and a magnification ratio to the Standard–GEM at $V_{\rm ref}$ = 300 V.

are the gain of the Thick–GEMs and the triple Standard–GEM structure at $V_{\rm ref} = 300$ V together with the gain ratio to the triple Standard–GEM structure. These values are obtained by extrapolating using the fitted functions except for the value of the 100 μm–GEM and are indicated by the dashed lines in Fig. 2. The gain of the 150 μm–GEM and the 100 μm–GEM are 1.3×10^3 times and 3.6×10^2 times higher than that of the triple Standard–GEM structure at $V_{\rm ref} = 300$ V.

4.3. Gain Stability

The gain stability of the 150 μm–GEM is measured using Ar(90%)/CH_4(10%). $V_{\rm ref}$ is kept to 230 V and the rate of a signal is about 2.5 Hz during the measurement.

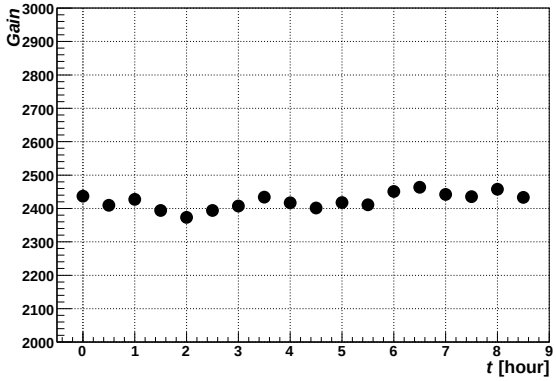

Figure 3. The gain stability of the 150 μm–GEM for Ar(90%)/CH_4(10%).

Figure 3 shows the gain stability of the 150 μm–GEM and the result is normalized to the condition of $P = 760$ Torr and $T = 300$ K i.e. $P/T \simeq 2.53$ Torr/K using the relation between the gain and P/T. The gain of the 150 μm–GEM is stable within about 1.0% (RMS) for 9 hours.

5. Summary and Outlook

The Thick–GEM is fabricated successfully using the dry etching technique in Japan. The electric field of the Thick–GEM is calculated and the $V_{\rm ref}$ dependence of gain and the gain stability of the Thick–GEM are measured. The electric field of the Thick–GEM is much stronger than that of the Standard–GEM and the Thick–GEM can attain much higher gain than the multi–layer structure of the Standard–GEM as expected. The Thick–GEM also has an excellent gain stability within 1.0% for 9 hours.

In the case of the 150 μm–GEM, however, discharge occurs continuously when the gain reaches to ~ 4000. The discharge might be caused due to dust remained inside holes of the 150 μm–GEM after the desmear process. In the case of the Thick–GEM, much more dust is produced in making holes. Now effort is on going to make the 150 μm–GEM more clean.

References

[1] F. Sauli, Nucl. Instr. and Meth. A **386** (1997) 531.

[2] M. Inuzuka, *et al.*, Nucl. Instr. and Meth. A **525** (2004) 529.

[3] T. Tamagawa, *et al.*, Nucl. Instr. and Meth. A **560**(2006) 418.

Development of a Gas Cherenkov Counter Using Gas Electron Multipliers (GEMs)

Y. Aramaki, H. Hamagaki, K. Ozawa, S.X. Oda, Y.L. Yamaguchi, S. Sano, K. Shigaki[a], D. Watanabe[a], S. Yokkaichi[b] and S. Sugawara[c]

Center for Nuclear Study, Graduate School of Science, University of Tokyo
[a]*Graduate School of Science, Hiroshima University*
[b]*RIKEN (The Institute of Physical and Chemical Research)*
[c]*Department of Physics, Waseda University*

1. Introduction

We developed an electron identification device which will be used for measuring low mass vector mesons in the heavy ion collisions. The device is a gas Cherenkov counter consisting of a gas radiator, photocathode for UV photons, and a multiple-Gas Electron Multiplier (GEM) [1]. Since the same gas material is used for both Cherenkov radiation and electron multiplication, no window is needed between a radiator part and a GEM part.

The GEM is a typically 50 μm thick polyimide sheet which coated with 5 μm thick copper at both sides and has regularly aligned holes. The typical diameter and pitch of the holes are 70 μm and 140 μm, respectively. High electric field for multiplication is realized inside the holes even with a low voltage difference between the both sides of the GEM and induces the charge.

Cesium iodide (CsI) is chosen as a photocathode for UV Cherenkov photons. CsI with the thickness of 200 nm is evaporated on the surface of the uppermost GEM foil. A reflective photocathode mode is chosen because the reflective photocathode mode has relatively high quantum efficiency (QE) and it can suppress photon feedback [2].

When ultraviolet (UV) photons impinged on the CsI coated on a GEM, photoelectrons are produced and are emitted from the CsI surface. The photoelectrons are attracted into the holes, and the charge multiplication is induced inside the holes.

We measured the QE of a CsI-coated GEM at the bench test in our laboratory. Meaurement of Cherenkov light with a gas Cherenkov counter using CsI-coated GEM was performed at REFER in Hiroshima university. We compared the number of detected photoelectrons at the performance test and the number of expected photoelectrons from the result of the QE.

2. QE of CsI-coated GEM

Figure 1 shows a schematic view of the experiment setup for the measuring QE of CsI photocathode. The magnesium fluoride (MgF_2) plate is used for the entrance window of the detector chamber. The cutoff wavelength, the diameter and the thickness of MgF_2 are 115 nm, 30 mm and 3 mm, respectively. The setup also includes a MgF_2 half mirror which splits the UV photons between the monitor PMT on the reflective side and the GEM-chamber on the transmissive side. The GEMs, the readout pads and the mesh were mounted inside the chamber made of stainless steel (the stainless box). The monochrometer has two slits

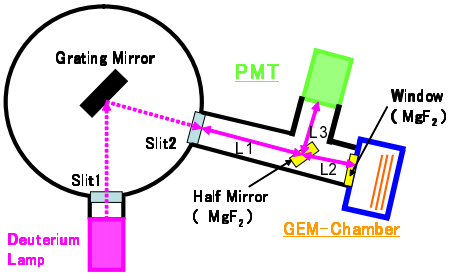

Figure 1. A schematic view of the setup for measurement of QE. The setup includes a vacuum ultraviolet (UVU) monochrometer equipped with a deuterium lamp (115–400 nm), which is connected to the detector chamber.

and the grating mirror. One slit in the UV light source side (slit1) is used for adjusting light intensity. The other slit (slit2) works as a wave length band filter and is fixed at 1 mm.

To read out signals, 5 by 5 array of pads with a 1×1 cm^2 square shape are used. The GEM chamber is pumped down to 10^{-4} Pa to reduce the water content. After pumping the chamber is filled with a mixed gas of Ar/CH_4 (90%/10%) or Ar/CO_2 (70%/30%). The monochrometer is also pumped down to 0.1 Pa and is kept in vacuum. The humidity in the stainless box was 9 ppm during the measurement.

The QE of the CsI-coated GEM at a given photon energy E is given by the following formula.

$$QE_{CsI}(E) = QE_{PMT}(E)\frac{R(E)}{T(E)}\frac{G_{PMT}}{G_{GEM}}\frac{I_{CsI}(E)}{I_{PMT}(E)\cdot C_1\cdot C_2} \quad (1)$$

R (T) represents reflection (transmission) of the half mirror. G_{GEM} is the gain of the multiple-GEM. C_1 is the mesh transparency ($C_1 = 0.81$), and C_2 is the opacity of the CsI layer due to the GEM holes ($C_2 = 0.833$). G_{PMT} (QE_{PMT}) is the gain (QE) of the reference PMT. The above values are taken from data sheet. I_{PMT} (I_{CsI}) is the photocurrent from the reference PMT (CsI photocathode). I_{PMT} and I_{CsI} are measured quantities.

Figure 2 shows the QE curve of the CsI-coated GEM. The QE starts to rise from 6 eV, which corresponds to the CsI efficiency cutoff. In the case where Ar/CO_2 (70 %/30 %) mixed gas is used, the drop of the QE of CsI-coated GEM occurs at about 7 eV due to absorption of UV photons because CO_2 gas efficiency cutoff is 7.2 eV [3]. In the case where Ar/CH_4 (90 %/10 %) mixed gas is used, the drop of the QE of CsI-coated GEM occurs at about 8.5 eV because

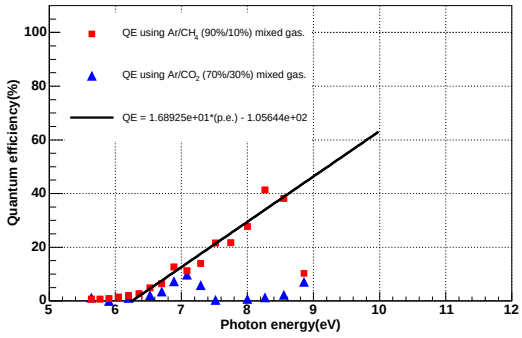

Figure 2. The QE of CsI-coated GEM as a function of photon energy. This QE of CsI-coated GEM involved extraction efficiency of GEM.

CH_4 gas efficiency cutoff is 8.7 eV [4]. The measured maximum QE is 40% at photon energy of 8.6 eV.

3. Performance test

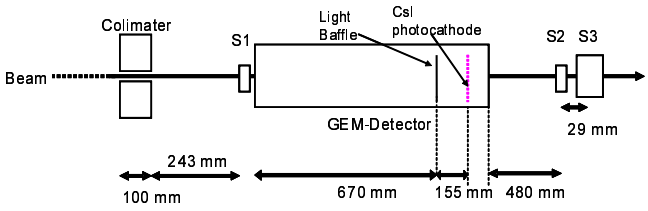

Figure 3. A schematic top view of the beam test setup.

A performance test was done at Relativistic Electron Facility for Education and Research (REFER) at Hiroshima University. REFER consists of a storage ring and an extraction line of electron beams. Electron beams of 150-MeV/c, which is an injector to the storage ring at Hiroshima university, is produced by the microtron. Since CF_4 gas has large photon energy cutoff ($E \sim 10.5$ eV) and large refractive index (1.00062), the performance evaluation of the gas Cherenkov counter was carried out with CF_4 gas. The configuration of detectors is shown in Fig. 3. Three plastic scintillation counters (S1, S2 and S3) and the Gas Cherenkov Counter (GEM-Detector) are placed along a beam line. The coincidence of S1, S2 and S3 were taken. Thus the incident electron beam can be defined to 10×10 mm^2.

Five GEMs including the CsI-coated GEM were used in order to keep the voltage applied to each GEM as low as possible. Thus this detector can achieve high gain and have low probability of discharge. The electric field (E_D) between the mesh and the CsI-coated GEM is set to positive when electrons from ionization energy loss are measured. E_D is set to negative in order to suppress electrons from ionization loss when electrons from Cherenkov light are measured. A light baffle is used for this to change path length of Cherenkov radiation.

The induced charge on the central pad is shown in Fig. 4. Since the direction of the electric field between the mesh and CsI-coated GEM in the right panel is opposite, electrons from ionization energy loss are suppressed. In Fig. 5, total charge from Cherenkov radiation and ionization energy loss are shown; left with light baffle ON and right with light baffle OFF, respectively. The direction and the strength of the electric field were set to the same values in the both cases.

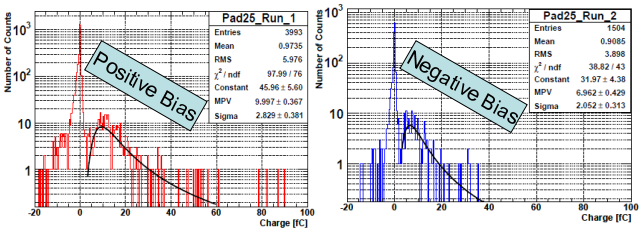

Figure 4. The charge from ionization energy loss in the different path length. The left (right) panel is positive (negative) bias.

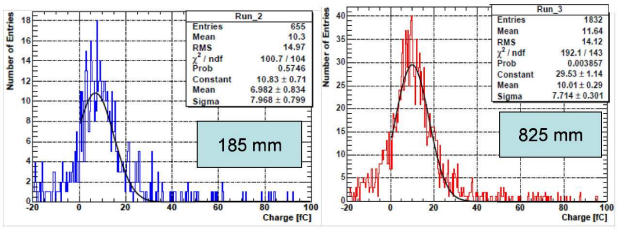

Figure 5. The charge from Cherenkov light in the different path length. The path length of the left (right) panel is 155 mm (855 mm).

The number of photoelectrons (49±28), obtained using the gain estimated from the ionization loss measurement, is smaller than the number (51) expected from the measured QE.

4. Summary

The gas Cherenkov counter using CsI-coated GEM was developed. The measured maximum QE is 40% at photon energy of 8.6 eV. The performance test has been done using an electron beam. The detected photoelectrons from Cherenkov light was 48±28 for net path length 624 mm. Smaller measured photoelectrons than expected one may be ascribed to the deliquescence of CsI.

References

[1] F. Sauli, Nucl. Instr. and Meth. A **386** (1997) 531.
[2] D. Mörmann *et al.*, Nucl. Instr. and Meth. A **471** (2001) 333.
[3] C. Lu, *et al.*, Nucl. Instr. and Meth. A **343** (1994) 135.
[4] R. Arnold, *et al.*, Nucl. Instr. and Meth. A **252** (1986) 188.

Design of readout circuit for 2-dimensional imaging with GEM

S. Sano, H. Hamagaki, Y. Tanaka[a], T. Fusayasu[a], and K. Kiyoyama[a]

Center for Nuclear Study, Graduate School of Science, University of Tokyo
[a]Nagasaki Institute of Applied Science

1. Introduction

The Gas Electron Multiplier (GEM) amplify a charge signal by avalanche process. GEM is a metal-coated polyimide foil with circular holes in a closed packed geometry. The metals at both sides are used as electrodes [1]. Typical thickness of a GEM foil is 50 μm, and the typical pitch and diameter of the holes are 140 μm and 70 μm, respectively [2]. With a few hundreds volts applied between the two electrodes, electron multiplication due to the avalanche process becomes active inside the holes. The gain of over 10^4 is obtained with multiple GEMs [3].

While GEM is utilized in physics experiments as HBD (Hadron Blind Detector) or TPC (Time Projection Chamber), so far GEM is also applicable to the 2-dimensional imaging detector of X-ray or neutron. This report describes the status of development of neutron 2D imaging using GEM, which is started recently.

Thermal neutron has small cross section for metal but large cross section for hydrogen atom included in water. Therefore the motion of the liquid in the engine of cars may be seen by using thermal neutron. Thermal neutron is caught with boron evaporated on the surface of GEM.

Imaging has a bottleneck in readout circuit for the signal from many pixels where the electrons multiplied by GEM reach finally. Therefore the CMOS chip involving the multi-channel readout electronics chain is required.

2. Conceptual design of readout module

Prototype with 1600 readout channels will be made with 25 CMOS chips each having 64-channel readout circuits. The size of the pixel is 1mm×1mm and imaging area is about 40mm×40mm. The readout electronics chain is shown in Fig. 1. The charge signal is integrated at the integrator, and the output of each channel is brought to one channel ADC by switching with the multiplexer. The rate of readout frame is chosen to be 1000 fps and readout rate of ADC is 1.6 MHz. The control of 25 chips and ADC-memory array is done with FPGA (Field Programmable Gate Array). The readout module consists of two boards, one has 1600 pixels to collect electrons and 25 chips and one ADC, the other has FPGA and memory, which is placed inside gas vessel. As the first step, the design of amplifier used as integrator was made.

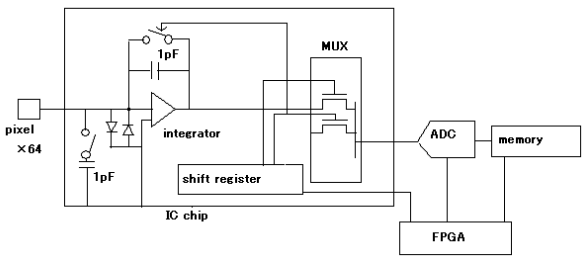

Figure 1. Block diagram of readout module including multi-channel readout electronics chain

3. Design of amplifier

It is necessary to know the shape of the charge signal form GEM for design of readout circuit. The charge signal of the pixels is induction charge due to electrons multiplied at last GEM. The upper panel of Fig. 2 shows the input

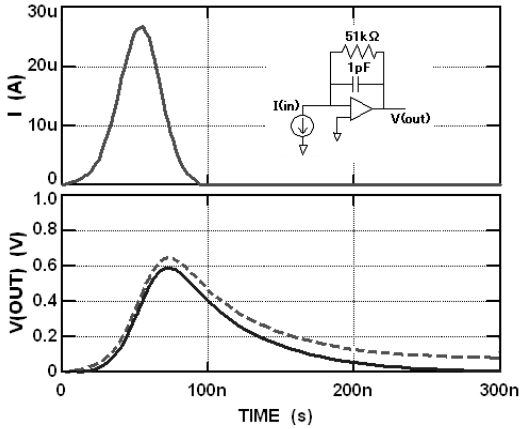

Figure 2. The upper panel shows the calculated input current signal. The lower panel shows the output of integrator with bipolar transistor input opamp (broken line) and FET input transistor opamp (solid line).

current signal calculated with the parameters describing the drift of electrons between GEM and pixels in gas ($ArCO_2$), where the distribution of drift velocity and production time at last GEM for the each electrons take account of diffusion coefficient. The lower panel of Fig. 2 shows the simulated output signal of integrator with bipolar transistor input opamp (separated line) and FET (field-effect transistor) input opamp (solid line). The reason that the separated line has the increasing offset is that bipolar transistor input opamp has large input bias current of micro-ampere order, while the input bias current of FET input opamp is so small that this effect can't be seen. Our requirement of gain band width and slew rate were also determined from the shape of the output of Fig.2. The specification of amplifier is as follows.

- FET input amplifier to minimize input bias current below 1 pA
- 60 dB open loop gain
- 60 MHz gain band width
- 100 V/μs slew rate

To satisfy these specifications, folded-cascode operational amplifier has been utilized, which has the differential input

and the single stage impedance, as shown in Fig. 3. Folded-cascode opamp can achieve a large gain with the high output impedance due to the use of cascode connections.

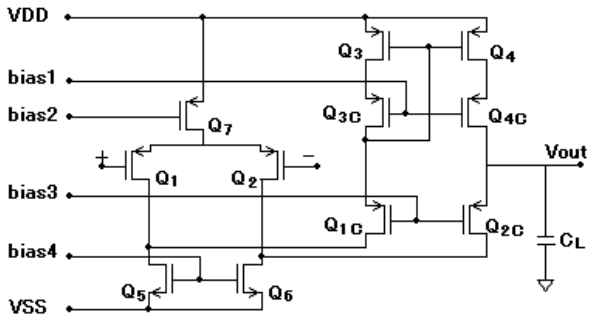

Figure 3. Folded-cascode operational amplifier

The current at output stage I_{ds} is determined from slew rate S_r as follows,

$$I_{ds} = S_r C_L$$

where C_L is the parasitic capacitance arising at the output connection, which is assumed to be 3 pF in this simulation. From requirement of slew rate of 100 V/μs, $I_{ds} = 300\ \mu A$ is obtained. The size of the input transistors Q_1 and Q_2 is determined from gain band width GBW as follows,

$$\frac{W}{L} = \frac{(2\pi \cdot GBW)^2 C_L^2}{4 k_p I_{ds}}$$

L and W is the gate length and width of FET, respectively. k_p is transconductance coefficient of p-channel transistor. The size of the other transistors $Q_3 - Q_7$ are determined from the relation of current I_{ds} to the effective voltage to work these transistors.

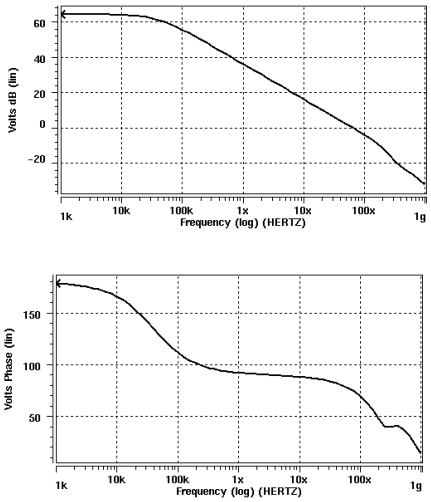

Figure 4. The upper is frequency-property of gain. The lower is frequency-property of phase.

The bias circuit was designed as all FET of amplifier work at saturation region. The current of amplifier is also determined from the main current of bias circuit with current mirror techniques, and the main current of bias circuit is adjustable with the resistance installed out of the chip.

The simulation is done with SPICE (Simulation Program with Integrated Circuit Emphasis) which can execute DC and AC analysis. Figure 4 shows the gain-frequency property (upper) and phase-frequency property (lower) resulting from the simulation. The AC simulation is done with a small trial signal of 1 mV to the differential input. The gain is the ratio of output voltage to input one. The gain at low frequency is higher than 60 dB and gain band width is 63 MHz, which satisfy our requirements. Figure 5 shows the result of simulation of the integrator involving the designed opamp, without discharge switch. The output voltage increases as the input charge and no offset increase exist, which means no input bias current.

The discharge switch will be made of CMOS switch which consists of the same size of p-channel and n-channel transistor. The on-resistance of the switch of the smallest size is about few kΩ and time constant of discharge is few nano-second which is enough short to discharge in one-clock of about 300 ns.

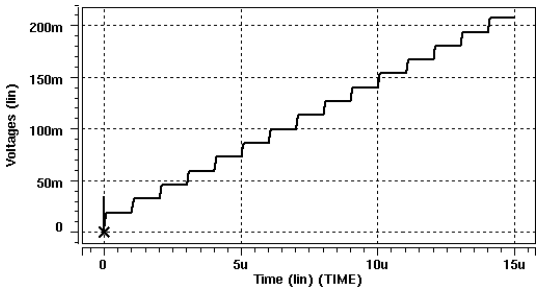

Figure 5. Output of integrator without discharge switch

4. Summary and Outlook

Design of readout electronics for 2-dimensional imaging with GEM by using CMOS analog techniques was started. Design work of opamp was completed, and integrator with this opamp and no discharge switch has sufficient property.

The other circuit, CMOS switch, multiplexer, and shift register, will be designed soon and layout will be designed based on the designed schematic diagram. After completion of the design and submitting to fabrication company, the readout electronics board will be designed and fabricated. The fabricated bare chip will be bonded to the board directly to make readout module compact. After that the board test will be done with test pulse, which contribute to the calibration of the real characteristics of imaging with GEM.

References

[1] F. Sauli, Nucl. Instrum. and Method. A 386 (1997) 531.
[2] S. Bachmann, *et al.*, Nucl. instrum. and Method. A 438 (1999) 376.
[3] Y. L. Yamaguchi, *et al.*, CNS Annual Report 2004 (2005) 93.

Theoretical Nuclear Physics

Large scale nuclear structure calculations in CNS

N. Shimizu[a], T. Otsuka[a,b,c], N. Itagaki[a], M. Honma[d] and Y. Utsuno[e]

[a] *Department of Physics, University of Tokyo*
[b] *Center for Nuclear Study, Graduate School of Science, University of Tokyo*
[c] *RIKEN (The Institute of Physical and Chemical Research)*
[d] *Center for Mathematical Sciences, University of Aizu*
[e] *Japan Atomic Energy Agency*

1. Introduction

Since the CNS started theoretical studies in 2001, we performed large-scale nuclear structure calculations in order to understand the structure of nuclei, which are complicated quantum many-body system. These theoretical works have been supported not only by the CNS, but also by the RIKEN Nishina Center and the Department of Physics, University of Tokyo [1]. In the fiscal year 2006, we investigated the role of the tensor-force part of the nuclear force and various other topics, which are summarized in Sects.2-6 individually [2, 3, 4, 5, 6, 7, 8, 9, 10, 11, 12, 13, 14, 15, 16, 17, 18, 19].

2. New models of nuclear force

The tensor force was implemented into the mean-field model so that the evolution of nuclear shells can be described for exotic nuclei as well as stable ones [2]. Besides the tensor-force part simulating the meson exchange, the model is an extension of the successful Gogny model. One of the major issues of rare isotope beam physics is a reduced spin-orbit splitting in neutron-rich exotic nuclei. It was shown that the effect of the tensor force on this splitting is larger than or about equal to the one due to the neutron skin. The discussions based on this achievement can be seen in Ref. [4, 5], and will be appeared in Sect.4, too. In addition, we evaluated the contribution of the nucleon-nucleon tensor interaction to single-particle energies with finite-range G-matrix potentials and with zero-range Skyrme potentials [3].

In the relativistic mean field (RMF) model, we constructed a new Lagrangian consisting of one-meson exchange terms and point coupling terms in order to predict properties of asymmetric nuclear matter [6]. We applied this Lagrangian for the investigation of asymmetric nuclear matter and found that the results for the symmetry energy as well as for the equation of state of pure neutron matter are in good agreement with either experimental data or with presently adopted theoretical predictions.

3. Molecular orbital approach in light nuclei

We performed several studies of the cluster structure of light nuclei. For example, we have demonstrated based on a microscopic α-cluster model that α-condensed states appear not only in light nuclei such as ^{12}C and ^{16}O but also in heavier nuclei with a core at excitation energies corresponding to multi-α-threshold energies [7]. To extend the study of normal-condensed state to the cases of heavier nuclei with an inner strongly bound core (^{16}O) and also to non-4N-nuclei, we have introduced a Monte Carlo technique, which are called "virtual Schuck" wave function. Another kind of exotic cluster configuration is a linear-chain structure of three α-clusters, and we have investigated the possibility in 10 MeV region of ^{13}C [8]. Furthermore, we have studied the cluster-shell competition in carbon isotopes. Two parameters have been introduced for the ^{12}C core to characterize the transition from a cluster state to a shell-model state as a measure of the cluster-shell competition: one expresses the relative distance between α-clusters and the other does the dissolution of one of the α clusters. As the neutron number increases, the α-α distance becomes smaller; on the contrary, the dissolution of α clusters is enhanced. The origins of the anomalously small B(E2) value of ^{16}C have been discussed from cluster-shell competition point of view [9].

4. Role of tensor force in exotic nuclei

We have investigated how the tensor force causes the shell evolution in exotic nuclei for the sd-pf shell region [10, 11]. Using the shell model, we can examine not only the evolution of the spherical shell structure but also its influence on the deformation. Performing a systematic calculation from $N = 20$ to 28, we have reproduced the inversion of the ordering of $1/2^+$ and $3/2^+$ in ^{47}K without any modification in the monopole interaction. The tensor force plays a predominant role in accounting for this feature. With the same effective interaction, ^{42}Si is predicted to be a deformed nucleus as shown in Fig. 1.

5. Structure of pf and pfg-shell nuclei

The structure of pf and pfg-shell nuclei has been investigated on the basis of the large-scale shell-model calculations. For ^{56}Ni, the exact solution with the GXPF1A interaction was obtained by state-of-the-art large-scale calculations including diagonalization of one-billion-dimensional matrix [15], and the results was compared with the our previous results. The high-spin structure of odd-odd nucleus ^{58}Co was studied [16]. It was found that the shell-model with the GXPF1 interaction describes the complicated energy levels and transition properties among them reasonably well, which supports the validity of our description of the double-magic ^{56}Ni core. The structure of neutron-rich ^{56,58,60}Cr isotopes was investigated [17]. It was shown that the GXPF1A interaction successfully reproduces the experimental energy levels for positive parity states of ^{56,58}Cr, while the good agreement is lost for N=36 ^{60}Cr, indicating the insufficiency of the pf-shell model space. A new effec-

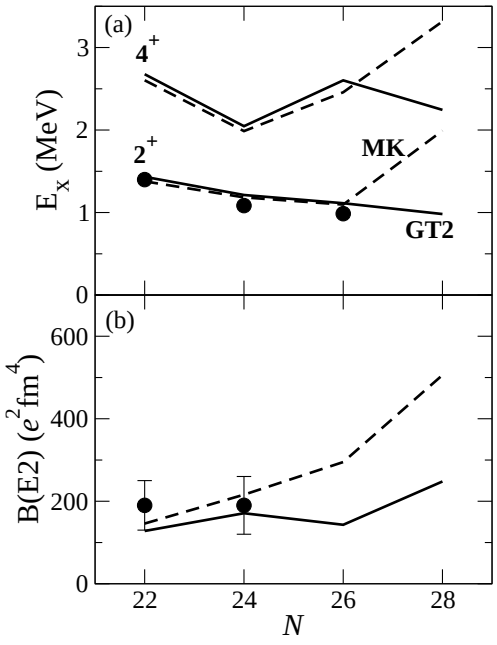

Figure 1. (a) The 2^+ energy levels and (b) $B(E2; 0^+ \rightarrow 2^+)$ values of neutron-rich Si isotopes compared between interactions with different strength in the tensor force. The tensor force of MK is about one third of GT2.

tive interaction JUN45 was presented for the model space consisting of the $(p_{3/2}, f_{5/2}, p_{1/2}, g_{9/2})$ orbits [18]. With this interaction, the structure of Ge isotopes was studied focusing on the irregular behavior of the second 0^+ state around N=40. Also, the nuclear matrix elements of the double-beta decay for the two-neutrino mode was estimated for ^{76}Ge and ^{82}Se.

6. Microscopic description of quadrupole collective states

The nuclear structure of the quadrupole collective states of even-even Te, Xe, and Ba isotopes was discussed using the nuclear shell model. It shows various phenomena, including the transition of spherical, axially symmetric deformed and triaxially deformed shapes. We show these phenomena are reproduced by our microscopic calculation, and the analysis of the anomalously small $B(E2)$ value of ^{136}Te. We also discuss the g-factors of Xe isotopes, which exhibit the transition between the spherical and the triaxially deformed shapes [19].

References

[1] N. Shimizu, T. Otsuka, N. Itagaki, T. Mizusaki, M. Honma, and Y. Utsuno, CNS Annual Report 2005 (2004) 93.

[2] T. Otsuka, T. Matsuo, and D. Abe, Phys. Rev. Lett. **97** (2006) 162501.

[3] A. Brown, T. Duguet, T. Otsuka, D. Abe, and T. Suzuki, Phys. Rev. C **74** (2006) 061303.

[4] A. Gade, B. A. Brown, D. Bazin, C. M. Campbell, J. A. Church, D. C. Dinca, J. Enders, T. Glasmacher, M. Horoi, Z. Hu, K. W. Kemper, W. F. Mueller, T. Otsuka, L. A. Riley, B. T. Roeder, T. Suzuki, J. R. Terry, K. L. Yurkewicz, and H. Zwahlen, Phys. Rev. C **74** (2006) 034322.

[5] Gaudefroy *et al.*, Phys. Rev. Lett. **97** (2006) 092501.

[6] S. Hirose, M. Serra, P. Ring, T. Otsuka and Y. Akaishi, Phys. Rev. C **75** (2007) 024301.

[7] N. Itagaki, M. Kimura, C. Kurokawa, M. Ito, and W. von Oertzen, Phys. Rev. C **75** (2007) 037303.

[8] N. Itagaki, W. von Oertzen, and S. Okabe, Phys. Rev. C **74** (2006) 067304.

[9] H. Masui and N. Itagaki, Phys. Rev. C **75** (2007) 054309.

[10] Y. Utsuno, T. Otsuka, T. Mizusaki, and M. Honma, J. Phys.: Conf. Ser. **49** (2006) 126.

[11] Y. Utsuno, T. Otsuka, T. Mizusaki, and M. Honma, AIP Conf. Proc. **865** (2006) 101.

[12] V. Tripathi *et al.*, Phys. Rev. C **73** (2006) 054303.

[13] A. Ozawa *et al.*, Phys. Rev. C **74** (2006) 021301(R).

[14] J. R. Terry *et al.*, Phys. Lett. B **640** (2006) 86.

[15] M. Horoi, B. A. Brown, T. Otsuka, M. Honma, and T. Mizusaki, Phys. Rev. C **73** (2006) 061305(R).

[16] M. A. G. Silveira, N. H. Medina, J. R. B. Oliveira, J. A. Alca'ntara-Nu'n ez, E. W. Cybulska, H. Dias, M. N. Rao, R. V. Ribas, W. A. Seale, K. T. Wiedemann, B. A. Brown, M. Honma, T. Mizusaki, and T. Otsuka, Phys. Rev. C **74** (2006) 064312.

[17] S. Zhu *et al.*, Phys. Rev. **C 74** (2006) 064315.

[18] M. Honma *et al.*, J. Phys.: Conf. Ser. **49** (2006) 45.

[19] N. Shimizu, T. Otsuka, T. Mizusaki, and M. Honma, J. Phys.: Conf. Ser.**49** (2006) 178.

Dependence of the $B(E2; 2_1^+ \rightarrow 0_1^+)$ in ^{16}C and ^{18}C on the Neutron Effective Charge

S. Fujii[a], T. Mizusaki[a,b] and T. Otsuka[a,c,d]

[a] *Center for Nuclear Study, Graduate School of Science, University of Tokyo*
[b] *Institute of Natural Sciences, Senshu University*
[c] *Department of Physics, University of Tokyo*
[d] *RIKEN (The Institute of Physical and Chemical Research)*

In the conventional shell model, effective charges are often introduced phenomenologically in calculating electric transition probabilities. Due to a limited model space in the shell model, the calculated wave function is generally insufficient. Because of this, if one calculates electric transition probabilities using the wave function obtained by the shell-model diagonalization and the bare charges, the results are usually smaller values than the experimental ones. Thus, in order to reproduce experimental values, some values are added to the values of the bare charges. Usually, the numbers of the effective charges in $E2$ transition are taken in the range $1.3 - 1.5e$ and $0.3 - 0.5e$ for the proton and neutron, respectively. From a theoretical point of view, although the values of the effective charges should be derived microscopically, the numbers are simply determined, in most of the cases, so as to reproduce experimental values. However, it is expected that the magnitudes of the effective charges can be closer to the bare ones as the model-space size becomes larger.

Recently, we have proposed a new microscopic shell model of no-core type [1] where the model-space size is taken larger than the conventional shell model. The model space is composed of the $0s$, $0p$, $1s0d$ and $1p0f$ shells in the calculation for neutron-rich carbon isotopes. The effective two-body interaction is microscopically derived from a bare nucleon-nucleon potential and the Coulomb force through a unitary transformation which is used in the unitary-model-operator approach (UMOA) [2,3]. In the actual calculation, the nucleon excitations from the hole states of ^{14}C are restricted up to two nucleons, and the excitations to the $1p0f$ shell are also up to two nucleons. Although this type of shell model has some restrictions as compared to the usual no-core shell model (NCSM) [4] and is thus less microscopic, it allows one to calculate some properties of heavier nuclei in an efficient way for which the NCSM calculation cannot be performed in a sufficiently large model space. In principle, a sort of effective operator must be employed in the calculation of the electric transition probabilities such as the $E2$ transition strength though the present model space is larger than the conventional one. However, as a first step, we use the bare operator and the bare charges for simplicity in the present study.

In the following calculations, the CD-Bonn potential [5] is employed as the two-body bare interaction, and the Coulomb force is also included for the proton-proton channel. The harmonic-oscillator frequency $\hbar\Omega = 15$ MeV is used, because the $\hbar\Omega$ dependences of calculated energy levels of ^{16}C and ^{18}C are weak in the range between $\hbar\Omega = 14$ and 16 MeV, and there appear energy minima in this region.

Isotopes	Original	Dressed	Expt.
^{16}C	1.30	0.84	$0.63^{\pm 0.11(\mathrm{stat})}_{\pm 0.16(\mathrm{syst})}$
^{18}C	1.19	2.10	

Table 1. The calculated and experimental $B(E2; 2_1^+ \rightarrow 0_1^+)$ values in units of $e^2\mathrm{fm}^4$ for ^{16}C and ^{18}C. The experimental value for ^{16}C is taken from Ref. [7].

In Fig. 1, calculated and experimental low-lying energy levels of ^{16}C are shown. The first column in Fig. 1, denoted by "original", represents the results obtained directly from the present method without any adjustable parameters. It is seen that the calculated 2_1^+, 2_2^+ and 4_1^+ states are in good agreement with the experimental values though the 0_2^+ and 3_1^+ states appear somewhat higher than the experiments.

We note here that, in the present shell-model calculation for ^{15}C, the $1/2_1^+$ state appears above the $5/2_1^+$ state, contrary to the experiment. This wrong ordering may be one of the reasons for the discrepancy between the results and the experiments in the excited states of ^{16}C for the case "original" in Fig. 1. If we consider a sufficiently large model space and calculate these energy levels using the same CD-Bonn potential within the UMOA framework, which is fully microscopic and appropriate for the description of the single-particle state, we can reproduce the correct ordering in ^{15}C as has been shown in Ref. [6]. In order to obtain the correct ordering in ^{15}C in the present shell model, we introduce a minimal refinement of neutron one-body energies on top of ^{14}C so as to reproduce the UMOA results for ^{15}C. In this way, we treat complex correlations coupled to a single-particle-like state within a rather simple framework. Thus, the present approach is a hybrid method combining a no-core type of shell model with single-particle information obtained by the UMOA. Hereafter, we refer to the calculated results with the minimal refinement as "dressed". As seen in the results for "dressed" in Fig. 1, the calculated results become better by introducing the dressed one-body energies. Namely, the correct ordering of the low-lying energy levels is obtained. As for energy levels of ^{18}C, the experimental value of the energy spacing between the first excited 2^+ and the ground 0^+ states is 1.62 MeV. Since our values for "original" and "dressed" are 1.44 and 1.73 MeV, respectively, both results are not so different from the experiment.

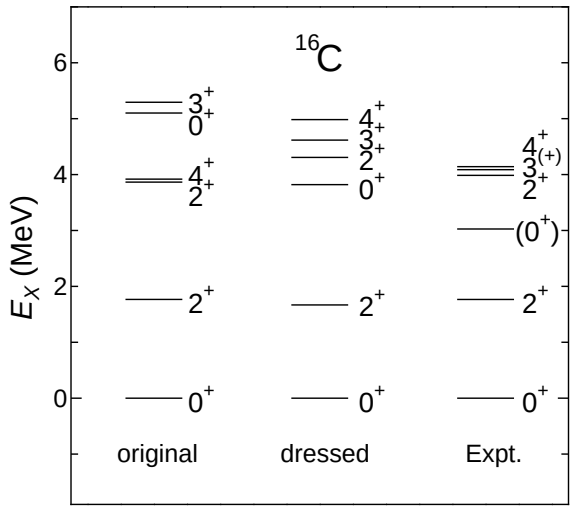

Figure 1. Low-lying energy levels of ^{16}C.

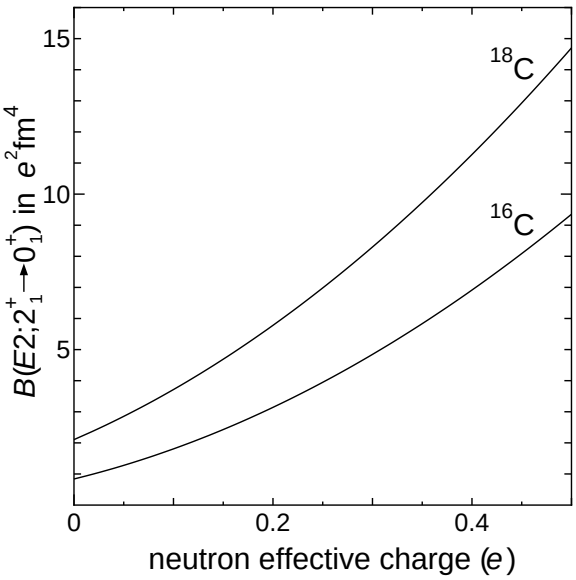

Figure 2. The dependence of the calculated $B(E2; 2_1^+ \rightarrow 0_1^+)$ values on the neutron effective charge $e_n^{\rm eff}$ for ^{16}C and ^{18}C for the case "dressed".

In Table 1, the calculated and experimental values of the $B(E2; 2_1^+ \rightarrow 0_1^+)$ in ^{16}C and ^{18}C are tabulated. Interestingly, for ^{16}C the result for "dressed" is smaller than that for "original", which is in contrast to the case of ^{18}C. For ^{16}C, the result for "dressed" is in good agreement with the anomalously hindered experimental value which has recently been found experimentally [7, 8, 9]. However, we should keep in mind that the present approach with the bare transition operator and the bare charges is nothing but an approximation though the model space is larger than the conventional shell model. Therefore, the good agreement may be accidental. For a deeper understanding of the validity of the present approach, we have also calculated the $B(E2; 5/2_1^+ \rightarrow 1/2_1^+)$ in ^{15}C of which experimental value is determined with high accuracy. The calculated result for "dressed" is $0.28\ e^2$fm^4, while the experimental value is $0.97 \pm 0.02\ e^2$fm^4. It seems that our result is considerably smaller than the experiment. However, it is noted that the experimental values of the $B(E2)$ in ^{15}C and ^{16}C are very small. Therefore, the comparisons between the results and experiments should be made carefully. As a matter of fact, we have found that the discrepancy of the $B(E2)$ in ^{15}C can be compensated by introducing the neutron effective charge as only $e_n^{\rm eff} = 0.164e$ which is much smaller than the usual neutron effective charge in the conventional shell model. This indicates that the neutron effective charge dependence of the $B(E2)$ in neutron-rich carbon isotopes are rather strong. In Fig. 2, we show the dependence of the $B(E2; 2_1^+ \rightarrow 0_1^+)$ in ^{16}C and ^{18}C on the neutron effective charge. For ^{16}C, the $B(E2)$ value is rapidly increasing as the neutron effective charge becomes larger. For $e_n^{\rm eff} = 0.5e$ which is the standard value in the conventional shell model, the calculated $B(E2)$ is $9.35\ e^2$fm^4. This value is about ten times larger than the result for the bare charge, namely, $e_n^{\rm eff} = 0$. Also for ^{18}C, a similar tendency of the strong dependence on the neutron effective charge is obtained.

Due to the strong dependence on the neutron effective charge, the $B(E2; 2_1^+ \rightarrow 0_1^+)$ values in ^{16}C and ^{18}C for the small number $e_n^{\rm eff} = 0.164e$, which is needed to reproduce the experimental $B(E2; 5/2_1^+ \rightarrow 1/2_1^+)$ in ^{15}C, become considerably larger as 2.62 and $4.98\ e^2$fm^4, respectively. This means that, in the present approach, we cannot reproduce the experimental $B(E2)$ values in ^{15}C and ^{16}C simultaneously with the same neutron effective charge. But, it should be noted that the $B(E2; 2_1^+ \rightarrow 0_1^+)$ in ^{16}C is very sensitive to the neutron effective charge, and thus it may be a difficult problem to derive the small $B(E2)$ value accurately from a microscopic point of view. For a more quantitative study, some improvements of the present approach may be needed, such as the enlargement of the model space and the derivation of an effective operator for the $E2$ transition strength. Results with these works will be reported in the near future.

References

[1] S. Fujii, T. Mizusaki, T. Otsuka, T. Sebe and A. Arima, Phys. Lett. B **650** (2007) 9.

[2] K. Suzuki and R. Okamoto, Prog. Theor. Phys. **92** (1994) 1045.

[3] S. Fujii, R. Okamoto and K. Suzuki, Phys. Rev. C **69** (2004) 034328.

[4] P. Navrátil, J. P. Vary, W. E. Ormand and B. R. Barrett, Phys. Rev. Lett. **87** (2001) 172502.

[5] R. Machleidt, F. Sammarruca and Y. Song, Phys. Rev. C **53** (1996) R1483.

[6] S. Fujii, R. Okamoto and K. Suzuki, J. Phys. Conf. Ser. **20** (2005) 83; nucl-th/0505076.

[7] N. Imai *et al.*, Phys. Rev. Lett. **92** (2004) 062501.

[8] Z. Elekes *et al.*, Phys. Lett. B **586** (2004) 34.

[9] H. J. Ong *et al.*, Phys. Rev. C **73** (2006) 024610.

Other Activities

The Fifth CNS International Summer School (CISS06)

E. Ideguchi, S. Shimoura, T. Otsuka[a], H. Sakai[a], S. Kubono, and T. Mizusaki[b]

Center for Nuclear Study, Graduate School of Science, University of Tokyo
[a]Department of Physics, Graduate School of Science, University of Tokyo
[b]Senshu University

The 5th CNS International Summer School (CISS06) was held at the Wako branch of the Center for Nuclear Study (CNS), the University of Tokyo, in the period of August 24–29, 2006.
This summer school is the fifth one in the series which aimed at providing graduate students and Post Docs with basic knowledge and perspectives of nuclear physics. Topics of this year were "Structure of exotic nuclei", "Nuclear mean field theory", "Fermion Molecular Dynamics", "Direct reaction with RI beams", "Effective interaction in nucleus", "Dense nuclear matter", "Supernova explosion","Nuclear moments", and "Shell model calculation". Short lectures on recent progress in physics with unstable nuclei were also presented.
The list of lecturers and the title of lectures are shown below.

I. Hamamoto (Lund)	"One-particle motion in deformed nuclei – from stable to drip line"
B. Sherrill (MSU)	"Experiments with radioactive ion beams at the National Superconducting Cyclotron Laboratory"
T. Neff (MSU)	"Nuclear structure and reactions in the Fermionic Molecular Dynamics approach"
W. Mittig (GANIL)	"Low to Medium Energy Experiments for the study of exotic nuclei"
M. Kohno (Kyushu dent.)	"Equivalent and effective interactions in nuclear physics"
T. Takatsuka (Iwate)	"Baryon Matter and Neutron Stars"
K. Sumiyoshi (Numazu)	"Supernova Simulations and the Role of Nuclear Physics"
H. Ueno (RIKEN)	"Study of unstable nuclei through the measurement of nuclear moments"
Y. Utsuno (JAEA)	"Shell-model approach to the island of inversion and beyond"

This year, 96 participants attended from 7 countries: Among them, 20 attendances were from Asian countries, China, Korea, Malaysia, Vietnam, and Myanmar. Domestic participants were from 15 universities and 1 institute over the country. The lectures were given from 10:00 in the morning to 18:00 in the evening. Student and Post Doc sessions were held in the school on Friday, Saturday and Monday evening after lectures. Thirteen talks were given by graduate students and Post Docs. Attendances also communicated each other in the Free Discussion time after dinner with a relaxed atmosphere. All information concerning the summer school is open for access at the following URL:

http://www.cns.s.u-tokyo.ac.jp/summerschool/

Organizers thank all participants and all members of the CNS who supported the summer school. They are also grateful to RIKEN for their supports in the preparation of the school. This school was supported in part by the International Exchange Program of Graduate School of Science, the University of Tokyo.

Laboratory Exercise for Undergraduate Students

T. Kawabata[a], K. Yako[b], H. Kimura[b], S. Noji[b], H. Sakai[b], and S. Shimoura[a]

[a]*Center for Nuclear Study, Graduate School of Science, University of Tokyo*
[b]*Department of Physics, University of Tokyo, Tokyo*

Nuclear scattering experiments were performed as a laboratory exercise for undergraduate students of the University of Tokyo. This program was aiming at providing undergraduate students with an opportunity to learn how to study the world of $< 10^{-14}$ m by using an ion beam from an accelerator. In 2006, 32 students joined this program.

The four beam times were scheduled in the second semester for juniors, and 8 students participated in each beam time. Before the beam time, the students learned the basic handling of the semiconductor detectors and electronic circuits at the Hongo campus, and attended a radiation safety lecture at RIKEN. They also joined a tour to the RI beam facility, which was under construction at RIKEN.

The experiment was performed at the RIKEN accelerator research facility (RARF) using a 26-MeV alpha beam accelerated by the AVF cyclotron. The alpha beam extracted from the AVF cyclotron was transported to the CRIB beam line in the E7 experimental room. In each beam time, the students were divided into two groups and took one of the following two subjects;

1. Measurement of elastic scattering of α particles from $^{197}\mathrm{Au}$.

2. Measurement of gamma rays emitted in the cascade decay of the rotational bands in $^{154}\mathrm{Gd}$ and $^{184}\mathrm{Os}$.

A snapshot of students and instructors during a beam time is shown in Fig. 1.

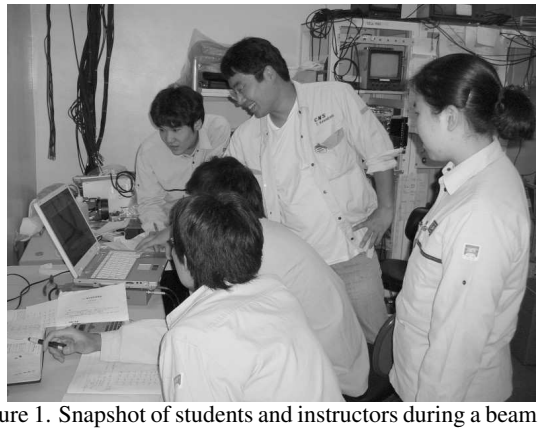

Figure 1. Snapshot of students and instructors during a beam time.

In the $\alpha+^{197}\mathrm{Au}$ measurement, α particles scattered from the Au target with a thickness of 1.42 mg/cm^2 were detected by a silicon PIN-diode located 11 cm away from the target. A plastic collimator with a diameter of 6 mm was attached on the silicon detector. The energy spectrum of the scattered α particles was recorded by a multi-channel analyzer (MCA) system. The beam was stopped by a Faraday cup in the scattering chamber. The cross section for the alpha elastic scattering was measured in the angular range of $\theta_{\mathrm{lab}} = 25$–$150^\circ$, and was compared with the calculated cross section for the Rutherford scattering as shown in Fig. 2. The cross section was also analyzed by the potential-model calculation, and the radius of the gold nucleus was discussed. Some students obtained the radius of $\sim$10 fm by using a classical model where the trajectory of the α particle in the nuclear potential is obtained by the Runge-Kutta method. Others tried to understand the scattering process by calculating the angular distribution by the distorted wave Born approximation with a Coulomb wave function and a realistic nuclear potential.

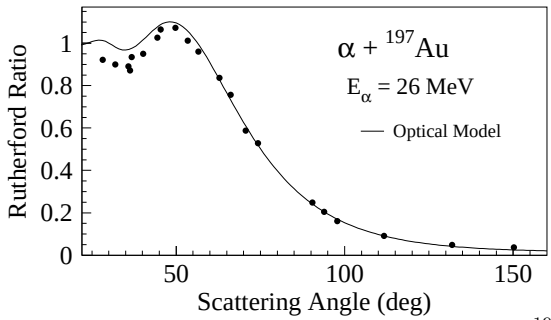

Figure 2. Ratio of the measured cross section for the $\alpha + {}^{197}\mathrm{Au}$ elastic scattering to Rutherford scattering. The solid line shows a result from an optical-model analysis by a student.

In the measurement of the rotational bands, excited states in $^{154}\mathrm{Gd}$ and $^{184}\mathrm{Os}$ nuclei were populated by the $^{152}\mathrm{Sm}(\alpha, 2n)$ and $^{182}\mathrm{W}(\alpha, 2n)$ reactions, respectively. The gamma rays emitted from the cascade decay of the rotational bands were measured by a high purity germanium detector located 50 cm away from the target. The energies of the gamma rays were recorded by the MCA system. The gain and the efficiency of the detector system had been calibrated with standard gamma-ray sources of $^{22}\mathrm{Na}$, $^{60}\mathrm{Co}$, $^{133}\mathrm{Ba}$, and $^{137}\mathrm{Cs}$. Based on the energies of the gamma rays, the ground-state rotational bands were identified. The moment of inertia and the deformation parameters of the excited states were discussed by using a classical rigid rotor model and an irrotational fluid model. The students found that the reality lies between the two extreme models. The initial population among the levels in the rotational band was also discussed by taking the effect of internal conversion into account.

We believe this program is very impressive for the students. It was the first time for most of the students to use large experimental equipments. They learned basic things about the experimental nuclear physics and how to extract physics from the data.

The authors would like to thank Dr. Y. Uwamino, Prof. Y. Sakurai, and the RARF cyclotron crew for their helpful effort in the present program.

Appendices

Symposium, Workshop, Seminar, PAC and External Review
CNS Reports
Publication List
Talks and Presentations
Personnel

Symposium, Workshop, Seminar, Colloquium, and PAC

A. Symposium

1. 21st Century COE International Symposium on "Neutrino Processes and Stellar Evolution (NEPSE07)"
   February 7-9, 2007, Sanjo Kaikan, University of Tokyo, Japan.

   The purpose of the NPSE07 symposium was to discuss various problems and issues on neutrino-nucleus reactions and their implications in stellar evolutions as well as recent developments of physics of neutrinos. It was timely to discuss such problems and issues at the time of the 20th anniversary of the supernovae 1987A.

   The organizing committee consisted of K. Sato(Univ. of Tokyo), K. Nomoto(Univ. of Tokyo), T. Kajita(ICRR, Univ. of Tokyo) K. Kubono(CNS, Univ. of Tokyo) T. Otsuka(Univ. of Tokyo, Chair of NEPSE07) H. Sakai(Univ. of Tokyo) S. Shimoura(CNS, Univ. of Tokyo) T. Kajino(NAO) A. Suzuki(KEK)

B. Workshop

1. 2nd German-Japanese Workshop on "Nuclear Structure and Astrophysics"
   October 4-7, 2006, RIKEN, Japan

   Second German-Japanese Workshop on Nuclear Structure and Astrophysics has been held during 4-7/Oct. 2006 at the conference room, RIBF building, RIKEN, which is a cooperative workshop between German and Japanese scientists, and many talks and discussion have been given.

   This workshop was the second time of the series after the first one held at GSI in December 2004. This time, not only from GSI, 20 scientists came to Japan from many districts of Germany and all of them gave presentations. From Japanese side, 71 persons registered and 49 presentation were given. To promote the collaborations between German and Japanese scientists, the collaboration meeting and facility tour to RIBF, which was near completion, were organized.

   The workshop was supported by University of Tokyo-RIKEN Joint International Program for Nuclear Physics (TORIJIN), and also from the German side, DFG and GSI have supported. The workshop corresponds to the activity of core-to-core program, JSPS.

   P. Ring (TU Munich), H. Emling (GSI), K. Langanke (GSI), T. Otsuka (Tokyo), T. Motobayashi (RIKEN), T. Kobayashi (Tohoku), and K. Yabana (Tsukuba)

2. Japanese French Workshop on "Exotic Femto Systems"
   March 13-16, 2007, GANIL, Caen, France

   This should be the first of a new serie of workshops aimed was to strengthen the links between theory and experiments, and collaborations between Japan and France.

   The workshop was supported by the core-to-core project "Exotic Femto Systems" by the JSPS and by GANIL.

   Organizers were T. Otsuka(Tokyo), T. Motobayashi(Tokyo), H. Utsunomiya(Kobe), A. Odahara(Osaka), G. Marcella(Orsay), M. Iolanda(Bordeaux), M. Wolfgang(Caen), and B. David(Caen)

3. International Workshop "Joint JUSTIPEN-LACM" Meeting
   March 2007, Oak Ridge National Laboratory, USA

   The meeting is a merger of two workshops: (i) the US-Japan theory meeting under the auspices of the Japan-US Theory Institute for Physics with Exoctic Nuclei (JUSTIPEN) and (ii) the annual NNSA-JIHIR meeting on the nuclear large amplitude collective motion (LACM) with an emphasis on fission.

   The purpose of the meeting, jointly organized by the JUSTIPEN Governing Board, by the UT/ORNL theory group, and by the JSPS Core-to-Core program "Exotic Femto Systems", is to bring together scientists (theorists and experimentalists) with interests in physics of radioactive nuclei, LACM, and theoretical approaches related to the SciDAC-2 UNEDF project. One emphasis of the meeting will be on topics related to future collaborations betwen US and Japanese groups (under JUSTIPEN). We are looking forward to an exiting meeting with stimulating discussions. The meeting is supported by the National Nuclear Security Administration under the Stewardship Science Academic Alliance program, JIHIR, JSPS, Todai-RIKEN Joint International Program for Nuclear Physics, and UNEDF.

The organizers are T. Otsuka (Tokyo), T. Motobayashi (RIKEN), H. Sakai (Tokyo), H. Horiuchi (RCNP/Osaka), M. Matsuo (Niigata), T. Noro (Kyushu), C. Bertulani(ORNL), D. Dean (ORNL), W. Nazarewicz (ORNL), and T. Papenbrock (ORNL).

C. CNS Seminar

1. "Suppression of fusion by quasi-fission in reactions forming heavy elements",
   David Hinde (Australian National University), Jun. 2nd, 2006.

2. "Barriers to Fusion: concept and application"
   Mahananda Dasgupta (Australian National University), Jun. 2nd, 2006.

D. CNS Colloquium

1. "Compression modes in (medium-)heavy nuclei: excitation and microscopic structure",
   M.N. Harakeh (KVI), July 20th, 2006.

2. "Recent study on unstable nuclei in Peking University",
   Tao Zheng (Peking Univ.), July 21th, 2006.

3. "The AGATA Spectrometer",
   B. Cederwall (Royal Institute of Technology, Sweden) August 22th, 2006

4. "The liquid, gas, and solid structure of light neutron-rich nuclei and role of the non-central interactions",
   N. Itagaki (Univ. of Tokyo) Nov. 28th, 2006

E. Program Advisory Committee for Nuclear-Physics Experiments at RI Beam Factory

The 1st NP-PAC meeting
Date: February 9–10, 2007
Place: Conference room, 2F RIBF building

To facilitate the exploration of the scientific opportunities, CNS and RIKEN Nishina Center for Accelerator-Based Science (RNC) decided to have a joint program advisory committee (PAC). Previously, the PAC for CRIB had been an independent body under the auspices of CNS. The new PAC will review all nuclear physics proposals, for RIBF facilities and CRIB, based on their scientific merits and feasibility. The PAC will submit reviewed papers to the director of RNC, while those proposals for CRIB experiments will be submitted to the director of CNS.

Eight experimental proposals for CRIB were examined in the 1st NP-PAC meeting.

CNS Advisory Committee

The 7th CNS AC meeting
Date: February 11, 2007.
Place: Seminar room in the 3rd floor of CNS building in Wako Campus

A CNS advisory committee meeting was held on February 11, 2007, to receive oral presentations of research activities and future plans of the Center. Committee members also attended the NP-PAC meeting of RIKEN on February 10 in order to hear presentations of proposals to be performed with CRIB.

The Committee members:

Prof. Kichiji Hatanaka (Chair, RCNP Osaka University)
Prof. Hideto En'yo (RIKEN Nishina Center)
Prof. Kazuhiro Yabana (University of Tsukuba)
Prof. Atsuko Odahara (Osaka University)
Prof. Ikuko Hamamoto (Lund University)
Prof. Wolfgang Mittig (GANIL)
Prof. Michael Wiescher (University of Notre Dame)

One of members (M. W.) was not present.

The Committee evaluated (i) scientific and educational activities of the research groups of CNS in fiscal year 2006, and (ii) research and education plans of each group from the fiscal year 2007.

CNS Reports

#68 "Search for 180 degree correlated equal-energy e^+e^- paris from e^+(^{82}Sr)+Th interactions",
M. Sakai, H. Kawakami, K. Omata, I. Sugai, I. Katayama, S. Shimizu K. Horie and T. Miura, Sept.2006.

#69 "CNS Annual Report 2005",
edited by K. Ozawa, Nov. 2006.

Publication List

A. Original Papers

1. S. S. Adler, H. Hamagaki, S. Kametani, T. Matsumoto, K. Oyama, K. Ozawa, T. Sakaguchi et al. (for the PHENIX Collaboration) "Evidence for a long-range component in the pion emission source in Au+Au collisions at $\sqrt{s_{NN}}$ = 200-GeV " Phys. Rev. Lett **98** (2007) 132301.

2. S. S. Adler, H. Hamagaki, S. Kametani, T. Matsumoto, K. Oyama, K. Ozawa, T. Sakaguchi et al. (for the PHENIX Collaboration) "High transverse momentum eta meson production in p+p, d+Au and Au+Au collisions at $\sqrt{s_{NN}}$ = 200-GeV " Phys. Rev. C **75** (2007) 024909.

3. S. S. Adler, H. Hamagaki, M. Inuzuka, F. Kajihara, S. Kametani, T. Matsumoto, K. Oyama, K. Ozawa, T. Sakaguchi et al. (for the PHENIX Collaboration) "Measurement of direct photon production in p + p collisions at $\sqrt{s}$ = 200-GeV " Phys. Rev. Lett. **98** (2007) 012002.

4. A. Adare, T. Gunji, H. Hamagaki, T. Isobe, F. Kajihara, S. Kametani, N. Kurihara, S. X. Oda, K. Ozawa,et al. (for the PHENIX Collaboration) "Measurement of high-p(T) single electrons from heavy-flavor decays in p+p collisions at $\sqrt{s}$ = 200-GeV " Phys. Rev. Lett. **97** (2006) 252002.

5. S. S. Adler, H. Hamagaki, M. Inuzuka, F. Kajihara, S. Kametani, T. Matsumoto, K. Oyama, K. Ozawa, T. Sakaguchi et al. (for the PHENIX Collaboration) "Jet properties from dihadron correlations in p+p collisions at $\sqrt{s}$ = 200-GeV " Phys. Rev. D **74** (2006) 072002.

6. S. S. Adler, H. Hamagaki, M. Inuzuka, F. Kajihara, S. Kametani, T. Matsumoto, K. Oyama, K. Ozawa, T. Sakaguchi et al. (for the PHENIX Collaboration) "Nuclear effects on hadron production in d + Au collisions at $\sqrt{s_{NN}}$ = 200-GeV with p+p data" Phys. Rev. C **74** (2006) 024904.

7. S. S. Adler, H. Hamagaki, S. Kametani, T. Matsumoto, K. Oyama, K. Ozawa, T. Sakaguchi et al. (for the PHENIX Collaboration) "Dense-Medium Modifications to di-induced hadron pair distributions in Au+Au collisions at $\sqrt{s_{NN}}$ = 200-GeV " Phys. Rev. Lett. **97** (2006) 052301.

8. S. S. Adler, H. Hamagaki, M. Inuzuka, F. Kajihara, S. Kametani, T. Matsumoto, K. Oyama, K. Ozawa, T. Sakaguchi et al. (for the PHENIX Collaboration) "Azimuthal angle correlations for rapidity separated hadron pairs in d + Au Collisions at $\sqrt{s_{NN}}$ = 200-GeV " Phys. Rev. Lett. **96** (2006) 222301.

9. S. S. Adler, T. Gunji, H. Hamagaki, M. Inuzuka, T. Isobe, F. Kajihara, S. Kametani, N. Kurihara, T. Matsumoto, K. Oyama, K. Ozawa, T. Sakaguchi, et al. (for the PHENIX Collaboration) "Improved measurement of double helicity asymmetry in inclusive midrapidity pi0 production for polarized p+p collisions at $\sqrt{s}$ = 200-GeV " Phys. Rev. D **73** (2006) 091102.

10. S. S. Adler, H. Hamagaki, S. Kametani, T. Matsumoto, K. Oyama, K. Ozawa, T. Sakaguchi et al. (for the PHENIX Collaboration) "Common suppression pattern of eta and pi0 mesons at high transverse momentum in Au+Au collisions at $\sqrt{s_{NN}}$ = 200-GeV " Phys. Rev. Lett. **96** (2006) 202301.

11. S. S. Adler, H. Hamagaki, M. Inuzuka, F. Kajihara, S. Kametani, T. Matsumoto, K. Oyama, K. Ozawa, T. Sakaguchi et al. (for the PHENIX Collaboration) "Jet structure from dihadron correlations in d+Au collisions at $\sqrt{s_{NN}}$ = 200-GeV" Phys. Rev. C **73** (2006) 054903.

12. S. X. Oda, H. Hamagaki, K. Ozawa, M. Inuzuka, T. Sakaguchi, T. Isobe, T. Gunji, Y. Morino, S. Saito, Y. L. Yamaguchi, et al. "Development of a time projection chamber using gas electron multipliers (GEM-TPC) " Nucl. Instrum. Meth. A **566** (2006) 312-320.

13. T. Isobe, H. Hamagaki, K. Ozawa, M. Inuzuka, T. Sakaguchi, T. Matsumoto, S. Kametani, F. Kajihara, T. Gunji, N. Kurihara, S.X. Oda, and Y.L. Yamaguchi "Development of a time projection chamber using CF4 gas for relativistic heavy ion experiments" Nucl. Instrum. Meth. A **564** (2006) 190-196.

14. T. Tamagawa, H. Hamagaki, M. Inuzuka et al. "Development of gas electron multiplier foils with a laser etching technique " Nucl. Instrum. Meth. A **560** (2006) 418-424.

15. R. Muto, H. Hamagaki, K. Ozawa et al. “Evidence for in-medium modification of the phi meson at normal nuclear density” Phys. Rev. Lett. **98** (2007) 042501.

16. T. Tabaru, H. Hamagaki, K. Ozawa et al. “Nuclear mass number dependence of inclusive production of omega and phi mesons in 12-GeV p + A collisions” Phys. Rev. C **74** (2006) 025201.

17. T. Fukuchi, S. Tanaka, T. Sasaki, Y. Gono, A. Odahara, T. Morikawa, M. Shibata, H. Watanabe, S. Motomura, T. Tsutsumi, O. Kashiyama, K. Saitoh, Y. Wakabayashi, T. Kishida, S. Kubono, and M. Ishihara: “ Level structure and excitation energy of a high-spin isomer in ^{150}Ho ”, Phys. Rev. C **73** (2006) 067303.

18. S. Michimasa, S. Shimoura, H. Iwasaki, M. Tamaki, S. Ota, N. Aoi, H. Baba, N. Iwasa, S. Kanno, S. Kubono, K. Kurita, M. Kurokawa, T. Minemura, T. Motobayashi, M. Notani, H.J. Ong, A. Saito, H. Sakurai, E. Takeshita, S. Takeuchi, Y. Yanagisawa, and A. Yoshida: “ Proton single-particle states in the neutron-rich ^{23}F nucleus”, Phys. Lett. B **638** (2006) 146–152.

19. S. Kubono, T. Teranishi, M. Notani, H. Yamaguchi, A. Saito, J. J. He, Y. Wakabayashi, H. Fujikawa, G. Amadio, H. Baba, T. Fukuchi, S. Shimoura, S. Michimasa, S. Nishimura, M. Nishimura, Y. Gono, A. Odahara, S. Kato, J. Y. Moon, J. H. Lee, Y. K. Kwon, C. S. Lee, K. I. Hahn, Zs. Fulop, V. Guimaraes, and R. Lichtenthaler: “Nuclear astrophysics at the east drip line”, Eur. Phys. J. A **27** (2006) 327–332.

20. Y. Togano, T. Gomi, T. Motobayashi, Y. Ando, N. Aoi, H. Baba, K. Demichi, Z. Elekes, N. Fukuda, Zs. Fulop, U. Futakami, H. Hasegawa, Y. Higurashi, K. Ieki, N. Imai, M. Ishihara, K. Ishikawa, N. Iwasa, H. Iwasaki, S. Kanno, Y. Kondo, T. Kubo, S. Kubono, M. Kunibu, K. Kurita, Y. U. Matsuyama, S. Michimasa, T. Minemura, M. Miura, H. Murakami, T. Nakamura, M. Notani, S. Ota, A. Saito, H. Sakurai, M. Serata, S. Shimoura, T. Sugimoto, E. Takeshita, S. Takeuchi, K. Ue, K. Yamada, Y. Yanagisawa, K. Yoneda, and A. Yoshida: “Study of the ^{26}Si(p,γ)^{27}P reaction through Coulomb dissociation of ^{27}P ”, Eur. Phys. J. A **27** (2006) 233–236.

21. C.J. Chiara, M. Devlin, E. Ideguchi, D.R. LaFosse, F. Lerma, W. Reviol, S.K. Ryu, D.G. Sarantites, O.L. Pechenaya, C. Baktash, A. Galindo-Uribarri, M.P. Carpenter, R.V.F. Janssens, T. Lauritsen, C.J. Lister, P. Reiter, D. Seweryniak, P. Fallon, A. Görgen, A.O. Macchiavelli, D. Rudolph, G. Stoitcheva, and W.E. Ormand: “Probing sd-fp cross-shell interactions via terminating configurations in ^{42,43}Sc” Phys. Rev. **C75** (2007) 054305 (18 pages)

22. K. Morita, K. Morimoto, D. Kaji, T. Akiyama, S. Goto, H. Haba, E. Ideguchi, K. Katori, H. Koura, H. Kudo, T. Ohnishi, A. Ozawa, T. Suda, K. Sueki, F. Tokanai, T. Yamaguchi, A. Yoneda, A. Yoshida: “Experiment on Synthesis of an Isotope ^{277}112 by ^{208}Pb + ^{70}Zn Reaction”, J. Phys. Soc. Jpn. **76** (2007) 043201 (5 pages)

23. K. Morita, K. Morimoto, D. Kaji, T. Akiyama, S. Goto, H. Haba, E. Ideguchi, K. Katori, H. Koura, H. Kikunaga, H. Kudo, T. Ohnishi, A. Ozawa, N. Sato, T. Suda, K. Sueki, F. Tokanai, T. Yamaguchi, A. Yoneda, A. Yoshida: “Observation of Second Decay Chain from ^{278}113”, J. Phys. Soc. Jpn. **76** (2007) 045001 (2 pages)

24. D. Rudolph, B.G. Carlsson, I. Ragnarsson, S. Aberg, C. Andreoiu, M.A. Bentley, M.P. Carpenter, R.J. Charity, R.M. Clark, M. Cromaz, J. Ekman, C. Fahlander, P. Fallon, E. Ideguchi, A.O. Macchiavelli, M.N. Mineva, W. Reviol, D.G. Sarantites, D. Seweryniak, S.J. Williams: “^{58}Ni: An Unpaired Band Crossing at New Heights of Angular Momentum for Rotating Nuclei”, Phys. Rev. Lett. **96** (2006) 092501 (4 pages)

25. Z. Elekes, Zs. Dombrádi, A. Saito, N. Aoi, H. Baba, K. Demichi, Zs. Fülöp, J. Gibelin, T. Gomi, H. Hasegawa, N. Imai, M. Ishihara, H. Iwasaki, S. Kanno, S. Kawai, T. Kishida, T. Kubo, K. Kurita, Y. Matsuyama, S. Michimasa, T. Minemura, T. Motobayashi, M. Notani, T. Ohnishi, H. J. Ong, S. Ota, A. Ozawa, H. K. Sakai, H. Sakurai, S. Shimoura, E. Takeshita, S. Takeuchi, M. Tamaki, Y. Togano, K. Yamada, Y. Yanagisawa, and K. Yoneda: “Proton inelastic scattering studies at the borders of the “island of inversion”: The ^{30,31}Na and ^{33,34}Mg case”, Phys. Rev. C **73** (2006) 044314.

26. Zs. Dombrádi, Z. Elekes, A. Saito, N. Aoi, H. Baba, K. Demichi, Zs. Fülöp, J. Gibelin, T. Gomi, H. Hasegawa, N. Imai, M. Ishihara, H. Iwasaki, S. Kanno, S. Kawai, T. Kishida, T. Kubo, K. Kurita, Y. U. Matsuyama, S. Michimasa, T. Minemura, T. Motobayashi, M. Notani, T. Ohnishi, H. J. Ong, S. Ota, A. Ozawa, H. K. Sakai, H. Sakurai, S. Shimoura, E. Takeshita, S. Takeuchi, M. Tamaki, Y. Togano, K. Yamada, Y. Yanagisawa, and K. Yoneda: “Vanishing N=20 Shell Gap: Study of Excited States in ^{27,28}Ne”, Phys. Rev. Lett. **96** (2006) 182501.

27. T. Nakamura, A. M. Vinodkumar, T. Sugimoto, N. Aoi, H. Baba, D. Bazin, N. Fukuda, T. Gomi, H. Hasegawa, N. Imai, M. Ishihara, T. Kobayashi, Y. Kondo, T. kubo, M. Miura, T. Motobayashi, H. Otsu, A. Saito, H. Sakurai, S. Shimoura, K. Watanabe, Y. X. Watanabe, T. Yakushiji, Y. Yanagisawa, K. Yoneda: “Observation of Strong Low-Lying E1 Strength in the Two-Neutron Halo Nucleus ^{11}Li”, Phys. Rev. Lett. **96** (2006) 252502.

28. Z. Elekes, Zs. Dombrádi, N. Aoi, S. Bishop, Zs. Fülöp, J. Gibelin, T. Gomi, Y. Hashimoto, N. Imai, N. Iwasa, H. Iwasaki, G. Kalinka, Y. Kondo, A. A. Korsheninnikov, K. Kurita, M. Kurokawa, N. Matsui, T. Motobayashi, T. Nakamura, T. Nakao, E.Yu. Nikolskii, T. K. Ohnishi, T. Okumura, S. Ota, A. Perera, A. Saito, H. Sakurai, Y. Satou, D. Sohler, T. Sumikama, D. Suzuki, M. Suzuki, H. Takeda, S. Takeuchi, Y. Togano, and Y. Yanagisawa: "Spectroscopic Study of Neutron Shell Closures via Nucleon Transfer in the Near-Dripline Nucleus ^{23}O", Phys. Rev. Lett. **98** (2007) 102502.

29. Z. Elekes, Zs. Dombrádi, N. Aoi, S. Bishop, Zs. Fülöp, J. Gibelin, T. Gomi, Y. Hashimoto, N. Imai, N. Iwasa, H. Iwasaki, G. Kalinka, Y. Kondo, A. A. Korsheninnikov, K. Kurita, M. Kurokawa, N. Matsui, T. Motobayashi, T. Nakamura, T. Nakao, E. Yu. Nikolskii, T. K. Ohnishi, T. Okumura, S. Ota, A. Perera, A. Saito, H. Sakurai, Y. Satou, D. Sohler, T. Sumikama, D. Suzuki, M. Suzuki, H. Takeda, S. Takeuchi, Y. Togano, and Y. Yanagisawa: "Search for neutron decoupling in ^{22}O via the (d,d$'\gamma$) reaction", Phys. Rev. C **74** (2006) 017306.

30. T. Shizuma, T. Ishii, H. Makii, T. Hayakawa, S. Shigematsu, M. Matsuda, E. Ideguchi, Y. Zheng, M. Liu, T. Morikawa, P.M. Walker, M. Oi: "Excited states in neutron-rich ^{188}W produced by an ^{18}O-induced 2-neutron transfer reaction", Euro. Phys. J. **A30** (2006) 391–396

31. K. Suda, H. Okamura, T. Uesaka, J. Nishikawa, H. Kumasaka, R. Suzuki, H. Sakai, A. Tamii, T. Ohnishi, K. Sekiguchi, K. Yako, S. Sakoda, H. Kato, M. Hatano, Y. Maeda, T. Saito, T. Ishida, N. Sakamoto, Y. Satou, K. Hatanaka, T. Wakasa, J. Kamiya: "Absolute Calibration of the Deuteron Beam Polarization at Intermediate Energies via the ^{12}C($\vec{d}, \alpha$)^{10}B*[2$^+$] Reaction", Nucl. Instrum. Methods. A **572** (2007) 745–753.

32. H. Fujita, Y. Fujita, T. Adachi, A. D. Bacher, G. P. A. Berg, T. Black, E. Caurier, C. C. Foster, H. Fujimura, K. Hara, K. Harada, K. Hatanaka, J. Jänecke, J. Kamiya, Y. Kanzaki, K. Katori, T. Kawabata, K. Langanke, G. Martinez-Pinedo, T. Noro, D. A. Roberts, H. Sakaguchi, Y. Shimbara, T. Shinada, E. J. Stephenson, H. Ueno, T. Yamanaka, M. Yoshifuku, M. Yosoi: "Isospin structure of $J^\pi = 1^+$ states in ^{58}Ni and ^{58}Cu studied by ^{58}Ni(p,p') and ^{58}Ni(^{3}He,t)^{58}Cu measurements", Phys. Rev. C **75** (2007) 034310.

33. T. Kawabata, H. Akimune, H. Fujita, Y. Fujita, M. Fujiwara, K. Hara, K. Hatanaka, M. Itoh, Y. Kanada-Enyo, S. Kishi, K. Nakanishi, H. Sakaguchi, Y. Shimbara, A. Tamii, S. Terashima, M. Uchida, T. Wakasa, Y. Yasuda, H. P. Yoshida, M. Yosoi: "$2\alpha + t$ cluster structure in ^{11}B", Phys. Lett. B **646** (2007) 6–11.

34. H. Mardanpour, H. R. Amir-Ahmadi, A. Deltuva, K. Itoh, N. Kalantar-Nayestanaki, T. Kawabata, H. Kuboki, Y. Maeda, J. G. Messchendorp, S. Sakaguchi, H. Sakai, N. Sakamoto, Y. Sasamoto, M. Sasano, K. Sekiguchi, K. Suda, Y. Takahashi, T. Uesaka, H. Witala, K. Yako: "Precision measurement of vector and tensor analyzing powers in elastic deuteron-proton scattering", Eur. Phys. J. A **31** (2007) 383–391.

35. H. Kuboki, A. Tamii, K. Fujita, K. Hatanaka, M. Hatano, J. Kamiya, T. Kudoh, Y. Maeda, K. Sagara, T. Saito, H. Sakai, Y. Sakemi, M. Sasano, K. Sekiguchi, Y. Shimizu, S. Shimomoto, M. Shiota, Y. Tameshige, T. Uesaka, T. Wakasa, K. Yako: "Search for supernarrow dibaryons via the pd $\rightarrow$ ppX and pd $\rightarrow$ pdX reactions", Phys. Rev. C **74** (2006) 035203.

36. A. L. Cole, H. Akimune, S. M. Austin, D. Bazin, A. M. van den Berg, G. P. A. Berg, J. Brown, I. Daito, Y. Fujita, M. Fujiwara, S. Gupta, K. Hara, M. N. Harakeh, J. Jänecke, T. Kawabata, T. Nakamura, D. A. Roberts, B. M. Sherrill, M. Steiner, H. Ueno, R. G. T. Zegers: "Measurement of the Gamow-Teller strength distribution in ^{58}Co via the ^{58}Ni(t, ^{3}He) reaction at 115 MeV/nucleon", Phys. Rev. C **74** (2006) 034333.

37. B. K. Nayak, U. Garg, M. Hedden, M. Koss, T. Li, Y. Liu, P. V. Madhusudhana Rao, S. Zhu, M. Itoh, H. Sakaguchi, H. Takeda, M. Uchida, Y. Yasuda, M. Yosoi, H. Fujimura, M. Fujiwara, K. Hara, T. Kawabata, H. Akimune, M. N. Harakeh: ""Bi-modal" isoscalar giant dipole strength in ^{58}Ni", Phys. Lett. B **637** (2006) 43–47.

38. H. Sakai, T. Saito, T. Ikeda, K. Itoh, T. Kawabata, H. Kuboki, Y. Maeda, N. Matsui, C. Rangacharyulu, M. Sasano, Y. Satou, K. Sekiguchi, K. Suda, A. Tamii, T. Uesaka, K. Yako: "Spin Correlations of Strongly Interacting Massive Fermion Pairs as a Test of Bell's Inequality", Phys. Rev. Lett. **97** (2006) 150405.

39. T. Uesaka, V. P. Ladygin, L. S. Azhgirey, Yu. V. Gurchin, A. Yu. Isupov, K. Itoh, M. Janek, J.-T. Karachuk, T. Kawabata, A. N. Khrenov, A. S. Kiselev, V. Kizka, J. Kliman, V. A. Krasnov, A. N. Livanov, Y. Maeda, A. I. Malakhov, V. Matoucek, M. Morhac, S. Nedev, S. Rangelov, S. G. Reznikov, S. Sakaguchi, H. Sakai, Y. Sasamoto, K. Sekiguchi, K. Suda, I. Turzo, T. A. Vasiliev, T. Wakui: "Proposal on the measurements of d-p elastic scattering analyzing powers at 0.3–2.0 GeV at the Internal Target Station of the Nuclotron", Phys. Part. and Nucl. Lett. **3** (2006) 305-311.

40. V. P. Ladygin, T. Uesaka, T. Saito, M. Hatano, A. Yu. Isupov, H. Kato, N.B. Ladygina, Y. Maeda, A. I. Malakhov, J. Nishikawa, T. Ohnishi, S. G. Reznikov, H. Sakai, N. Sakamoto, S. Sakoda, Y. Satou, K. Sekiguchi, K. Suda, A. Tamii, N. Uchigashima, and K.Yako: "Tensor Analyzing Power T_{20} of the $dd \longrightarrow {}^3\mathrm{He}n$ and $dd \longrightarrow {}^3\mathrm{H}p$ Reactions at Zero Angle for Energies 140, 200, and 270 MeV", Phys. Atom. Nucl. **69** (2006) 1271–1278.

41. H. Kamada, S. Fujii, E. Uzu, M. Yamaguchi, R. Okamoto and Y. Koike: "Separability of a Low-Momentum Effective Nucleon-Nucleon Potential", Prog. Theor. Phys. **115** (2006) 839–844.

B. Proceedings

1. S. V. Green for the PHENIX Collaboration: "Highlights from the PHENIX experiment-Part1" Nucl. Phys. A 774 (2006) 93-102, Proceedings of The 18th International Conference on Ultra-Relativistic Nucleus-Nucleus Collisions, Budapest, Hungary, Aug., 4–9, 2005.

2. H. Busching for the PHENIX Collaboration: "Highlights from the PHENIX experiment-Part2" Nucl. Phys. A 774 (2006) 102-112, Proceedings of The 18th International Conference on Ultra-Relativistic Nucleus-Nucleus Collisions, Budapest, Hungary, Aug., 4–9, 2005.

3. Y. Akiba for the PHENIX Collaboration: "Probing the properties of dense partonic matter at RHIC" Nucl. Phys. A 774 (2006) 403-408, Proceedings of The 18th International Conference on Ultra-Relativistic Nucleus-Nucleus Collisions, Budapest, Hungary, Aug., 4–9, 2005.

4. M. Shimomura for the PHENIX Collaboration: "High p_T π^0, η identified and inclusive charged hadron spectra from PHENIX" Nucl. Phys. A 774 (2006) 457-460, Proceedings of The 18th International Conference on Ultra-Relativistic Nucleus-Nucleus Collisions, Budapest, Hungary, Aug., 4–9, 2005.

5. M. Konno for the PHENIX Collaboration: "Systematic Study of identified particle production in PHENIX" Nucl. Phys. A 774 (2006) 461-464, Proceedings of The 18th International Conference on Ultra-Relativistic Nucleus-Nucleus Collisions, Budapest, Hungary, Aug., 4–9, 2005.

6. D. Pal for the PHENIX Collaboration: "Nuclear Modification and elliptic flow measurement for ϕ mesons $\sqrt{s_{NN}}$ = 200 GeV d+Au and Au+Au collisions by PHENIX" Nucl. Phys. A 774 (2006) 489-492, Proceedings of The 18th International Conference on Ultra-Relativistic Nucleus-Nucleus Collisions, Budapest, Hungary, Aug., 4–9, 2005.

7. H. Masui for the PHENIX Collaboration: "Anisotropic flow in $\sqrt{s_{NN}}$ = 200 GeV Cu+Cu and Au+Au collisions at PHENIX" Nucl. Phys. A 774 (2006) 511-514, Proceedings of The 18th International Conference on Ultra-Relativistic Nucleus-Nucleus Collisions, Budapest, Hungary, Aug., 4–9, 2005.

8. D. Winter for the PHENIX Collaboration: "PHENIX measurement of particle yields at high p_T with respect to reaction plane in Au+Au collisions at $\sqrt{s_{NN}}$ = 200 GeV" Nucl. Phys. A 774 (2006) 545-548, Proceedings of The 18th International Conference on Ultra-Relativistic Nucleus-Nucleus Collisions, Budapest, Hungary, Aug., 4–9, 2005.

9. N. Grau for the PHENIX Collaboration: "Probing cold and hot dense nuclear medium via high p_T jets with di-hadron and γ-hadron correlations at PHENIX" Nucl. Phys. A 774 (2006) 565-568, Proceedings of The 18th International Conference on Ultra-Relativistic Nucleus-Nucleus Collisions, Budapest, Hungary, Aug., 4–9, 2005.

10. N. N. Ajitanand for the PHENIX Collaboration: "Two and three particle flavor dependent correlations" Nucl. Phys. A 774 (2006) 585-588, Proceedings of The 18th International Conference on Ultra-Relativistic Nucleus-Nucleus Collisions, Budapest, Hungary, Aug., 4–9, 2005.

11. P. Chung for the PHENIX Collaboration: "Evidence for a long range structure in the pion emission source in Au+Au collisions at RHIC" Nucl. Phys. A 774 (2006) 607-610, Proceedings of The 18th International Conference on Ultra-Relativistic Nucleus-Nucleus Collisions, Budapest, Hungary, Aug., 4–9, 2005.

12. M. Csanad for the PHENIX Collaboration: "Measurement and analysis of two and three particle correlations" Nucl. Phys. A 774 (2006) 611-614, Proceedings of The 18th International Conference on Ultra-Relativistic Nucleus-Nucleus Collisions, Budapest, Hungary, Aug., 4–9, 2005.

13. S. A. Butsyk for the PHENIX Collaboration: "PHENIX results on open heavy flavor production and flow in Au+Au collisions at $\sqrt{s_{NN}}$ = 200 GeV" Nucl. Phys. A 774 (2006) 669-672, Proceedings of The 18th International Conference on Ultra-Relativistic Nucleus-Nucleus Collisions, Budapest, Hungary, Aug., 4–9, 2005.

14. X. Wei for the PHENIX Collaboration: "Study of J/ψ production in $\sqrt{s_{NN}}$ = 200 GeV $p+p$ and d+Au collisions in PHENIX" Nucl. Phys. A 774 (2006) 693-696, Proceedings of The 18th International Conference on Ultra-Relativistic Nucleus-Nucleus Collisions, Budapest, Hungary, Aug., 4–9, 2005.

15. Y. Kwon for the PHENIX Collaboration: "Heavy flavor production in $p+p$ and d+Au collisions at $\sqrt{s_{NN}}$ = 200 GeV from single leptons over a wide kinematic range" Nucl. Phys. A 774 (2006) 705-708, Proceedings of The 18th International Conference on Ultra-Relativistic Nucleus-Nucleus Collisions, Budapest, Hungary, Aug., 4–9, 2005.

16. A. Toia for the PHENIX Collaboration: "Measurement of low mass dielectron continuum in $\sqrt{s_{NN}}$ = 200 GeV Au-Au collisions with PHENIX experiment at RHIC" Nucl. Phys. A 774 (2006) 743-746, Proceedings of The 18th International Conference on Ultra-Relativistic Nucleus-Nucleus Collisions, Budapest, Hungary, Aug., 4–9, 2005.

17. H. Pereira for the PHENIX Collaboration: "PHENIX results on J/ψ production in Au+Au and Cu+Cu collisions at $\sqrt{s_{NN}}$ = 200 GeV" Nucl. Phys. A 774 (2006) 747-750, Proceedings of The 18th International Conference on Ultra-Relativistic Nucleus-Nucleus Collisions, Budapest, Hungary, Aug., 4–9, 2005.

18. I. Ravinovich, H. Hamagaki, S. Oda, K. Ozawa *et al*, "A hadron blind detector for the PHENIX experiment at RHIC" Nucl. Phys. A 774 (2006) 903-906, Proceedings of The 18th International Conference on Ultra-Relativistic Nucleus-Nucleus Collisions, Budapest, Hungary, Aug., 4–9, 2005.

19. F. Kajihara for the PHENIX Collaboration: "Heavy Quark Measurement by Single Electrons in the PHENIX Experiment", J. Phys. G: Nucl. Part. Phys. - G/242500/SPE, Proc. of The 19th International Conference on Ultra-Relativistic Nucleus-Nucleus Collisions, Shanghai, China, Nov., 14–20, 2006.

20. T. Horaguchi (PHENIX Collaboration): "The measurement of the polarized gluon distribution function at PHENIX" AIP Conf. Proc. **870**, 651 (2006).

21. T. Isobe, for the PHENIX Collaboration: "Direct photon production in Au+Au collisions at RHIC-PHENIX", Proc. of the Hard Probes 2006, Jun. 9–16, 2006, Asilomar CA USA, Nucl. Phys. A **783** (2007) 569c–572c.

22. T. Isobe, for the PHENIX Collaboration: "Measurement of neutral mesons in $\sqrt{s_{NN}}$=200GeV Au+Au and Cu+Cu collisions at RHIC-PHENIX", Proc. of 17th Particles and Nuclei International Conference (PANIC05), Oct. 24–28, 2005, Santa Fe NM USA, AIP Conference Proceedings **842** (2006) 56–58.

23. T. Gunji, for the PHENIX Collaboration: "Measurements of J/ψ yield at forward-rapidity and mid-rapidity in Au + Au collisions $\sqrt{s_{NN}}$ = 200-GeV by PHENIX at RHIC" Proc. of 17th Particles and Nuclei International Conference (PANIC05), Oct. 24–28, 2005, Santa Fe NM USA, AIP Conference Proceedings **842** (2006) 44–46.

24. T. Isobe, for the PHENIX Collaboration: "Measurement of neutral pions in $\sqrt{s_{NN}}$ = 200 GeV and 62.4 GeV Au+Au collisions at RHIC-PHENIX", Proc. of the 18th International Conference on Ultra-Relativistic Nucleus-Nucleus Collisions (QM2005), Aug. 04–09, 2005, Budapest, Hungary, Acta. Phys. Hung. A **27** (2006) 227–230.

25. A. Saito, H. Sakai, S. Shimoura, T. Uesaka, T. Kawabata, K. Nakanishi, Y. Sasamoto, E. Ideguchi, H. Yamaguchi, S. Kubono, G. P. Berg, T. Ichihara and T. Kubo: " SHARAQ project ", Proc. of Tours Symposium on Nuclear Physics, Tours, France, Sept. 5-8 (2006) AIP Conf. Proc. 891 (2007) 131-137.

26. A. Saito, S. Shimoura, T. Minemura, Y. U. Matsuyama, H. Baba, N. Aoi, T. Gomi, H. Higurashi, K. Ieki, N. Imai N. Iwasa, H. Iwasaki, S. Kanno, S. Kubono, M. Kunibu, S. Michimasa, T. Motobayashi, T. Nakamura, H. Ryuto, H. Sakurai, M. Serata, E. Takeshita, S. Takeuchi, T. Teranishi, K. Ue, K. Yamada and Y. Yanagisawa: " Exotic cluster states in ^{11}Be via α-inelastic scattering", Proc. of Tours Symposium on Nuclear Physics, Tours, France, Sept. 5-8, 2006, AIP Conf. Proc. 891 (2007) 205-213.

27. S. Kubono, H. Yamaguchi, Y. Wakabayashi, G. Amadio, S. Hayakawa, J.J. He, A. Saito, T. Teranishi, S. Nishimura, N. Fukunishi, N. Iwasa, K. Inafuku, S. Kato, M.H. Tanaka, Y. Fuchi, J.Y. Moon, K. Kwon, C.S. Lee, L.H. Khiem, A. Chen, and J. Pearson: " Experimental Study of Stellar Reactions at CNS", Proc. of the 6th Chine-Japan Joint Nuclear Physics Symposium, Shanghai, May 16-20, 2006, AIP Conf. Proc. 865 (2006) 200-207.

28. S. Shimoura: "In-beam spectroscopy of exotic nuclei probed by α-induced direct reactions", Proc. Int. Symposium on Structure of Exotic Nuclei and Nuclear Forces, eds. M. Honma, T. Otsuka and N. Aoi, J. Phys. Conf. Ser. **49** (2006) 155–160

29. Y. Satou, T. Nakamura, N. Fukuda, T. Sugimoto, Y. Kondo, N. Matsui, Y. Hashimoto, T. Nakabayashi, T. Okumura, M. Shinohara, T. Motobayashi, Y. Yanagisawa, N. Aoi, S. Takeuchi, T. Gomi, Y. Togano, S. Kawai, H. Sakurai, H.J. Ong, T.K. Onishi, S. Shimoura, M. Tamaki, T. Kobayashi, H. Otsu, Y. Matsuda, N. Endo, M. Kitayama, M. Ishihara: "(p, p') and (p, n) reactions on halo nuclei", Proc. Int. Symposium on Structure of Exotic Nuclei and Nuclear Forces, eds. M. Honma, T. Otsuka and N. Aoi, J. Phys. Conf. Ser. **49** (2006) 27–28

30. Zs. Dombrádi, Z. Elekes, A. Saito, N. Aoi, H. Baba, K. Demichi, Zs. Fülöp, J. Gibelin, T. Gomi, H. Hasegawa, N. Imai, M. Ishihara, H. Iwasaki, S. Kanno, S. Kawai, T. Kishida, T. Kubo, K. Kurita, Y. Matsuyama, S. Michimasa, T. Minemura, T. Motobayashi, M. Notani, H.J. Ong, S. Ota, A. Ozawa, H.K. Sakai, H. Sakurai, S. Shimoura, E. Takeshita, S. Takeuchi, M. Tamaki, Y. Togano, K. Yamada, Y. Yanagisawa, K. Yoneda: "Evolution of the N = 20 shell gap", Proc. Int. Symposium on Structure of Exotic Nuclei and Nuclear Forces, eds. M. Honma, T. Otsuka and N. Aoi, J. Phys. Conf. Ser. **49** (2006) 140–145

31. H.J. Ong, N. Imai, N. Aoi, H. Sakurai, Zs. Dombrádi, A. Saito, Z. Elekes, H. Baba, K. Demichi, Zs. Fülöp, J. Gibelin, T. Gomi, H. Hasegawa, M. Ishihara, H. Iwasaki, S. Kanno, S. Kawai, T. Kubo, K. Kurita, Y.U. Matsuyama, S. Michimasa, T. Minemura, T. Motobayashi, M. Notani, S. Ota, H.K. Sakai, S. Shimoura, E. Takeshita, S. Takeuchi, M. Tamaki, Y. Togano, K. Yamada, Y. Yanagisawa, K. Yoneda: "Inelastic proton scattering on ^{16}C", Proc. Int. Symposium on Structure of Exotic Nuclei and Nuclear Forces, eds. M. Honma, T. Otsuka and N. Aoi, J. Phys. Conf. Ser. **49** (2006) 13–14

32. S. Takeuchi, N. Aoi, H. Baba, T. Fukui, Y. Hashimoto, K. Ieki, N. Imai, H. Iwasaki, S. Kanno, Y. Kondo, T. Kubo, K. Kurita, T. Minemura, T. Motobayashi, T. Nakabayashi, T. Nakamura, T. Okumura, T.K. Onishi, S. Ota, H. Sakurai, S. Shimoura, R. Sugou, D. Suzuki, H. Suzuki, M.K. Suzuki, E. Takeshita, M. Tamaki, K. Tanaka, Y. Togano, K. Yamada: "Proton inelastic scattering on ^{32}Mg", Proc. Int. Symposium on Structure of Exotic Nuclei and Nuclear Forces, eds. M. Honma, T. Otsuka and N. Aoi, J. Phys. Conf. Ser. **49** (2006) 153–154

33. T. Sugimoto, T. Nakamura, N. Fukuda, M. Miura, Y. Kondo, N. Aoi, H. Baba, D. Bazin, T. Gomi, H. Hasegawa, Y. Hashimoto, N. Imai, T. Kobayashi, T. Kubo, T. Motobayashi, M. Ohara, A. Saito, H. Sakurai, S. Shimoura, A.M. Vinodkumar, K. Watanabe, Y.X. Watanabe, T. Yakushiji, Y. Yanagisawa, K. Yoneda, M. Ishihara: "Invariant-mass spectroscopy of the neutron-drip line nucleus ^{14}Be", Proc. Int. Symposium on Structure of Exotic Nuclei and Nuclear Forces, eds. M. Honma, T. Otsuka and N. Aoi, J. Phys. Conf. Ser. **49** (2006) 43–44

34. S. Michimasa, S. Shimoura, H. Iwasaki, M. Tamaki, S. Ota, N. Aoi, H. Baba, N. Iwasa, S. Kanno, S. Kubono, K. Kurita, M. Kurokawa, T. Minemura, T. Motobayashi, M. Notani, H.J. Ong, A. Saito, H. Sakurai, E. Takeshita, S. Takeuchi, Y. Yanagisawa, A. Yoshida: "Single-particle States in ^{23}F", Proc. Int. Symposium on Structure of Exotic Nuclei and Nuclear Forces, eds. M. Honma, T. Otsuka and N. Aoi, J. Phys. Conf. Ser. **49** (2006) 196–197

35. H. Iwasaki, M. Tamaki, S. Michimasa, M. Niikura, S. Shimoura, N. Aoi, S. Takeuchi, S. Ota, T.K. Onishi, E. Takeshita, H.J. Ong, H. Baba, Z. Elekes, T. Fukuchi, Y. Ichikawa, M. Ishihara, N. Iwasa, S. Kanno, R. Kanungo, S. Kawai, T. Kubo, K. Kurita, A. Saito, Y. Satou, H. Suzuki, M.K. Suzuki, Y. Togano, Y. Yanagisawa, H. Sakurai, T. Motobayashi: "Spectroscopy on neutron-rich nuclei near $N = 50$ via two-step Coulomb excitation at intermediate energies", Proc. Int. Symposium on Structure of Exotic Nuclei and Nuclear Forces, eds. M. Honma, T. Otsuka and N. Aoi, J. Phys. Conf. Ser. **49** (2006) 65–66

36. Z. Elekes, Zs. Dombrádi, A. Saito, N. Aoi, H. Baba, K. Demichi, Zs. Fülöp, J. Gibelin, T. Gomi, H. Hasegawa, N. Imai, M. Ishihara, H. Iwasaki, S. Kanno, S. Kawai, T. Kishida, T. Kubo, K. Kurita, Y. Matsuyama, S. Michimasa, T. Minemura, T. Motobayashi, M. Notani, T.K. Ohnishi, H.J. Ong, S. Ota, A. Ozawa, H.K. Sakai, H. Sakurai, S. Shimoura, E. Takeshita, S. Takeuchi, M. Tamaki, Y. Togano, K. Yamada, Y. Yanagisawa, K. Yoneda: "Bound excited states in ^{27}F", Proc. 12th Int. Symposium on Capture Gamma-Ray Spectroscopy and Related Topics, eds. A. Woehr and A. Aprahamian, AIP Conf. Proc. **819** (2006) 383–385

37. Y. Togano, T. Gomi, T. Motobayashi, Y. Ando, N. Aoi, H. Baba, K. Demichi, Z. Elekes, N. Fukuda, Zs. Fülöp, U. Futakami, H. Hasegawa, Y. Higurashi, K. Ieki, N. Imai, M. Ishihara, K. Ishikawa, N. Iwasa, H. Iwasaki, S. Kanno, Y. Kondo, T. Kubo, S. Kubono, M. Kunibu, K. Kurita, Y.U. Matsuyama, S. Michimasa, T. Minemura, M. Miura, H. Murakami, T. Nakamura, M. Notani, S. Ota, A. Saito, M. Serata, S. Shimoura, T. Sugimoto, E. Takeshita, S. Takeuchi, K. Ue, K. Yamada, Y. Yanagisawa, K. Yoneda, A. Yoshida: "Coulomb Dissociation of

^{27}P for Study of ^{26}Si(p,γ)^{27}P Reaction", Proc. Int. Symposium on Origin of Matter and Evolution of Galaxies (OMEG2005), eds. S. Kubono, W. Aoki, T. Kajino, T. Motobayashi, K. Nomoto AIP Conf. Proc. **847** (2006) 281–286

38. S. Shimoura: "Nuclear Spectroscopy Using Direct Reactions of RI Beams", Proc. 6th China-Japan Joint Symposium on Nuclear Physics Trends, eds. Y-G Ma and A. Ozawa, AIP Conf. Proc. **865** (2006) 34–41

39. E. Ideguchi: "Study of High-spin States by Using Stable and Unstable Nuclear Beams", Proc. 6th China-Japan Joint Symposium on Nuclear Physics Trends, eds. Y-G Ma and A. Ozawa, AIP Conf. Proc. **865** (2006) 125–130

40. Z. Elekes, Zs. Dombrádi, A. Saito, N. Aoi, H. Baba, K. Demichi, Zs. Fülöp, J. Gibelin, T. Gomi, H. Hasegawa, N. Imai, M. Ishihara, H. Iwasaki, S. Kanno, S. Kawai, T. Kishida, T. Kubo, K. Kurita, Y. Matsuyama, S. Michimasa, T. Minemura, T. Motobayashi, M. Notani, T. Ohnishi, H.J. Ong, S. Ota, A. Ozawa, H.K. Sakai, H. Sakurai, S. Shimoura, E. Takeshita, S. Takeuchi, M. Tamaki, Y. Togano, K. Yamada, Y. Yanagisawa, K. Yoneda: "Study of exotic nuclei around the "island of inversion" " Proc. Tours Symposium on Nuclear Physics VI (TOURS2006), AIP Conf. Proc. **891** (2007) 122–130

41. Y. Togano, T. Gomi, T. Motobayashi, Y. Ando, N. Aoi, H. Baba, K. Demichi, Z. Elekes, N. Fukuda, Zs. Fülöp, U. Futakami, H. Hasegawa, Y. Higurashi, K. Ieki, N. Imai, M. Ishihara, K. Ishikawa, N. Iwasa, H. Iwasaki, S. Kanno, Y. Kondo, T. Kubo, S. Kubono, M. Kunibu, K. Kurita, Y. U. Matsuyama, S. Michimasa, T. Minemura, M. Miura, H. Murakami, T. Nakamura, M. Notani, S. Ota, A. Saito, H. Sakurai, M. Serata, S. Shimoura, T. Sugimoto, E. Takeshita, S. Takeuchi, K. Ue, K. Yamada, Y. Yanagisawa, K. Yoneda, and A. Yoshida: "Study of the ^{26}Si(p,γ)^{27}P reaction through Coulomb dissociation of ^{27}P", Eur. Phys. J. A **27**, Supplement 1 (2006) 233.

42. H. Yamaguchi, A. Saito, J.J. He, Y. Wakabayashi, G. Amadio, H. Fujikawa, S. Kubono, L.H. Khiem, Y.K. Kwon, M. Niikura, T. Teranishi, S. Nishimura, Y. Togano, N. Iwasa and K. Inafuku: "Proton resonance scattering of 7Be", Proc. of Int. Conf. on Origin of Matter and Evolution of Galaxies (OMEG05), AIP conference proceeding **847** (2006) 275-280.

43. Y. Sasamoto, T. Kawabata, T. Uesaka, K. Suda, Y. Maeda, S. Sakaguchi, K. Itoh, K. Hatanaka, M. Fujiwara, A. Tamii, Y. Shimizu, K. Nakanishi, K. Kawase, H. Hashimoto, Y. Tameshige, H. Matsubara, M. Itoh, H. P. Yoshida, M. Uchida: "Cluster states in ^{13}C", Proc. of the RCNP Osaka Spring Workshop on Cluster Condensation and Nucleon Correlation in Nuclei, Apr. 26–28, 2006, Research Center for Nuclear Physics, Osaka, Japan, Mod. Phys. Lett. A **21** (2006) 2393–2401.

44. T. Kawabata, H. Akimune, H. Fujita, M. Fujiwara, K. Hara, K. Hatanaka, K. Nakanishi, Y. Shimbara, A. Tamii, H. P. Yoshida, M. Yosoi, Y. Fujita, M. Itoh, Y. Kanada-Enyo, S. Kishi, H. Sakaguchi, S. Terashima, Y. Yasuda, M. Uchida, T. Wakasa: "$2\alpha + t$ cluster state in ^{11}B", Proc. of the RCNP Osaka Spring Workshop on Cluster Condensation and Nucleon Correlation in Nuclei, Apr. 26–28, 2006, Research Center for Nuclear Physics, Osaka, Japan, Mod. Phys. Lett. A **21** (2006) 2383–2392.

45. A. Tamii, T. Adachi, K. Fujita, K. Hatanaka, H. Hashimoto, M. Itoh, H. Matsubara, K. Nakanishi, Y. Sakemi, Y. Shimbara, Y. Shimizu, Y. Tameshige, M. Yosoi, Y. Fujita, H. Sakaguchi, J. Zenihiro, T. Kawabata, Y. Sasamoto, M. Dozono, J. Carter, H. Fujita, B. Rubio, A. Perez: "^{12}C(p,p') scattering measurement at forward angles", Proc. of the RCNP Osaka Spring Workshop on Cluster Condensation and Nucleon Correlation in Nuclei, Apr. 26–28, 2006, Research Center for Nuclear Physics, Osaka, Japan, Mod. Phys. Lett. A **21** (2006) 2367–2371.

46. T. Kawabata, H. Akimune, H. Fujita, Y. Fujita, M. Fujiwara, K. Hara, K. Hatanaka, M. Itoh, Y. Kanada-Enyo, S. Kishi, K. Nakanishi, H. Sakaguchi, Y. Shimbara, A. Tamii, S. Terashima, M. Uchida, T. Wakasa, Y. Yasuda, H. P. Yoshida, M. Yosoi: "$2\alpha + t$ cluster state in ^{11}B", Proc. of International Symposium on Structure of Exotic Nuclei and Nuclear Forces (SENUF06), March 9–12, University of Tokyo, Tokyo, Japan, J. Phys. Conf. Ser. **49** (2006) 210–211.

47. T. Uesaka: "Experimental studies of spin-dependent interactions in unstable nuclei with polarized proton target", Proc. of International Symposium on Structure of Exotic Nuclei and Nuclear Forces (SENUF06), March 9–12, University of Tokyo, Tokyo, Japan, J. Phys. Conf. Ser. **49** (2006) 172–172.

48. S. Fujii, T. Mizusaki, T. Otsuka, T. Sebe and A. Arima: "Shell-model description of ^{16}C with the Idaho N^{3}LO NN potential", Proc. of the International Symposium on Structure of Exotic Nuclei and Nuclear Forces (SENUF06), Mar. 9–12, 2006, Tokyo, Japan, Journal of Physics: Conference Series **49** (2006) 7–12.

C. Theses

1. S. Michimasa: "Proton Shell Structure in Neutron-rich Nucleus ^{23}F", Doctor Thesis, University of Tokyo, December (2006)
2. F. Kajihara: "Measurement of Single Electrons from Semi-Leptonic Decay of Heavy Quarks in Au + Au Collisions at 200 A GeV", PhD. Thesis, the University of Tokyo, March 2007.
3. T. Gunji "J/ψ Production in High Energy Heavy Ion Collisions at RHIC" PhD. Thesis, the University of Tokyo, March 2007.
4. Y.L. Yamaguchi: "Research and Development of Gas Electron Multiplier (GEM) with a dry etching technique" Master Thesis, University of Tokyo, March 2007.
5. Y. Aramaki: "Development of a Gas Cherenkov Counter Using Gas Electron Multipliers (GEMs)" Master Thesis, University of Tokyo, March 2007.
6. S. Saito "" Master Thesis, University of Tokyo, March (2007).
7. G. Amadio: "Study of the Resonant Scattering of ^{7}Be+p", Master Thesis, University of Tokyo, March (2007).

Talks and Presentations

A. Conferences

1. A. Saito, H. Sakai, S. Shimoura, T. Uesaka, T. Kawabata, K. Nakanishi, Y. Sasamoto, E. Ideguchi, H. Yamaguchi, S. Kubono, G. P. Berg, T. Ichihara and T. Kubo (Oral): "SHARAQ project", Tours Symposium on Nuclear Physics VI (TOURS2006), Sep. 5–8, 2006, Tours, France.

2. A. Saito, S. Shimoura, T. Minemura, Y. U. Matsuyama, H. Baba, N. Aoi, T. Gomi, Y. Higurashi, K. Ieki, N. Imai, N. Iwasa, H. Iwasaki, S. Kanno, S. Kubono, M. Kunibu, S. Michimasa, T. Motobayashi, T. Nakamura, H. Ryuto, H. Sakurai, M. Serata, E. Takeshita, S. Takeuchi, T. Teranishi, K. Ue, K. Yamada and Y. Yanagisawa (Oral): "Exotic cluster states in ^{12}Be via α-inelastic scattering", Tours Symposium on Nuclear Physics VI (TOURS2006), Sep. 5–8, 2006, Tours, France.

3. A. Saito (Oral): "Exotic cluster states in ^{12}Be via α-inelastic scattering", 2nd German-Japanese Workshop on Nuclear Structure and Astrophysics, Oct. 4–7, 2006, RIKEN, Japan.

4. A. Saito (Oral): "Study of cluster structures in ^{12}Be via α-inelastic scattering", RCNP workshop on Clustering phenomena in nuclear many-body systems, Feb. 14–16, 2007, RCNP, Osaka University, Japan.

5. S. Kubono (Invited): " Experimental Approach to Stellar Reactions with RI Beams - Overview of Exper iments on the Neutron-Deficient Side -", The IX International Conference on Nucleus Nucleus Collisions, August 28 - Septe mber 1, 2006, Rio de Janeiro.

6. S. Kubono (Invited): " Experimental Study of Stellar Reactions at CNS", The 6th Chine-Japan Joint Nuclear Physics Symposium, May 16-20, 2006, Shanghai.

7. S. Kubono (Invited): " Nuclear Astrophysics Study at CRIB", The 2nd German-Japanese Workshop on Nuclear Structure and Astrophysics, Oct. 4-6 , 2006, Wako, Japan.

8. S. Kubono (Invited): " Experimental Study of Nuclear Reactions in the pp-Chain", The International Symposium on Neutrino Processes and Stellar Evolution, Februar y 7-9, 2007, Tokyo.

9. S. Kubono (Invited): " CRIB Status and Progress", The Workshop of Slow and Stopped RI Beam Workshop, Nov. 13-15, 2006, Osaka.

10. S. Kubono (Invited): " Nuclear Reaction Study for Astrophysics", The Workshop on Nuclear Data and the Analysis, Nov. 24, 2006, Tsukuba.

11. S. Kubono (Invited): " Atomic Clusters in Nuclear Astrophysics", The Workshop on Clustering Phenomena in Many-Body Nucleon System, Feb. 14-16, 2007, Osaka.

12. S. Kubono (Invited): " Nuclear Astrophysics at RIBF", The workshop on Evolution of the Early Universe and the Nucleosynthesis, Feb. 22-23, 2007, Sapporo.

13. H. Yamaguchi, S. Kubono, Y. Wakabayashi, G. Amadio, and S. Hayakawa (Oral): "High-intensity target for low-energy RI-beam production at CNS CRIB", Second expert meeting on critical issues of next-generation high-intensity fragment separators, May 10–13, 2006, RIKEN, Tokyo, Japan.

14. H. Yamaguchi, A. Saito, J.J. He, Y. Wakabayashi, G. Amadio, H. Fujikawa, S. Kubono, L.H. Khiem, Y.K. Kwon, M. Niikura, T. Teranishi, S. Nishimura, Y. Togano, N. Iwasa and K. Inafuku (Oral): "Proton resonance scattering on ^{7}Be", Nuclei in the Cosmos - IX (NIC-IX) Jun. 25–30 2006, CERN, Geneva, Switzerland.

15. H. Yamaguchi, A. Saito, J.J. He, Y. Wakabayashi, G. Amadio, H. Fujikawa, S. Kubono, L.H. Khiem, Y.K. Kwon, M. Niikura, T. Teranishi, S. Nishimura, Y. Togano, N. Iwasa and K. Inafuku (Oral): "Proton resonance scattering of ^{7}Be", 21st Century COE International Symposium on Neutrino Processes and Stellar Evolution (NEPSE07), February 7–9, 2007, University of Tokyo, Tokyo, Japan

16. S. Shimoura (invited): "Nuclear Spectroscopy Using Direct Reactions of RI Beams", 6th China-Japan Joint Nuclear Physics Symposium on Nuclear Physics Trends, May 16–20, 2006, Shanghai, China

17. E. Ideguchi (invited): "Study of High-spin States by Using Stable and Unstable Nuclear Beams", 6th China-Japan Joint Nuclear Physics Symposium on Nuclear Physics Trends, May 16–20, 2006, Shanghai, China

18. S. Shimoura (invited): "High resolution magnetic spectrometer SHARAQ in RIBF", International Symposium on Exotic Nuclei (EXON2006), July 17–22, 2006, Khanty-Mansiysk, Russia

19. S. Michimasa, S. Shimoura, H. Iwasaki, M. Tamaki, S. Ota, N. Aoi, H. Baba, N. Iwasa, S. Kanno, S. Kubono, K. Kurita, M. Kurokawa, T. Minemura, T. Motobayashi, M. Notani, H.J. Ong, A. Saito, H. Sakurai, E. Takeshita, S. Takeuchi, Y. Yanagisawa and A. Yoshida (Oral): "Proton Shell Structure in Neutron-rich ^{23}F", IX International Conference on Nucleus-Nucleus Collisions (NN2006), August 28–Sep. 1, 2006, Rio de Janeiro, Brazil

20. S. Shimoura (invited): "Spectroscopy of exotic nuclei using direct reactions of RI beams at RIPS", 1st RIBF Annual Users Meeting, August 3–4, 2006, RIKEN, Saitama, Japan

21. S. Shimoura (invited): "High resolution spectroscopy using RI beams – SHARAQ project", 2nd German-Japanese Workshop on Nuclear Structure and Astrophysics, October 4–7, 2006, RIKEN, Saitama, Japan

22. S. Shimoura (invited): "Physics programs at SHARAQ", International Collaboration Workshop on Experiments at the RIBF (RIBF-ICW06), November 6–9, 2006, RIKEN, Saitama, Japan

23. S. Shimoura (invited): "Determination of weak matrix elements from charge exchange reactions of unstab le nuclei", 21th Century COE International Symposium on Neutrino Processes and Steller Evolu tion (NEPSE07), February 7–9, 2007, University of Tokyo, Tokyo, Japan

24. S. Shimoura (invited): "High Resolution Spectrometer SHARAQ at the RIBF", Japanese-French Workshop on Exotic Femto Systems, March 13–16, 2007, Caen, France

25. S. Michimasa (oral): "Study of Excited States in ^{23}F Using Direct Reactions", Japanese French Workshop on Exotic Femto Systems, Mar. 13–16, 2007, Caen, France

26. E. Ideguchi: "Isomer measurement by recycle use of ejectiles", RIBF Mini Workshop on Gamma-ray spectroscopy at RIBF III, February 6, 2007, RIKEN, Saitama, Japan

27. E. Ideguchi: "Gamma-ray spectroscopy with slowed down RI beam", RIBF Mini Workshop on Gamma-ray spectroscopy at RIBF II, October 16–17, 2006, RIKEN, Saitama, Japan

28. S. Shimoura: "CNS-GRAPE collaboration for high-resolution gamma-ray spectroscopy at RIBF", RIBF Mini Workshop on Gamma-ray spectroscopy at RIBF II, October 16–17, 2006, RIKEN, Saitama, Japan

29. S. Shimoura (oral): "Molecular resonance states in unstable nuclei", RCNP workshop on Clustering Phenomena in Nuclear Many-Body Systems, February 14–16, 2007, RCNP, Osaka, Japan

30. S. Ota (oral): "Proton Intruder State in ^{13}B", RCNP workshop on Clustering Phenomena in Nuclear Many-Body Systems, February 14–16, 2007, RCNP, Osaka, Japan

31. E. Ideguchi: "Study of Superdeformed States in A$\sim$40 region and Future Perspectives" RCNP workshop on Clustering Phenomena in Nuclear Many-Body Systems, February 14–16, 2007, RCNP, Osaka, Japan

32. S. Shimoura (oral): "Physics Programs in the SHARAQ project", RCNP workshop on New studies developen in upgrade of RCNP AVF Cyclotron, February 19–20, 2007, RCNP, Osaka, Japan

33. E. Ideguchi (oral): "Study of High-Spin Deformed States in A=30–40 and 100", RCNP workshop on New studies developen in upgrade of RCNP AVF Cyclotron, February 19–20, 2007, RCNP, Osaka, Japan

34. E. Ideguchi: "Study of High-Spin States in A$\sim$40 Region", JAEA workshop on Nuclear Structure and Nuclear Data by Gamma-ray Spectroscopy, JAEA, Ibaraki, Japan, March 13, 2007

35. H. Hamagaki: "Electromagnetic Measurements at RHIC", the 1st Asian Triangle Heavy Ion Conference (ATHIC 2006), June 29 – July 1, 2006, Yonsei University, Seoul, Republic of Korea.

36. H. Hamagaki: "GEM R&D Efforts at CNS", the Workshop on the Current Status and Outlook of the Tracking Detectors using GEM (in Japanese), March 23, 2007, RIKEN, Wako-shi, Saitama, Japan

37. T. Gunji "J/psi Production in Au+Au and Cu+Cu Collisions at RHIC" Workshop on "Strong Coupled Quark-Gluon-Plasma : SPS, RHIC and LHC", Feb. 16–17, 2007, Nagoya University, Nagoya, Japan

38. T. Gunji "J/psi Production in Heavy Ion Collisions at RHIC" Workshop on "Relativistic Heavy Ion Physics" Feb. 10–11, 2007, Matsumoto Univ. Nagano, Japan

39. T. Gunji for the PHENIX Collaboration (oral): "Centrality dependence of J/psi production in Au+Au and Cu+Cu Collisions by th e PHENIX Experiment at RHIC ", The 19th International Conference on Ultra-Relativistic Nucleus-Nucleus Collisio ns, Nov. 14–20, 2006, Shanghai Science Hall, Shanghai, China.

40. T. Gunji "J/psi Measurement in Heavy Ion Collisions at RHIC" Workshop on "Frontiers in the physics of quark-gluon-plasma", July 17-18, RIKEN, Saitama, Japan

41. T. Gunji for the PHENIX Collaboration "PHENIX Charomonium Measurement" June 6–8, RHIC AGS Annual Users' Meeting, Brookhaven National Laboratory, Ner Y owrk, USA

42. F. Kajihara (Invited): "Heavy Quark Measurement by Single Electrons in the PHENIX Experiment", The 19th International Conference on Ultra-Relativistic Nucleus-Nucleus Collisions, Shanghai, China, Nov., 14–20, 2006

43. T. Isobe for the PHENIX collaboration (Invited): "Systematic Study of High-p_T Direct Photon Production with the PHENIX Experiment at RHIC", The 19th International Conference On Ultra relativistic Nucleus-Nucleus Collisions (Quark Matter 2006), Nov. 14–20, 2006, Shanghai, China.

44. T. Isobe for the PHENIX collaboration (Poster): "Measurement of Direct Photons with the EMCal in $\sqrt{s_{\rm NN}}$ = 200 GeV Au+Au Collisions at RHIC-PHENIX", The 19th International Conference On Ultra relativistic Nucleus-Nucleus Collisions (Quark Matter 2006), Nov. 14–20, 2006, Shanghai, China.

45. T. Isobe for the PHENIX collaboration (Oral): "Direct photon production in Au+Au collisions at RHIC-PHENIX", Hard Probes 2006, Jun. 9–16, 2006, Asilomar CA, USA.

46. T. Isobe for the PHENIX collaboration (Poster): "Neutral pion measurement in $\sqrt{s_{\rm NN}}$ = 200 GeV Au+Au collisions at RHIC-PHENIX", 2006 RHIC-AGS Annual Users meeting, Jun. 5–9, 2006, Brookhaven Nat. Lab. NY, USA.

47. S.X. Oda for the PHENIX Collaboration (poster): "Measurement of J/psi mesons via di-electrons in Cu+Cu collisions at RHIC-PHENIX", The 19th International Conference on Ultra-Relativistic Nucleus-Nucleus Collisions, Nov. 14–20, 2006, Shanghai Science Hall, Shanghai, China.

48. S.X. Oda (oral): "Development of GEM and detectors using GEM at the PHENIX experiment and CNS, University of Tokyo", First workshop of JSPS Creative Research Project 'Research and development of a novel detector system for the international linear collider', Dec. 20–22, 2006, High Energy Accelerator Research Organization, Ibaraki, Japan.

49. Y. Morino for the PHENIX collaboration (Poster): "A search for condensed double anti-K bound state at PHENIX", Quark Matter 2006, Nov. 14–20, 2006. Shanghai, Chana.

50. Y.L. Yamaguchi (Oral): "Measurement of basic properties of GEM at CNS, Univ. of Tokyo", at the Micro Pattern Gas Detector Workshop, Jan. 26, 2007, Saga University, Saga, Japan.

51. T. Horaguchi for the PHENIX Collaboration (Oral): "The Measurement of the Polarized Gluon Distribution Function at PHENIX", Conference on the International of Particle and Nuclear Physics, May 30–Jun. 3, 2006, Westin Rio Mar Beach, Puerto Rico

52. T. Horaguchi for the PHENIX Collaboration (Oral): "Measurement of the direct photon production in polarized proton-proton collisions at $\sqrt{s} = 200$ GeV with PHENIX", The 17th International Spin Physics Symposium, Oct. 2–7, 2006, Kyoto, Japan.

53. S. Fujii (Invited): "Microscopic approaches to exotic nuclei with the bare nuclear force", Opening Ceremony of Japan-US Theory Institute for Physics with Exotic Nuclei (JUSTIPEN), Jul. 11, 2006, RIKEN, Wako, Japan.

54. S. Fujii, T. Mizusaki, T. Otsuka, T. Sebe and A. Arima (Oral): "A new microscopic shell-model approach to neutron-rich carbon isotopes", International Conference on Nuclear Structure '06 (NS06), Jul. 24–28, 2006, ORNL, Knoxville, USA.

55. S. Fujii, T. Mizusaki, T. Otsuka, T. Sebe and A. Arima (Oral): "Structure of ^{16}C from a large-scale shell-model calculation with modern nucleon-nucleon interactions" (in Japanese), KEK workshop on Modern Nuclear Physics, Oct. 1–3, 2007, KEK, Tsukuba, Japan.

56. S. Fujii, T. Mizusaki, T. Otsuka, T. Sebe and A. Arima (Oral): "Microscopic shell-model description of neutron-rich carbon isotopes", 2nd German-Japanese Workshop on Nuclear Structure and Astrophysics, Oct. 4–7, 2006, RIKEN, Wako, Japan.

57. S. Fujii, T. Mizusaki, T. Otsuka, T. Sebe and A. Arima (Oral): "Effective charge in shell-model calculations for nuclei around ^{16}C" (in Japanese), YITP workshop on Effective Interaction Theory and Nuclear Models, Feb. 5–8, 2007, Kyoto, Japan.

58. S. Fujii, T. Mizusaki, T. Otsuka, T. Sebe and A. Arima (Oral): "Microscopic shell-model calculations for neutron-rich carbon isotopes in the $spsdpf$ space", International Workshop, Joint JUSTIPEN-LACM Meeting, Mar. 5–8, 2007, ORNL, Knoxville, USA.

59. T. Kawabata, Y. Sasamoto, Y. Maeda, K. Nakanishi, S. Sakaguchi, K. Suda, T. Uesaka, M. Fujiwara, H. Hashimoto, K. Kawase, K. Hatanaka, Y. Shimizu, Y. Tameshige, A. Tamii, H. P. Yoshida, K. Itoh, M. Itoh, Y. Kanada-En'yo and M. Uchida (Oral): "Cluster states in ^{11}B and ^{13}C", RCNP Workshop on Cluster Condensation and Tensor Correlation in Nuclei, Mar. 22–23, 2007, Research Center for Nuclear Physics, Osaka, Japan.

60. Y. Maeda (Oral): "Study of 3NF effects via the pd breakup reactioin at 250 MeV", RCNP Workshop on Fewbody System and Baryon-Baryon interaction, Mar. 6–7, 2007, Research Center for Nuclear Physics, Osaka, Japan.

61. T. Kawabata, S. Shimoura, T. Uesaka, K. Nakanishi, Y. Sasamoto, H. Sakai, A. Saito, T. Kubo and G. P. A. Berg (Oral): "SHARAQ Project $\sim$ New Spin-Isospin Modes in Nuclei $\sim$", International Workshop as Joint JUSTIPEN-LACM Meeting, Mar. 5–8, 2007, Joint Institute for Heavy Ion Research, Oak Ridge, Tennessee, USA.

62. S. Sakaguchi, T. Uesaka, T. Wakui, T. Kawabata, N. Aoi, Y. Hashimoto, M. Ichikawa, Y. Ichikawa, K. Itoh, M. Itoh, H. Iwasaki, T. Kawahara, H. Kuboki, Y. Maeda, R. Matsuo, T. Nakao, H. Okamura, H. Sakai, N. Sakamoto, Y. Sasamoto, M. Sasano, Y. Satou, K. Sekiguchi, M. Shinohara, K. Suda, D. Suzuki, Y. Takahashi, A. Tamii, K. Yako and M. Yamaguchi (Oral): "Analyzing Power Measurement for Elastic Scattering on ^{6}He on Polarized Protons", RI Beam Factory mini Workshop on Proton Elastic Scattering on Unstable Nuclei, Mar. 2, 2007, RIKEN, Saitama, Japan.

63. T. Kawabata (Oral): "Dilute cluster states", RCNP Workshop on Frontier Explored by the Upgraded RCNP Cyclotron, Feb. 19–20, 2007, Research Center for Nuclear Physics, Osaka, Japan.

64. T. Kawabata, Y. Sasamoto, Y. Maeda, K. Nakanishi, S. Sakaguchi, K. Suda, T. Uesaka, M. Fujiwara, H. Hashimoto, K. Kawase, K. Hatanaka, Y. Shimizu, Y. Tameshige, A. Tamii, H. P. Yoshida, K. Itoh, M. Itoh, Y. Kanada-En'yo and M. Uchida (Oral): "Cluster states in ^{11}B", RCNP Workshop on Clustering Phenomena in Nuclear Many-Body Systems, Feb. 14–16, 2007, Research Center for Nuclear Physics, Osaka, Japan.

65. Y. Sasamoto, T. Kawabata, T. Uesaka, K. Suda, Y. Maeda, S. Sakaguchi, K. Itoh, K. Hatanaka, M. Fujiwara, A. Tami, Y. Shimizu, K. Nakanishi, K. Kawase, H. Hashimoto, Y. Tameshige, H. Matsubara, M. Itoh, H. P. Yoshida and M. Uchida (Oral): "Cluster states in ^{13}C", RCNP Workshop on Clustering Phenomena in Nuclear Many-Body Systems, Feb. 14–16, 2007, Research Center for Nuclear Physics, Osaka, Japan.

66. S. Sakaguchi, T. Uesaka, T. Wakui, T. Kawahara, A. Tamii and H. Sakai (Oral): "Solid Polarized Proton Target Using Ar-ion Laser", RI Beam Factory mini Workshop on Accelerater Experiments with Laser, Nov. 30, 2006, RIKEN, Saitama, Japan.

67. Y. Sasamoto, T. Kawabata, T. Uesaka, M. Hamagaki, I. Sugai and Y. Takeda (Oral): "Preparation of self-supporting target of ^{11}B", International Nuclear Target Development Society (INTDS2006), Oct. 16–20, 2006, Tsukuba Epochal International Congress Center, Tsukuba, Ibaraki, Japan.

68. K. Suda, T. Uesaka, V. P. Ladygin, Y. Maeda, P. K. Kurilkin, Yu. V. Gurchin, A. Yu. Isupov, K. Itoh, M. Janek, J.-T. Karachuk, T. Kawabata, A. N. Khrenov, A. S. Kiselev, V. A. Kizka, J. Kliman, V. A. Krasnov, A. N. Livanov, A. I. Malakov, V. Matoucek, M. Morhac, S. M. Piyadin, S. G. Reznikov, S. Sakaguchi, H. Sakai, Y. Sasamoto, K. Sekiguchi, I. Turzo and T. A. Vasiliev (Oral): "Development of Deuteron Polarimeter at Internal Target Station of Nuclotron", 17th International Spin Physics Symposium (SPIN2006), Oct. 2–7, 2006, Kyoto, Japan.

69. Y. Maeda, T. Uesaka, T. Kawabata, K. Suda, Y. Sasamoto, S. Sakaguchi, H. Sakai, K. Yako, M. Sasano, S. Noji, K. Hatanaka, A. Tamii Y. Shimizu, M. Takechi, Y. Tameshige, H. Matsubara, K. Sagara, T. Wakasa, M. Dozono, E. Ihara and K. Sekiguchi (Oral): "Measurement of A_y for the pd Breakup Reaction at 250 MeV", 17th International Spin Physics Symposium (SPIN2006), Oct. 2–7, 2006, Kyoto, Japan.

70. S. Sakaguchi, T. Uesaka, T. Wakui, T. Kawabata, N. Aoi, Y. Hashimoto, M. Ichikawa, Y. Ichikawa, K. Itoh, M. Itoh, H. Iwasaki, T. Kawahara, H. Kuboki, Y. Maeda, R. Matsuo, T. Nakao, H. Okamura, H. Sakai, N. Sakamoto, Y. Sasamoto, M. Sasano, Y. Satou, K. Sekiguchi, M. Shinohara, K. Suda, D. Suzuki, Y. Takahashi, A. Tamii, K. Yako and M. Yamaguchi (Oral): "Analyzing Power Measurement for Elastic Scattering of ^{6}He on Polarized Protons", 17th International Spin Physics Symposium (SPIN2006), Oct. 2–7, 2006, Kyoto, Japan.

71. S. Sakaguchi, T. Uesaka, T. Wakui, T. Kawabata, N. Aoi, Y. Hashimoto, M. Ichikawa, Y. Ichikawa, K. Itoh, M. Itoh, H. Iwasaki, T. Kawahara, H. Kuboki, Y. Maeda, R. Matsuo, T. Nakao, H. Okamura, H. Sakai, N. Sakamoto, Y. Sasamoto, M. Sasano, Y. Satou, K. Sekiguchi, M. Shinohara, K. Suda, D. Suzuki, Y. Takahashi, A. Tamii, K. Yako and M. Yamaguchi (Oral): "Analyzing Power Measurement for the Proton Elastic Scattering on ^{6}He at 71 MeV/u", CNS International Summer School (CISS06), Aug. 24–29, 2006, Center for Nuclear Study, University of Tokyo, Saitama, Japan.

72. T. Kawabata, H. Akimune, H. Fujita, Y. Fujita, M. Fujiwara, K. Hara, K. Hatanaka, M. Itoh, Y. Kanada-En'yo, S. Kishi, K. Nakanishi, H. Sakaguchi, Y. Shimbara, A. Tamii, S. Terashima, M. Uchida, T. Wakasa, Y. Yasuda, H. P. Yoshida and M. Yosoi (Oral): "Three-body cluster state in ^{11}B", 18th International IUPAP Conference on Few-Body Problems in Physics (FB18), Aug. 21–26, 2006, Santos, Brazil.

73. Y. Maeda, H. Sakai, K. Fujita, M. Hatano, J. Kamiya, T. Kawabata, H. Kuboki, K. Hatanaka, H. Okamura, T. Saito, Y. Sakemi, M. Sasano, K. Sekiguchi, Y. Shimizu, K. Suda, Y. Tameshige, A. Tamii, T. Wakasa, K. Yako, M.B. Greenfield, H. Kamada and H. Witała (Oral): "Measurements of the $\vec{n}d$ scattering at 250 MeV", 18th International IUPAP Conference on Few-Body Problems in Physics (FB18), Aug. 21–26, 2006, Santos, Brazil.

74. T. Kawabata, H. Akimune, H. Fujita, Y. Fujita, M. Fujiwara, K. Hara, K. Hatanaka, M. Itoh, Y. Kanada-En'yo, S. Kishi, K. Nakanishi, H. Sakaguchi, Y. Shimbara, A. Tamii, S. Terashima, M. Uchida, T. Wakasa, Y. Yasuda, H. P. Yoshida and M. Yosoi (Oral): "Dilute cluster state in ^{11}B", International Workshop on Alpha Particle Condensation in Nuclear Systems, Aug. 17–19, 2006, Munich, Germany.

75. Y. Sasamoto, T. Kawabata, T. Uesaka, K. Suda, Y. Maeda, S. Sakaguchi, K. Itoh, K. Hatanaka, M. Fujiwara, A. Tami, Y. Shimizu, K. Nakanishi, K. Kawase, H. Hashimoto, Y. Tameshige, H. Matsubara, M. Itoh, H. P. Yoshida and M. Uchida (Oral): "Cluster states in ^{13}C", International Workshop on Alpha Particle Condensation in Nulcear Systems, Aug. 17–19, 2006, Munich, Germany.

76. S. Sakaguchi, T. Uesaka, T. Wakui, T. Kawahara and H. Sakai (Oral): "CNS Polarized Proton Target for RI-Beam Experiment", Annual RI Beam Factory Users Meeting 2006, Aug. 3–4, 2006, RIKEN, Saitama, Japan.

77. T. Kawabata, H. Akimune, H. Fujita, Y. Fujita, M. Fujiwara, K. Hara, K. Hatanaka, M. Itoh, Y. Kanada-En'yo, S. Kishi, K. Nakanishi, H. Sakaguchi, Y. Shimbara, A. Tamii, S. Terashima, M. Uchida, T. Wakasa, Y. Yasuda, H. P. Yoshida and M. Yosoi (Oral): "Dilute cluster state in ^{11}B", 2nd International Conference on Collective Motion in Nuclei under Extreme Conditions (COMEX2), Jul. 20–23, 2006, Sankt Goar, Germany.

78. S. Sakaguchi, T. Uesaka, T. Wakui, T. Kawabata, N. Aoi, Y. Hashimoto, M. Ichikawa, Y. Ichikawa, K. Itoh, M. Itoh, H. Iwasaki, T. Kawahara, H. Kuboki, Y. Maeda, R. Matsuo, T. Nakao, H. Okamura, H. Sakai, N. Sakamoto, Y. Sasamoto, M. Sasano, Y. Satou, K. Sekiguchi, M. Shinohara, K. Suda, D. Suzuki, Y. Takahashi, A. Tamii, K. Yako and M. Yamaguchi (Poster): "Measurement of the Analyzing Power for the p+^{6}He Elastic Scattering at 71MeV/u", 7th International Conference on Radioactive Nuclear Beams (RNB7), Jul. 3–7, 2006, Cortina d'Ampezzo, Italy.

79. S. Sakaguchi, T. Uesaka, T. Wakui, T. Kawabata, N. Aoi, Y. Hashimoto, M. Ichikawa, Y. Ichikawa, K. Itoh, M. Itoh, H. Iwasaki, T. Kawahara, H. Kuboki, Y. Maeda, R. Matsuo, T. Nakao, H. Okamura, H. Sakai, N. Sakamoto, Y. Sasamoto, M. Sasano, Y. Satou, K. Sekiguchi, M. Shinohara, K. Suda, D. Suzuki, Y. Takahashi, A. Tamii, K. Yako and M. Yamaguchi (Oral): "Analyzing Power Measurement for Proton Elastic Scattering on ^{6}He", RI Beam Factory mini Workshop on Elastic Scattering of Unstable Nuclei, Jun. 24, 2006, RIKEN, Saitama, Japan.

80. T. Kawabata, H. Akimune, H. Fujita, Y. Fujita, M. Fujiwara, K. Hara, K. Hatanaka, M. Itoh, Y. Kanada-Enyo, S. Kishi, K. Nakanishi, H. Sakaguchi, Y. Shimbara, A. Tamii, S. Terashima, M. Uchida, T. Wakasa, Y. Yasuda, H. P. Yoshida and M. Yosoi (Oral): "$2\alpha + t$ cluster state in ^{11}B", RCNP Osaka Spring Workshop on Cluster

Condensation and Nucleon Correlation in Nuclei, Apr. 26–28, 2006, Research Center for Nuclear Physics, Osaka, Japan.

81. Y. Sasamoto, T. Kawabata, T. Uesaka, K. Suda, Y. Maeda, S. Sakaguchi, K. Itoh, K. Hatanaka, M. Fujiwara, A. Tami, Y. Shimizu, K. Nakanishi, K. Kawase, H. Hashimoto, Y. Tameshige, H. Matsubara, M. Itoh, H. P. Yoshida and M. Uchida (Oral): "Cluster states in ^{13}C", RCNP Osaka Spring Workshop on Cluster Condensation and Nucleon Correlation in Nuclei, Apr. 26–28, 2006, Research Center for Nuclear Physics, Osaka, Japan.

82. T. Uesaka (Invited): "Polarized Proton Target at High Temperature and Low Magnetic Field", 17th International Spin Physics Symposium (SPIN2006), Oct. 2–7, 2006, Kyoto, Japan.

83. T. Uesaka (Oral): "Elastic Scattering Experiment at SHARAQ", RI Beam Factory mini Workshop on Elastic Scattering of Unstable Nuclei, Jun. 23–24, 2006, RIKEN, Saitama, Japan.

84. T. Uesaka, T. Wakui, S. Sakaguchi, T. Kawahara, and H. Sakai (Oral): "Polarized proton target for RI beam experiments", 7th International Conference on Radioactive Nuclear Beams (RNB7), Jul. 3–7, 2006, Cortina d'Ampezzo, Italy.

85. T. Uesaka, S. Shimoura, H. Sakai T. Kawabata, G. P. A. Berg, A. Saito, K. Nakanishi, Y. Sasamoto, T. Kubo, S. Kubono, E. Ideguchi, H. Yamaguchi (Poster): "The high resolution SHARAQ spectrometer", 7th International Conference on Radioactive Nuclear Beams (RNB7), Jul. 3–7, 2006, Cortina d'Ampezzo, Italy.

86. T. Uesaka, S. Shimoura, T. Kawabata, H. Sakai, A. Saito, K. Nakanishi, Y. Sasamoto, S. Kubono, E. Ideguchi, H. Yamaguchi, T. Kubo, G. P. A. Berg (Invited): "Design of the high-resolution SHARAQ spectrometer", Annual RI Beam Factory Users Meeting 2006, Aug. 3–4, 2006, RIKEN, Saitama, Japan.

87. T. Uesaka (Oral), "Quasifree knockout reaction with Polarized Protons" ,International Collaboration Workshop on Experiments at the RIBF, Nov. 6–9, 2006, RIKEN, Saitama, Japan.

B. JPS Meetings

1. Y. Wakabayashi, T. Fukuchi, Y. Gono, A. Odahara, S. Tanaka, M. Inoue, T. Sasaki, M. Kibe, N. Hokoiwa, T. Shinozuka, M. Fujita, A. Yamazaki, T. Sonoda, C.S. Lee, Y.K. Kwon, J.Y. Moon and J.H. Lee (Oral): "High-spin states of ^{93}Nb" at the JPS Fall meeting, Sep 20–23, 2006, Nara Women's University, Nara, Japan.

2. H. Yamaguchi, Y. Wakabayashi, G. Amadio, H. Fujikawa, S. Kubono, A. Saito, J.J. He, T. Teranishi, S. Nishimura, Y. Togano, Y.K. Kwon, N. Iwasa, K. Inafuku, and L. H. Khiem: "Proton resonance scattering of 7Be at CRIB facility of CNS", JPS Autumn Meeting Sep. 20–23, Nara, Japan.

3. E. Ideguchi: "Study of High-Spin States Using RI Beams" Symposium on New Domain in High Spin and Isospin via γ-ray Spectroscopy, JPS Fall Meeting, September 20–23, Nara, Japan

4. M. Niikura, E. Ideguchi, N. Aoi, H. Baba, T. Fukuchi, Y. Ichikawa, H. Iwasaki, T. Kubo, M. Kurokawa, M. Liu, S. Michimasa, T.K. Onishi, S. Ota, S. Shimoura, H. Suzuki, D. Suzuki, Y. Wakabayashi, K. Yoshida, Y. Zheng: "Study of High Spin States around ^{48}Ca via Fusion Reaction of Secondary Be ams", JPS Fall Meeting, September 20–23, Nara, Japan

5. T. Gunji

   "J/ψ Measurement in Heavy Ion Collisions at RHIC" at the JPS Spring meeting, Sep. 20–23, 2006, Symposium on "Strong Coupled Quark-Gluon-Plasma observed at RHIC", Nara Women's Univ. Nara. Japan

6. Y. Morino for the PHENIX Collaboration (Oral): "A search for condensed double anti-K bound state at PHENIX", at the JPS Fall meeting, Sep. 20–23, 2006, Nara Woman University, Nara, Japan.

7. T. Horaguchi for the PHENIX Collaboration (Oral): "Measurement of the direct photon production in polarized proton-proton collisions at $\sqrt{s}$ = 200 GeV with PHENIX", at the JPS Fall meeting, Sep. 20–23, 2006, Nara Women's University, Tokyo, Japan.

8. Y. Aramaki, H. Hamagaki, K. Ozawa, S.X. Oda, Y.L. Yamaguchi, S. Yokkaichi[a] Univ. of Tokyo, RIKEN[a]: "Development of a Cherenkov light detector using a CsI evaporated GEM", at the JPS Fall meeting, Sep. 20–23, 2006, Nara Woman's University, Nara, Japan.

9. Y.L. Yamaguchi, H. Hamagaki, K. Ozawa, S.X. Oda, Y. Aramaki, S. Sano, S. Yokkaichi, T. Tamagawa, S. Iwamoto (Oral): "Study for Thickness Dependence of Gain of GEM", at the JPS Fall meeting, Sep. 20–23, 2006, Nara Women's University, Nara, Japan.

10. S. Fujii, T. Mizusaki, T. Otsuka, T. Sebe and A. Arima (Oral): "Large-scale shell-model calculations for neutron-rich carbon isotopes with modern NN forces", at the JPS Fall meeting, Sep. 20–23, 2006, Nara Women's University, Nara, Japan.

11. Y. Sasamoto, T. Kawabata, T. Uesaka, K. Suda, Y. Maeda, S. Sakaguchi, K. Itoh, K. Hatanaka, M. Fujiwara, A. Tami, Y. Shimizu, K. Nakanishi, K. Kawase, H. Hashimoto, Y. Tameshige, H. Matsubara, M. Itoh, H. P. Yoshida and M. Uchida: "Cluster states in ^{13}C", JPS Autumn Meeting, Sep. 20–23, 2006, Nara Women's University, Nara, Japan.

12. Y. Maeda, T. Uesaka, T. Kawabata, K. Suda, Y. Sasamoto, S. Sakaguchi, K. Itoh, H. Sakai, K. Yako, M. Sasano, S. Noji, K. Miki, K. Hatanaka, Y. Sakemi, A. Tamii Y. Shimizu, Y. Tameshige, H. Matsubara, T. Wakasa, M. Dozono and K. Sekiguchi: "Study of 3NF effects via the pd breakup reactioin at 250 MeV", JPS Autumn Meeting, Sep. 20–23, 2006, Nara Women's University, Nara, Japan.

13. S. Sakaguchi, T. Uesaka, T. Wakui, T. Kawabata, N. Aoi, Y. Hashimoto, M. Ichikawa, Y. Ichikawa, K. Itoh, M. Itoh, H. Iwasaki, T. Kawahara, H. Kuboki, Y. Maeda, R. Matsuo, T. Nakao, H. Okamura, H. Sakai, N. Sakamoto, Y. Sasamoto, M. Sasano, Y. Satou, K. Sekiguchi, M. Shinohara, K. Suda, D. Suzuki, Y. Takahashi, A. Tamii, K. Yako and M. Yamaguchi: "Measurement of Analysing Power for Proton Elastic Scattering on ^{6}He", JPS Autumn Meeting, Sep. 20–23, 2006, Nara Women's University, Nara, Japan.

14. T. Uesaka, S. Shimoura, H. Sakai T. Kawabata, G. P. A. Berg, A. Saito, K. Nakanishi, Y. Sasamoto, T. Kubo, S. Kubono, E. Ideguchi, H. Yamaguchi, "Current Status of the SHARAQ Spectrometer I", JPS Autumn Meeting, Sep. 20–23, 2006, Nara Women's University, Nara, Japan.

15. A. Saito, S. Shimoura, T. Kawabata, Y. Sasamoto, T. Uesaka, and H. Sakai (Oral): "Development of low-pressure multi-wire drift chamber", at the JPS Spring meeting, Mar. 25–28, 2007, Tokyo Metropolitan University, Tokyo, Japan.

16. S. Shimoura, S. Ota, H. Iwasaki, M. Kurokawa, S. Michimasa, S. Kubono, T. Teranishi, M. Notani, M. Tamaki, T. Murakami, N. Iwasa, T. Motobayashi, Y. Yanagisawa, T. Minemura, S. Takeuchi, T. Gomi, K. Yamada, A. Saito, H. Baba, Y.U. Matsuyama, S. Kanno, E. Takeshita, K. Demichi, K. Hasegawa, K. Kurita, H. Sakurai, N. Aoi, E. Ideguchi, A. Odahara, T. Fukuchi, K. Miller, Z. Elekes, M. Ishihara: "Lifetime of Isomeric 0^+ State in ^{12}Be", JPS Spring Meeting, Mar. 25–28, Hachioji, Japan

17. S. Ota, S. Shimoura, H. Iwasaki, M. Kurokawa, S. Michimasa, S. Kubono, T. Teranishi, M. Notani, M. Tamaki, T. Murakami, N. Iwasa, T. Motobayashi, Y. Yanagisawa, T. Minemura, S. Takeuchi, T. Gomi, K. Yamada, A. Saito, H. Baba, Y.U. Matsuyama, S. Kanno, E. Takeshita, K. Demichi, K. Hasegawa, K. Kurita, H. Sakurai, N. Aoi, E. Ideguchi, A. Odahara, T. Fukuchi, K. Miller, Z. Elekes, M. Ishihara: "Proton Intruder State in ^{13}B via Proton Transfer Reaction on ^{12}Be", JPS Spring Meeting, Mar. 25–28, Hachioji, Japan

18. Y. Zheng, E. Ideguchi, S. Ota, M. Niikura, M. Liu, S. Michimasa, S. Shimoura, H. Yamaguchi, H. Baba, M. Kurokawa, T. Fukuchi, T. Morikawa, S. Mitarai, A. Yoshida, T. Murakami, D. Suzuki, T. Nakao, T. Suzuki, T. Koike, T. Komatsubar a: "Study of high-spin states in ^{108}In", JPS Spring Meeting, Mar. 25–28, Hachioji, Japan

19. S.X. Oda for the PHENIX Collaboration (oral): "J/ψ production in $\sqrt{s_{NN}}$=200 GeV Cu+Cu Collisions at mid-rapidi ty RHIC-PHENIX", at the JPS Spring meeting, Mar. 25–28, 2007, Tokyo Metropolitan University, Tokyo, Japan.

20. Y. Morino for the PHENIX Collaboration (Oral): "Study of electron-hadron correlation at p+p 200GeV collisions at PHENIX", at the JPS Spring meeting, Mar. 25–28, 2007,Tokyo MetroPolitan University, Tokyo, Japan.

21. S. Sano, H. Hamagaki, Y. Tanaka, T. Fusayasu, K. Kiyoyama, S.X. Oda, Y. Aramaki, Y.L. Yamaguchi: "Development of readout circuit for 2-dimensional imaging with Gas Electron Multiplier (GEM)" at the JPS Spring meeting, Mar. 25–28, 2007,Tokyo MetroPolitan University, Tokyo, Japan.

22. S. Fujii, T. Mizusaki and T. Otsuka (Oral): "Effective charge in shell-model calculations for nuclei around ^{16}C", at the JPS Spring meeting, Mar. 25–28, 2007, Tokyo Metropolitan University, Hachioji, Japan.

23. T. Uesaka, S. Shimoura, H. Sakai T. Kawabata, G. P. A. Berg, A. Saito, K. Nakanishi, Y. Sasamoto, S. Michimasa, T. Kubo, S. Kubono, E. Ideguchi, H. Yamaguchi, "Current Status of the SHARAQ Spectrometer II", JPS Spring meeting, Mar. 25–28, 2007, Tokyo Metropolitan University, Tokyo, Japan.

24. T. Kawahara, T. Uesaka, S. Sakaguchi, T. Wakui and K. Itoh: "The polarized proton solid target using the high power LED", JPS Spring meeting, Mar. 25–28, 2007, Tokyo Metropolitan University, Tokyo, Japan.

25. T. Kawabata: "Cluster states in ^{11}B and ^{13}C", JPS Spring meeting, Mar. 25–28, 2007, Tokyo Metropolitan University, Tokyo, Japan.

26. Y. Sasamoto, T. Kawabata, T. Uesaka, K. Suda, Y. Maeda, S. Sakaguchi, K. Itoh, K. Hatanaka, M. Fujiwara, A. Tami, Y. Shimizu, K. Nakanishi, K. Kawase, H. Hashimoto, Y. Tameshige, H. Matsubara, M. Itoh, H. P. Yoshida and M. Uchida: "Cluster states in ^{13}C", JPS Spring Meeting, Mar. 25–28, 2007, Tokyo Metropolitan University, Tokyo, Japan.

C. Lectures

1. S. Shimoura: "Special Lectures on Variety of Structure in Asymmetric Nuclei", June 5–7, 2006, Tohoku University

2. S. Kubono: "Nuclear Astrophysics", Feb. 14-19, 2005, Canpo de Jordan, Brazil.

D. Seminars

1. A. Saito: "Exotic cluster states in ^{12}Be via α-inelastic scattering", May 30, 2006, RIBF Nuclear Physics Seminar at RIKEN, Japan

2. E. Ideguchi: "Study of Large Deformed Nucleus in High-Spin States", November 28, 2006, Tohoku University

3. T. Uesaka, "Studies of Unstable Nuclei with Polarized Proton Target", Tsukuba Seminar on Unstable Nuclei, Aug. 30, 2006, JAEA, Tokai, Japan.

4. T. Uesaka, "SHARAQ Project – high resolution spectroscopy with RI beams –", the Regular Seminar of the Physics Department of University of Notre Dame, Oct. 30, 2006, University of Notre Dame, South Bend, USA.

Personnel

Director

OTSUKA, Takaharu	*Professor, Department of Physics, Graduate School of Science*

Scientific Staff

1. Accelerator Research

WATANABE, Shin-ichi	*Research Associate*

2. Heavy-Ion Collisions

SHIMOURA, Susumu	*Professor*
UESAKA, Tomohiro	*Associate Professor*
IDEGUCHI, Eiji	*Lecturer*
IWASAKI, Hironori	*Research Associate*
KAWABATA, Takahiro	*Research Associate*
MICHIMASA, Shin'ichiro (November 2006 $\sim$)	*Research Associate*

3. Nuclear Structure in Extreme States

KUBONO, Shigeru	*Professor*
HAMAGAKI, Hideki	*Associate Professor*
YAMAGUCHI, Hidetoshi	*Research Associate*
OZAWA, Kyoichiro ($\sim$ October 2006)	*Research Associate*

Guest Professors

MIZUSAKI, Takahiro	*Senshu University*

Technical Staff

OHSHIRO, Yukimitsu YAMAZAKI, Norio

Technical Assistants

YAMAKA, Shoichi
NAGATA, Takeshi
YOSHINO, Ryo

Post Doctoral Associates

SUDA, Kenji
FUJII, Shinichiro
MAEDA, Yukie
HORAGUCHI, Takuma ($\sim$ October 2006)
LIU, Minlang
ZHENG, Yong
OTA, Shinnsuke
WAKABAYASHI, Yasuo
NAKANISHI, Kosuke

Graduate Students

KAJIHARA, Fukutaro
GUNJI, Taku
ISOBE, Tadaaki
NIIKURA, Megumi
ODA, Susumu
MORINO, Yuhei
SAKAGUCHI, Satoshi
SAITO, Shota
SASAMOTO, Yoshiko
AMADIO, Guilherme
YAMAGUCHI, Yorito
ARAMAKI, Youki
SANO, Satoshi
HAYAKAWA, Seiya

Administration Staff

HIRANO, Midori
KISHI, Yukino (May 2006 $\sim$)
YAMAMOTO, Ikuko
ITAGAKI, Toshiko
FUJIWARA, Yuko
ENDO, Takako

Committees

Council

IWASAWA, Yasuhiro (chair)	*Dean, Graduate School of Science*
SAKAI, Hideyuki	*Department of Physics, Graduate School of Science*
MATSUURA, Mitsuhiro	*Department of Earth and Planetary Science*
UCHIDA, Shinichii	*Department of Physics, Graduate School of Science*
OTSUKA, Takaharu	*Department of Physics, Graduate School of Science*
Hayano, Ryugo	*Department of Physics, Graduate School of Science*
KUBONO, Shigeru	*Center for Nuclear Study, Graduate School of Science*
SHIMOURA, Susumu	*Center for Nuclear Study, Graduate School of Science*
NAGAMIYA, Shoji	*J-PARC Project Office,* *High Energy Accelerator Research Organization*

Steering Committee

OTSUKA, Takaharu	*Department of Physics, Graduate School of Science*
SHIMOURA, Susumu	*Center for Nuclear Study, Graduate School of Science*
KUBONO, Shigeru	*Center for Nuclear Study, Graduate School of Science*
HAMAGAKI, Hideki	*Center for Nuclear Study, Graduate School of Science*
SAKAI, Hideyuki	*Department of Physics, Graduate School of Science*
AIHARA, Hiroaki	*Department of Physics, Graduate School of Science*
HAYANO, Ryugo	*Department of Physics, Graduate School of Science*
HAMAGUCHI, Hiroo	*Department of Chemistry, Graduate School of Science*
KOBAYASHI, Tomio	*International Center for Elementary Particle Physics*
YAMAZAKI, Yasunori	*Institute of Physics, Graduate School of Arts and Sciences*
MADARAME, Haruki	*Department of Nuclear Engineering and Management*

Program Advisory Committee

HATANAKA, Kichiji (chair)	*Research Center for Nuclear Physics, Osaka University*
EN'YO, Hideto	*The Institute of Physical and Chemical Research, Nishina Center*
YABANA, Kazuhiro	*University of Tsukuba*
ODAHARA, Atsuko	*Osaka University*
HAMAMOTO, Ikuko	*University of Lund, Sweden*
MITTING, Wolfgang	*Grand Accelerateur National D'Ions Lourds*
WIESCHER, Michael	*University of Notre Dame*